Phase transitions in driven diffusive systems far from equilibrium

Szavits Nossan, Juraj

UNIVERSITY OF ZAGREB
FACULTY OF SCIENCE
DEPARTMENT OF PHYSICS

Juraj Szavits Nossan

PHASE TRANSITIONS IN DRIVEN DIFFUSIVE SYSTEMS FAR FROM EQUILIBRIUM

DOCTORAL THESIS

Zagreb, 2011

SVEUČILIŠTE U ZAGREBU
PRIRODOSLOVNO-MATEMATIČKI FAKULTET
FIZIČKI ODSJEK

Juraj Szavits-Nossan

FAZNI PRIJELAZI U VOĐENIM DIFUZIJSKIM SUSTAVIMA DALEKO OD RAVNOTEŽE

DOKTORSKI RAD

Zagreb, 2011.

TEMELJNA DOKUMENTACIJSKA KARTICA

Sveučilište u Zagrebu
Prirodoslovno-matematički fakultet, Fizički odsjek
Sveučilišni poslijediplomski studij prirodnih znanosti
Fizika - smjer Fizika kondenzirane materije

Doktorska disertacija

FAZNI PRIJELAZI U VOĐENIM DIFUZIJSKIM SUSTAVIMA DALEKO OD RAVNOTEŽE

Juraj Szavits-Nossan, dipl. ing.

Institut za fiziku, Zagreb

Mentor: Dr. sc. Katarina Uzelac, znan. savj., Institut za fiziku, Zagreb

U ovom radu promatramo fazne prijelaze daleko od ravnoteže u nekoliko predloženih generalizacija tzv. asimetričnog jednostavnog procesa iskjučenja (skraćeno ASEP). ASEP je jednostavni model iz klase tzv. vođenih difuzijskih sustava koji se održavaju daleko od ravnoteže vanjskim poljem i/ili rubnim uvjetima. U prvom dijelu predlažemo generalizacija ASEP-a na dugodosežne skokove, pri čemu se duljina skoka bira iz raspodjele koja slijedi potencijski zakon $p_l \propto l^{-(1+\sigma)}$, gdje je $\sigma > 1$ parametar dosega. Iako dugodosežni model ima isti fazni dijagram kao i kratkodosežni, opažamo razlike na svim linijama prijelaza za $1 < \sigma < 2$, dok kratkodosežna granica nastupa za $\sigma > 2$. Iz perspektive dugodosežnog modela razmatramo i ASEP s jednim defektnim čvorom koji usporava tok čestica i inducira separaciju faza. Za razliku od kratkodosežnog modela u kojem postoji otvoreno pitanje da li se separacija faza javlja za sve jačine defekta, u dugodosežnom modelu pokazujemo da je scenarij bez separacije moguć, te izvodimo egzaktnu točku prijelaza između dva režima. U slučaju konačne koncentracije defekata (tj. nereda) pokazujemo da u dvodimenzionalnom ASEP-u postoji režim u kojem separacije faza nema bez obzira na detalje nereda, za razliku od jednodimenzionalnog ASEP-a u kojem nered uvijek inducira separaciju faza.

(118 stranica, 55 slika, 1 tablica, 159 literarnih navoda, 1 prilog, jezik izvornika: engleski)

Ključne riječi: vođeni difuzijski sustavi, stacionarna stanja, fazni dijagrami, defekti, neuređeni sustavi
Datum obrane: 20. listopada 2011.
Povjerenstvo za obranu:

1. Akademik Slaven Barišić, PMF-Fizički odsjek (Predsjednik povjerenstva)
2. Dr. sc. Katarina Uzelac (Mentor), Institut za fiziku
3. Profesor Dr. sc. Gunter M. Schütz, Institut für Festkörperforschung, Forschungszentrum Jülich, Njemačka
4. Profesor Dr. sc. Denis. K. Sunko, PMF-Fizički odsjek
5. Profesor Dr. sc. Antonije Dulčić, PMF-Fizički odsjek

Rad je pohranjen u Središnjoj knjižnici za fiziku Prirodoslovno-matematičkog fakulteta u Zagrebu, Bijenička cesta 32.

BASIC DOCUMENTATION CARD

University of Zagreb
Faculty of Science, Department of Physics
Postgraduate study in Condensed matter physics

Ph.D. Thesis

PHASE TRANSITIONS IN DRIVEN DIFFUSIVE SYSTEMS FAR FROM EQUILIBRIUM

Juraj Szavits-Nossan, dipl. ing.

Institute of Physics, Zagreb

Supervisor: Dr. sc. Katarina Uzelac, Institute of Physics, Zagreb

Nonequilibrium phase transitions are studied in several proposed generalizations of the asymmetric simple exclusion process (ASEP). ASEP is a simple model belonging to the class of so-called driven diffusive systems maintained far from equilibrium by external field and nonequilibrium boundary conditions. We propose a generalization of ASEP that replaces short-range with long-range hopping, where hopping length l is taken from the probability distribution that follows a power law $p_l \propto l^{-(1+\sigma)}$ with $\sigma > 1$. Although the resulting phase diagram remains the same, we observe changes both at the first- and the second-order transition lines for $1 < \sigma < 2$, while the short-range limit sets in for $\sigma > 2$. Using the same model we also address the long-standing question of whether a "slow" site in ASEP always induces phase separation. By including a "slow" site in the long-range model we show that the transition to the non-separated phase is possible and we find the exact transition point. In the case of finite concentration of defects (i.e. disorder), we show that contrary to the one-dimensional case where disorder always induces phase separation, in the two-dimensional ASEP a regime exists in which phase separation is absent.

(118 pages, 55 figures, 1 table, 159 references, 1 appendix, original in: English)

Keywords: driven diffusive systems, stationary states, phase diagrams, defects, disordered systems
Date of thesis defense: 20th of October 2011
Thesis committee:

1. Academician Slaven Barišić (Committee Chair), Physics Department, Faculty of Science, University of Zagreb
2. Dr. Katarina Uzelac (Mentor), Institute of Physics, Zagreb
3. Professor Dr. Gunter M. Schütz, Institut für Festkörperforschung , Forschungszentrum Jülich, Germany
4. Professor Dr. Denis K. Sunko, Physics Department, Faculty of Science, University of Zagreb
5. Professor Dr. Antonije Dulčić, Physics Department, Faculty of Science, University of Zagreb

Thesis is deposited in Central Physics Library, Faculty of Science, Physics Department, Bijenička cesta 32.

The work presented in this dissertation has been conducted at the Institute of Physics, Zagreb under the supervision of Dr. Katarina Uzelac, as part of the Postgraduate doctoral studies in Condensed matter physics at the Physics Department, Faculty of Science, University of Zagreb.

For Martina and Aron

Ja ne znam tko si? Čuj me, dobri druže,
kad padne veče ponad tvoga krova,
kroz mrak se javi ćuk i hukne sova,
a oblaci ko jata ptica kruže
nad tornjevima sela i gradova -

izađi u noć... idi... Divlje ruže
opijat će te putem. Trn će cvasti,
otvorit oči lopoči na vodi.

Izađi... idi... Srebrn plašt će pasti
dalekom cestom, kud te srce vodi.

(Gustav Krklec)

Acknowledgement

The work presented here has been conducted in the statistical physics group of Dr. Katarina Uzelac at the Institute of Physics, Zagreb. It is my duty, and before all, my pleasure to thank Dr. Uzelac for introducing me to the lively field of non-equilibrium statistical physics. I wish to express my gratitude for the patience and the care she showed towards all my ideas, both good and bad ones, playing often a role of a strict referee that leaves no room for thin arguments. I am especially in debt to Professor Gunter M. Schütz for his useful comments, suggested references and many clarifications that have significantly improved the presentation.

I thank my colleagues Ivan Balog and Tomislav Ivek for sharing all the good and all the bad moments in a life of a graduate student, of which, hopefully, we should remember only the good ones (one example being the fact the most breakthrough ideas happened curiously on Friday afternoons!). I thank my parents for being supportive and understanding. Special thanks goes to Ivan Katona for helping me with English version when I was running out of time.

Last but not least, I thank my wife Martina, who was all these years the best friend I could ever have, and my son Aron, whose joy and smile mean the whole world to me.

Contents

1 Introduction

In this paper we are dealing with a class of so-called driven diffusive systems [1,2], of which a typical representative is shown in Figure 1.1. Driven diffusive systems are macroscopic systems consisting of classical particles which are brought in contact with two reservoirs of different densities (Figure 1.1) or temperatures, with whom they exchange either particles or energy. In particular, we are interested in a situation in which the system is exposed to an external field (for example, electric or gravitational), which drives particles in the preferred direction, so that a current of mass or energy is established. Due to unequal densities or temperatures at boundaries and an external field which may be of arbitrary strength, a system will eventually reach a steady, but nonequilibrium state different from the one described by the Gibbs-Boltzmann distribution.

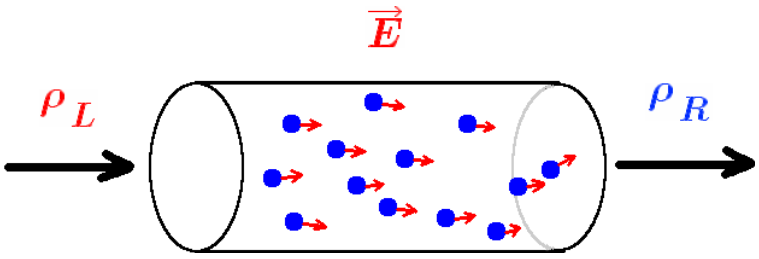

Figure 1.1: An example of a driven diffusive system in contact with two reservoirs at different densities and also subjected to an external field which drives particles in the preferred direction.

Such a nonequilibrium steady state is generally unknown, except for some one-dimensional models from this class [3–5] which we present in Section 2. As opposed to equilibrium [6], this fact denies us a straightforward way of calculating expectation values of macroscopic variables and their fluctuations bringing us back to one of the central issues of nonequilibrium statistical physics - how to derive a time evolution of macroscopic (thermodynamical) variables from microscopic equations of motion. Since this problem, except when we are close to equilibrium [7], is only slowly beginning to appear in standard textbooks on statistical physics (as an exception see e.g. [8]), we shall attempt to give a brief historical overview

of its main approaches in Section 1.1, distancing in advance from the illusion that we can be either exhaustive or complete in this task.

The lack of knowledge of stationary distribution in systems far from the equilibrium sets the first motivation for studying driven diffusion system. In the absence of a unified approach to the problem of nonequilibrium, one idea is to study simple systems from which one hopes to deduce a catalogue of general principles. Historically, a similar approach can be found in the development of the theory of phase transitions, where long before [10] the discovery of the renormalization group [11], many conclusions were drawn from exact solutions of certain microscopic models, such as the two-dimensional Ising model [12]. Following this idea, a microscopic model of a driven diffusive system, the asymmetric simple exclusion process (ASEP) [3–5], will be introduced briefly in Section 1.2 and studied in depth later in Chapter 2. Its various generalizations, presented in Chapters 3, 4 and 5, are the main subject of this thesis.

ASEP in contact with particle reservoirs of different densities is an important example of a system exhibiting boundary-induced phase transitions in one dimension [13], which brings us to the second motivation for studying this class of far-from-equilibrium systems. Its significance is further emphasized by the fact that equilibrium phase transitions (with short-range interactions) in one dimension are generally ruled out by the Peierls' argument [14]. On the other hand, such a rich behaviour found in systems far from the equilibrium should not be that surprising given that once the conditions that bring system to the equilibrium are lifted, the problem becomes essentially a dynamical one and the stationary state will generally depend on the details of dynamics (in some cases, it may even never be reached). This means that on the level of stochastic model like ASEP, we are left with the ambiguity of possible ways a system can be driven out of equilibrium. The experience from equilibrium phase transitions tells us, on the other hand, that the guiding principle in dealing with various mathematical models is the concept of *universality*, i.e. the fact that the character of phase transition is affected only by few ingredients (symmetry of the order parameter, range of interactions, dimension, etc.). Important steps in applying similar concept to nonequilibrium phase transitions have been recently put together in an exhausting review by Ódor [9], however, many issues still remain. Some examples of phase transitions in driven diffusive systems will be presented in section 1.2.

Finally, the last, equally important motivation for studying driven diffusion systems is applications to real systems. Although from the perspective of mathematical models this motivation may often seem neglected, by studying simplified microscopic models one hopes to identify the key (minimum) ingredients necessary to explain a certain phenomenon. Serving as starting point, these models are then often generalized for the purpose of obtaining better quantitative predictions. Historically, one of the first models in the class of driven diffusive system,

the so-called KLS model (named after its authors S. Katz, J. L. Lebowitz and H. Spohn [15]), was originally introduced to model transport in superionic conductors (e.g. α-AgI), in which mobile ions behave like a fluid immersed in the crystal lattice of static ions and are subjected to an external electric field [16]. ASEP, as its one-dimensional version in the limit of strong external field, has found many other applications including quantum spin chains, surface growth, protein synthesis and traffic, details of which are presented in Chapter 2.2. These examples teach us that in many macroscopic systems, "particles" can be imagined in a much broader sense than the one we are accustomed to in condensed matter physics, ranging from proteins in cytoplasm to cars in traffic. The last case is a good example of a system for which the traditional Hamiltonian approach and concept of equilibrium make little sense, since the forces involved are not actually physical, but "social". One can think of many other examples of such "non-thermodynamical" systems, found either in biology our in our society [1] that are slowly becoming the subjects of nonequilibrium statistical mechanics as well. Having that in mind, it is not pretentious to say that, in the world around us, the equilibrium is actually rather the exception than the rule.

1.1 Systems out of equilibrium: a short overview

Despite numerous efforts conducted in the last century, the understanding of macroscopic systems out of equilibrium is still far from being put in a systematic theory. One of the reasons is that nonequilibrium is essentially an *dynamical* problem, in a sense that one must know how to deduce the behaviour of few macroscopic variables from a time evolution of many microscopic degrees of freedom.

Historically, a first step in this direction was already made by Boltzmann, one of the founding fathers of statistical mechanics. Boltzmann derived the equation which, under the assumption of "molecular chaos" (*"Strosszahlansatz"*), explained the relaxation of rarefied gas towards the equilibrium, Maxwell-Boltzmann distribution (the famous H-theorem). At that time, Boltzmann equation was highly criticized by Loschmidt for deducing irreversibility from the reversible, Newton's laws of motion. It soon turned out that irreversibility was already implemented in the equation by the assumption of molecular chaos and the question of the so-called "arrow of time" began its long history. Today's prevailing opinion[2] sees irreversibility as a *typical* behaviour of *macroscopic* systems, which is not in contradiction to the reversible *microscopic* equations of motion [20]. This opinion has been recently put on rigorous grounds with the discovery of fluctuation theorems

[1] For an overview see Chapter *"Monte Carlo methods outside of physics"* in [17]; in the context of diffusive systems see [18].

[2] An opposite view, that irreversibility is intrinsic to dynamical systems, was advocated by the 1977 Nobel Laureate I. Prigogine (for an informal introduction see [19]).

(FT) [21–25], a collection of related theorems[3] which reveal the time asymmetry in fluctuations that either increase or decrease entropy. Roughly, the theorems state the following. Let us consider the probability $\pi(\sigma_\tau)$ that during the time interval τ, the average phase-space contraction rate is equal to σ_τ. According to the Liouville's theorem, the phase-space contraction rate is identically zero in Hamiltonian systems with conservative forces, but it is different from zero and equal to the entropy production rate in systems with dissipation. Fluctuation theorem then states that in systems with dissipation,

$$\frac{\pi(\sigma_\tau)}{\pi(-\sigma_\tau)} = e^{\tau\sigma_\tau}. \tag{1.1}$$

In other words, trajectories that decrease entropy are exponentially suppressed relative to the ones that increase it. There is even more in it: since entropy production is an extensive variable, the exponential factor in 1.1 becomes huge for macroscopic systems, thus explaining the origin of irreversibility in the world around us. Fluctuation theorems are valid quite generally and differ only in whether the system under consideration is either deterministic or stochastic system as well as whether we are interested in transient (as in 1.1) or stationary state (i.e. in the limit $\tau \to \infty$). For example, Gallavotti and Cohen proved the fluctuation theorem for the so-called thermostated dissipative, but *reversible* systems, mathematical idealizations of real thermostated systems (for a recent review, see [27]). Regarding the second law of thermodynamics and the "arrow of time", their result clearly shows no intrinsic "arrow of time", but rather a possibility of observing one *locally* in the direction determined by the sign of entropy production[4].

Another important result for systems far from equilibrium is the Jarzynski equality [29], which itself turns out to be a special kind of the fluctuation theorem [30] (Moreover, Harris and Schütz have shown that all fluctuation theorems can be derived from a fundamental time-reversal property of Markov processes, see [30].) To state the Jarzynski equality imagine a system in contact with environment such that the system's energy depends on the external time-dependent parameter λ. If λ is varied adiabatically, the total average work $\langle W \rangle$ performed on a system by external force is given by the difference in the free energy of the final (2) and initial (1) equilibrium states, $\langle W \rangle = F_2 - F_1 = \Delta F$ [31]. If, however, λ is varied at finite rate, the second law of thermodynamics states only that $\langle W \rangle \geq \Delta F$. Jarzynski's result gives the following *equality* for *any* finite rate $\dot{\lambda}$,

$$\langle exp(-\beta_1 W) \rangle_{1\to 2} = exp(-\beta \Delta F), \tag{1.2}$$

where although the final state 2 does not even have to be the equilibrium one,

[3] For a discussion about their similarities and differences see [26].

[4] In the context of cosmology, these lines of thought ultimately imply the Universe being born in the highly ordered state, see for example [28]

the expression 1.2 still refers to F_2! From the above expression, the second law of thermodynamics follows easily using the Jensen's inequality, $\langle exp(A)\rangle \geq exp(\langle A\rangle)$. Jarzynski equality finds its importance in experiments, since the measurement of free energy no longer requires equilibrium conditions to be met in a laboratory. From the point of view of the experimental physics, fluctuation theorems and Jarzynski equality find their application mostly in mesoscopic systems, typically biological ones, where due to a small number of degrees of freedom, deviations from classical thermodynamics become inevitable (for an experimentalist's view on the fluctuations theorems and Jarzynski equality, see [32]).

Fluctuation theorems are the crowning achievement of the so-called dynamical approach to the problem of nonequilibrium (see, for example, [33]), which evolves around the exact Liouville equation and uses all the "artillery" known from the theory of dynamical systems, like the Lyapunov exponents. Historically, a much older approach is the stochastic one, introduced by A. Einstein in 1905 in order to explain the Brownian movement [34]. Basically, the stochastic approach consists of distinguishing the fast and the slow degrees of freedom, the latter ones often being a consequence of, for example, conservation laws or critical slowing down at the second-order phase transition. In Brownian movement of pollen grains, the position and the momentum of grains are examples of slow degrees of freedom, compared to the motion of molecules of water that surrounds them, whose motion is fast and irregular. This separation of time scales enables us to write down the mesoscopic equation for the time evolution of slow degrees of freedom, the celebrated Langevin equation [35],

$$m\frac{d\vec{v}}{dt} = -\lambda\vec{v} + \vec{\eta}, \tag{1.3}$$

where stochastic noise $\vec{\eta}$ models the fast degrees of freedom,

$$\langle \eta(\vec{x},t)\eta(\vec{x}',t')\rangle = 2\lambda k_B T\delta(\vec{x}-\vec{x}')\delta(t-t'). \tag{1.4}$$

Langevin equation, in its general form, is the basis of the linear irreversible thermodynamics (see, for example, [7])), the theory that covers small deviations from equilibrium in the linear-response regime. Developed by the end of 1960s, this theory gave a complete description of thermodynamical fluctuations close to equilibrium. Employing the concept of local equilibrium [7], it was later successfully extended to spatially varying thermodynamic variables. The central idea of linear irreversible thermodynamics is the Onsager's hypothesis of regression of fluctuations [36], proved explicitly for Gaussian Markov processes in [37], which states that the relaxation of a system perturbed by the linear perturbation follows the *same* time evolution as the spontaneous fluctuations in the equilibrium state. In other words, in the linear-response regime a system typically does not distinguish the way the initial state was prepared. From the practical side, this enables us to

relate the response of a system to the external perturbation to equilibrium fluctuations, a fact that is mathematically expressed by the fluctuation-dissipation theorem (FDT) [38, 39] and Green-Kubo (GK) relations [40]. Since then, there has been many attempts to generalise FDT and GK relations to non-linear response and/or arbitrary far from equilibrium, of which a significant interest is recorded especially in the recent years (see [41] and references therein).

There are, of course, important examples of systems that are not in local equilibrium. This brings us to the beginning of this chapter and to driven diffusive system, which we proceed to describe in the following Section.

1.2 Driven diffusive systems

A representative mathematical model for driven diffusive systems is the driven lattice gas, introduced by Katz, Lebowitz and Spohn in 1984 [15] as a simple modification of the Ising model for the purpose of studying conductivity in superionic conductors, e.g. in anorganic crystals like β-Al_2O_3), in glasses like AgI-Ag_2MoO_4) and in polymers like (polyethylene-oxide)-$NaBF_4$. Their main characteristic is a sudden drop of conductivity in several orders of magnitude at lower temperatures, which is considered as an example of a *nonequilibrium* phase transition.

As one of the simplest realization of driven lattice gases we may consider a system consisting of (classical) particles distributed on a cubic lattice in d dimensions conditioned to accommodate at most one particle per lattice site ($\sigma_{\vec{r}} = 0, 1$). Apart from this exclusion principle, particles interact via short-range interactions, so that the total energy of a system is equal to

$$\mathcal{H} = -4J \sum_{|\vec{r}-\vec{r}'|=1} \sigma_{\vec{r}}\sigma_{\vec{r}'}. \tag{1.5}$$

In addition, the system is subjected to an external electric field $\vec{E}$, in which particles behave as positively charged ions. In the context of superionic conductors, particles represent "liquid" phase of conducting ions which diffuse through the crystal lattice of static ions. Due to the Coulomb screening, the resulting interaction is modelled by the exclusion principle on very short distances and by the short-range interactions at distances of few lattice spacings.

In contact with thermal reservoir at temperature T and subjected to electric field $\vec{E}$, driven lattice gas evolves according to the following master equation

$$\frac{\partial P_E(\vec{\sigma}, t)}{\partial t} = \sum_{\vec{\sigma}^{\vec{r}\vec{r}'}} [c_E(\vec{\sigma}^{\vec{r}\vec{r}'}, \vec{r}, \vec{r}')P_E(\vec{\sigma}^{\vec{r}\vec{r}'}, t) - c_E(\vec{\sigma}, \vec{r}, \vec{r}')P_E(\vec{\sigma}, t)], \tag{1.6}$$

where state $\vec{\sigma}^{\vec{r}\vec{r}'}$ is obtained by exchanging particles or holes at sites $\vec{r}$ and $\vec{r}'$, $P_E(\vec{\sigma}, t)$ is probability to find the system in the state $\vec{\sigma}$ at time t and $c_E(\vec{\sigma}, \vec{r}, \vec{r}')$ is the transition rate from $\vec{\sigma}$ to $\vec{\sigma}^{\vec{r}\vec{r}'}$. The hopping of particles $\vec{r} \leftrightharpoons \vec{r}'$ is restricted to

nearest neighbours only, $|\vec{r}-\vec{r}'|=1$, provided that $\sigma_{\vec{r}}-\sigma_{\vec{r}'}\neq 0$. Transition rates $c_E(\vec{\sigma},\vec{r},\vec{r}')$ are defined as follows,

$$c_E(\vec{\sigma},\vec{r},\vec{r}')=\phi(\beta\Delta\mathcal{H}-\epsilon\beta E), \tag{1.7}$$

where $\Delta\mathcal{H}=\mathcal{H}(\vec{\sigma}^{\vec{r}\vec{r}'})-\mathcal{H}(\vec{\sigma})$ and $-\epsilon E$ is the work[5] required to move a particle to the adjacent site, ϵ being $-1, 0$ and 1 for particle hopping against the field $\vec{E}$, perpendicular to it and in the direction of the field, respectively. Function ϕ is chosen such that in the absence of an external field, $c_E(\vec{\sigma},\vec{r},\vec{r}')$ satisfies detail balance[6],

$$\phi(\beta\Delta\mathcal{H})=e^{-\beta\Delta\mathcal{H}}\phi(-\beta\Delta\mathcal{H}). \tag{1.8}$$

which ensures thermal equilibrium described by the Gibbs-Boltzmann distribution

$$P_{E=0}(\vec{\sigma})=\frac{1}{Z}e^{-\beta\mathcal{H}(\vec{\sigma})}. \tag{1.9}$$

In that case the usual ferromagnetic phase transition takes place at $\rho=1/2$ and T equal to 0, 2.27 J/k_B and 4.5 J/k_B in $1, 2$ and 3 dimensions, respectively.

If the external field is present, the system still exhibits continuous phase transition to the ordered phase (in $d>2$), but at the critical temperature that generally depends on it, $T_c(E)$. Compared to equilibrium phase transitions, the most surprising differences are[7]:

- long-ranged correlations in the paramagnetic phase ($T>T_c(E)$), $G(\vec{r})\sim|\vec{r}|^{-d}$, which seem to be a generic feature of *nonequilibrium* systems with conserved order parameter [44], and
- the fact that $T_c(E)$ increases with increasing E and saturates at $T_c(\infty)>T_c(0)$, contrary to the expectation that the stronger fields would break the correlations and decrease the critical temperature.

The above findings, among others, initiated interest for studying even simpler driven diffusive systems, possibly more prone to analytic calculations than the KLS model, whose studying was mainly restricted to Monte Carlo simulations and renormalization group calculations. One such example is the asymmetric simple exclusion process (ASEP), a special case of the KLS model in one dimension and without nearest-neighbour interactions ($J=0$).

ASEP was first introduced as a model for transport of ribosomes along the mRNA in 1968 [45, 46] and then in 1970 as a purely mathematical model of interacting particles [47]. In the context of driven diffusive systems, the exact steady

[5] We assume charge and lattice spacing equal to 1

[6] For example, the choice $\phi(x)=\min\{1,e^{-x}\}$ refers to Metropolis dynamics.

[7] For a more comprehensive review, see [1, 42, 43]

state of ASEP with open boundary conditions (i.e. in contact with left and right particle reservoirs of densities ρ_L and ρ_R, respectively) was found in 1993 [4, 5]. The exact solution aroused great interest in this model and several important results, relevant for the general theory of nonequilibrium steady states, followed. Using the exact solution, Derrida, Lebowitz and Speer have derived the probability distribution for an arbitrary coarse-grained fluctuation $\rho(x)$ in density profile,

$$P_L(\rho(x)) \sim exp[-L\mathcal{F}(\{\rho(x)\})], \tag{1.10}$$

where $\mathcal{F}(\{\rho(x)\})$ plays the role equivalent to the free energy in equilibrium. The expression for the functional $\mathcal{F}(\{\rho(x)\})$ is rather complex, so we shall point out here only its main features. First, as opposed to the equilibrium free energy ($\rho_L = \rho_R$), the functional $\mathcal{F}(\{\rho(x)\})$ is *non-local* function of $\rho(x)$. Second, $\mathcal{F}(\{\rho(x)\})$ is not necessarily convex function, depending on the boundary conditions. Third, fluctuations around the most probable density profile are not always Gaussian.

The expression for $\mathcal{F}(\{\rho(x)\})$ was later derived from the purely hydrodynamic theory of Bertini *et al.* [48], not invoking the knowledge of the exact steady state. Their theory covers all driven diffusive systems whose macroscopic behaviour follows the hydrodynamic equation

$$\frac{\partial \rho}{\partial t} = -\frac{\partial j}{\partial x}. \tag{1.11}$$

where $j(x,t)$ consists of diffusive term $-D\partial\rho/\partial x$ and linear response to the external field, $\sigma(\rho)E$,

$$j(x,t) = -D(\rho)\frac{\partial \rho}{\partial x} + \sigma(\rho)E. \tag{1.12}$$

(In chapter 2 it will be shown that for ASEP, $D(\rho) = const.$ and $\chi(\rho) = \rho(1-\rho)$). The *macroscopic theory of fluctuations* of Bertini *et al.*, besides spatial, deals with dynamical fluctuations as well, and therefore represents a generalization of the Onsager-Machlup theory [37], which gives the probability distribution of time-dependent fluctuations around the equilibrium state. Regarding the property of the microscopic reversibility, inherent to the Onsager-Machlup theory, the macroscopic theory of Bertini *et al.* clearly distinguishes the time evolution of spontaneous fluctuations from relaxation, which in the presence of dissipation are no longer time inverse of each other. In that sense ASEP, as a simple model in which these observations have been first grasped, has already justified its role as a window to the world of nonequilibrium phenomena.

2

Asymmetric simple exclusion process (ASEP)

ASEP is interesting to study for because it can be brought into connection with various models describing seemingly different phenomena including surface growth, protein biosynthesis and traffic. On the other hand, ASEP takes important place in nonequilibrium statistical physics as the exactly solvable model of nonequilibrium, boundary-induced phase transitions. From pedagogical reasons, we first present phase diagram of ASEP obtained in the mean-field approximation and then the exact stationary solution, which due to its complexity and applicability to various generalizations is somewhat of a theoretical achievement. Along with the exact stationary solution, we also give a phenomenological, domain-wall approach describing the first-order phase transition, which relies on the properties of the Burgers' equation obtained in the hydrodynamical limit. A second-order phase transition, characterized by the diverging length, is then analysed and its corresponding critical exponent is discussed. Finally, we discuss several possible generalizations which will later prove helpful in better understanding the robustness of phase transitions in ASEP.

2.1 Definition of the model

In ASEP, classical particles occupy discrete sites on an one-dimensional lattice under the exclusion principle, which forbids two particles to occupy the same site (τ_i being equal to 0 and 1 for an unoccupied and occupied site, respectively). Dynamics of ASEP can be defined in several ways depending on the problem. For example, in modelling traffic phenomena one usually deploys so-called *parallel* dynamics, in which all particles hop simultaneously in discrete time steps. In other problems more common is *random-sequential* dynamics, in which randomly chosen particles hop one at a time. In that case, the time evolution is described by the following master equation

$$\frac{d}{dt}P(C,t) = \sum_{C'} \left[W(C' \to C)P(C',t) - W(C \to C')P(C,t)\right], \tag{2.1}$$

where $P(C,t)$ is the probability distribution of finding a system in the state C at time t, C being completely determined by the occupancy of sites, $C = \{\tau_1, \tau_2, \dots\}$. In one dimension, the transition rates $W(C \to C')$ are given by

$$W(C \to C') = \begin{cases} p, & C = \{\dots, \tau_i = 1, \tau_{i+1} = 0, \dots,\}, \\ & C' = \{\dots, \tau_i = 0, \tau_{i+1} = 1, \dots,\}, \\ q = 1 - p, & C = \{\dots, \tau_i = 0, \tau_{i+1} = 1, \dots,\}, \\ & C' = \{\dots, \tau_i = 1, \tau_{i+1} = 0, \dots,\}, \\ 0, & other. \end{cases} \tag{2.2}$$

Depending on the choice of parameters p and q, we speak of the totally asymmetric process ($p = 1$, $q = 0$) in which particles hop only to the right, partially asymmetric process ($p \neq q \neq 0$) in which particles hop in both directions but with asymmetric rates and symmetric process ($p = q$) in which particles hop equally in both directions. Physical quantities of interest are local density $\langle \tau_i \rangle$ and current $j_i = \langle \tau_i(1 - \tau_{i+1}) \rangle$, where $\langle \dots \rangle$ designates averaging over probability distribution $P(C,t)$, $\langle \dots \rangle = \sum_C (\dots) P(C,t)$. Local density and current connects the following continuity equation,

$$\frac{d}{dt}\langle \tau_i \rangle = j_{i-1} - j_i, \tag{2.3}$$

from where it immediately follows that the steady state current is constant across the chain, $j_i \equiv j$. On a finite lattice of L sites, boundary conditions that are usually considered are either periodic ($\tau_1 = \tau_{L+1}$) or open (figure 2.1). The latter denote the exchange of particles with (infinite) reservoirs of constant densities, which are needed to be non-equal in order to achieve a nonequilibrium state.

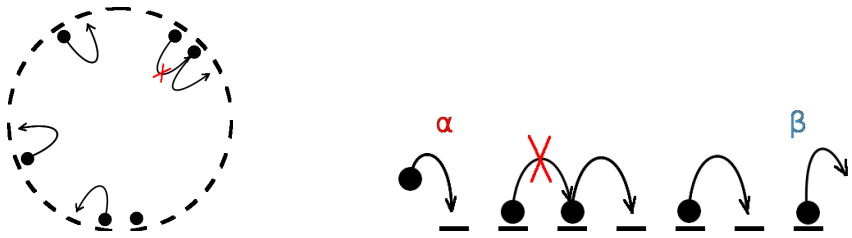

Figure 2.1: Schematic picture of ASEP with periodic (left figure) and open boundary conditions (right figure).

2.1.1 Periodic boundary conditions

The full, time-dependent solution of the above master equation has been found only recently using the Bethe *Ansatz* [49]. Here we are interested only in the stationary limit, in which it is rather easy to see that all probabilities become equal,

$$P(C) = \frac{1}{\binom{L}{N}}, \tag{2.4}$$

where $N = \rho L$ is the number of particles and ρ is the particle density. Accordingly, the density profile is constant across the chain and the correlation function is being factorized

$$\langle \tau_i \rangle = \frac{N}{L} = \rho, \quad \langle \tau_i \tau_j \rangle = \frac{(N-1)N}{(L-1)L} \approx \rho^2, \tag{2.5}$$

leading to the following expression for the current

$$j = \frac{N}{L}\frac{L-N}{L-1} = \rho(1-\rho) + O(L^{-1}). \tag{2.6}$$

From figure 2.2 we see that the current reaches maximum at density 1/2, which is a consequence of the exclusion principle. In physics community that deals with traffic, current-density relation is often called the *fundamental diagram*.

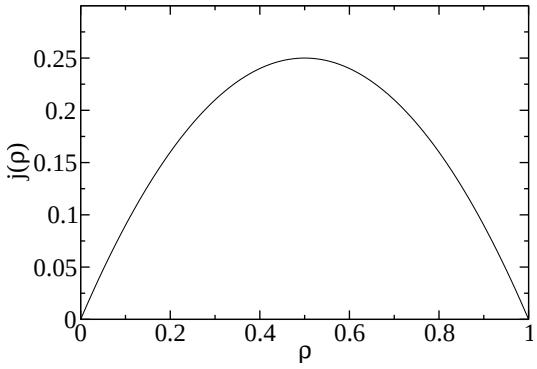

Figure 2.2: Current-density relation $j(\rho)$ in TASEP with periodic boundary conditions.

2.1.2 Open boundary conditions

In case of open boundary conditions, system exchanges particles at both ends in a way that particles enter and leave the chain with certain probability. For example, in the totally asymmetric case, particles enter chain at site $i = 1$ with the probability α provided the site $i = 1$t is empty. Similarly, particles leave

the chain from the site $i = L$ with the probability β, provided the site $i = L$ is occupied. In the master equation (2.1), the transition rates (2.2) should be supplemented with

$$W(C \to C') = \begin{cases} \alpha, & C = \{\tau_1 = 0, \dots\}, C' = \{\tau_1 = 1, \dots\}, \\ \beta, & C = \{\dots, \tau_L = 1\}, C' = \{\dots, \tau_L = 0\}, \\ 0, & other. \end{cases} \tag{2.7}$$

Since the current at boundaries equals $j = \alpha(1-\langle\tau_1\rangle) = \beta\langle\tau_L\rangle$, the boundaries may be interpreted as particle reservoirs held at fixed densities $\rho_L = \alpha$ and $\rho_R = 1-\beta$. For $\rho_L = \rho_R$, which corresponds to $\alpha = 1-\beta$, it is easy to show that the stationary state is similar to the one achieved in the case of periodic boundary conditions, in a sense that the density profile is constant and that the correlation function factorizes

$$\langle\tau_i\rangle = \alpha, \quad \langle\tau_i\tau_j\rangle = \alpha^2, \quad \alpha = 1-\beta. \tag{2.8}$$

A nontrivial behaviour, interesting for the occurrence of various phases, is expected for $\rho_L \neq \rho_R$. As we shall see in chapter 2.3, phase transitions that separate these phases have a lot in common with equilibrium phase transitions.

2.2 Connection to other models and applications

2.2.1 Surface growth

ASEP can be mapped to a discrete model of surface growth [66], in which surface is exposed to the beam of atoms followed by their absorption or desorption at surface "valleys" ($h_i - h_{i\pm1} = -1$) or "hills" ($h_i - h_{i\pm1} = 1$), respectively, where h_i is the surface height at site i. Mapping a surface configuration $\{h_i | i = 1, \dots, L\}$ to a particle configuration in ASEP $\{\tau_i | i = 1, \dots, L\}$ is done using the following relation

$$h_{i+1} - h_i = 1 - 2\tau_i, \tag{2.9}$$

meaning that moving particles to the right (or left) increases (or decreases) surface height by 2, $h_i \to h_i + 2$ ($h_i \to h_i - 2$), as depicted in figure 2.3. In this way a surface grows with an average speed $v = 2j$, where $j = (p-q)\rho(1-\rho)$ corresponds to the stationary current in ASEP,

$$\bar{h} = \frac{1}{L}\sum_{i=1}^{L} h_i \approx vt, \quad t \to \infty. \tag{2.10}$$

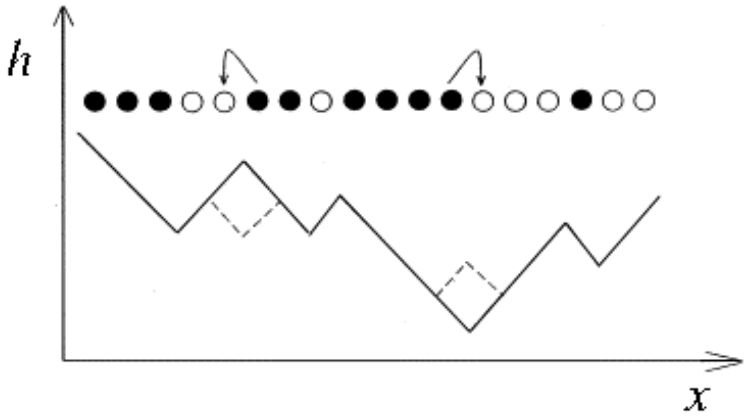

Figure 2.3: Mapping of ASEP to the model of surface growth by ballistic deposition. In ASEP, particle movements to the right or left correspond to increase or decrease in surface height, $h_i \to h_i + 2$ or $h_i \to h_i + 2$, respectively.

The surface is said to be rough in a sense that

$$\xi = \left[\frac{1}{L}\sum_{i=1}^{L}(h_i - \bar{h})^2\right]^{1/2} \propto L^{\chi}, \quad t \to \infty. \tag{2.11}$$

In the continuous limit in which $h_i \to h(x,t)$ [67], the symmetric case $p = q$ is described by the so-called Edwards-Wilkinson (EW) equation,

$$\frac{\partial}{\partial t}h(x,t) = \nu\nabla^2 h(x,t) + \eta(x,t). \tag{2.12}$$

In the asymmetric case $p \neq q$, the corresponding equation is the Kardar-Parisi-Zhang (KPZ) equation,

$$\frac{\partial}{\partial t}h(x,t) = \nu\nabla^2 h(x,t) + \frac{\lambda}{2}(\nabla h)^2 + \eta(x,t) \tag{2.13}$$

where $\eta(x,t)$ denotes the white noise having the following covariance

$$\langle \eta(x,t)\eta(x',t')\rangle = D\delta(x-x')\delta(t-t'). \tag{2.14}$$

Characteristic length ξ of surface roughness is found to satisfy the following scaling relation,

$$\xi(\bar{h}, L) = L^{\chi} f(\bar{h}L^{-z}), \tag{2.15}$$

where $f(x) \approx$ const. for $x \to \infty$ and $f(x) \propto x^{\chi/z}$ for $x \to 0$. In other words, ξ grows as $\xi \propto \bar{h}^{\chi/z}$ for finite time t and then saturates to $\xi \propto L^{\chi}$ when $t \to \infty$. Due to EW equation being linear, it is rather easy to show that $\chi = 1/2$ and $z = 2$, the corresponding task being less trivial for the KPZ equation, for which the values

$\chi = 1/2$ and $z = 3/2$ have been obtained using the methods of renormalization group [68].

2.2.2 Quantum spin chains

A formal similarity between stochastic and quantum system resides in the fact that both master and Schrödinger equation are linear in time. In order to write down the master equation in the quantum language, let us start from its general form,

$$\frac{d}{dt}P(C,t) = \sum_{C'} \left[W(C' \to C)P(C',t) - W(C \to C')P(C,t)\right], \tag{2.16}$$

and let us assign to each configuration C a ket vector $|C\rangle$. If we define vector $|P(t)\rangle \equiv \sum_C P(C,t)|C\rangle$, the master equation becomes the equation for $|P(t)\rangle$,

$$\frac{\partial}{\partial t}|P(t)\rangle = -H|P(t)\rangle, \tag{2.17}$$

where H is the "Hamiltonian" defined by its matrix elements

$$\langle C|H|C'\rangle = \begin{cases} -W(C' \to C) & C \neq C' \\ \sum_{C'' \neq C} W(C \to C'') & C = C'. \end{cases} \tag{2.18}$$

From here two immediate properties of the "Hamiltonian" H follow. By introducing vector $\langle S| \equiv \sum_C \langle C|$, the first property follows from the normalization of the probability distribution $\sum_C P(C,t) = 1$,

$$\langle S|P(t)\rangle = \sum_C P(C,t) = 1 \quad \forall t, \tag{2.19}$$

which further leads to

$$\langle S|H = 0. \tag{2.20}$$

The second property is related to the stationary state (if it exists), which corresponds to the ground state of the "Hamiltonian",

$$\frac{d}{dt}|P(t)\rangle = 0 \quad \Rightarrow \quad H|P^*\rangle = 0. \tag{2.21}$$

The similarity with the quantum formalism can be pushed even further, as follows. The observable F can be defined as the diagonal matrix $F(t) = \sum_C F(C)|C\rangle\langle C|$, which gives $\langle F(t)\rangle = \sum_C F(C)P(C,t) = \langle S|F|P(t)\rangle$. Using the identity operator written in the "energy" basis, $\hat{1} = \sum_\epsilon |\epsilon\rangle\langle\epsilon|$, the expectation value of the observable $F(t)$ can be written as

$$\langle F(t)\rangle_{P_0} = \sum_{\epsilon} \langle S|F|\epsilon\rangle\langle\epsilon|P_0\rangle e^{-\epsilon t}, \tag{2.22}$$

where $|P_0\rangle$ designates an initial state. In the long-time limit, we expect the above sum to be dominated by the first excited state (of energy ϵ_1), which leads to

$$\langle F(t)\rangle_{P_0} \to \langle F\rangle^* + \langle S|F\epsilon_1\rangle\langle\epsilon_1|P_0\rangle e^{-\epsilon_1 t}, \quad t \to \infty \tag{2.23}$$

where $\langle F\rangle^*$ is the expectation value of the observable F in the stationary state. This correspondence thus enables us to calculate the characteristic time scale τ, which determines the relaxation of the stochastic system to its stationary state, from the spectrum of the corresponding quantum system, $\tau \sim 1/|\mathrm{Re}(\epsilon_1)|$.

The reason we quoted the word "Hamiltonian" is because the real quantum Hamiltonian is always Hermitian and consequently, its eigenvalues are all real and positive. In stochastic systems, that is the case only if detailed balance holds [1],

$$P^*(C)W(C \to C') = P^*(C')W(C' \to C), \tag{2.24}$$

while otherwise, the "Hamiltonian" is *non-Hermitian.*

In ASEP, a configuration C is given by the occupation numbers $C = \{\tau_1, \ldots, \tau_L\}$, which gives $|C\rangle$ equal to

$$|C\rangle = |\tau_1 \ldots \tau_L\rangle \equiv |\tau_i\rangle \otimes \cdots \otimes |\tau_L\rangle. \tag{2.25}$$

Since we are dealing with only two states per site, it is natural to use the Pauli matrices,

$$\sigma^x = \begin{pmatrix} 0 & 1 \\ 1 & 0 \end{pmatrix}, \qquad \sigma^y = \begin{pmatrix} 0 & -i \\ i & 0 \end{pmatrix}, \qquad \sigma^z = \begin{pmatrix} 1 & 0 \\ 0 & -1 \end{pmatrix}, \tag{2.26}$$

from which one constructs operators $s^{\pm}$ and n,

$$s^+ = \begin{pmatrix} 0 & 1 \\ 0 & 0 \end{pmatrix}, \qquad s^- = \begin{pmatrix} 0 & 0 \\ 1 & 0 \end{pmatrix}, \qquad n = \begin{pmatrix} 0 & 0 \\ 0 & 1 \end{pmatrix}, \tag{2.27}$$

such that

$$s^+|0\rangle = 0, \quad s^+|1\rangle = |0\rangle \tag{2.28}$$

$$s^-|0\rangle = |1\rangle, \quad s^-|1\rangle = 0 \tag{2.29}$$

$$n|0\rangle = 0, \quad n|1\rangle = |1\rangle. \tag{2.30}$$

Let us recall the transition rates in ASEP, which correspond to particles moving either to the right or to the left,

[1] The proof is elementary; for further reading see [2].

$$1_i 0_{i+1} \xrightarrow{p} 0_i 1_{i+1}, \tag{2.31}$$

$$0_i 1_{i+1} \xrightarrow{q} 1_i 0_{i+1}. \tag{2.32}$$

Expressed in terms of operators $s^{\pm}$, the above processes lead to the non-diagonal elements in H of the form $-ps_i^- s_{i+1}^+$ and $-qs_i^+ s_{i+1}^-$. The diagonal elements are then easily obtained if we recognize that

$$\langle S|s_i^+ = \langle S|n_i \quad \text{i} \quad \langle S|s_i^- = \langle S|(1-n_i). \tag{2.33}$$

In order to satisfy the condition $\langle S|H = 0$, each non-diagonal term has to be supplemented with a similar diagonal one, but in which s_i^- and s_i^+ are replaced with n_i and $1-n_i$, respectively. In the end, this reduces to

$$H_{\text{ASEP}} = \sum_{i=1}^{L} [pn_i(1-n_{i+1}) + q(1-n_i)n_{i+1} - ps_i^- s_{i+1}^+ - qs_i^+ s_{i+1}^-]. \tag{2.34}$$

From the expression above, the Hamiltonian of the Heisenberg XXZ quantum is obtained using the similarity transformation $H \to BH_{\text{ASEP}}B^{-1}$[2] [2],

$$H_{XXZ} = -J \sum_i [\sigma_i^x \sigma_{i+1}^x + \sigma_i^y \sigma_{i+1}^y + \Delta(\sigma_i^z \sigma_{i+1}^z - 1)], \tag{2.35}$$

where

$$J = \frac{\sqrt{pq}}{2}, \quad \Delta = \frac{\sqrt{p/q} + \sqrt{q/p}}{2} \quad \text{i} \quad B = e^{\ln(p/q)\sum_i i\sigma_i^z}. \tag{2.36}$$

Spectrum of the above Hamiltonian can be then determined using the Bethe *Ansatz*. In the case of periodic boundary conditions, the first excited state has the following complex "energy" ϵ_1 [50],

$$\epsilon_1 = -2\sqrt{\rho(1-\rho)}\frac{6.509189...}{L^{3/2}} + \pm\frac{2i\pi(2\rho-1)}{L}. \tag{2.37}$$

In the expression above, the real part corresponds to the relaxation towards the stationary state and leads to the dynamical exponent $z = 3/2$, while the imaginary part corresponds to the oscillatory behaviour originating from kinematic waves travelling with the group velocity $v_g = 1 - 2\rho$. Similar result may be obtained also in the case of open boundary conditions, see [51, 52]. In the low- and in the high-density phases, the resulting ϵ_1 is constant leading to the exponential relaxation. On the other hand, on the coexistence line $\alpha = \beta < 1/2$ and in the

[2]Depending on the boundary conditions, some non-Hermitian terms may appear as well

maximum-current phase one finds gap that vanishes as $\epsilon_1 \propto L^{-2}$ and $\epsilon_1 \propto L^{-3/2}$, respectively.

2.2.3 Zero-range process

Another example of a driven diffusive system is the zero-range process (ZRP), which differs from ASEP in that particles are not restricted by the exclusion principle ($n_i = 0, 1, 2, \dots$) and propagate at rate $u(n_i)$ which depends on the number of particles at a given site. ZRP is interesting for condensation appearing in the stationary state (for a review see [53] and references therein), in a sense that the macroscopic number of particles ($\propto N$) condensates on a single site provided $u(i)$ decays slower than

$$u(i) \simeq \beta \left(1 + \frac{2}{i}\right), \quad i \gg 1. \tag{2.38}$$

Real systems that can be modelled by ZRP include shaken granular gases (e.g. grains of sand or plastic balls) and traffic jams. The experiment described in [54] has shown that shaken granular gas of particles distributed over L connected compartments condenses eventually in a single compartment (figure 2.4). Traffic phenomena is related to ZRP using the connection between TASEP and ZRP, which maps sites and particles in ZRP to particles and holes in TASEP, respectively (figure 2.5). Condensation in ZRP then corresponds to the macroscopic depletion of particles in front of a single particles, i.e. to a macroscopic queue behind it.

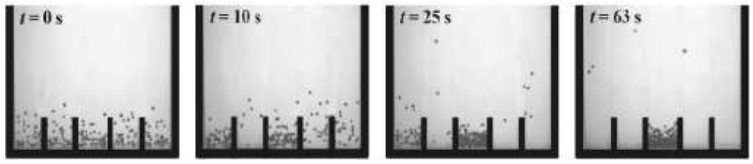

Figure 2.4: Time evolution of a granular gas vertically shaken with amplitude $a = 1$ mm and frequency $f = 21$ Hz. Picture is taken from [54].

2.2.4 Traffic phenomena

Figure 2.6(a) depicts trajectories of cars photographed from air, each line designating trajectory of a single car. It is interesting to notice the so-called "phantom" traffic jam moving in the *opposite* direction with respect to the cars. The term "phantom" relates to the fact that slowing down is not caused by an external perturbation (e.g. road works, car accidents, etc.) but rather emerges spontaneously (caused e.g. by the overreaction of a driver) and propagates to other

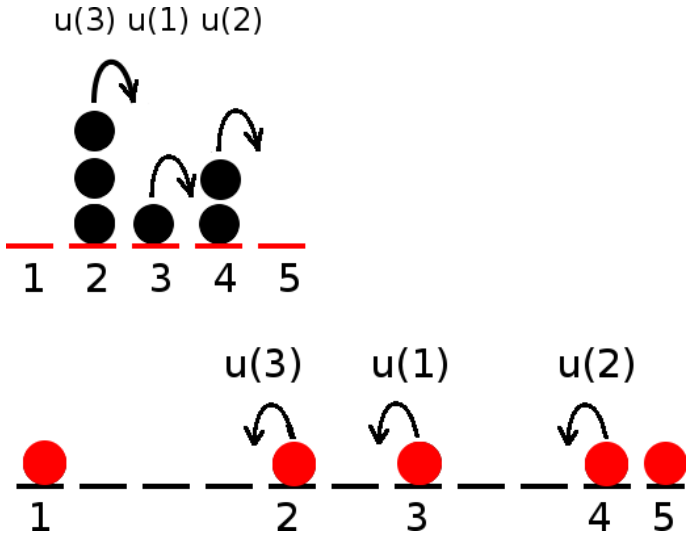

Figure 2.5: Mapping of ZRP to TASEP. Sites in ZRP (denoted by numbers) correspond to particles in TASEP, while a number of particles at site $i = 1, \ldots, L$ in ZRP corresponds to a number of holes in front of i-th particle in TASEP.

cars. Whether a "phantom" traffic jam will appear or not depends on the particular form of the fundamental diagram. An example of the fundamental diagram obtained experimentally in real traffic is shown in figure 2.6(b), consisting of free-flow regime, where current grows linearly with density and congested-flow regime, where current decreases with increasing density.

Fundamental diagram in figure 2.6(a) reminds us of the current-density relation in TASEP, as depicted in figure 2.2. Indeed, TASEP with parallel dynamics can be mapped to the so-called Nagel-Schreckenberg (NG) model of traffic [55] in the limit $v_{\max} = 1$. NG model is an one-dimensional lattice model subjected to either periodic or open boundary conditions, in which each car has been assigned a discrete value of speed, $v_i = 0, 1, \ldots, v_{\max}$. The cars move simultaneously in discrete time steps according to the following rules:

1. **acceleration**: if $v_i < v_{\max}$, then $v_i \to v_i + 1$
2. **slowing down**: if distance $d_i = x_{i+1} - x_i$ to the car in front is less than v_i, then $v_i \to d_i - 1$
3. **randomization**: $v_i \to v_i - 1$ with probability p
4. **car motion**: i-th car moves v_i sites forward

NG model is a minimal model of traffic in a sense that all four rules are needed to capture the essence of real traffic. First rule designates the driver's intention to achieve the maximum (allowed) speed. The second rule ensures that drivers adjust

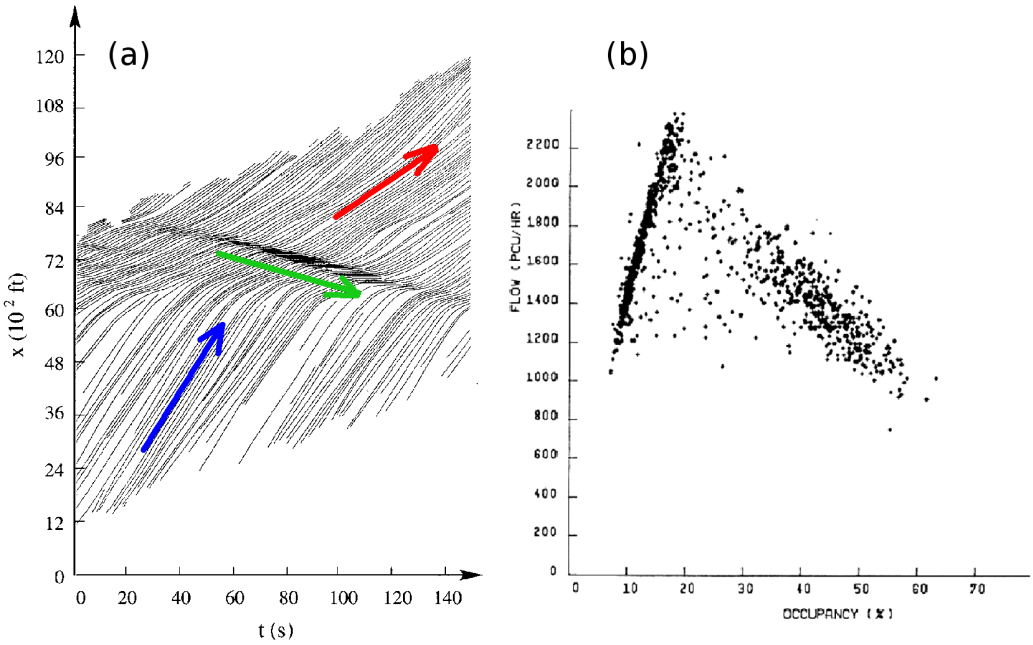

Figure 2.6: (a) Trajectories of cars photographed from air and their corresponding velocity vectors (denoted by red and blue arrows); notice a "phantom" traffic jam travelling backwards, its velocity vector being denoted by green arrow. (b) Fundamental diagram of real traffic, taken from [55].

their speed in order to avoid crashing in other cars. Third rule is a simplified way of capturing individual characteristics of each driver (e.g. overreaction leading to slowing down) and is essential to the formation of "phantom" traffic jams. NS model later experienced various generalizations more relevant to real traffic (for a recent review see [56] and [18]).

From a practical point of view, traffic modelling is important for better understanding and, finally, avoiding the congested phase. It is interesting to note that this field of research also gave the first experimental observation of the first-order boundary-induced phase transition, observed on the streets of Köln in Germany [57].

2.2.5 Protein biosynthesis

Protein biosynthesis is one of the most important processes within cell in which a genetic code encoded in DNA is translated into proteins involved in various regulatory tasks. The process begins with transcription creating messenger RNA from DNA with the help of RNA polymerase (figure 2.7).

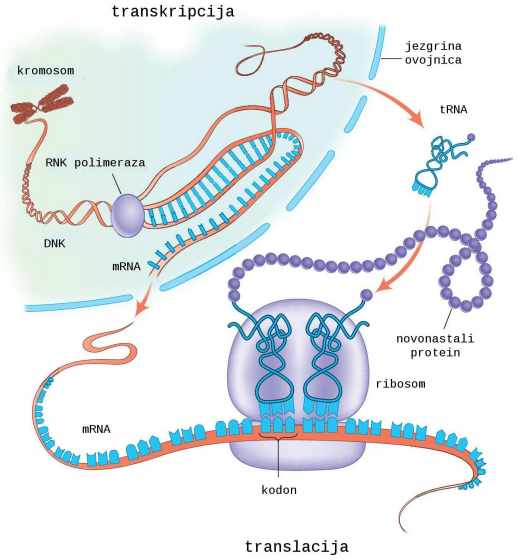

Figure 2.7: Schematic picture of protein biosynthesis consisting of transcription (mRNA assembly from DNA) in cell nucleus and translation (ribosome motion along mRNA) in cytoplasm. Picture is taken from [58].

The mRNA then diffuses through the cell membrane into cytoplasm, where translation begins by binding ribosomes to mRNA. Ribosomes move along the mRNA looking for a start codon. When it is found, a transfer RNA (tRNA) attaches to it using its anticodon, a nucleotide triplet complementary to the mRNA triplet at the binding site of mRNA and ribosome. tRNA carries an amino acid which is then released and added to the polypeptide chain . Ribosome moves one codon further repeating the process until it reads the stop codon which terminates the translation and releases the newly created protein from the ribosome.

The idea of MacDonald *et al.* [45] was to model the process of translation using TASEP with open boundary conditions, left and right reservoirs being stop and start codons, respectively, and particles being ribosomes. TASEP has been later generalized to the so-called l-TASEP [46], in which each particle occupies l sites ($l \approx 12$), reflecting the fact that ribosomes bind to more than one codon at a time. Further improvement consists in taking into account spatial inhomogeneities in hopping rates, since codons with lower concentrations of corresponding tRNA locally suppress ribosome motion across them, acting as if they are defects in TASEP. Even in TASEP with periodic boundary conditions, already a single defect site drastically changes the stationary state [59]. In the case of open boundary conditions, TASEP with one or more defects has been considered in the context of protein biosynthesis by several authors [60–62, 64]. A general conclusion is that the current and therefore the rate of protein synthesis strongly depend on defect positions within the chain.

2.3 Boundary-induced phase transitions

2.3.1 Phase diagram in the mean-field approximation

Let us return now to TASEP with open boundary conditions. Inserting expression for the current in the continuity equation (2.3), we arrive at the following equation

$$\frac{d}{dt}\langle\tau_i\rangle = \langle\tau_{i-1}(1-\tau_i)\rangle - \langle\tau_i(1-\tau_{i+1})\rangle. \tag{2.39}$$

The problem with the above equation is that it contains unknown terms $\langle\tau_{i-1}\tau_i\rangle$ and $\langle\tau_i\tau_{i+1}\rangle$, bearing resemblance with Bogoliubov-Born-Green-Kirkwood-Yvon (BBGKY) hierarchy. The usual approximation used to bypass this problem is the so-called mean-field approximation, which approximates $\langle\tau_i\tau_{i+1}\rangle \approx \langle\tau_i\rangle\langle\tau_{i+1}\rangle$. If we denote $\langle\tau_i\rangle$ with ρ_i in the mean-field approximation, we arrive at the following recursion in the stationary limit $d\rho_i/dt = 0$

$$\rho_{i+1} = 1 - \frac{C}{\rho_i}, \quad i = 1, \ldots, L-1 \tag{2.40}$$

where $C = \alpha(1-\rho_1) = \beta\rho_L$ corresponds to the stationary current. The upper recursion can be solved [3] by recognizing that the r.h.s of (2.40) is a homographic function [3] of the form $f(x) = (x-C)/x$. This means that from the solution of the quadratic equation $f(x) = x$,

$$\rho_\pm = \frac{1 \pm \sqrt{1-4C}}{2}, \quad 1-4C > 0 \tag{2.41}$$

a series $\{b_i\}$ can be constructed with b_i depending on whether the quadratic equation (2.41) has one or two real solutions, $b_i = \rho_i - 1/2$ in the first case and $b_i = (\rho_i - \rho_-)/(\rho_i - \rho_+)$ in the second case, respectively. Inserting recursion (2.40) in the expression for b_i, it is easy to show that the series $\{b_i\}$ is arithmetic in the first case and geometric in the second case, the fact that eases further calculation. The final expression for ρ_i is given by

$$\rho_i = \frac{-\rho_+\rho_-(\rho_+^{i-1} - \rho_-^{i-1}) + (\rho_+^i - \rho_-^i)\rho_1}{-\rho_+\rho_-(\rho_+^{i-2} - \rho_-^{i-2}) + (\rho_+^{i-1} - \rho_-^{i-1})\rho_1}. \tag{2.42}$$

where $\rho_1 = 1 - C/\alpha$ and the current C is the solution of the implicit equation $\rho_L = C/\beta$. Depending on the parameters α and β, four different types of solution are possible, as displayed below.

[3] A special form of the rational function

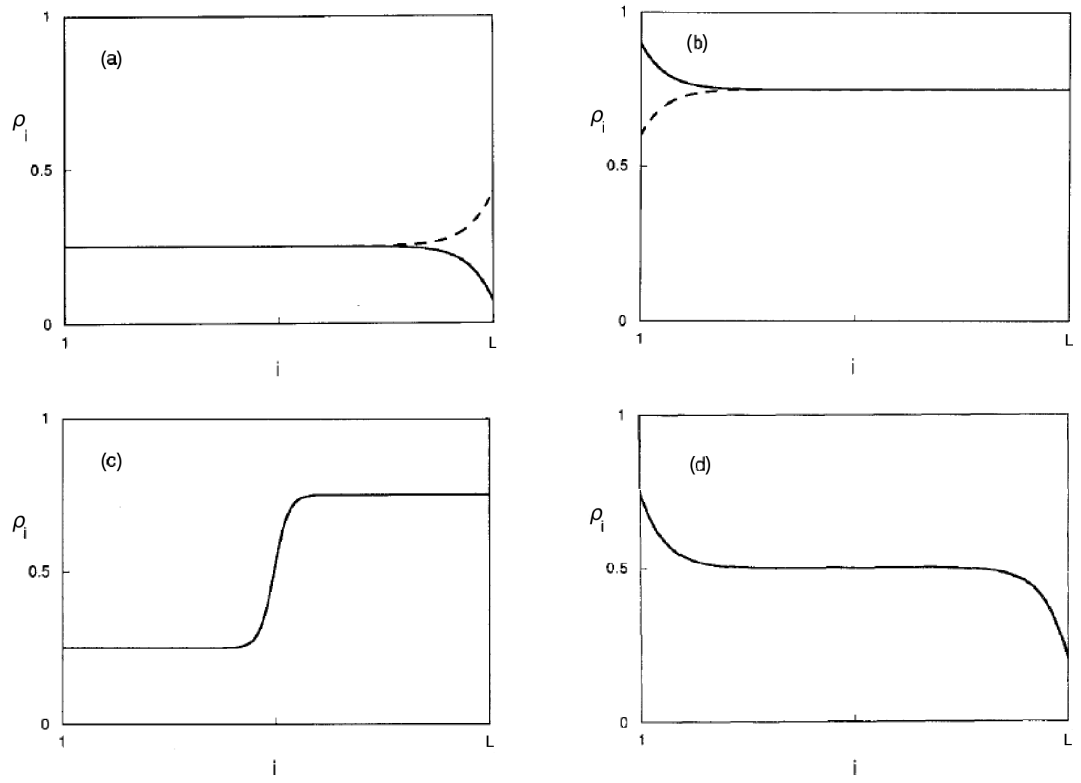

Figure 2.8: Density profiles in TASEP obtained by the mean-field approximation (a) in the low-density phase A ($\alpha \leq 1/2$, $\beta > \alpha$), (b) in the high-density phase B ($\beta \leq 1/2$, $\beta < \alpha$), (c) on the coexistence line between phases A and B ($\alpha = \beta < 1/2$) and (d) in the maximum-current phase C ($\alpha > 1/2$, $\beta > 1/2$).

The low-density phase (A). In this phase $\rho_1 = \rho_- + 0^{\pm}$, which gives stationary current $C = \alpha(1-\alpha)$. By iterating the recursion one arrives at the nearly constant profile $\rho_i \approx \alpha$ (figure 2.8a), except close to $i = L$, where $\rho_L = \alpha(1-\alpha)/\beta < \rho_+$. Such values of ρ_1 and ρ_L correspond to the following α and β,

$$\alpha \leq 1/2, \qquad \beta > \alpha. \tag{2.43}$$

The high-density phase (B). In this phase $\rho_L = \rho_+ + 0^{\pm}$, which gives stationary current $C = \beta(1-\beta)$ i $\rho_L = 1-\beta$. By iterating the recursion one arrives at the nearly constant profile $\rho_i \approx 1-\beta$ (figure 2.8b), except close to $i = 1$, where $\rho_1 = 1-\beta(1-\beta)/\alpha < \rho_+$. Such values of ρ_1 and ρ_L correspond to the following α and β,

$$\beta \leq 1/2, \qquad \beta < \alpha. \tag{2.44}$$

Note that phases A and B are related by the combination of particle-hole ($\tau_i \leftrightarrow 1-\tau_i$) and mirror symmetry ($i \leftrightarrow L-i+1$ and $\alpha \leftrightarrow \beta$)

$$\langle\tau_i\rangle(\alpha,\beta) = 1 - \langle\tau_{L-i+1}\rangle(\beta,\alpha). \tag{2.45}$$

The coexistence line $\alpha = \beta < 1/2$**.** On the line separating phases A and B, the recursion begins with ρ_1 infinitesimally below ρ_- and ends at ρ_L infinitesimally above ρ_+, which gives $C = \alpha(1-\alpha)$. The density profile has the shape of a domain wall (figure 2.8c), which happens for,

$$\alpha = \beta < 1/2. \tag{2.46}$$

The maximum-current phase (C). Finally, when $\rho_1 > 1/2$ and $\rho_L < 1/2$, the current attains the maximum possible value, $C = 1/4$, for

$$\alpha > 1/2, \qquad \beta > 1/2, \tag{2.47}$$

In the bulk, the density attains the value 1/2 (figure 2.8d), while the deviations near the boundaries follow the power law with the exponent 1. Near the left boundary, density profile takes the form

$$\rho_i - \frac{1}{2} \sim \frac{1}{2i}. \tag{2.48}$$

A similar behaviour is found near the right boundary using the mentioned symmetry (2.45).

To summarize, we display the phase diagram obtained in the mean-field approximation in figure 2.9. As the exact stationary state will reveal below, the mean-field approximation yields correct phase diagram containing all phases, but the density profiles turn out to be incorrect, especially on the coexistence line and in the maximum-current phase.

2.3.2 Exact solution

The exact stationary state of TASEP with open boundary conditions was first given by Derrida, Domany and Mukamel in 1992 [3], by recognizing that the unnormalized solution $f_L(\tau_1,\ldots,\tau_L)$ to the stationary master equation (2.1) is related to $f_{L-1}(\tau_1,\ldots,\tau_{L-1})$ using the following construction. Given a configuration $C = \{\tau_i | i = 1,\ldots,L\}$, for each pair of neighbouring sites with occupation numbers $\tau_i = 1$ and $\tau_{i+1} = 0$ it holds that

$$\begin{aligned} f_L(\tau_1,\ldots,\tau_{i-1},1,0,\tau_{i+2},\ldots,\tau_L) &= f_{L-1}(\tau_1,\ldots,\tau_{i-1},1,\tau_{i+2},\ldots,\tau_L) + \\ &+ f_{L-1}(\tau_1,\ldots,\tau_{i-1},0,\tau_{i+2},\ldots,\tau_L). \end{aligned} \tag{2.49}$$

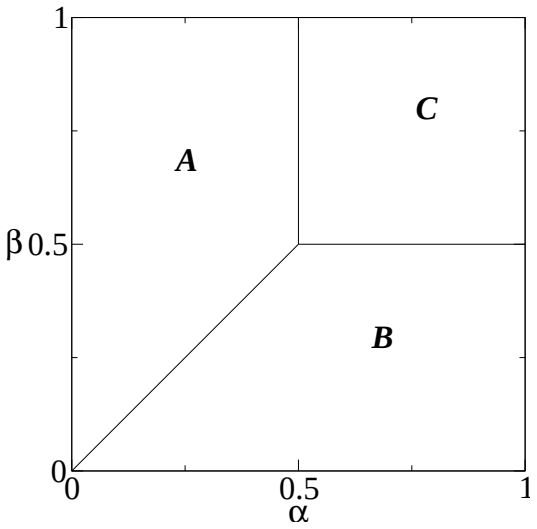

Figure 2.9: Phase diagram of TASEP obtained by the mean-field approximation and consisting of the low-density phase (A), the high-density phase (B) and the maximum-current phase (C).

Additionally, the following relations hold at boundaries when $\tau_1 = 0$ or $\tau_L = 1$,

$$f_L(0, \tau_2, \ldots, \tau_L) = \frac{1}{\alpha} f_{L-1}(\tau_2, \ldots, \tau_L) \tag{2.50}$$

$$f_L(\tau_1, \ldots, \tau_{L-1}, 1) = \frac{1}{\beta} f_{L-1}(\tau_1, \ldots, \tau_{L-1}). \tag{2.51}$$

Starting from the solution of the master equation for system size $L = 1$, $f_1(0) = 1/\alpha$ and $f_L(1) = 1/\beta$, the above recursion relations are sufficient to determine weights $f_L(\tau_1, \ldots, \tau_L)$ e.g. using computer, but the real trouble is, of course, to find the analytical expression for general L. This was accomplished first by Derrida, Domany and Mukamel for $\alpha = \beta = 1$ and later that year for general α and β by Schütz and Domany [4]. Due to the fact that the mentioned solutions are rather exhaustive, here we display a more compact solution by Derrida, Evans, Hakim and Pasquier from 1993 [5] obtained using the matrix-product *Ansatz* (MPA).

The idea behind the recursions (2.49) and (2.51) is to write the weights $f_L(\tau_1, \ldots, \tau_L)$ as a product of matrices D or E and vectors $\langle W|$ and $|V\rangle$,

$$f_L(\tau_1, \ldots, \tau_L) = \langle W| \prod_{i=1}^{L} [\tau_i D + (1 - \tau_i) E] |V\rangle, \tag{2.52}$$

which reduces (2.49) and (2.51) to matrix equations for D, E, $\langle W|$ i $|V\rangle$,

$$DE = D + E \tag{2.53}$$

$$\langle W|E = \frac{1}{\alpha} \langle W| \tag{2.54}$$

$$D|V\rangle = \frac{1}{\beta}|V\rangle. \tag{2.55}$$

System of equations (2.53)-(2.55) is often referred to as DEHP algebra, named after its authors (Derrida, Evans, Hakim and Pasquier). The matrices D and E are generally infinite unless $\alpha + \beta = 1$ [5], in which case they are one-dimensional (i.e. scalars). There are many different choices (representations) for matrices D and E and vectors $\langle W|$ and $|V\rangle$, for example

$$D = \begin{pmatrix} 1 & 1 & 0 & 0 & \cdots \\ 0 & 1 & 1 & 0 & \\ 0 & 0 & 1 & 1 & \\ 0 & 0 & 0 & 1 & \\ \vdots & & & & \ddots \end{pmatrix}, \qquad E = \begin{pmatrix} 1 & 0 & 0 & 0 & \cdots \\ 1 & 1 & 0 & 0 & \\ 0 & 1 & 1 & 0 & \\ 0 & 0 & 1 & 1 & \\ \vdots & & & & \ddots \end{pmatrix}, \tag{2.56}$$

$$\langle W| = \kappa \left(1, \left(\frac{1-\alpha}{\alpha}\right), \left(\frac{1-\alpha}{\alpha}\right)^2, \ldots, \right), \quad |V\rangle = \kappa \begin{pmatrix} 1 \\ \left(\frac{1-\beta}{\beta}\right) \\ \left(\frac{1-\beta}{\beta}\right)^2 \\ \vdots \end{pmatrix}, \tag{2.57}$$

where the value of $\kappa = \sqrt{(\alpha+\beta-1)/\alpha\beta}$ is taken in order to satisfy the condition $\langle W|V\rangle = 1$.

Once the matrices D and E and the vectors $\langle W|$ and $|V\rangle$ are known, it is easy to show that the normalization constant $Z_L = \sum_{\{\tau_i\}} f_L(\{\tau_i\})$ is equal to $\langle W|C^L|V\rangle$, where $C = D + E$. The average local density $\langle \tau_i \rangle_L$ and the current $j_L = \langle \tau_i(1-\tau_i)\rangle$ are then given by the following expressions, respectively,

$$\langle \tau_i \rangle = \frac{\langle W|C^{i-1}DC^{L-i}|V\rangle}{\langle W|C^L|V\rangle}, \tag{2.58}$$

$$j = \frac{Z_{L-1}}{Z_L}. \tag{2.59}$$

If we calculate the density profile and the current from here using the properties of DEHP algebra (2.53)-(2.55) [5], we arrive at the same phase diagram as the one obtained in the mean-field approximation. There are, however, two exceptions. The first is found on the coexistence line $\alpha = \beta < 1/2$, where the following linear profile replaces the sharp domain wall

$$\langle \tau_{Lx} \rangle_L \simeq \alpha + x(1-2\alpha), \quad 0 < x < 1, \quad \alpha = \beta < 1/2. \tag{2.60}$$

The second exception is found near the boundaries. Depending on the value of β, one distinguishes three possible cases in the low-density phase, where density approaches its bulk value α exponentially,

$$\langle \tau_{L-i} \rangle_L = \alpha + \begin{cases} \left(\frac{\alpha(1-\alpha)}{\beta(1-\beta)}\right)^{i+1}(1-2\beta) & \beta < 1/2 \\ \frac{[4\alpha(1-\alpha)]^{i+1}}{2\sqrt{\pi} i^{1/2}} & \beta = 1/2 \\ \frac{[4\alpha(1-\alpha)]^{i+1}}{\sqrt{\pi} i^{3/2}} \frac{(\alpha-\beta)(1-\alpha-\beta)}{(1-2\alpha)^2(1-2\beta)^2} & \beta > 1/2. \end{cases} \tag{2.61}$$

A closer look at the expressions in (2.61) reveals two characteristic lengths,

$$\xi_\alpha^{-1} = -\ln[4\alpha(1-\alpha)] \quad \text{i} \tag{2.62}$$

$$\xi_\beta^{-1} = -\ln[4\beta(1-\beta)]. \tag{2.63}$$

A deviation from the bulk value near the left boundary is determined by characteristic lengths $1/\xi = |1/\xi_\alpha - 1/\xi_\beta|$ and $\xi = \xi_\alpha$ for $\alpha < \beta < 1/2$ and $\beta \geq 1/2$, where in the latter case we used the fact that $\xi_\beta \to \infty$. The fact that ξ_β diverges reflects in the density decaying with a power law away from the boundary, where the corresponding exponents of power-law decay equal $1/2$ for $\beta = 1/2$ and $3/2$ for $\beta > 1/2$. As we see, the exact solution reveals two different shapes of density profile within the phase A, one being a purely exponential decay (phase AI), the other being a product of the exponential and the power-law decay (phase AII). Similar expressions and conclusions are obtained in the high-density phase as well by exploiting the mentioned symmetry (2.45).

Finally, the deviation from the bulk density $1/2$ in the maximum-current phase follows a power-law, but the corresponding exponent is $1/2$ rather than the mean-field value 1. Close to the left boundary, density profile is given by

$$\langle \tau_i \rangle_L \simeq \frac{1}{2} + \frac{1}{2\sqrt{\pi} i^{1/2}} + \mathrm{O}(i^{-3/2}), \tag{2.64}$$

and similar behaviour is found close to the right boundary as well by exploiting the symmetry (2.45). The exact phase diagram is depicted in 2.10.

The fact that the mean-field approximation fails to give the correct density profile on the coexistence line ($\alpha = \beta < 1/2$), as well as in the maximum-current phase (C), is not unexpected. Our experience of equilibrium teaches us that phase transitions are precisely the situations in which the mean-field approximation usually fails, since then fluctuations become important. Below we shall show that phases A and B are separated by the transition that may be characterized as a first-order one due to discontinuity present in the first derivative of current with respect to α. Similarly, the transition from phases A or B to phase C, having discontinuity in the second derivative of current, is being characterized as a second-order one. Similarity with the equilibrium phase transitions increases further with the fact that the first-order transition is accompanied by a phase coexistence, while the second-order transition is accompanied by the diverging length ξ.

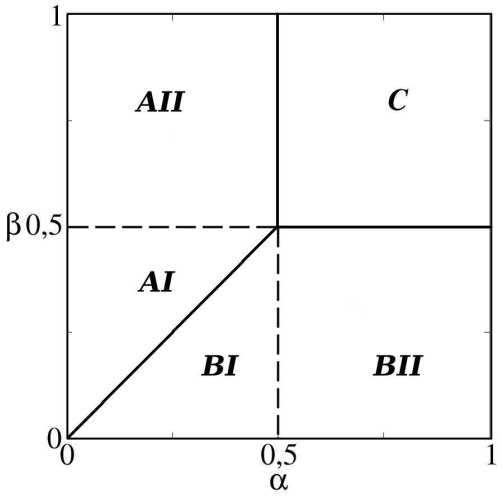

Figure 2.10: The exact phase diagram of TASEP consisting of the low-density phase (AI and AII), the high-density phase (BI and BII) and the maximum-current phase (C).

2.3.3 First-order phase transition and the domain-wall dynamics

Let us recall the expression for current in phases A, B and C,

$$j(\alpha,\beta) = \begin{cases} \alpha(1-\alpha), & \alpha < 1/2, \alpha \leq \beta \quad \text{(phase A)} \\ \beta(1-\beta), & \beta < 1/2, \beta \leq \alpha \quad \text{(phase B)} \\ 1/4 & \alpha \geq 1/2, \beta \geq 1/2 \quad \text{(phase C)}. \end{cases} \tag{2.65}$$

From the above expression it is straightforward to notice that for fixed $\beta < 1/2$, the first derivative of current with respect to α has a discontinuity at $\alpha = \beta < 1/2$,

$$\lim_{\alpha \to \beta^+} \frac{\partial J(\alpha,\beta)}{\partial \alpha} = 0 \tag{2.66}$$

$$\lim_{\alpha \to \beta^-} \frac{\partial J(\alpha,\beta)}{\partial \alpha} = 1 - 2\beta, \tag{2.67}$$

which, inspired by the equilibrium phase transitions, allows us to speak of the first-order phase transition. On the other hand, a first-order phase transition is usually accompanied by phase coexistence and finite correlation length. We may therefore ask whether such picture is present in this case too.

Answer to this question may be found beginning with the mean-field approximation and the corresponding density profile for $\alpha = \beta < 1/2$ (figure 2.8c), where a domain wall separates areas of low density α and high density $1 - \alpha$. Such stationary solution is easier to understand by considering the equation for $\rho_i(t)$,

$$\frac{d\rho_i}{dt} = \rho_{i-1}(1-\rho_i) - \rho_i(1-\rho_{i+1}), \tag{2.68}$$

in the continuous (hydrodynamic) limit when lattice constant $a = 1/L \to 0$ with $i \to x = ia$, $t \to ta$ and $\rho_i(t) \to \rho(x,t)$. At the same time the equation for ρ_i assumes the form of the so-called inviscid Burgers equation for $\rho(x,t)$, defined on the interval $[0,1]$,

$$\frac{\partial\rho}{\partial t} = -(1-2\rho)\frac{\partial\rho}{\partial x}, \tag{2.69}$$

where the corresponding boundary conditions are $\rho(0,t) = \alpha$ and $\rho(1,t) = 1-\beta$ and an initial condition $\rho_0(x,0)$ is assumed. Burgers equation as a nonlinear partial differential equation is famous for its shock-like solutions [69]. In order to see that, it is useful to define the so-called characteristics $x = X(t)$ along which the density $\rho(X(t),t)$ remains constant [69],

$$\rho(X(t),t) = \rho(X(0),0) = \rho_0(X(0)). \tag{2.70}$$

Taking derivative of the above expression with respect to t, one arrives at

$$\frac{d}{dt}\rho(X(t),t) = \frac{\partial\rho}{\partial t} + \frac{dX}{dt}\frac{\partial\rho}{\partial x} = 0, \tag{2.71}$$

whereby it follows that

$$\frac{dX}{dt} = 1 - 2\rho \equiv c(\rho). \tag{2.72}$$

Neglecting for a moment the fact that the system is finite, the characteristics turn out to be straight lines

$$x = X(t) = x_0 + c(\rho_0(x_0))t, \quad -\infty < x_0 < \infty. \tag{2.73}$$

Let us take a look at the time evolution of the initially upward step-like density profile $\rho_0(x)$ as depicted in figure 2.11a, where $\rho_0(-\infty) = \rho_L$, $\rho_0(\infty) = \rho_R < \rho_L$ and density $\rho_0(0) = 1/2$ is taken to be at the origin. It is easy to see that $c(\rho_0(x)) < 0$ for all $x < 0$, while $c(\rho_0(x)) > 0$ for all $x > 0$. In other words, for the fixed density $\rho_1 > 1/2$ (i.e. the one that corresponds to $x_0 < 0$, where x_0 is given by $\rho(x_0) = \rho_1$), a point x implicitly defined by $\rho(x,t) = \rho_1$ assumes more negative values in the course of time. At the same time, if we fix density $\rho < 1/2$ (i.e. the one that corresponds to $x_0 > 0$), a position $x > 0$ in the characteristic line (2.73) assumes more positive values in the course of time. As a result, the initial step-like profile stretches in time behaving as a "rarefaction fan".

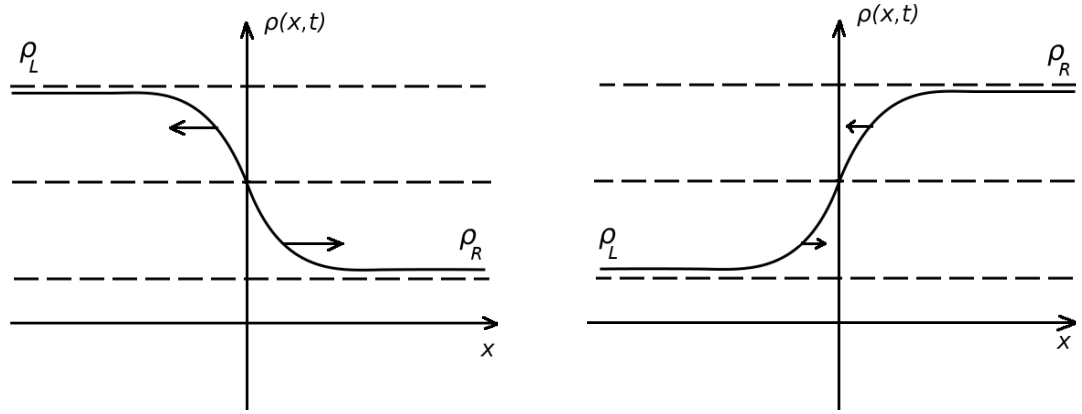

Figure 2.11: Time evolution of the density profile governed by the inviscid Burgers equation (2.69) for the initial conditions that result in a rarefaction fan (figure on the left) and a shock wave (figure on the right).

On the other hand, an initially downward step-like profile (i.e. when $\rho_L < \rho_R$, as depicted in figure 2.11b) will lead to the opposite effect - a shock wave. The trouble is, however, that the crest of the wavefront will eventually "spill over" itself, in particular when two characteristics cross each other. Since each characteristic line corresponds to the different density, this would mean that $\rho(x,t)$ takes two different values for the same x and t, i.e. that $\rho(x,t)$ is ill-defined. Of course, such scenario never happens in a discrete model, in which $\langle \tau_i \rangle$, $i = 1, \ldots, L$ denote the average occupancy of sites. Trouble arises, obviously, in taking the limit $a = 1/L \to 0$, in which one considers density profiles on spatial scales much larger than the microscopic width $\sim a$ of the shock wave. The idea is, therefore, to keep the higher order terms in a in series expansion of $\rho_{i\pm1}$, which results in the viscous Burgers equation,

$$\frac{\partial \rho}{\partial t} = -(1-2\rho)\frac{\partial \rho}{\partial x} + a\frac{\partial^2 \rho}{\partial x^2}, \tag{2.74}$$

containing diffusive term with diffusion constant a. It turns out that by adding this additional diffusive term, which is a well known procedure in mathematics called the parabolic regularization (see for example [70]), the solutions of the Burgers equation become smooth for all times. In particular, the domain wall remains stable and travels with the velocity

$$V = \frac{j(\rho_L) - j(\rho_R)}{\rho_L - \rho_R}. \tag{2.75}$$

The stability of the shock wave in the presence of dissipation is rather easy to understand having in mind that the diffusive term intents to dissipate ("stretch") the wave, which is balanced with its intention to spill it over itself. The presence of both nonlinearity and dissipation, characteristic of Burgers equation, is essential

to the occurrence of *solitons* - waves that retain their shape in time (for further reading see one of the introductory textbooks, e.g. [71]).

Setting the aforementioned discussion in the context of first-order transition on the coexistence line in TASEP, we see how a stable domain wall, connecting domains of low and high density imposed by boundary conditions, naturally emerges in the time evolution of the Burgers equation. On the contrary, the exact solution of TASEP (2.60) for $\alpha = \beta < 1/2$ displays linear density profile. A way to improve the domain wall picture by including fluctuations, obviously neglected in the mean-field approximation, was proposed by Kolomeisky *et al.* in [72]. They start from the idea that in a system which has not yet reached a stationary state, the two possible stationary states, imposed by boundary conditions $\rho_L = \alpha$ and $\rho_R = 1 - \beta$, are coerced into a *metastable* state which emerges in the form of a domain wall. In order that such a domain wall is stable, it is required that $\rho_L < 1/2$ and $\rho_R > 1/2$, i.e. $\alpha < 1/2$ and $\beta < 1/2$ (the phases AI and BI). According to the expression (2.75), the velocity of the domain wall then reads

$$V = \beta - \alpha, \qquad \alpha < 1/2, \beta < 1/2. \tag{2.76}$$

For $\alpha < \beta$ (phase AI), the domain wall travels toward the right boundary resulting in density being equal to $\rho_L = \alpha$. On the other hand, for $\alpha > \beta$, the domain wall travels to the left boundary and density attains the value $\rho_R = 1 - \beta$. When $\alpha = \beta < 1/2$ precisely, the domain-wall velocity vanishes, but due to the fluctuations one cannot expect that it will remain stationary. For example, a particle entering the system from the left reservoir travels fast across the low-density domain until it reaches the domain wall, which results in the growth of the high-density domain and movement of the domain wall one step to the left. On the other hand, when a particle exits the system it leaves a hole behind travelling fast across the high-density domain until it reaches the domain wall. By joining the domain wall, the high-density domain shrinks and the domain wall moves one step to the right. Since particles entering and leaving system are both random and uncorrelated events, the domain wall behaves as a random walker moving leftwards and rightwards with the probabilities D_L and D_R, respectively,

$$D_L = \frac{j(\rho_L)}{\rho_L - \rho_R}, \qquad D_R = \frac{j(\rho_R)}{\rho_L - \rho_R}, \tag{2.77}$$

and reflecting at both ends (figure 2.12).

If we assume that the width of the domain wall is equal to a[4], which enables us to pinpoint its position to a single bond, the probability distribution $P_i(t)$ of finding it at the bond $(i, i+1)$ satisfies the following master equation

[4]That shock waves in TASEP are of microscopic sizes has been rigorously proved, see e.g. [74] and reference therein.

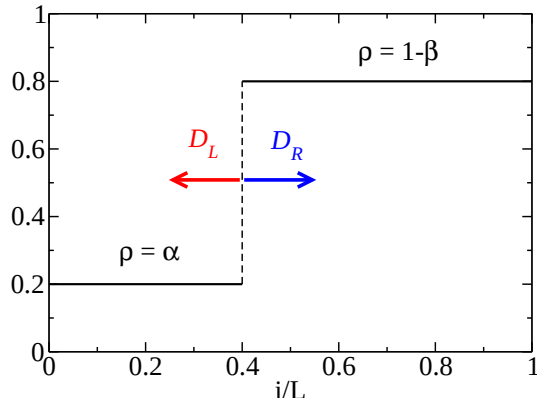

Figure 2.12: The domain wall in the approach of Kolomeisky *et al.* as a random walker moving leftwards and rightwards with the probabilities D_L and D_R, respectively.

$$\frac{dP_i}{dt} = D_R P_{i-1} + D_L P_{i+1} - (D_L + D_R)P_i, \quad i = 1, \ldots, L-1, \tag{2.78}$$

$$\frac{dP_0}{dt} = D_L P_1 - D_R P_0, \tag{2.79}$$

$$\frac{dP_L}{dt} = D_R P_{L-1} - D_L P_L, \tag{2.80}$$

In the above expressions, we have taken that the positions $i = 0$ and $i = L$ correspond to flat density profiles $\langle \tau_j \rangle = \rho_L$ and $\langle \tau_j \rangle = \rho_R$, $j = 1, \ldots, L$, respectively. Once the solution to system of equations (2.78) and (2.80) is known, the density profile ρ_i^{DW} easily follows from

$$\rho_i^{DW}(t) = \sum_{j=0}^{i} P_j(t)\rho_L + \sum_{j=i+1}^{L} P_j(t)\rho_R. \tag{2.81}$$

Although the solution to the system of equations (2.78) and (2.80) is known for any t [73], here we are interested only in the stationary solution when $dP_i/dt = 0$. In that case, the equations (2.78) and (2.80) are solved by assuming the form $P_i = exp(-ki)/\mathcal{N}$, where $k = \ln(D_L/D_R)$, which finally gives

$$P_i = \begin{cases} \frac{e^{-(L-i)/\xi}}{\mathcal{N}} & \alpha < \beta < 1/2 \\ \frac{e^{-i/\xi}}{\mathcal{N}} & \beta < \alpha < 1/2, \end{cases} \qquad \mathcal{N} = \frac{1 - e^{-(L+1)/\xi}}{1 - e^{-1/\xi}}, \tag{2.82}$$

where ξ is the characteristic length

$$\xi^{-1} = \left| \ln \left(\frac{\alpha(1-\alpha)}{\beta(1-\beta)} \right) \right|. \tag{2.83}$$

The characteristic length obtained in the domain-wall approach of Kolomeisky *et al.*, as we see, attains the exact value. The exact agreement is found for the stationary density profile on the coexistence line $\alpha = \beta < 1/2$ as well, where density profile displays a linear shape. This is intuitively clear, as $\alpha = \beta < 1/2$ corresponds to $D_L = D_R$, i.e. to a symmetric random walker with P_i being constant everywhere.

Finally, let us mention how well the domain-wall approach describes the phase diagram of TASEP. When we modelled the dynamics of a domain wall, we conveniently assumed that the domain wall is sharp. This is true for $\alpha < 1/2$ and $\beta < 1/2$, which may be understood by examining the speed $c(\rho)$ of propagation of local density fluctuations. If a small change in α is taken as such a perturbation (with $\beta < 1/2$ fixed), we get $c(\alpha) > 0$ for $\alpha < 1/2$ meaning that the perturbation in α propagates across the system. On the other hand, for $\alpha > 1/2$ $c(\alpha)$ is negative and the perturbation remains localized near the boundary. If we recall the exact stationary solution giving the characteristic lengths ξ_α and ξ_β, we see that the change of sign of c coincides with ξ_α diverging in phase AII ($\alpha \geq 1/2$). This of course is not a coincidence - the domain-wall approach of Kolomeisky *et al.* gives the following microscopic interpretation of the transition (not a phase one!) from AI to AII: the reason that the characteristic length ξ depends only on β is due to the fact that no further change in $\alpha \geq 1/2$ propagates across the system. On the other hand, since for $\alpha > 1/2$ and $\beta < 1/2$ a perturbation does not propagate across the system any more and the domain-wall picture ceased to be valid. The area of its validity is depicted in figure 2.13.

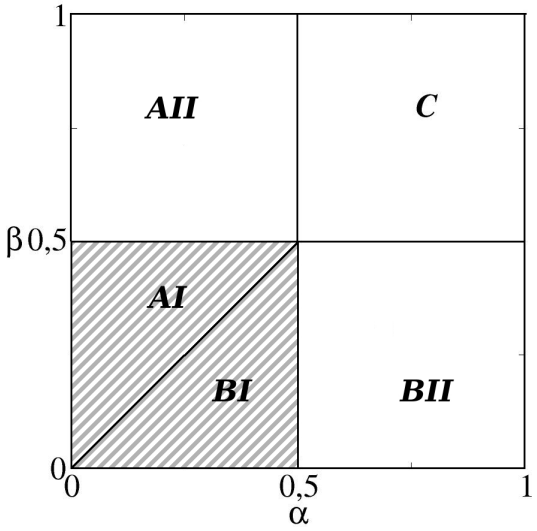

Figure 2.13: A part of the phase diagram in TASEP to which the domain-wall approach of Kolomeisky *et al.* applies (shaded area).

Since ASEP has been solved exactly, the lengthy discussion presented in this

chapter might seem redundant. Its importance, however, becomes apparent when various generalizations of TASEP are considered, most of which are not exactly solvable, like the one presented in Chapter 3.

2.3.4 Second-order phase transition and critical exponents

Unlike on the coexistence line $\alpha = \beta < 1/2$, the first derivative of current (2.65) with respect to α or β is continuous on lines $\alpha = 1/2$, $\beta > 1/2$ and $\alpha > 1/2$, $\beta = 1/2$ separating the low-density and the high-density phases from the maximum-current phase, respectively, but a discontinuity is found in the second derivative

$$\lim_{\alpha \to 1/2^+} \frac{\partial^2 J(\alpha,\beta)}{\partial \alpha^2} = 0 \tag{2.84}$$

$$\lim_{\alpha \to 1/2^-} \frac{\partial^2 J(\alpha,\beta)}{\partial \alpha^2} = -2. \tag{2.85}$$

The exact solution reveals that this transition is followed by a divergence of the characteristic length ξ and a power law form of the density profile with exponent $1/2$, as displayed in (2.64). As the exact exponent differs from the mean-field exponent 1, we may wonder if there is a phenomenological theory, as successful as the domain-wall approach to the first-order transition, that improves the mean-field treatment by including fluctuations and leading to the correct exponent in the maximum-current phase.

Such a theory has been proposed by Hager *et al. et al.* [75], which starts from the stochastic viscous Burgers equation for local density fluctuations, $\phi(x,t) \equiv \rho(x,t) - \overline{\rho}$,

$$\frac{\partial \phi}{\partial t} = -c(\overline{\rho})\frac{\partial \phi}{\partial x} - \kappa\phi\frac{\partial \phi}{\partial x} + \nu\frac{\partial^2 \phi}{\partial x^2} - \frac{\partial \eta}{\partial x}, \tag{2.86}$$

where $c(\overline{\rho})$ and κ are given by,

$$c(\overline{\rho}) = \left.\frac{dj(\rho)}{d\rho}\right|_{\rho=\bar{\rho}} = 1 - 2\bar{\rho}, \tag{2.87}$$

$$\kappa = \left.\frac{d^2 j(\rho)}{d\rho^2}\right|_{\rho=\bar{\rho}} = -2. \tag{2.88}$$

Stochastic term in (2.86) describes density fluctuations originating from fluctuations of current and therefore appears as a gradient of stochastic current $\eta(x,t)$, a Gaussian variable with covariance

$$\langle \eta(x,t)\eta(x',t')\rangle = D\delta(x-x')\delta(t-t'). \tag{2.89}$$

Moving to the coordinate system travelling at the speed $c(\overline{\rho})$ (or alternatively by

choosing $\overline{\rho} = 1/2$) and using the transformation $\phi = \partial h/\partial t$, the above equation assumes the form of the Kardar-Parisi-Zhang (KPZ) equation

$$\frac{\partial h}{\partial t} = \nu \frac{\partial^2 h}{\partial x^2} + \frac{|\kappa|}{2}\left(\frac{\partial h}{\partial x}\right)^2 + \eta. \tag{2.90}$$

In one-dimension, KPZ equation has an important property that D/ν and $|\kappa|$ are both invariant to the renormalization [76] and therefore we can relate them using dimensional analysis [76] that yields

$$\xi(t) \sim [(D/\nu)^{1/2} \cdot |\kappa| \cdot t]^{2/3}, \tag{2.91}$$

where $z = 3/2$ is recognized as the dynamical exponent. In order to apply this result to an open system in the maximum-current phase, Hager *et al.* start from an infinite system on real and positive semi-axis ($x > 0$) with boundary condition $\rho(0) = \rho_L$. In the stationary state, they show that the only combination of parameters D, ν, $|\kappa|$ and $\Delta\rho \equiv \rho_L - 1/2$ that has dimension of length is of the form

$$l = (D/\nu)(\Delta\rho)^{-2}. \tag{2.92}$$

Assuming that in the stationary limit $\langle\phi(x)\rangle = \rho(x) - 1/2$ takes the following form [13]

$$\langle\phi(x)\rangle = \Delta\rho\mathcal{F}(x/l), \tag{2.93}$$

where $\mathcal{F}(0) = 1$, and that no information of the boundary does spreads in the bulk due to the speed $c(1/2)$ being equal to zero (in the maximum-current phase), Hager *et al.* conclude that the function $\mathcal{F}$ assumes the following asymptotic form

$$\mathcal{F}(x) \sim x^{-1/2}, \quad x \to \infty, \tag{2.94}$$

yielding the desired exponent 1/2. We should note that the same exponent, as well as the asymptotic form of the function $\mathcal{F}(x)$, has been obtained earlier in [77] using the $2-\epsilon$ expansion of the corresponding Martin-Siggia-Rose functional describing spatial and temporal fluctuations in the viscous Burgers equation (2.86).

The exponent 1/2 has proved universal in a sense that it remains unchanged in various proposed generalizations of ASEP including the partially asymmetric hopping rates ($p \neq q$) [78], the parallel dynamics [79, 80], the presence of bulk reservoirs (i.e. Langmuir kinetics) [81] and inhomogeneities in hopping rates assigned to particles (i.e. particle-wise disorder) [82]. Inspired by the search for the universality in nonequilibrium systems, we may ask ourselves what are the essential "ingredients" that lead to such universality. The answer to this question will be given in chapter 3.

2.4 Generalizations

Recalling the examples of real systems commonly modelled by ASEP, it is obvious that ASEP is an oversimplified model. Most of the proposed generalizations of ASEP were indeed motivated by the intent to develop more realistic models, most of which are originating in traffic or biology. Some of the generalizations related to traffic include multiple lanes [83–85], crossings [86, 87], several types of vehicles [88, 90–92], adjustment of speed to road conditions [93] etc. In biology, some of generalizations include particles occupying more than one site [94, 95], site-wise disorder [60], desorption and adsorption of particles in the bulk (i.e. Langmuir kinetics) [96], particles with internal states [97], etc.

From the theoretical viewpoint, a part of these generalizations, of which some are cited in what follows, helps to build a catalogue of driven diffusive systems and those of their characteristics that lead to the universal behaviour.

2.4.1 Langmuir kinetics

Inspired by the Langmuir process of adsorption and desorption of atoms, ions and molecules at surface, Parmeggiani, Franosch and Frey proposed a generalization of ASEP exchanging particles with bulk reservoir at each lattice site [96]. Their inspiration stems from dynamics of molecular motors - proteins that translate chemical energy into mechanical. Molecular motors move along the cytoskeleton from which they can detach and later reattach [98]. Schematic picture of TASEP with Langmuir kinetics is depicted in figure 2.14, where ω_A and ω_D denote the rates of adsorption and desorption, respectively.

$$\text{adsorption} \quad 0 \overset{\omega_A}{\to} 1 \tag{2.95}$$

$$\text{desorption} \quad 1 \overset{\omega_D}{\to} 0 \tag{2.96}$$

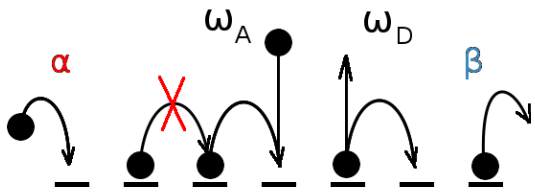

Figure 2.14: Schematic picture of TASEP with Langmuir kinetics.

The most interesting results regarding this model are achieved when ω_A and ω_D are inversely proportional to the system size, $\omega_A \equiv \Omega_A/L$ and $\omega_D \equiv \Omega_D/L$, as then both the short-range hopping and the Langmuir kinetics happen at the same time scales. Parmeggiani, Franosch and Frey have shown that this further

results in the localization of the domain wall (i.e. phase coexistence) in the limit $L \to \infty$ in a sense that the domain wall's width ξ_{DW} in the stationary density profile diverges slower than L, $\xi_{DW} \propto L^{1/2}$. The exponent 1/2, which differs from the one predicted by the mean-field theory, has been explained by Evans, Juhaśz and Santen [99], who demonstrated that domain wall performs random walk with spatially dependent hopping rates $D_L(x)$ and $D_R(x)$ (an idea of spatially dependent hopping rates describing the domain-wall dynamics was introduced independently of [99] by Rakós, Paessens and Schütz in [100])

$$D_L(x) = \frac{j_L(x)}{\rho_R(x) - \rho_L(x)}, \qquad D_R(x) = \frac{j_R(x)}{\rho_R(x) - \rho_L(x)}. \tag{2.97}$$

where $j_L(x)$ and $j_R(x)$ denote the current of particles entering the low-density and the high-density domain, respectively,

$$j_L(x) = \sum_{y<x} \Omega_A[1 - \rho_s(y)] - \sum_{y<x} \Omega_D \rho_s(y) \tag{2.98}$$

$$j_R(x) = \sum_{y>x} \Omega_D \rho_s(y) - \sum_{y>x} \Omega_A[1 - \rho_s(y)]. \tag{2.99}$$

The spatial dependence of $D_L(x)$ and $D_R(x)$ originates in the non-trivial shape of the domain wall $\rho_s(x)$, $\rho_s(x)$ being the solution to the following mean-field equation

$$(1 - 2\rho_s)\frac{\partial \rho_s}{\partial x} - \Omega_A(1 - \rho_s) + \Omega_D \rho_s = 0. \tag{2.100}$$

The stationary probability distribution $P(x)$ of the domain wall's position can be calculated explicitly as it satisfies detailed balance condition (due to the reflecting boundary conditions)

$$D_R(x)P(x) = D_L(x + a)P(x + a), \tag{2.101}$$

$a = 1/L$ being a unit of domain wall's movement, yielding $P(x) \propto exp(-E(x))$ where $E(x + a) - E(x) = D_L(x + a)/D_R(x)$. Density profile of the domain wall can be then calculated explicitly from the equation (2.100) in the symmetric case $\Omega_A = \Omega_D = \Omega$, yielding function $E(x)$ that has a minimum at position x_s where the domain wall's velocity $V = D_R(x) - D_L(x)$ vanishes. The standard deviation of x_s then easily follows from the Taylor expansion of $P(x)$ around x_s up to the quadratic term and is $\propto L^{1/2}$. Similar calculation will be used in chapter 3 concerning a generalization of ASEP to the long-range hopping.

We should mention that spatially dependent hopping rates of the domain wall in some cases lead to a completely different function $E(x)$. For example, Rakós, Paessens and Schütz have modified Langmuir kinetics by including nearest-neighbouring interaction between particles [100]. In that case, $E(x)$ displays a global maximum that increases with system size leading to ergodicity breaking

and hysteresis.

2.4.2 Inhomogeneities in hopping rates

Apart from inducing a localization of the domain wall by supplementing ASEP with Langmuir kinetics, phase separation can be achieved by assigning inhomogeneous hopping rates either to particles or sites. TASEP with one of particles that hops at rate $\alpha < 1$ and passes other particles at rate β has been independently solved by Mallick [88] and Kim *et al.* [89]. The exact solution revealed that in the coordinate frame of a slow particle, a macroscopic domain wall can be seen for certain α and β. A model with inhomogeneous hopping rates assigned to all particles but without a possibility of passing ($\beta = 0$) can be also solved exactly by mapping it to the zero-range process [90, 91], where the phase separation turns out to be induced by the slowest particle in the system. Assigning inhomogeneous hopping rates to the particles is predominantly used in the traffic modelling, where slower particles correspond to vehicles with lesser speed limit (e.g. trucks).

On the other hand, stationary state of TASEP with inhomogeneities assigned to sites rather than to particles is generally rarely known. Janowsky and Lebowitz [59] have shown that already the presence of a single defect site from which particles hop at reduced rate $r < 1$ induces global phase separation. A similar problem was addressed by Wolf and Tang in the context of surface growth portrayed by the KPZ equation [101], where a surface grows slower along the line defect. Despite vast attempts, both problems are still left with the question of whether the regime in which a defect does not induce phase separation exists. A historical overview of this problem, as well as our contribution to it, can be found in chapter 4.

Besides localized defects, sometimes is necessary to consider full disorder, e.g. in biological processes. In that case each site has been assigned a hopping probability chosen from the given probability distribution. Once chosen, hopping probabilities do not vary in time, i.e. they are *quenched*. ASEP with quenched site-wise disorder differs from ASEP with few localized defects in the mechanism of phase separation. A detailed clarification of these differences is left for chapter 5.

3

Phase transitions in ASEP with long-range hopping

In the previous chapter we have shown that the phase transitions in ASEP display phenomena characteristic of phase transitions in equilibrium, like the domain wall occurring at the first-order transition or the diverging characteristic length at the second-order transition. The second-order transition in ASEP shares at least two similarities with the phase transitions in equilibrium. First, the same power law $\langle \tau_i \rangle - 1/2 \propto i^{-1/2}$ is found in other generalizations of the model [78–82], which brings us to the concept of *universality* (for a thorough review of the concept of universality away from the equilibrium see [9]). Second, the application of mean-field theory is shown to be inadequate, because it neglects the relevant contribution stemming from the fluctuations.

One of the (few) ways of directly influencing the fluctuations is to increase the range of interaction. If we introduce the interaction that decays with length l as power law $l^{-(\sigma+1)}$, then by varying the parameter of range σ we can interpolate the two borderline cases, short-range one for $\sigma \to \infty$ and effectively infinite-dimensional case $\sigma = -1$. In equilibrium systems, depending on the particular model and values of σ, we may expect e.g. a change in the universality class (see [105]), phase transition in one dimension [106] or better agreement with the mean-field theory (see [10]).

This chapter shall deal with the generalization of short-range ASEP, as proposed in the papers [107, 108]. The generalization is concerning particles that propagate in long-range jumps whose length is chosen from the distribution $p_l \propto l^{-(1+\sigma)}$. Except the mentioned general motivation, the non-local correlations occurring in the short-range model (see [109] and contained reference), which were shown to be a generic characteristic of numerous systems away from equilibrium, provide another motive. In that context, it seems justified to introduce non-local correlations *directly*, and investigate their influence over the phase diagram in the sense of universality. The chapter 3.3 also presents a possible application to the description of the transport of DNA regulatory proteins.

3.1 Definition of the model

Instead of short-range hops, the particles are allowed long-range jumps of length $1 \leq l \leq L$, while the exclusion principle is retained. The length of hopping l is selected from the distribution

$$p_l \propto \frac{1}{l^{\sigma+1}}, \tag{3.1}$$

where σ is the range parameter. If we limit ourselves to the random-sequential dynamics, that means that in each infinitesimal time interval $[t, t+dt]$ a randomly selected particle on site i moves by l sites either to the left to the site $i-l$ (with the probability of $q \cdot p_l$) or to the right to the site $i+l$ (with the probability of $p \cdot p_l$), but only given the condition that the target site it jumps on is empty. Similar to the short-range case, for $p = 1$ and $q = 0$ we speak of totally asymmetric, for $p \neq q \neq 0$ of partially asymmetric, and for $p = q$ of a symmetric process.

The choice of range parameter σ in this model is not completely arbitrary. We shall later demonstrate that the current in the long-range model is equal to the current in the short-range one enlarged by factor $\lambda_{L-1}(\sigma) = \langle l \rangle = \sum_{l=1}^{L-1} l \cdot p_l$, which diverges for $\sigma \leq 1$ in the limit $L \to \infty$. On the other hand, in the limit $\sigma \to \infty$ the probability (3.1) becomes the Kronecker delta function $\delta_{l,1}$, thus giving us the standard short-range ASEP. The range of σ we turn our attention to is therefore $1 < \sigma < \infty$.

3.1.1 Periodic boundary conditions

In the case of periodic boundary conditions ($\tau_{i+L} = \tau_i$), the probability of finding a system in a particular configuration $C = \{\tau_i | i = 1, \ldots, L\}$ satisfies the following master equation

$$\frac{d}{dt} P(C,t) = \sum_{C'} W(C' \to C) P(C',t) - \sum_{C'} W(C \to C') P(C,t), \tag{3.2}$$

where for every $i = 1, \ldots, L$ and $l = 1, \ldots, L-1$, the rate of transition from C toC' equals

$$W(C \to C') = \begin{cases} p \cdot p_l, & C = \{\ldots, \tau_i = 1, \tau_{i+l} = 0, \ldots,\}, \\ & C' = \{\ldots, \tau_i = 0, \tau_{i+l} = 1, \ldots,\}, \\ q \cdot p_l, & C = \{\ldots, \tau_i = 0, \tau_{i+1} = 1, \ldots,\}, \\ & C' = \{\ldots, \tau_i = 1, \tau_{i+1} = 0, \ldots,\}, \\ 0, & other, \end{cases} \tag{3.3}$$

where $p_l = l^{-(1+\sigma)}/\zeta_{L-1}(\sigma+1)$, and $\zeta_{L-1}(\sigma+1) = \sum_{l=1}^{L-1} l^{-(1+\sigma)}$ is the partial sum of Riemann zeta function. The upper expression produces the equation for the

mean local density $\langle \tau_i \rangle$, which denoted as a continuity equation,

$$\frac{d}{dt}\langle \tau_i \rangle = j_{i-1} - j_i, \tag{3.4}$$

defines the current j_i as total current of all particles hopping over the site i, and those hopping from it,

$$j_i = \sum_{l=1}^{L-1} \sum_{k=i-l+1}^{i} p_l \langle \tau_k (1 - \tau_{k+l}) \rangle. \tag{3.5}$$

As in the short-range model with periodic boundary conditions, all probabilities $P(C)$ are equal (for a detailed explanation see [110]) giving a constant density profile and the current of form

$$\langle \tau_i \rangle = \frac{N}{L} = \rho, \quad j = \frac{\zeta_{L-1}(\sigma)}{\zeta_{L-1}(\sigma+1)} \frac{N(N-1)}{L(L-1)} = \lambda_{L-1}(\sigma)\rho(1-\rho) + O(L^{-1}). \tag{3.6}$$

This means that the current-density relation $j(\rho)$ has the same form $\propto \rho(1-\rho)$ as in the short-range model, but is enlarged by a factor $\lambda_{L-1}(\sigma)$ (figure 3.1), corresponding to the mean length of jumps with respect to the probability distribution p_l, $\lambda_{L-1}(\sigma) = \langle l \rangle$. In the thermodynamic limit in which $L \to \infty$, the mean length of jumps is equal to the ratio of two Zeta functions, $\zeta(\sigma)/\zeta(\sigma+1)$, where $\zeta(\sigma) < \infty$ only for $\sigma > 1$. Therefore we are interested only in the value of the parameter $\sigma > 1$ for which the current is finite.

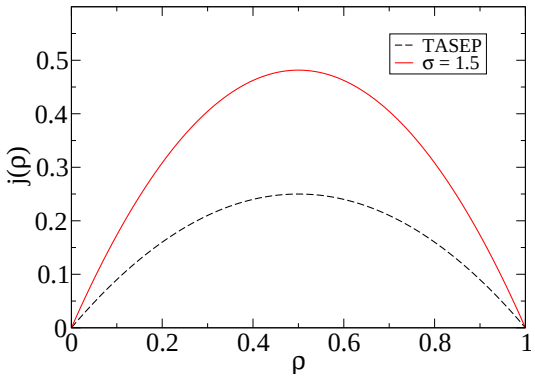

Figure 3.1: The fundamental diagram of the totally asymmetric simple exclusion process with short-range (dashed line) and long-range hopping (full line) for $\sigma = 1.5$.

3.1.2 Open boundary conditions

Unlike the short-range model, the long-range hopping generally leads to non-local "boundary" conditions. In order to demonstrate this, we shall look into a

situation in which a particle in the system selects such an l that the site $i+l$ where it needs to jump to happens to be outside of the system. If we ban such a jump and force a particle to jump outside of the system only from the boundary site L (as in the short-range model), a behaviour drastically different from the one in the bulk would be introduced at the boundaries. A more natural choice of boundary conditions would be to let the particle leave the system from the site i, but with an additional probability β for the target site in the right reservoir to be empty. This leads to the total probability β_i for a particle on site i to leave the system,

$$\beta_i = \frac{\beta}{\zeta_L(\sigma+1)} \sum_{j=L-i+1}^{L} \frac{1}{j^{\sigma+1}}. \tag{3.7}$$

A similar reasoning brings us to the definition of the left "boundary" condition, which allows only the particles from the left reservoir that are within a distance L from the site i to jump to the site i. Taking into account the density of the left reservoir α, the probability α_i that the particle enters the system at the site i is given by

$$\alpha_i = \frac{\alpha}{\zeta_L(\sigma+1)} \sum_{j=i}^{L} \frac{1}{j^{\sigma+1}}. \tag{3.8}$$

A schematic picture of the non-local boundary conditions defined above is depicted in figure 3.2. It should be noted that our choice of boundary conditions (3.7) and (3.8) retains the symmetry of the short-range model with respect to $\alpha \leftrightarrow \beta$ and $\tau_i \leftrightarrow 1 - \tau_{L-i+1}$.

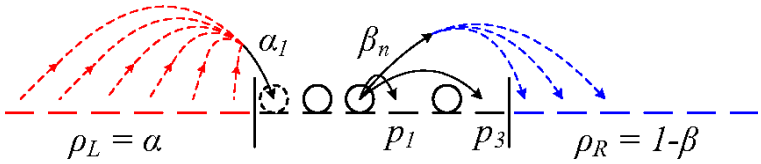

Figure 3.2: Schematic picture of the totally asymmetric simple exclusion process with long-range hopping and open boundary conditions.

The choice of boundary conditions (3.7) and (3.8) introduces exchange of particles with reservoirs at every site. In the lattice equations for the mean densiy, this fact reflects in the coupling of the mean local density $\langle\tau_i\rangle$, $1 \le i \le L$, to the "external fields" α_i and β_i,

$$\begin{aligned}\frac{d}{dt}\langle\tau_i\rangle = \alpha_i(1-\langle\tau_i\rangle) + \sum_{j=1}^{i-1} p_{i-j}\langle\tau_j(1-\tau_i)\rangle - \\ - \sum_{j=i+1}^{L} p_{j-i}\langle\tau_i(1-\tau_j)\rangle - \beta_i\langle\tau_i\rangle,\end{aligned} \tag{3.9a}$$

$$\frac{d}{dt}\langle\tau_1\rangle = \alpha_1(1-\langle\tau_1\rangle) - \sum_{j=2}^{L} p_{j-1}\langle\tau_1(1-\tau_j)\rangle - \beta_1\langle\tau_1\rangle, \tag{3.9b}$$

$$\frac{d}{dt}\langle\tau_L\rangle = \alpha_L(1-\langle\tau_L\rangle) + \sum_{j=1}^{L-1} p_{L-j}\langle\tau_j(1-\tau_L)\rangle - \beta_L\langle\tau_L\rangle, \tag{3.9c}$$

A more condensed form of the equations above can be attained in the form of the continuity equation,

$$\frac{d}{dt}\langle\tau_i(t)\rangle = j_i - j_{i+1}, \tag{3.10}$$

where current j_i is defined as the total current of all particles jumping from or over the site i,

$$j_i = \sum_{k=i+1}^{L} \alpha_k(1-\langle\tau_k\rangle) + \sum_{k=1}^{i}\sum_{l=i+1}^{L} p_{l-k}\langle\tau_k(1-\tau_l)\rangle + \sum_{k=1}^{i}\beta_k\langle\tau_k\rangle. \tag{3.11}$$

By including the sites $i = 0$ and $i = L+1$ in the definition above gives the total current of particles entering and exiting the system,

$$j_{\text{in}} = \sum_{i=1}^{L} \alpha_i(1-\langle\tau_i\rangle) \tag{3.12}$$

$$j_{\text{out}} = \sum_{i=1}^{L} \beta_i\langle\tau_i\rangle \tag{3.13}$$

Of course, in the stationary state the current is conserved, i.e. $j_{\text{in}} = j_1 = \cdots = j_L = j_{\text{out}}$.

3.2 Hydrodynamic approach in the mean-field approximation

Let us consider the process on an infinite lattice for an arbitrary p and q with the probability of hopping $p_l = l^{-(1+\sigma)}/\zeta(\sigma+1)$. Starting with the master equation, the time evolution of the mean local density $\langle\tau_n\rangle$ follows the equation

$$\frac{d}{dt}\langle\tau_n\rangle(t) = \langle K_n^{(1)}\rangle, \tag{3.14}$$

where

$$K_n^{(1)} = \sum_{r>0} p_r(\Delta_r^+\tau_n - \Delta_r^-\tau_n) - (p-q)\sum_{r>0} p_r\left[(1-\tau_n)\Delta_r^+\tau_n + \tau_n\Delta_r^-\tau_n\right], \tag{3.15}$$

abd the following notation has been introduced, $\Delta_r^+\tau_n \equiv \tau_{n+r} - \tau_n$ and $\Delta_r^-\tau_n \equiv \tau_n - \tau_{n-r}$. We are interested in the so-called hydrodynamic limit in which the microscopic details are averaged on appropriate spatial and temporal scales. In mathematics, such a procedure is rigorously defined and was performed for an arbitrary p in a short-range case [111, 112], and recently for $p = q$ in a long-range case [113]. In the short-range case the results are the Burgers equation for $p \neq q$

$$\frac{\partial \rho}{\partial t} = -(p-q)\frac{\partial}{\partial x}[\rho(1-\rho)], \tag{3.16}$$

and the diffusion equation for $p = q$,

$$\frac{\partial \rho}{\partial t} = \frac{1}{2}\frac{\partial^2 \rho}{\partial x^2}. \tag{3.17}$$

In upper equations the local density $\rho(x,t)$ represents the microscopic local density $\langle \tau_n \rangle$ averaged either over a so-called Euler scale for $p \neq q$ ($t \to t/a$, $x \to x/a$) or over the diffusion scale for $p = q$ ($t \to t/a^2$, $x \to x/a$). The reason that this procedure yields the same result as the "naive" Taylor series in the lattice constant a lies in the fact that the stationary solution of the master equation $P(C)$ is the uniform measure, which approximates the product measure up to small finite size corrections that become unimportant in the hydrodynamic limit.

In the long-range case the rigorous calculation in a symmetric case $p = q$ [113] yields a so-called fractional diffusion equation in the form

$$\frac{\partial \phi}{\partial t} = \nu_\sigma \Delta_\sigma \phi(x,t), \quad 1 < \sigma < 2, \tag{3.18}$$

where $\nu_\sigma = -2p\Gamma(-\sigma)cos(\pi\sigma/2)/\zeta(\sigma+1) > 0$ and Δ_σ is fractional Laplacian with the property that for an appropriately selected function $f(x)$, the Fourier transform of $\Delta_\sigma f(x)$ equals

$$\mathcal{F}\{\Delta_\sigma f(x)\} = -|k|^\sigma \hat{f}(k). \tag{3.19}$$

In real space the fractional Laplacian (also known as the Riesz fractional derivation, see [114,115]) is defined as a linear combination of Weyl fractional derivatives,

$$\Delta_\sigma f(x) \equiv -\frac{{}_{-\infty}\mathcal{D}_x^\sigma + {}_x\mathcal{D}_\infty^\sigma}{2cos(\pi\sigma/2)}, \tag{3.20}$$

$${}_{-\infty}\mathcal{D}_x^\sigma f(x) = \frac{1}{\Gamma(n-\sigma)}\frac{d^n}{dx^n}\int_{-\infty}^{x} f(\xi)(x-\xi)^{n-\sigma-1}, \tag{3.21a}$$

$${}_x\mathcal{D}_\infty^\sigma f(x) = \frac{(-1)^n}{\Gamma(n-\sigma)}\frac{d^n}{dx^n}\int_{x}^{\infty} f(\xi)(\xi-x)^{n-\sigma-1}, \tag{3.21b}$$

which have the following property with respect to the Fourier transformation,

$$\mathcal{F}\{{}_{-\infty}\mathcal{D}_x^{\sigma} f(x)\} = (-ik)^{\sigma}\hat{f}(k), \tag{3.22a}$$

$$\mathcal{F}\{{}_{x}\mathcal{D}_{\infty}^{\sigma} f(x)\} = (ik)^{\sigma}\hat{f}(k). \tag{3.22b}$$

Derivatives of fractional order were first mentioned in works by Leibnitz, Euler, Laplace, Fourier and others, while a systematic theory was formed independently by both Riemann and Liouville in the 19th century (see [116]). In physics the fractional derivatives are useful in modelling *subdiffusive* ($\mu < 2$) and *superdiffusive* ($\mu > 2$) motion where the mean squared deviation in particle's position does not grow linearly with time, but rather follows a power law with a non-integer μ (see e.g. [117]),

$$\langle(\Delta\vec{r})^2\rangle = \langle(\vec{r} - \langle\vec{r}\rangle)^2\rangle \propto t^{\mu}. \tag{3.23}$$

The application of fractional derivatives is commonly found in biophysics (the aforementioned anomalous diffusion), polymer physics (Levy's random walk), chaos theory, rheology, in description of relaxation of disordered systems (amorphous metals, spin glass, ferroelectric crystals , etc.), electronics (circuit elements with fractional impedance $|Z| \propto \omega^{-1/2}$) - to mention just a few (for a more thorough overview of the applications in physics and engineering see [118] and [119]).

Returning to the equation (3.14), by applying the mean-field approximation $\langle\tau_n\tau_m\rangle \to \langle\tau_n\rangle\langle\tau_m\rangle$, $n \neq m$, we get the equation of the form

$$\frac{d\phi_n}{dt} = \sum_{r>0}\frac{p_r}{2}(\Delta_r^{+}\phi_n - \Delta_r^{-}\phi_n) + (\Delta\rho + \phi_n)(p-q)\sum_{r>0} p_r(\Delta_r^{+}\phi_n + \Delta_r^{-}\phi_n), \tag{3.24}$$

where ϕ_n denotes the deviation of local density from the mean density $\bar{\rho}$, and $\Delta\rho = \bar{\rho} - 1/2$ is introduced to distinguish two important cases, $\bar{\rho} \neq 1/2$ and $\bar{\rho} = 1/2$. In order to get the equation for $\phi(x,t)$ in the limit $a \to 0$, we shall use the procedure described in [120]. The idea consists of taking $\phi_n(t)$ as coefficients of the Fourier series of a certain function $\phi(\hat{k},t)$ defined on the interval $[-K/2, K/2]$,

$$\hat{\phi}(k,t) = \sum_{n=-\infty}^{\infty}\phi_n(t)e^{-ikx_n}, \tag{3.25a}$$

$$\phi_n(t) = \frac{1}{K}\int_{-K/2}^{K/2}\hat{\phi}(k,t)e^{ikx_n}dk, \tag{3.25b}$$

where $x_n = na$ and $K = 2\pi/a$. By using (3.25a) and (3.25b), the equation (3.24) can be writen in the inverse Fourier space as follows,

$$\frac{d}{dt}\hat{\phi}(k,t) = \hat{\phi}(k,t)[D(ka) - D(0)] + \Delta\rho\hat{\phi}(k,t)B(ka) + \tag{3.26}$$

$$+ \frac{1}{K^2}\int_{-K/2}^{K/2} dk_1 \int_{-K/2}^{K/2} dk_2 \hat{\phi}(k_1,t)\hat{\phi}(k_2,t) \sum_{n=-\infty}^{\infty} e^{i(k_1+k_2-k)na} B(ka), \tag{3.27}$$

where $D(ka)$ and $B(ka)$ are given by

$$D(ka) = \frac{1}{2}\left[Li_{\sigma+1}(e^{ika}) + Li_{\sigma+1}(e^{-ika})\right], \tag{3.28a}$$

$$B(ka) = (p-q)[Li_{\sigma+1}(e^{ika}) - Li_{\sigma+1}(e^{-ika})]. \tag{3.28b}$$

In upper expressions $Li_s(z)$ is the so-called polylogarithm defined by the following series

$$Li_s(z) = \sum_{n=1}^{\infty} \frac{z^n}{n^s}, \tag{3.29}$$

which also appears in physics in relation to Bose-Einsten and Fermi-Dirac distributions [121],

$$Li_s(z) = \frac{1}{\Gamma(s)}\int_0^{\infty} \frac{t^{s-1}}{e^t/z - 1} dt \tag{3.30a}$$

$$-Li_s(-z) = \frac{1}{\Gamma(s)}\int_0^{\infty} \frac{t^{s-1}}{e^t/z + 1} dt. \tag{3.30b}$$

Using the known expansion of polylogarithm $Li_s(e^z)$ around $z = 0$ [121],

$$Li_s(e^z) = \Gamma(1-s)(-z)^{s-1} + \sum_{k=0}^{\infty} \frac{\xi(s-k)}{k!} z^k, \quad |z| < 2\pi, \quad s \neq 1, 2, 3, \ldots, \tag{3.31}$$

yields the following expansion of $D(ka)$ and $B(ka)$ in ka,

$$D(ka) - D(0) = \frac{1}{2\zeta(\sigma+1)}\left[2\Gamma(-\sigma)cos\frac{\pi\sigma}{2}|k|^\sigma a^\sigma + \right.$$

$$\left. + 2\sum_{n=1}^{\infty} \frac{\zeta(\sigma+1-2n)}{(2n)!}(ik)^{2n}a^{2n}\right], \tag{3.32a}$$

$$B(ka) = \frac{p-q}{\zeta(\sigma+1)}\left[-2i\Gamma(-\sigma)sin\frac{\pi\sigma}{2}sgn(k)|k|^\sigma a^\sigma + \right.$$

$$\left. + 2\sum_{n=1}^{\infty} \frac{\zeta(\sigma+2-2n)}{(2n-1)!}(ik)^{2n-1}a^{2n-1}\right]. \tag{3.32b}$$

Finally, we are interested in taking the limit $a \to 0$ which allows us to replace the sum in (3.25a) with an integral,

$$\hat{\phi}(k,t) = \sum_{n=-\infty}^{\infty} \phi_n(t) e^{-ikx_n} = \frac{1}{a} \sum_{n=-\infty}^{\infty} \phi_n(t) e^{-ikx_n} \overbrace{\Delta x_n}^{a} \tag{3.33}$$

$$\Rightarrow \quad lim_{a\to 0}[a\hat{\phi}(k,t)] = \int_{-\infty}^{\infty} \phi(x,t) e^{-ikx} dk \equiv \tilde{\phi}(k,t), \tag{3.34}$$

$$\phi(x,t) = \frac{1}{2\pi} \int_{-\infty}^{\infty} \tilde{\phi}(k,t) e^{ikx} dk, \tag{3.35}$$

where $\tilde{\phi}(k,t)$ and $\phi(k,t)$ denote $\hat{\phi}(k,t)$ and $\phi_n(t)$, respectively, in the continuous limit. In addition, the time scale has to be transformed as $t \to t/a^z$, where z is the smallest exponent in a that appears in (3.32a) and (3.32b). With respect to values of p and q, we recognize two distinct cases: symmetric ($p = q$) and asymmetric ($p \neq q$).

3.2.1 The symmetric case $p = q$

For $p = q$, $B(ka)$ equals 0 and $z = \min\{\sigma, 2\}$. For $\sigma > 2$, this yields the usual diffusion equation

$$\frac{\partial \phi}{\partial t} = \nu_2 \frac{\partial^2 \phi}{\partial x^2}, \quad \sigma > 2, \tag{3.36}$$

where ν_2 is the diffusion coefficient, $\nu_2 = \zeta(\sigma - 1)/2\zeta(\sigma + 1) > 0$. On the other hand, for $1 < \sigma < 2$ the usual diffusion equations is replaced by the fractional diffusion equation

$$\frac{\partial \phi}{\partial t} = \nu_\sigma \Delta_\sigma \phi, \quad 1 < \sigma < 2, \tag{3.37}$$

where $\nu_\sigma = -\Gamma(-\sigma) cos(\pi\sigma/2)/\zeta(\sigma + 1) > 0$, identical to the rigorous result of [113].

3.2.2 The asymmetric case $p \neq q$

In the asymmetric case $z = \min\{\sigma, 1\}$, which for $\sigma > 1$ yields the inviscid Burgers equation with additional term $-v\partial/\partial x \phi(x,t)$,

$$\frac{\partial \phi}{\partial t} = -c(\bar{\rho}) \frac{\partial \phi}{\partial x} - \kappa \phi \frac{\partial \phi}{\partial x}, \quad \sigma > 1, \tag{3.38}$$

where $c(\bar{\rho})$ and κ are

$$c(\bar{\rho}) = (p-q)(1-2\bar{\rho})\lambda(\sigma) = \left.\frac{dj(\rho)}{d\rho}\right|_{\rho=\bar{\rho}}, \tag{3.39}$$

$$\kappa = -2(p-q)\lambda(\sigma) = \left.\frac{d^2 j(\rho)}{d\rho^2}\right|_{\rho=\bar{\rho}} .. \tag{3.40}$$

In this way we have recovered the functional form of the current $j(\sigma) = \lambda(\sigma)\rho(1-\rho)$ and the mean hopping lenght $\lambda(\sigma)$,

$$j(\rho) = (p-q)\lambda(\sigma)\rho(1-\rho), \quad \lambda(\sigma) = \frac{\zeta(\sigma)}{\zeta(\sigma+1)}. \tag{3.41}$$

The original Burgers equation (2.69) is obtained easily by the Galilean transformation $x \to x - c(\bar{\rho})t$, or alternatively by taking $\bar{\rho} = 1/2$ corresponding to $c = 0$.

The result (3.38) is a bit surprising because it suggests that the long-range jumps have no visible effect on large space and time scales. The equation (3.38) also implies the same conclusions discussed in chapter (2.3), which pertain to the occurrence of the domain walls and their instability in a inviscid case. Therefore it is justified to look at higher order terms in a, which were omitted in the limit $a \to 0$, but which become relevant if we wish to describe the behaviour on smaller scales. For $1 < \sigma < 2$, the next lower-order terms in (3.32a) and (3.32b are of order a^σ, which in the real space correspond to the fractional Laplacian $\Delta_\sigma\phi$ and the non-linear term $\phi H_\sigma \phi$, where the non-local operator H_σ is given by the following linear combination of Weyl fractional derivatives,

$$H_\sigma \equiv \frac{-\infty\mathcal{D}_x^\sigma - {}_x\mathcal{D}_\infty^\sigma}{2sin(\pi\sigma/2)}, \tag{3.42}$$

and has the following property considering the Fourier transformation $\mathcal{F}$ with respect to a chosen function $f(x)$

$$\mathcal{F}\{H_\sigma f(x)\} = -isgn(k)|k|^\sigma \hat{f}(k), \quad \hat{f}(k,t) = \mathcal{F}\{f(x)\}. \tag{3.43}$$

Although both of these terms are non-local and of the same order in a, we may assume that because of the non-linearity the term $\phi H_\sigma \phi$ will generally be of a higher order than the diffusive term. By neglecting the non-linear term we then get a viscous Burgers equation with a fractional diffusive term for $1 < \sigma < 2$, and a standard diffusive term for $\sigma > 2$,

$$\frac{\partial\phi^a}{\partial t} = a^{\sigma-1}\nu_\sigma\Delta_\sigma\phi^a - \kappa\phi^a\frac{\partial\phi^a}{\partial x}, \quad 1 < \sigma < 2, \tag{3.44}$$

$$\frac{\partial\phi^a}{\partial t} = a\nu_2\Delta\phi^a - \kappa\phi^a\frac{\partial\phi^a}{\partial x}, \quad \sigma > 2, \tag{3.45}$$

where the local deviation of density was denoted as $\phi^a(x,t)$ to stress its dependence on a.

The upper equations lead to two important conclusions. The first states that the short-range limit occurs *effectively* already for $\sigma > 2$, which is the result that will surface many times later when the open boundary conditions will be considered. The other concerns the regularity of the solution of the Burgers equation with the fractional diffusive term. In fact, the equation in the form of (3.44) was already investigated by several authors (see [122] and the respective references), who have all shown that the fractional diffusive term has a similar effect as the standard diffusive term in the sense that the solution of the equation (3.44) is expected to attain stable (smooth) domain walls as well.

3.2.3 Relaxation to the stationary state

Before introducing the boundary conditions (3.8) and (3.7) into the previous discussion, it would be interesting to verify the conclusions of previous chapter, attained in the hydrodynamic limit, for a discrete model. It is also clear that the numerical simulations restrict us to finite systems and periodic boundary conditions must be considered if we wish to keep the translational invariance. Instead of a (trivial) stationary state discussed in chapter 3.1.1, we are now investigating the relaxation of the system towards the stationary state by looking at the longest relaxation time τ.

We have shown in the chapter 2.2 that in the short range case τ is inversely proportional to the gap between the ground state energy and the energy of the first excited state of XXZ spin chain. The quantum spin chain with the short-range interaction in $1d$ can be treated with the Bethe *Ansatz*. As a result, depending on asymmetry in p and q and for a fixed density[1], we get a diffusive relaxation for $p = q$ [50],

$$\tau \propto L^z, \quad z = 2, \quad p = q, \tag{3.46}$$

while in the asymmetric case, $p \neq q$, τ diverges as $\tau \propto L^z$ with $z = 3/2$ [50, 123]. A similar behaviour is found in the case of open boundary conditions [51, 52] on the coexistence line ($\tau \propto L^2$ due to diffusive motion of the domain wall) and in the maximum-current phase ($\tau \propto L^{3/2}$), except in the low- and in the high-density phases where τ is found to be finite.

As mentioned earlier in chapter 2.2, the other way of determining τ consists of investigating the invariance to a change of time and spatial scales of hydrodynamic equations, specifically their stochastic versions. Using the transformation $\phi(x,t) = \partial h(x,t)/\partial x$, the diffusion equation in the symmetrical ($p = q$) case and the Burgers

[1] If instead of density we fix number of particles, the gap scales as L^2, see [124]

equation in the asymmetrical ($p \neq q$) case are transformed into the Edwards-Wilkinson (EW) and Kardar-Parisi-Zhang (KPZ) equations, respectively,

$$\frac{\partial h}{\partial t} = \nu \Delta h + \eta, \tag{3.47}$$

$$\frac{\partial h}{\partial t} = \nu \Delta h + \frac{\lambda}{2}\left(\frac{\partial h}{\partial x}\right)^2 + \eta, \tag{3.48}$$

For the stochastic processes described in the upper equations the autocorrelation function $\langle \phi(0,0)\phi(x,t)\rangle$ is a homogeneous function determined by the exponents χ and z,

$$C(\lambda x, \lambda^{1/z} t) = \lambda^{2\chi - 2} C(x,t), \tag{3.49}$$

where the averaging $\langle \dots \rangle$ is executed along all possible time evolutions of the noise η. Considering the linearity of EW equation, χ and z can be determined from the dimensional analysis, which yields $\chi = 1/2$ and $z = 2$. In the case of KPZ equation the calculation is more complicated and it consists in proving two important properties of the KPZ equation. The first property is the relation $\chi + z = 2$ that follows from the invariance of KPZ equation with respect to the special kind of Galileo transformation parameterized by the vector $\vec{v}$ [76],

$$h'(\vec{x}, t) = h(\vec{x} - \vec{v}t) - \frac{1}{\lambda}\vec{v}\cdot\vec{x} + \frac{1}{2\lambda}\vec{v}^2 t \tag{3.50}$$

which applies for an arbitrary dimension d. The other property is characteristic only of $d = 1$, and is reflected in the fact that the stationary probability distribution of heights $P[h(x)]$, as in EW equation, is given by the Gauss distribution [76],

$$P[h] \propto exp\left[-\frac{\nu}{D}\int dx (\nabla h)^2\right], \tag{3.51}$$

where D is defined by the relation (2.89). Consequence of this is that $\chi = 1/2$, which together with $\chi + z = 2$ gives $z = 3/2$.

Non-local variations of EW and KPZ equation have been studied in [125, 126], where the local diffusive term $\Delta h(x,t)$ was replaced with the fractional $\Delta_\sigma h(x,t)$,

$$\frac{\partial h}{\partial t} = \nu \Delta_\sigma h + \eta, \quad 0 < \sigma \leq 2, \tag{3.52}$$

$$\frac{\partial h}{\partial t} = \nu \Delta_\sigma h + \frac{\lambda}{2}\left(\frac{\partial h}{\partial x}\right)^2 + \eta, \quad 0 < \sigma \leq 2. \tag{3.53}$$

In the case of fractional EW equation (FEW), $\chi = (\sigma - 1)/2$ and $z = \sigma$ follow from the dimensional analysis [125]. The fractional KPZ equation (FKPZ), on the other hand, shows significantly more complex behaviour with several distinct regimes,

depending on the value of the parameter σ and on whether the noise $\eta(x,t)$ is spatially correlated or not [126]. If the noise is uncorrelated the calculation shows the existence of two regimes: the first is the fractional EW regime $\sigma < 3/2$ with $\chi = (\sigma - 1)/2$ and $z = \sigma$, and the other is the standard KPZ regime for $\sigma > 3/2$ with $\chi = 1/2$ and $z = 3/2$. The regime change in $z(\sigma)$ at $3/2$ can be intuitively understood as system's tendency to relax itself through its fastest component which for $\sigma > 3/2$ ceases to be a fractional diffusion, because then $z_{FEW} < z_{FKPZ}$.

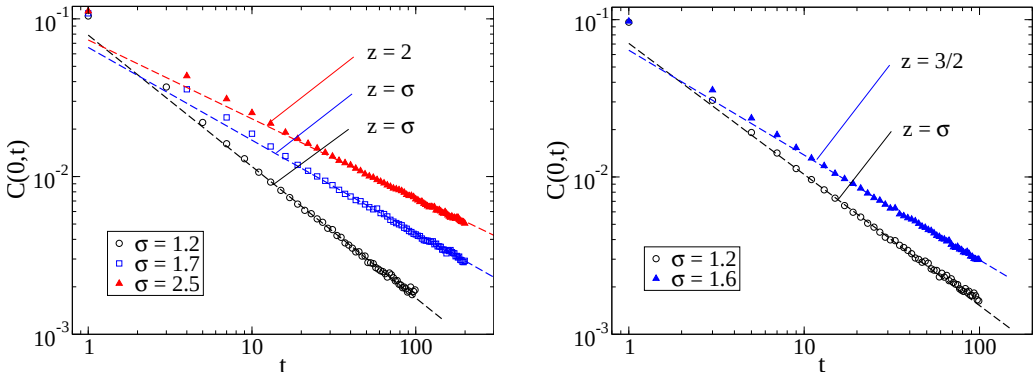

Figure 3.3: Autocorrelation function $C(0,t)$ in the symmetric (left) and in the totally asymmetric (right) simple exclusion process with long-range hopping on a periodic lattice of size $L = 10^4$ and the particle density $\rho = 1/2$. Autocorrelation function was obtained by averaging over 10^7 independent Monte Carlo simulations with $t = 100$ Monte Carlo steps per site. Dashed lines denote the analytical result $C(0,t) \propto t^{-1/z}$ with $z = \min\{\sigma, 2\}$ (left) and $z = \min\{\sigma, 3/2\}$ (right).

The upper estimates were checked in a discrete model by calculating the autocorrelation function $C(i-j,t)$ using the Monte Carlo simulations. For that purpose, we considered the symmetric and the totally asymmetric model with long-range hopping and periodic boundary conditions on a lattice of length $L = 10^4$ and density $\rho = 1/2$, and calculated the autocorrelation function $\langle[\tau_i(0) - \rho][\tau_j(t) - \rho]\rangle$, averaged over over 10^7 independent Monte Carlo simulations with $t = 100$ Monte Carlo steps per site. If we limit ourselves to just calculating the dynamic exponent z, we can determine z from $C(i-j,t)$ by setting $i - j = ct$, since then

$$C(ct,t) \propto t^{-1/z}. \tag{3.54}$$

The time dependence of $C(0,t)$ (where we have taken $\rho = 1/2$ so that $c = 0$) in the symmetric and the totally asymmetric case is depicted in figures 3.3a and 3.3b, respectively. In both cases we get excellent concordance with estimated values $z = \min\{\sigma, 2\}$ for $p = q$ and $z = \min\{\sigma, 3/2\}$ for $p \neq q$ in the case of spatially uncorrelated noise.

3.3 Long-range effects in transport of DNA regulatory proteins

DNA regulatory proteins bind to a DNA molecule and participate in various important processes in cell like transcription or chromosome packaging. Some of them, like transcription factors, bind only to specific sites on DNA molecule activating or inhibiting the transcription of genes. The rate k_a of binding of a protein P to the specific site S on DNA molecule,

$$P + S \leftrightharpoons PS, \tag{3.55}$$

can be measured experimentally [127] by calculating the ration

$$k_a = \frac{d[PS]/dt}{[P][S]} \tag{3.56}$$

In the beginning, the protein-DNA search was considered to be a purely diffusive process. Theoretically, this assumption leads to $k_{3D} = 4\pi D_{3D} ba \approx 10^8$ $\mathrm{M}^{-1}\mathrm{s}^{-1}$, where D_{3D} is the diffusion constant of the protein, b is the cross-section of the binding reaction and a is the fraction of the molecular surface of the protein that contains the reactive binding interface. The predicted value of k_{3D}, however, differs from the experimentally determined values by two orders of magnitude. To stress this discrepancy a term *facilitated* diffusion was coined. Nowadays we know that the protein-DNA search consists of alternating rounds of $3d$ and $1d$ diffusion (for a more detailed overview, see [128]), as depicted in figure 3.4.

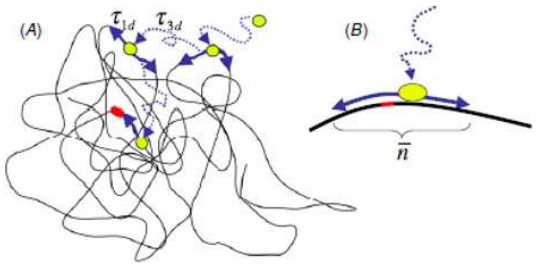

Figure 3.4: (A) Schematic picture of the mechanism of facilitated diffusion by which a DNA regulatory protein (yellow) searches for a specific site on DNA (red). (B) Between absorption and desorption the protein visits on average $\bar{n}$ sites (i.e. base pairs, bp) increasing the cross-section b from 1 bp to $\bar{n}$. The picture is taken from [128].

If the DNA molecule is long enough and folded, two its parts may come close enough to each other initiating an intersegmental transfer occurs (figure 3.5). Lomholt *et al.* described this process using the one-dimensional fractional diffusion equation [129], considering the fact that the probability of finding a loop of length l follows the power law $p_l \propto l^{-1-\sigma}$, where σ is $1 < \sigma < 2$ in good solvents [130].

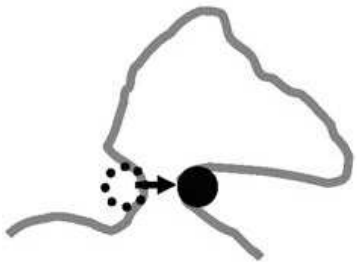

Figure 3.5: Schematic picture of intersegmental transfer as one of the processes explaining fast (facilitated) diffusion.

In that context, long-range jumps in TASEP could be taken as a discrete version of fractional diffusion in describing protein-DNA search on long DNA chains.

3.4 Boundary-induced phase transitions

Due to the fact that in the thermodynamic limit of an infinite system with long-range hopping we get the same (Burgers) equation as in the short-range case and that the long-range effects are described only by higher-order terms suggests a phase diagram same or similar to the standard one. On the other hand, if we consider the open chain we must bear in mind that the boundary conditions are non-local. In what follows we shall, first by using Monte Carlo simulations and later on analytically, show that this fact does not affect the phase diagram, but only the behavior on transition lines.

3.4.1 Phase diagram

In order to determine the phase diagram we are performing Monte Carlo (MC) simulations with the usual random-sequential dynamics, in a way that for each discrete time step we randomly select one site $1 \leq i \leq L$ on a lattice (L such steps define one Monte Carlo step/site). If the site i is empty ($\tau_i = 0$), a particle from the left reservoir of density $\rho_L = \alpha$ jumps to it with the probability α_i. If the site i is occupied the length $1 \leq l \leq L$ is randomly selected from the distribution p_l, and two distinct cases are possible . In the first case the particle moves by l sites to site $i+l$, given the condition that the site $i+l$ is empty. In the case $i+l > L$, the particle exits the system with the probability β. The stationary density profile $\langle \tau_i \rangle$ and the current j_i are calculated only after the system has relaxed t_0 MC steps/site, which ensures that the stationary state has been reached.

In figures 3.6a to 3.6d the density profiles of typical α and β are depicted. In contrast to the short-range model, the figure present us with several similarities and differences. The phases of low and high density are still present (figures 3.6a and 3.6b), but display greater deviation from the mean density close to the edges. Secondly, the line $\alpha = \beta < 1/2$ shows a non-trivial profile which does not correspond to the linear profile from the short-range model (figure 3.6c). Finally,

in the maximum-current phase the mean density is still 1/2, but with significantly higher deviations close to the edges (figure 3.6d).

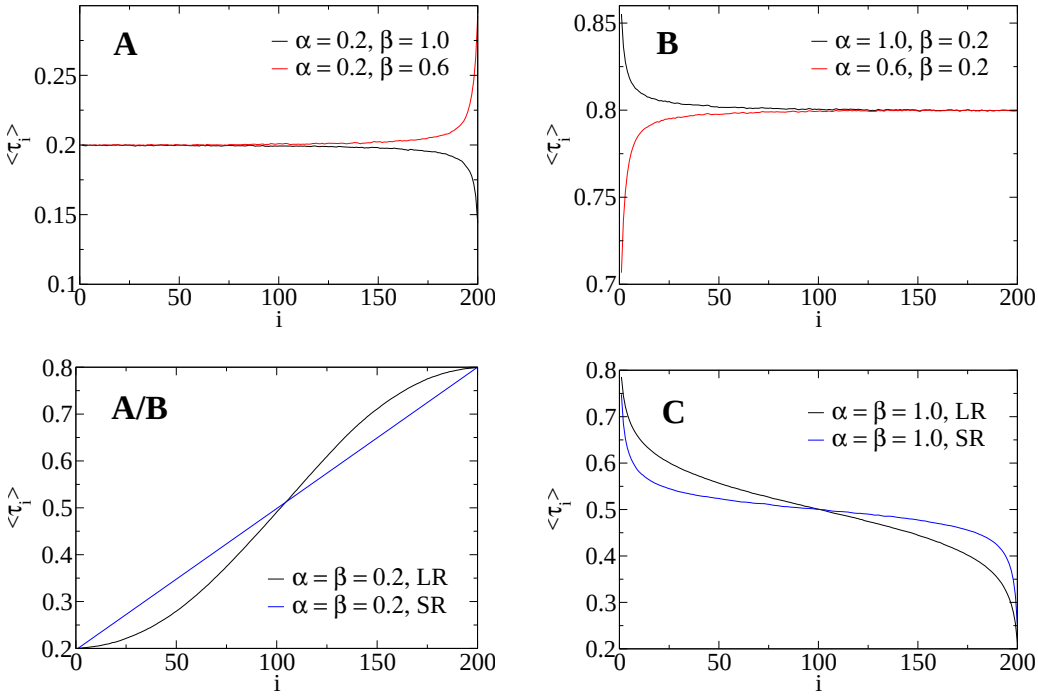

Figure 3.6: Density profiles in the totally asymmetric simple exclusion process with long-range hopping for $\sigma = 1.5$ obtained by Monte Carlo simulations: (a) in the low-density phase A, (b) in the high-density phase B, (c) on the coexistence line and (d) in the maximum-current phase. For an easier comparison, the figures (c) and (d) show also density profiles in the short-range model (SR) obtained for the same α and β. The parameters of all simulations are $L = 200$ and $t_0 = t = 10^7$ MC steps/site.

In order to determine the nature of phase transition we are looking at the mean density $\bar{\rho} = \langle N \rangle / L = \sum_{i=1}^{L} \langle \tau_i \rangle / L$ and the current j_L as functions of α for two fixed parameter values β, $\beta < 1/2$ (figure 3.7a) and $\beta > 1/2$ (figure 3.7b) [Considering that the phase diagram is symmetric to $\alpha \leftrightarrow \beta$, a similar results can be obtained by varying the β with a fixed α.] The figure 3.7a shows how the mean density $\bar{\rho}$ has a sudden increase on the line $\alpha = \beta = 0.3 < 1/2$, like in the short-range model. The figure 3.7b depicts the dependence of the current j_L/λ_L on α for the fixed $\beta = 0.7 > 1/2$, which follows the expected current-density relation $j_L = \alpha(1-\alpha)$ for $\alpha < 1/2$ and $j_L = 1/4$ for $\alpha > 1/2$ (figure 3.7b). In both figures we presented the results for $\sigma < 1$ as well to show that the divergence of current destroys phase transitions.

Based on Monte Carlo simulations, we can now deduce that the phase diagram has indeed remained unchanged in the long-range model, but differences can be seen on the coexistence line $\alpha = \beta < 1/2$ and in the maximum-current phase.

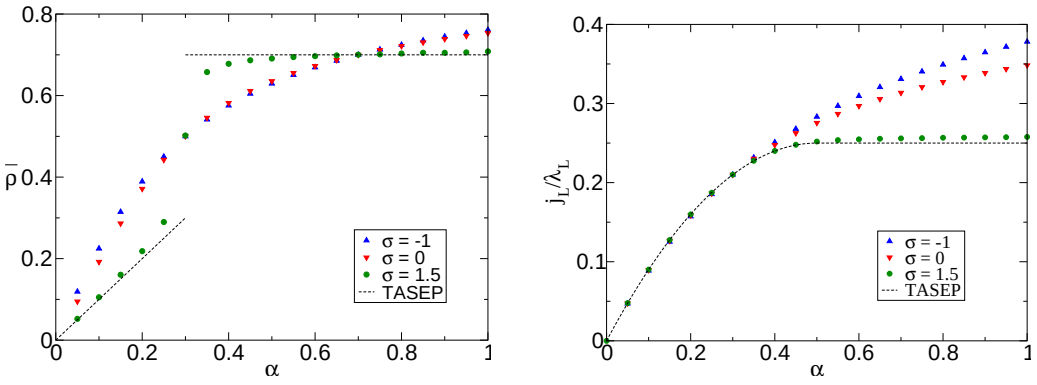

Figure 3.7: (a) The mean density $\bar{\rho}$ as a function of α for $\beta = 0.3$ and (b) the current j_L/λ_L as a function of α for $\beta = 0.7$, for different values of the parameter σ. The parameters of all simulations are $L = 200$ and $t_0 = t = 2 \cdot 10^6$ MC steps/site. The corresponding dependencies in the short-range case are depicted by dashed lines.

These differences will be the subject of the rest of this chapter.

3.4.2 Domain-wall localization at the first-order transition

A non-trivial density profile on the coexistence line $\alpha = \beta < 1/2$ can be explained by the domain-wall approach discussed in detail in chapter 2.3.3. Justification of this approach stems from the fact that in the hydrodynamic limit we got a viscous Burgers equation with fractional diffusive term that gives stable shock as a possible solution. As the width of the shock is of the order of the lattice constant a, for the instantaneous profile of the domain wall we can assume a step function,

$$\rho_s(x) = \begin{cases} \alpha & x < x_s \\ 1-\beta & x > x_s. \end{cases}, \tag{3.57}$$

where x_s is the current position of the domain wall. As in TASEP with Langmuir kinetics described in chapter 2.4.1, the hopping probabilities of the domain wall to the neighbouring sites turn out to be spatially dependent because of the spatial dependence of the total current of particles entering the left or exiting the right of the domain wall's position. According to the expression (2.97), the probability r_i that the domain wall moves from i to $i+1$ is equal to the difference of currents of particles entering to and exiting from the domain of density $1-\beta$, divided by the height of the domain wall $1-\alpha-\beta$,

$$r_i = \frac{1}{1-\alpha-\beta}\left[\sum_{j=i}^{L}\beta_j(1-\beta) - \sum_{j=i}^{L}\alpha_j\beta\right], \quad i = 1, ..., L. \tag{3.58}$$

Similarly, the probability l_i that the domain wall moves from i to $i-1$ is equal to

the difference of currents of particles entering to and exiting from the domain of density α, divided by the height of the domain wall $1-\alpha-\beta$,

$$l_i = \frac{1}{1-\alpha-\beta}\left[\sum_{j=1}^{i-1}\alpha_j(1-\alpha) - \sum_{j=1}^{i-1}\beta_j\alpha\right], \quad i = 2, ..., L+1. \tag{3.59}$$

Since the domain wall is reflecting at the boundaries, we also have $l_1 = r_{L+1} = 0$.

If the domain-wall's velocity $v_i = r_i - l_i$ is calculated from the expressions (3.58) and (3.59), it becomes clear that for $\alpha < \beta$ the velocity is always positive, $v_i > 0$, which means that the domain wall remains close to the right boundary yielding low-density phase in the bulk. For $\alpha > \beta$ its velocity is on the other hand always negative, $v_i < 0$, and the domain wall resides close to the left boundary resulting in the high-density phase in the bulk. Compared to the short-range model, a difference is found on the coexistence line $\alpha = \beta < 1/2$ where v_i does not vanishes (except at the special site $i = L/2+1$), but is instead positive for $1 \leq i < L/2+1$ and negative for $L/2+1 < i \leq L+1$, while its absolute value increases as the boundaries are approached. In other words, the velocity of the domain wall is always directed towards centre but increases away from it. A question that immediately arises is whether a localization of the domain wall is possible in the centre in a sense that the standard deviation of its position $\Delta_L = [\langle x_s^2\rangle - \langle x_s\rangle^2]^{1/2}$ increases slower than L in the limit $L \to \infty$,

$$\lim_{L\to\infty} \Delta_L/L = 0 \quad \Leftrightarrow \quad \text{localization} \tag{3.60}$$

[In upper expression, thermodynamic limit is necessary since a finite system is always ergodic and therefore no localization occurs.]

An answer to this question brings us to the stationary equations for the probability distribution P_i of the domain wall's position i

$$r_{i-1}P_{i-1} + l_{i+1}P_{i+1} - (r_i + l_i)P_i = 0, \quad i = 2, ..., L \tag{3.61}$$

$$l_2P_2 - r_1P_1 = 0 \tag{3.62}$$

$$r_LP_L + -l_{L+1}P_{L+1} = 0. \tag{3.63}$$

The solution to the upper system of equations can be found in the closed form [73],

$$P_i = \frac{1}{Z_L}\prod_{j=1}^{i-1}\frac{r_j}{l_{j+1}} \equiv \frac{1}{Z_L}e^{-V_i}, \tag{3.64}$$

where Z_L is the normalization constant, and V_i is the "potential" defined as

$$V_i = -\sum_{j=1}^{i-1}\ln\frac{r_j}{l_{j+1}}, \qquad q < i \leq L+1. \tag{3.65}$$

Once P_i's are known, stationary density profile follows from [73]

$$\langle \tau_i \rangle^{DW} = \left(\sum_{j=i+1}^{L+1} P_j \right) \alpha + \left(\sum_{j=1}^{i} P_j \right) (1 - \beta). \tag{3.66}$$

The upper expression can be used to calculate density profiles and to compare them to the results of numerical simulations, as depicted in figures 3.8a and 3.8b for $\sigma = 1.5$ and 3, respectively, which show excellent agreement in all cases. We also notice that for $\sigma = 1.5$ the deviation in domain wall's position decreases as the system size L is increased, contrary to the case $\sigma = 3$ where density profiles attain almost linear profile. A way to determine if localization occurs or not would be to calculate Δ_L as a function of L for several values of σ. As depicted in figure 3.9, Δ_L displays a rather good agreement with a power law

$$\Delta_L \sim \begin{cases} L^{\frac{\sigma}{2}} & 1 < \sigma < 2 \\ L & \sigma > 2. \end{cases} \tag{3.67}$$

meaning that the domain wall is localized for $1 < \sigma < 2$ and delocalized for $\sigma > 2$.

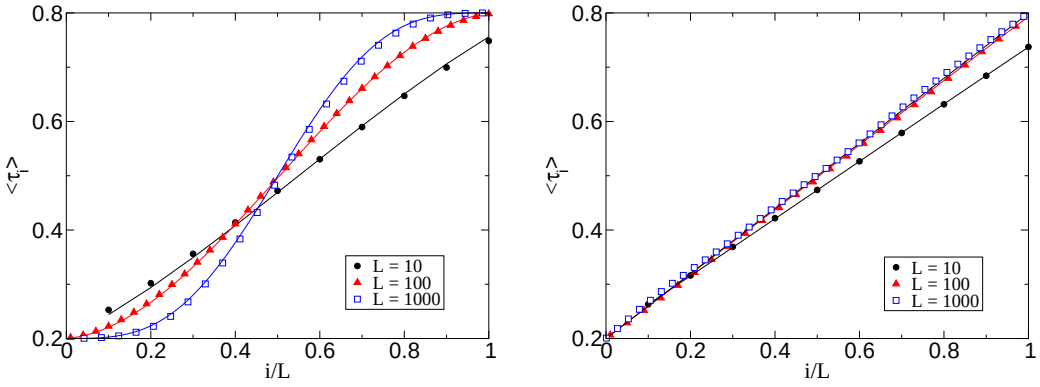

Figure 3.8: Comparison of density profiles obtained from Monte Carlo simulations (symbols) and using the domain-wall approach (lines) for various systems sizes L and for (a) $\sigma = 1.5$ and (b) $\sigma = 3$. In both cases $\alpha = \beta = 0.2$.

The power law dependence 3.67 can be in fact derived analytically. The starting point is to replace r_i, l_i, P_i and V_i with their continuous counterparts $r(x)$, $l(x)$, $P(x)$ and $V(x)$ for fixed $x = i/L$ in the limit $L \to \infty$. For example,

$$L \cdot P_{i/L} \to P(x). \tag{3.68}$$

If we define a discrete n-th order derivative of V_i at site i as $\Delta_i^{(n)} \equiv \Delta_{i+1}^{(n-1)} - \Delta_i^{(n-1)}$ with $\Delta_i^{(1)} = V_i - V_{i-1}$, then the continuous limit yields

$$L^n \cdot \Delta_i^{(n)} \to \frac{d^n}{dx^n} V(x). \tag{3.69}$$

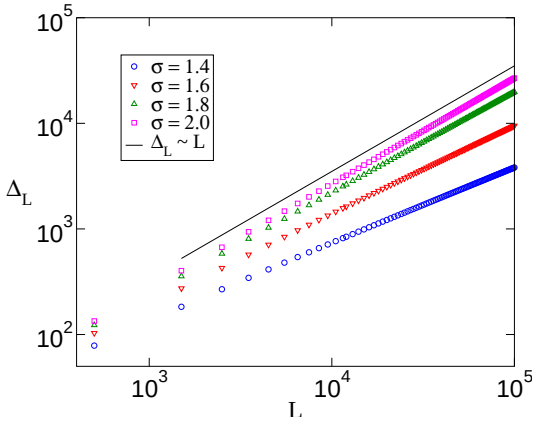

Figure 3.9: Standard deviation of the domain wall's position Δ_L as a function of the system size L for various σ and for $\alpha = \beta = 0.1$.

For example, the first- and the second-order derivatives are

$$L \cdot \ln\left(\frac{r_{i-1}}{l_i}\right) \to \frac{d}{dx}V(x) \tag{3.70}$$

$$L^2 \cdot \ln\left(\frac{r_i \cdot l_i}{r_{i-1} \cdot l_{i+1}}\right) \to \frac{d^2}{dx^2}V(x). \tag{3.71}$$

For $\alpha = \beta$ we have $r_i = l_{L-i+2}$ yielding a Taylor series of the "potential" $V(x)$ around $x = 1/2 + 2/L$ that contains only even powers of $(x - 1/2)$,

$$V(x) = V(1/2) + \underbrace{\frac{1}{2!}\left.\frac{d^2V}{dx^2}\right|_{x=1/2}}_{c_2}\left(x - \frac{1}{2}\right)^2 + \underbrace{\frac{1}{4!}\left.\frac{d^4V}{dx^4}\right|_{x=1/2}}_{c_4}\left(x - \frac{1}{2}\right)^4 + \dots \tag{3.72}$$

From here, the lowest-order approximation gives the Gaussian distribution from where the standard deviations Δ_L proportional to $L/\sqrt{c_2}$ follows. The calculation of Δ_L is thus reduced to the calculation of c_2 related to the second-order derivative of $V(x)$ at $x = 1/2$. Spatial dependence of V_i justifying the Gaussian approximation is depicted in figure 3.10.

To calculate c_2 we start from the more compact form of sums that are found in expressions (3.58) and (3.59) for r_i and l_i,

$$\sum_{j=1}^{i-1}\alpha_i = \alpha\left\{\lambda_L\frac{\zeta_{i-1}(\sigma)}{\zeta_L(\sigma)} + (i-1)\left[1 - \frac{\zeta_{i-1}(\sigma+1)}{\zeta_L(\sigma+1)}\right]\right\}, \tag{3.73}$$

$$\sum_{j=i}^{L}\alpha_i = \alpha\lambda_L - \sum_{j=1}^{i-1}\alpha_i \tag{3.74}$$

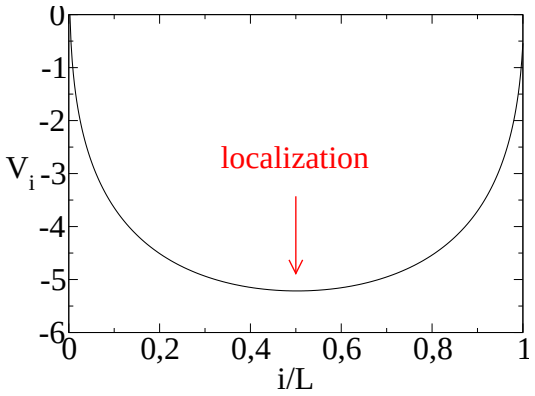

Figure 3.10: Spatial dependence of "potential" V_i for $1 < \sigma < 2$. Minimum of the "potential" is located at the localization site of the domain wall in the limit $L \to \infty$.

$$\sum_{j=1}^{i-1} \beta_i = \beta \left\{ \lambda_L \left[1 - \frac{\zeta_{L-i}(\sigma)}{\zeta_L(\sigma)} \right] - (L - i + 1) \left[1 - \frac{\zeta_{L-i}(\sigma+1)}{\zeta_L(\sigma+1)} \right] \right\}, \tag{3.75}$$

$$\sum_{j=i}^{L} \beta_i = \beta\lambda_L - \sum_{j=1}^{i-1} \beta_i \tag{3.76}$$

where $\zeta_n(s)$ denotes the partial sum of the Zeta function $\zeta(s)$,

$$\zeta_n(s) = \sum_{k=1}^{n} \frac{1}{k^s}. \tag{3.77}$$

To estimate $\zeta_n(s)$, we may use the Euler-Maclaurin series, which yields

$$\zeta_n(s) = \zeta(s) - \frac{1}{(s-1)} \frac{1}{n^{s-1}} + \int_n^\infty \frac{x - \lfloor x \rfloor}{x^{s+1}} dx, \tag{3.78}$$

where the last term can be neglected because it is of order $O(n^{-s})$. Inserting (3.78) in (3.58) and (3.59), and replacing i with $x = i/L$, in the limit $L \to \infty$ we get

$$r(x) \simeq \frac{\beta(1-\beta)}{1-\alpha-\beta} \left[\lambda_L + \frac{f(x,\sigma,\alpha,\beta)}{L^{\sigma-1}} \right], \quad 0 \ll x \ll 1, \tag{3.79}$$

$$l(x) \simeq \frac{\alpha(1-\alpha)}{1-\alpha-\beta} \left[\lambda_L + \frac{f(1-x+2/L,\sigma,\beta,\alpha)}{L^{\sigma-1}} \right]., \quad 0 \ll x \ll 1, \tag{3.80}$$

where $f(x,\sigma,\alpha,\beta)$ is analytic for $0 < x < 1$, which is all that matters. Inserting $r(x)$ and $l(x)$ in $\Delta_i^{(2)}$ and $\Delta_i^{(4)}$ we arrive at

$$c_2 = \frac{1}{2} \frac{d^2}{dx^2} V(x) \Big|_{x=1/2} \simeq -\frac{2f'(1/2,\sigma,\alpha,\alpha)}{\lambda\alpha(1-\alpha)} L^{2-\sigma}, \tag{3.81}$$

$$c_4 = \frac{1}{24}\,\frac{d^4}{dx^4}V(x)\bigg|_{x=1/2} \simeq -\frac{2f'''(1/2,\sigma,\alpha,\alpha)}{\lambda\alpha(1-\alpha)}L^{2-\sigma}, \tag{3.82}$$

which gives the desired dependence Δ_L on L.

Let us mention that the functional form $\Delta_L \propto L^{a/2}$ for $1 < a < 2$ is found in the short-range model with Langmuir kinetics as well, where rates of absorption and desorption equal [81],

$$\omega_A = \frac{\Omega_A}{L^a}, \quad \omega_D = \frac{\Omega_D}{L^a}. \tag{3.83}$$

A similarity with the long-range model is unveiled only when α_i and β_i are calculated in the continuous limit,

$$\alpha_i \quad \to \quad \alpha(x) \simeq \frac{\alpha}{\zeta(\sigma+1)\sigma}\left[(x-1/L)^{-\sigma}-1\right]L^{-\sigma}, \tag{3.84}$$

$$\beta_i \quad \to \quad \beta(x) \simeq \frac{\beta}{\zeta(\sigma+1)\sigma}\left[(1-x)^{-\sigma}-1\right]L^{-\sigma}, \tag{3.85}$$

where they display the same power law in L, but of the different origin: in [81] the power law is postulated while in the long-range model it follows naturally from the non-local transport on a finite segment.

3.4.3 σ-dependent exponent at the second-order transition

The results of Monte Carlo simulations, as presented in chapter 3.4.1, have shown that even in the long-range model there occurs a continuous phase transition from the low- or high-density phase to the maximum current phase. In the short-range model we have seen that this transition is, much like the whole maximum-current phase, characterized by long-range correlations reflected in power-law decay of the local density away from the boundaries with the exponent 1/2. Considering our experience with equilibrium phase transitions in systems with long-range interactions, it is to be expected that the long-range hopping will alter this behaviour as well.

The power-law dependence of the density profile in the maximum current phase can be checked using Monte Carlo simulations. If such a dependence exists then for the deviation of the local density from the mean density 1/2, $\Delta\rho(n,L) \equiv |\langle\tau_n\rangle - 1/2|$, the following scaling relation applies

$$\Delta\rho(n,L) = L^{-\mu}f(n/L), \tag{3.86}$$

where $f(x) \propto x^{-\mu}$ for $0 \ll x \ll 1/2$, and μ is the appropriate critical exponent. The upper relation means that for two different system sizes L_1 and L_2 one must have

$$\Delta\rho(n, L_1) = \left(\frac{L_2}{L_1}\right)^{\mu} \Delta\rho(n, L_1). \tag{3.87}$$

Figures 3.11a and 3.11b depict $\Delta\rho(n, L)$ and $L^{\mu}\Delta\rho(n, L)$, respectively, for three different system sizes, $L = 800$, 1500 and 5000, and $\sigma = 1.5$, where the best graph overlapping is obtained for $\mu = 0.25$. The same analysis was performed in figure 3.12 for different values $\sigma = 1.2$, 1.5 and 1.8 yielding the dependence $\mu(\sigma) = (\sigma - 1)/2$ for $1 < \sigma < 2$. Together with $\mu = 1/2$, obtained in the short-range limit $\sigma > 2$ in which the normal diffusive term is replaced by the fractional one, we conclude the following expression for $\mu(\sigma)$

$$\mu(\sigma) = \min\left\{\frac{\sigma - 1}{2}, \frac{1}{2}\right\}, \quad \sigma > 1. \tag{3.88}$$

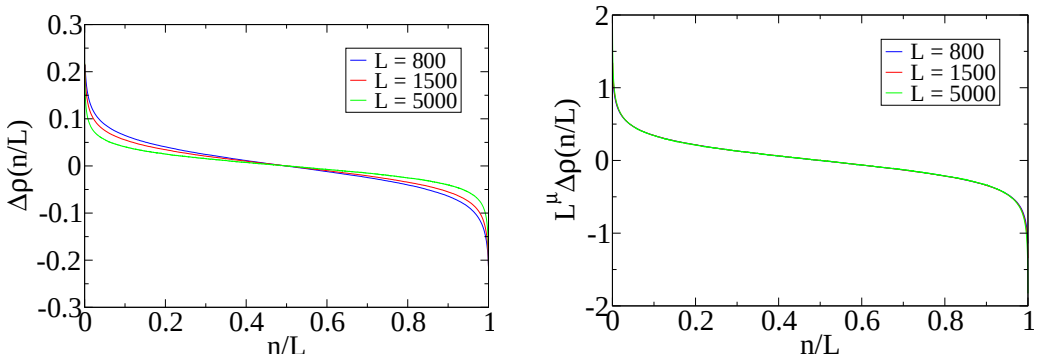

Figure 3.11: Deviation of the local density from the mean density 1/2 for $\alpha = \beta = 0.8$, $\sigma = 1.5$ and different system sizes L (a) before applying the scaling relation (3.86) and (b) after.

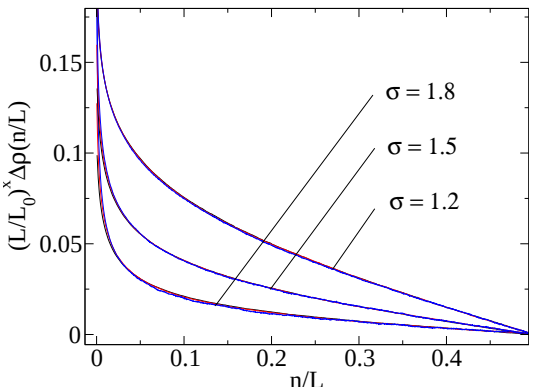

Figure 3.12: Deviation of the local density from the mean density 1/2 for $\alpha = \beta = 0.8$ and various σ. All profiles $\Delta\rho(n, L)$ corresponding to the same σ, but different system size $L = 800$, 1500 and 5000 have been scaled to the one for $L_0 = 5000$ according to the expression (3.87).

In the reminder of this chapter we are going to derive the conjectured expression (3.88). Unfortunately, in doing so the long range of hopping deprive us of many analytical approaches that were applied earlier to the short-range model. In a situation like this, the only approach that surfaces is the mean-field approximation. Besides being a natural choice to start with, the motivation inspires from the work of Krug [13], who starts from the stationary viscous Burgers equation with boundary conditions $\rho(0) = \rho_0$ and $\rho(L) = 0$, $L \to \infty$

$$D\frac{d\rho}{dx} = \rho(1-\rho) - j, \tag{3.89}$$

where current j is an unknown. For $\rho_0 > \rho^*$, where $\rho^* = 1/2$ is density at which $j(\rho)$ attains its maximum, Krug shown that the deviation of the local density from its bulk value ρ^* obeys a power law,

$$\rho(x) \simeq \frac{1}{2} + \frac{D}{x}, \quad x \gtrsim D/(\rho_0 - \rho^*), \quad \rho_0 > \rho^*. \tag{3.90}$$

Although it is, of course, the same power law (2.48) that follows from the analytical solution of the discrete mean-field equations, the above approach gains in importance when the exact solution to the mean-field equations is unknown. In the case of long-range hopping, this motivate us to use the hydrodynamic equations (3.44) and (3.45) with appropriate non-local "boundary" conditions to calculate the unknown exponent $\mu(\sigma)$.

We start from the equations for the mean density ρ_n, $n = 1, \ldots, L$, written in the mean-field approximations,

$$\frac{d}{dt}\rho_n = \alpha_n(1-\rho_n) + \sum_{m=1}^{n-1} p_{n-m}\rho_m(1-\rho_n) - \sum_{m=n+1}^{L} p_{m-n}\rho_n(1-\rho_m) - \beta_n\rho_n, \tag{3.91}$$

$$\frac{d}{dt}\rho_1 = \alpha_1(1-\rho_1) - \sum_{m=2}^{L} p_{m-1}\rho_1(1-\rho_m) - \beta_1\rho_1, \tag{3.92}$$

$$\frac{d}{dt}\rho_L = \alpha_L(1-\rho_L) + \sum_{m=1}^{L-1} p_{L-m}\rho_m(1-\rho_L) - \beta_L\rho_L, \tag{3.93}$$

Assuming non-local "boundary" conditions,

$$\rho_n = \begin{cases} \alpha, & -L < n \le 0 \\ 1-\beta, & L < n \le 2L, \end{cases} \tag{3.94}$$

the upper equations can be written in a form as if the system was infinite

$$\frac{d}{dt}\rho_n(t) = \sum_{r=1}^{L} p_r(\Delta_r^+\rho_n - \Delta_r^-\rho_n) - \sum_{r=1}^{L} p_r\left[(1-\rho_n)\Delta_r^+\rho_n + \rho_n\Delta_r^-\rho_n\right]. \tag{3.95}$$

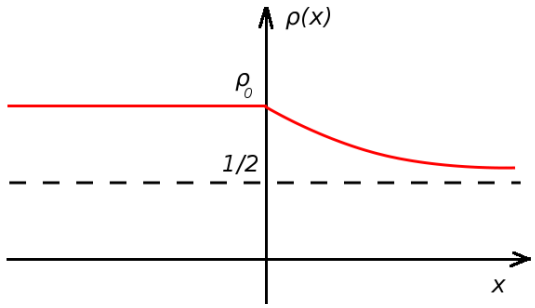

Figure 3.13: Schematic picture of the assumed solution $\rho(x)$ consisting of power-law decay for $x > 0$ and a constant profile for $x < 0$ which is equivalent to the boundary condition (3.96).

In this way the coupling of local density to α_n and β_n is already implied by the definition of the boundary conditions (3.94), which opens a pathway to the application of the hydrodynamic equations to an open system. Since we are interested solely in obtaining the exponent $\mu(\sigma)$ instead of the full solution, we may instead consider an equivalent infinite system and assume the stationary solution of the following form (figure 3.13),

$$\rho(x) = \begin{cases} \rho_0, & -\infty < x < 0 \\ \frac{1}{2} + \phi(x), & 0 < x < \infty \\ 1/2, & x \to \infty. \end{cases} \tag{3.96}$$

where the function $\phi(x)$ is assumed to take the asymptotic form $\phi(x) \propto (x/a)^{-\bar{\mu}} = n^{-\bar{\mu}}$. By inserting (3.96) in hydrodynamic equations (3.44) and (3.45) we obtain the following terms in a for $1 < \sigma < 2$,

$$-\kappa\phi(x)\frac{\partial\phi(x)}{\partial x} \simeq -\bar{\mu}|\kappa|a^{2\bar{\mu}}x^{-2\bar{\mu}-1}, \tag{3.97}$$

$$a^{\sigma-1}\nu_\sigma\Delta_\sigma\phi(x) \simeq \frac{\phi(0)}{\sigma\zeta(\sigma+1)}a^{\sigma-1}x^{-\sigma} + O(a^{\sigma-1+\bar{\mu}}x^{-\sigma-\bar{\mu}}), \tag{3.98}$$

where $\phi(0) = \rho_0 - 1/2$. It turns out that the lowest-order term in powers of a in equation (3.98) originates from the constant density profile for $x < 0$. [One should not worry about the non-linear term $a^{\sigma-1}\phi H\phi$, already neglected in our earlier calculations, because it happens to be of the higher order $O(a^{\sigma-1+\bar{\mu}}x^{-\sigma-\bar{\mu}})$.] Since in the stationary limit the l.h.s. of (3.44) equals zero, $\partial\phi/\partial t = 0$, the two lowest-order terms must be of the same order (but of the opposite sign!) yielding

$$2\bar{\mu} = \sigma - 1 \quad \Rightarrow \quad \bar{\mu} = \frac{\sigma-1}{2}, \quad 1 < \sigma < 2. \tag{3.99}$$

A similar analysis can be performed for $\sigma > 2$, differing only in the fact that now both local $a\Delta\phi(x)$ and non-local $a^{\sigma-1}\Delta_\sigma\phi$ diffusive terms must be taken into account. The only new term to estimate is $a\Delta\phi(x)$,

$$a\nu_2\Delta\phi(x) \sim |\nu_2|\bar{\mu}(1+\bar{\mu})a^{1+\bar{\mu}}x^{-\bar{\mu}-2}. \tag{3.100}$$

If we compare the lowest-order term we arrive at the following equation for μ, $2\bar{\mu} = \min\{\sigma - 1, 1 + \bar{\mu}\}$, yielding the following $\bar{\mu}$

$$\bar{\mu} = \begin{cases} \frac{\sigma-1}{2}, & 2 < \sigma < 3, \\ 1, & \sigma > 3 \end{cases} \tag{3.101}$$

The expressions (3.99) and (3.101) can be written in the more compact form

$$\bar{\mu}(\sigma) = \min\left\{\frac{\sigma-1}{2}, 1\right\}. \tag{3.102}$$

For $1 < \sigma < 2$, the exponent $\bar{\mu}$ is identical to the one that was conjectured based on Monte Carlo simulations. On the other hand, the difference is found in the limiting σ for which the (mean-field) short-range regime $\bar{\mu} = 1$ sets in: according to (3.102), the limiting σ is 3 instead of 2. Based on that we may conclude that the mean-field approximation is applicable for $1 < \sigma < 2$, while for $2 < \sigma < 3$ the non-local boundary terms are obviously of higher order than the missing terms that stem from the correlations neglected by the mean-field approximation.

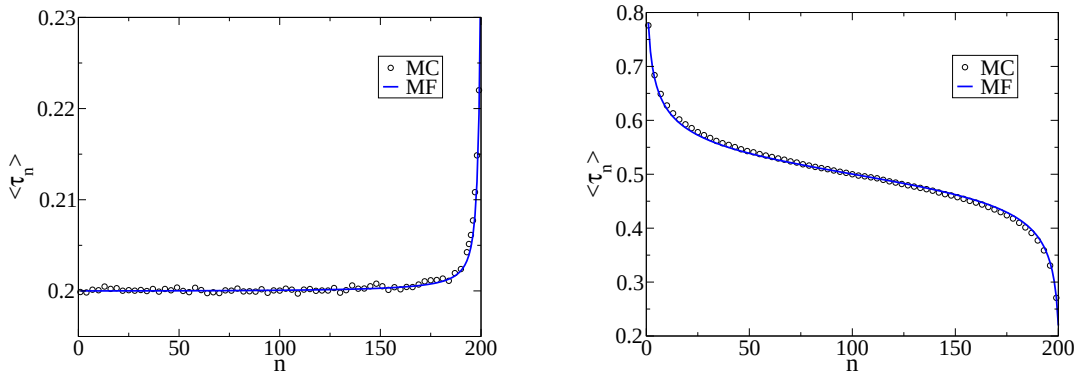

Figure 3.14: Comparison of the density profiles in TASEP with long-range hopping (a) in the low-density phase ($\alpha = 0.2$ and $\beta = 0.7$) and (b) in the maximum-current phase ($\alpha = 1.0$ and $\beta = 1.0$), obtained by Monte Carlo simulations (symbols) and in the mean-field approximation (line) for $\sigma = 1.8$.

3.4.3.1 Numerical solution of the mean-field equations

The upper conclusions can be checked directly by solving the mean-fied equations (3.91)-(3.93) numerically in the stationary limit, reducing the problem to finding a zero of a non-linear system of L equations in L unknowns. Of various available software packages, we decided to use the HYBRD algorithm taken from the MIN-

PACK library[2]. Figures (3.14a) and (3.14b) depict numerical solutions for $\sigma = 1.8$ and α and β which correspond to the low-density phase and the maximum-current phase (the high-density phase can be easily obtained using the symmetry (2.45)). We find an excellent agreement generally in all cases, the only two exceptions being the profiles on the coexistence line $\alpha = \beta < 1/2$ (figure 3.15a) and naturally, in the short-range limit for $\sigma > 2$ (figure 3.15b). In the first case the disagreement is displayed in the smearing out of the density profile and can be fixed by taking into account fluctuations in the domain wall's position, as it was discussed in length in the previous chapter. The second case, on the other hand, is "hopeless" - mean-field approximation in the short-range limit neglects the crucial contribution stemming from the correlations and cannot describe the maximum-current phase correctly.

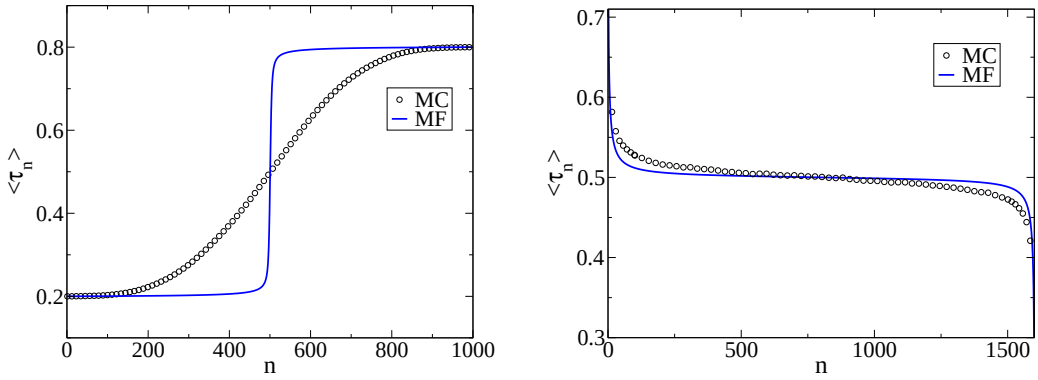

Figure 3.15: Comparison of the density profiles in TASEP with long-range hopping (a) on the coexistence line ($\alpha = \beta = 0.2$, $\sigma = 1.8$) and (b) in the maximum-current phase ($\alpha = 1.0$ and $\beta = 1.0$, $\sigma = 2.5$), obtained by Monte Carlo simulations (symbols) and in the mean-field approximation (line).

* * *

The long-range model, pictured to examine the robustness and universality of phase transitions in ASEP, has in many ways met our initial expectations. We have shown that the phase diagram remained the same except at the transition lines. The applicability of the mean-field approximation, common to many models with long-range interactions, enabled us to investigate the character of phase transitions using the underlying hydrodynamic equation yielding several important results: (a) the long-range hopping being reflected in the non-local diffusion that ensures that the domain wall remains microscopically sharp in the course of the time evolution, (b) the value of the dynamical exponent $z = \min\{\sigma, 3/2\}$ related to the

[2]http://www.netlib.org/minpack/

relaxation towards the stationary state in the maximum-current phase and (c) the short-range limit being attained for $\sigma > 2$.

Applying the hydrodynamic approach to an open system gives a correct σ-dependent exponent in the maximum-current phase and predicts the localization of the domain wall on the coexistence line. Compared to the results obtained by Monte Carlo simulations, the smearing of the density profile turns out to be too short, while the correct result is obtained by picturing domain wall as a random walker moving in a potential with a global minimum.

4

Phase separation induced by a single defect

In previous two chapters we achieved a non trivial stationary state by bringing the system in contact with reservoirs of different densities. This chapter shall deal with a different problem in which a non trivial stationary state is achieved by adding a single localized defect or impurity from which the particles move with reduced probability $r < 1$. The importance of the model also lies in the fact that the question of whether the defect will necessary cause phase separation irrespective of the value of the parameter r, still remains open.

Aside from the fact that the exact solution is eluding us for over 20 years, an additional issue is that the mean-field approximation gives a trivial result $r_c = 1$ i.e. homogeneous limit without defect. In chapter 4.2 we shall introduce an impurity in TASEP with long-range hopping in which it is possible to achieve a transition into a regime without phase separation by varying the range of hopping σ. Finally, we shall present a way to determine (possibly) the exact transition point using the mean field approximation [131].

4.1 Short-range ASEP with a defect site

We consider TASEP on a periodic lattice consisting of L sites and $N = \rho \cdot L$ particles whose propagation on a lattice is described by the random-sequential dynamics with hopping probability 1. The exception is a fixed site e.g. $i = L$, from which the particle moves with a probability r smaller than 1, $0 < r < 1$ (figure 4.1).

TASEP with a static defect and the random-sequential dynamics was first investigated by Janowsky and Lebowitz [59, 132]. In the stationary state they have found a domain wall that separates the macroscopic density phases ρ_- and ρ_+ (figure 4.2). They determined the densities ρ_- and ρ_+ in the mean-field approximation while neglecting any spatial dependence of the density $\langle \tau_i \rangle$,

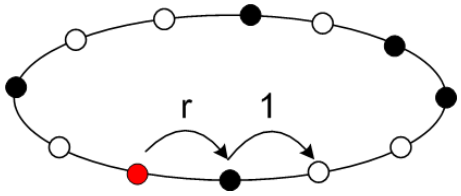

Figure 4.1: Schematic picture of TASEP with a static defect from which the particles move with reduced probability $0 < r < 1$. The probability of hopping from other sites is 1.

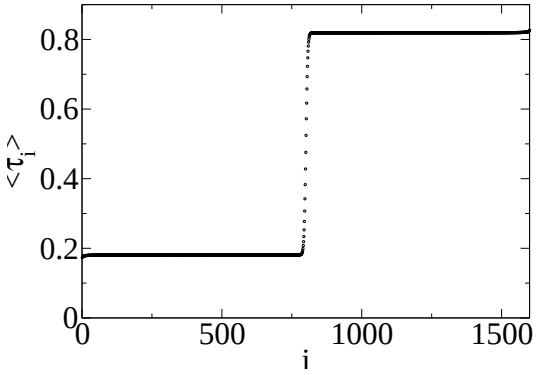

Figure 4.2: Density profile in TASEP with a single defect on site $i = L$ for $\rho = 1/2$ and $r = 0.2$ obtained with a Monte Carlo simulation of a system size $L = 1600$.

$$\langle \tau_i \rangle \approx \begin{cases} \rho_- & 1 \leq i < i_s \\ \rho_+ & i_s \leq i \leq L \end{cases} . \tag{4.1}$$

where i_s is the position of a domain wall. Considering that the density is homogeneous both far from defect and the domain wall, and that the current j is always preserved, we have

$$j = \rho_-(1 - \rho_-) = \rho_+(1 - \rho_+), \tag{4.2}$$

which leads to $\rho_- = \rho_+$ or $\rho_- = 1 - \rho_+$. Ignoring the correlations close to the defect, the conservation of the current furthermore leads to

$$j = r\rho_-(1 - \rho_+), \tag{4.3}$$

giving

$$\rho_- = \frac{r}{1+r}, \quad \rho_+ = \frac{1}{1+r}. \tag{4.4}$$

If we additionally use the conservation of the total number of particles then we can determine the position of the domain wall from

$$\rho_- i_s + \rho_+(L - i_s) = \rho, \tag{4.5}$$

which gives

$$i_s = \frac{1 - \rho(1 + r)}{1 - r} L. \tag{4.6}$$

To determine the smearing out of the domain wall, Janowsky and Lebowitz use the concept of *second-class* particles, that in interaction with other (ordinary) particles behave like a hole and in interaction with holes like an ordinary particle. In accordance with this rule, the movement of the second-class particle is always directed towards the domain wall, and it turns out that it loosely follows its current position, which gives a simple means to follow its movement through the system. By using the Monte Carlo simulations, Janowsky and Lebowitz have demonstrated that the standard deviation of position ξ_L of the second-class particle depends on the system size L as $\xi_L \propto L^{1/2}$ if $\rho \neq 1/2$ and $\xi_L \propto L^{1/3}$ if $\rho = 1/2$. The difference in the behaviour for $\rho \neq 1/2$ and $\rho = 1/2$ can be interpreted in the following way [59]. The hop of the particle from the defect site $i = L$ consists of the two dependent events: hopping of the particle to the right and the hopping of the hole to the left. The particle then moves towards the domain wall with an average velocity $1 - \rho_-$, while the hole moves with the velocity $-\rho_+ = -(1 - \rho_-)$. For $\rho \neq 1/2$ the position of the domain wall is stay away from the centre, from which it follows that the arrivals of the particles and holes at the domain wall are mutually independent events. The fluctuations in the position of the domain wall are in that case determined by the statistics of the particle hopping over the defect, i.e. by the statistics of creating pairs of particles/holes. On the other hand, for $\rho = 1/2$ the domain wall is in the centre, so that the arrivals of particles and holes occur at the same time. Unlike the previous case, the fluctuations in the position of the domain wall are now determined by the deviations of the local velocity of particles and holes from their mean velocities $1 - \rho_-$ and $-\rho_+$.

4.1.1 Unresolved issues

For this model the open question is whether there exists such an r_c that for all r such that $r_c < r < 1$ the defect does not induce phase separation ($\rho_- \neq \rho_+$), but instead gives the local density $\langle \tau_i \rangle \approx \rho_- = \rho_+ = 1/2$. History of this problem is long, stretching way back to 1990 when Wolf and Tang proposed the so-called RSOS model of surface growth in the presence of a line defect [101]. This model can be translated on to TASEP by the transformation $h_i - h_{i-1} = 1 - 2\tau_i$, where h_i is the height of the surface on the location i (see 2.2.1), in which case the defect corresponds to the line defect on the line $x = x_0$ along which the surface grows slower. If we denote $h(x, t)$ the height of the surface at the point x and at the time t, the deviation $h(x, t)$ from the average surface slope $[h(0, t) - h(L, t)]/L$ equals

$$\Delta\bar{h}(x) = \frac{1}{T}\int_0^T \left[h(x,t) - h(0,t) - x\frac{h(L,t) - h(0,t)}{L}\right] dt, \tag{4.7}$$

where the time averaging is made over a long time interval $T \to \infty$. By introducing the defect at x_0, surface deformation occurs in the sense that

$$d = \frac{1}{L}\sum_{x=0}^{L} \Delta\bar{h}(x) - \Delta\bar{h}(x_0) \neq 0 \tag{4.8}$$

as depicted in figure 4.3. The surface is said to be deformed either *weakly* if $d \sim L^\gamma$ with $\gamma < 1$, because then $lim_{L\to\infty} d/L = 0$, or *strongly* when $\gamma = 1$ for which $lim_{L\to\infty} d/L > 0$. In their paper Wolf and Tang concluded that $\gamma = 1$, i.e. that the surface is always strongly deformed, by using computer simulations of the RSOS model and by solving the KPZ equation analytically. In a similar growth model, a one that can be directly mapped to TASEP, Kandel and Mukamel demonstrated both regimes, depending on the strength of the defect [133].

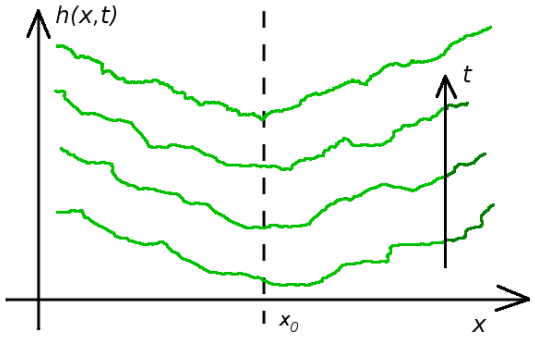

Figure 4.3: The sketch of the surface growth in a so-called RSOS model in the presence of a line defect on the line $x = x_0$ alogn which the growth speed is smaller.

If we map the problem of surface deformation back to TASEP, the order parameter d can be annotated as

$$d = \frac{2}{L}\sum_{i=1}^{L} i\left(\langle\tau_i\rangle - \frac{1}{2}\right) - \frac{L(L+1)\Delta}{2L^2}, \tag{4.9}$$

where Δ denotes average surface tilt, which in TASEP corresponds to $L - 2N$ and is constant in time due to periodic boundary conditions. From here we easily deduce that by inserting e.g. the approximate solution (4.1) into the expression for d we get only strong deformation $d \propto L$. There is, however, some more recent research that leaves the possibility of a weak deformation [134].

Using the KPZ equation, TASEP can be also linked to the model of directed polymer in disordered media. On a plain, a polymer can be described using

a directed path from $(0,0,)$ to (x,t) but without intersections. The model then describes the transverse fluctuations of a polymer as described by the Hamiltonian

$$\mathcal{H}[x(t)] = \int dt' \left[\frac{\gamma}{2} \left(\frac{dx}{dt'} \right) + \eta(x',t') + V(x) \right] \tag{4.10}$$

where γ denotes the tension, $\eta(x,t)$ is the white noise describing the influence of the medium, $\langle \eta(x,t)\eta(x',t') \rangle = 2D\delta(x-x')\delta(t-t')$ and $V(x) = -\epsilon\delta(x)$ is the attractive potential localized on the line $x = 0$ (figure 4.4). If we denote partition function with $Z(x,t)$

$$Z(x,t) = \int_{(0,0)}^{(x,t)} \mathcal{D}x'(t') exp\{-\mathcal{H}/k_B T\}, \tag{4.11}$$

the connection with surface growth is obtained using the expression for the free energy $\mathcal{F}(x,t) = -k_B T Z(x,t)$ [135], which in the absence of defect ($V(x) = 0$) satisfies the KPZ equation

$$\frac{\partial \mathcal{F}}{\partial t} = \nu \frac{\partial^2 \mathcal{F}}{\partial x^2} + \frac{\lambda}{2} \left(\frac{\partial \mathcal{F}}{\partial x} \right)^2 + \eta, \tag{4.12}$$

where $\nu = k_B T/2\gamma$ with $\lambda = -1/\gamma$. Without defect, the transverse deviation of the polymer end $\delta x = \langle [x(t)]^2 \rangle^{1/2}$ behaves like $\delta x \propto t^{1/z}$, where $z = 3/2$ is the dynamical exponent of the KPZ equation. If we introduce the line defect using the potential $V(x) = -\epsilon\delta(x)$, then by varying its strength ϵ we can achieve the saturation $\delta x = \text{const.}$, i.e. the localization of polymer, which in TASEP corresponds to the phase coexistence. The non-trivial issue remains the value of threshold ϵ_c, which is such that the localization is lost for $\epsilon < \epsilon_c$. Due to the lack of an exact solution, the problem was addressed by several authors, often arriving to contradicting conclusions [136–141].

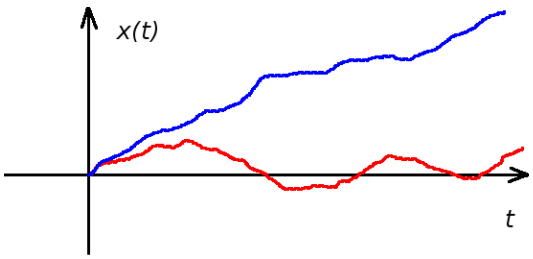

Figure 4.4: Visualisation of a delocalized (blue line) and a localized polymer (red line) in a presence of a line defect on a line $x = 0$.

In TASEP, the problem of absence of phase separation was researched by several authors. Schütz studied a version of TASEP in which the time evolution evolves in discrete time steps divided into two sub-steps [142]. In the first sub-

step the particles on sites $1, 3, \ldots$ are propagated one step to the right. Then in the second step only particles on sites $2, 4, \ldots$ propagate, the exception being the particle on site L, which in the second sub-step (L is even!) is propagated stochastically, i.e. with a probability $r < 1$. A model formulated in this manner can be solved exactly [142] and gives $r_c = 1$. One must bear in mind that the time evolution is here almost deterministic, and that the correlations between the particles are larger than in the model with the random-sequential dynamics.

The question of threshold r_c was tackled by both Janowsky and Lebowitz in their later paper [132], in which they solved the master equation for small systems consisting of only several sites and open boundary conditions, and calculated the current $j(r, \alpha = \beta = 1)$ for $\rho = 1/2$. If there is a threshold, there should be a change in current at r_c from the r-dependent function to a constant, $j = 1/4$. By expanding the current for a small r, Janowsky and Lebowitz shown that the lowest order terms do not change by increasing the system size L, and thus they obtained the expansion in r of the exact current $j_\infty(r, 1)$ of the infinite system,

$$j_\infty(r, 1) = r - \frac{3}{2}r^2 + \frac{19}{16}r^3 - \frac{21535}{27648}r^4 + \ldots. \tag{4.13}$$

By extrapolating the above expression to the larger values of r, they shown that there is no change of regime at least for $r \lesssim 0.8$.

The problem was again revived by Ha *et al.* in year 2003 [143]. They studied the problem of defect on a site $L/2$ in TASEP with open boundary conditions for $\alpha = 1 - \beta$. By observing how the appropriately selected order parameter $\rho_+(r, L) - \rho_-(r, L)$ scales with L, Ha *et al.* have arrived to best concordance with the power-law for $r_c = 0.80(2)$, surprisingly close to the result of Janowsky and Lebowitz. Their other interesting result considered the density profile. In the domain-wall phase, Ha *et al.* observed a power-law decay with the distance n from the defect

$$\langle \tau_n \rangle - \rho_- \sim -n^{-\nu}, \qquad \langle \tau_{L-n} \rangle - \rho_+ \sim n^{-\nu}, \quad 1 \ll n \ll L, \tag{4.14}$$

where $\nu = 1/2$[1] Similar power-law for $\rho_- = \rho_+ = 1/2$ can be observed in the shock-free phase, but with the corresponding exponent $\nu = 1/3$. In the surface growth context, such a profile leads to the weak deformation, which can be demonstrated by inserting $\langle \tau_i \rangle - 1/2 = L^{-1/3} f(i/L)$ into the expression (4.8) for the depth d of surface deformation

$$d(\Delta = 0) = \frac{2}{L} \sum_{i=1}^{L} i \left(\langle \tau_i \rangle - \frac{1}{2} \right) \approx \frac{2}{L} L^2 \int_0^1 dx \cdot x \cdot f(x) L^{-1/3} \propto L^{2/3}, \tag{4.15}$$

From here we see that the exponent γ in $d \propto L^\gamma$ is less than 1.

[1] A similar power-law behaviour was found by Janowsky and Lebowitz in their first paper on TASEP with a defect [59], but with the exponent $\nu = 1$.

The following part of the chapter 4 shall deal with our contribution to the problem of defect in TASEP by generalizing the model to long-range hopping. We will demonstrate that this enables us to keep the essential features of the short-range model, but it will also enable us to apply successfully the mean-field approximation that will provide us the way to determine analytically the non-trivial transition point at which the phase separation disappears.

4.2 Absence of phase separation in ASEP with long-range hopping

We consider TASEP on a $1d$ dimensional lattice with $L+1$ sites and $N = \rho L$ particles, and with periodical boundary conditions, where the site $L+1$ is acting as a static defect and cannot accept particles (figure 4.5). The particles are propagated by long range hopping and random-sequential dynamics, while the length of jumps $1 \leq l \leq L$ is selected from the probability distribution $p_l = l^{-(1+\sigma)}/\zeta_L(\sigma+1)$, where $\zeta_L(\sigma+1)$ is partial sum of the Zeta function. The jump is accepted if the site $i+l$ is empty, and is otherwise rejected. Impurity on site $L+1$ acts an obstacle because the particles have to jump over it, which is possible as long as $\sigma < \infty$. The advantage of the model lies in the fact that to vary the strength of impurity, one does not need any additional parameter beside σ. Thus any change of the regime in the model, if it exists, is a result of the change of parameter σ.

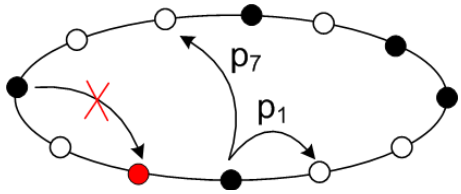

Figure 4.5: Schematic picture of TASEP with long-range hopping and a static impurity that is excluded from particle dynamics.

4.2.1 The results of Monte Carlo simulations

Typical results of Monte Carlo simulations for $\rho = 1/2$ are shown in figure 4.6. Similarly to the short-range model, we can observe two regimes separated by the threshold σ_c: for $\sigma > \sigma_c$ impurity in the system induces a domain wall that separates the macroscopic domains of density ρ_+ to the left and $\rho_- = 1 - \rho_+$ to the right of the impurity. On the other hand, for $1 < \sigma < \sigma_c$ the density profile organizes itself so that the domain wall does not exist, and that the current equals to the maximum current in the pure long-range model, $\lambda_L(\sigma)/4$. Similarity with a

short-range model is also seen in the spreading of the density profile, which is the result of the fluctuations in the domain wall's current position. Figure 4.7 depicts the dependence of the characteristic width ξ_L of this spreading on the system size L, derived by fitting the difference $\langle \tau_{n+1} \rangle - \langle \tau_n \rangle$ on the Gauss distribution for two different densities, $\rho = 0.5$ and $\rho = 0.55$. In both cases the results are in accordance with the aforementioned prediction that ξ_L is proportional to $L^{1/2}$ for $\rho \neq 1/2$ and to $L^{1/3}$ for $\rho = 1/2$.

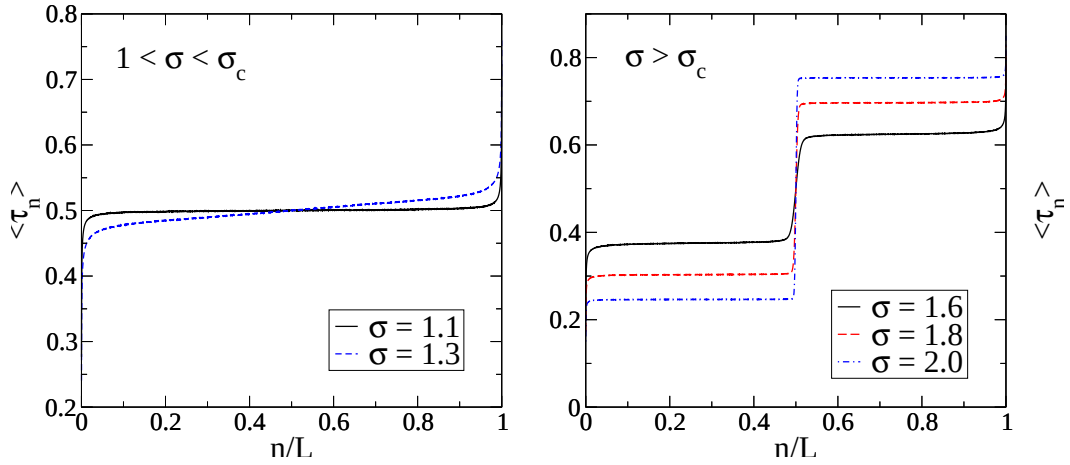

Figure 4.6: Density profiles in the phase without a domain wall for $\sigma = 1.1$ and 1.3 (left) and in the phase with a domain wall for $\sigma = 1.6, 1.8$ and 2 (right), derived from Monte Carlo simulations for a system of size $L = 6400$ and density $\rho = 1/2$, averaging by $t = 10^8$ MC steps/site.

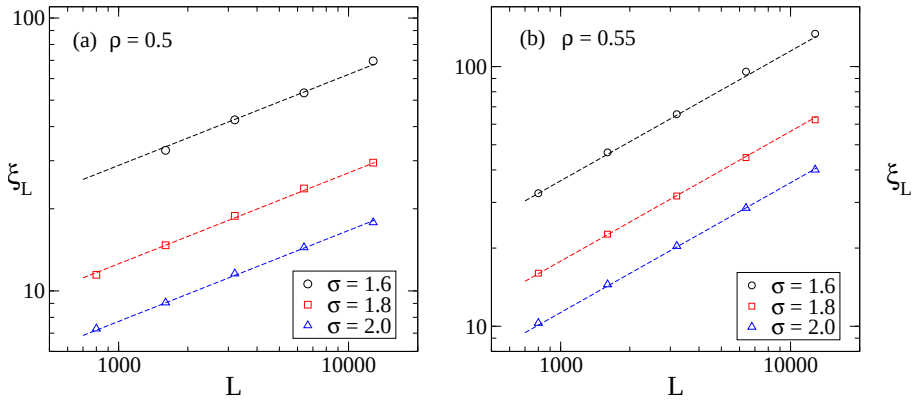

Figure 4.7: The width of the spreading of the density profile ξ_L as a function of system size for different values of parameter σ and density (a) $\rho = 1/2$ and (b) $\rho \neq 1/2$. Dashed lines represent the guide for the eye with slopes (a) 1/3 and (b) 1/2.

Considering the results of Ha *et al.*, it is interesting to check the deviation of density profiles from their mean densities ρ_- and ρ_+ in the shock phase, or from

their mean densities $\rho_- = \rho_+ = 1/2$ in the shock-free phase. As the densities ρ_- and ρ_+ are unknown, we will consider the deviations from densities $\langle\tau_{L/4}\rangle$ and $\langle\tau_{3L/4}\rangle$, considering the fact that sites $L/4$ and $3L/4$ are on the furthest point away from the domain wall and the impurity. In the domain of density $\rho_- = \langle\tau_{L/4}\rangle$, we assume the following density profile

$$\Delta\rho_-(n,L) \equiv \langle\tau_n\rangle - \langle\tau_{L/4}\rangle = L^{-\nu} f_-(n/L), \quad 1 \ll n \ll L/2, \tag{4.16}$$

where $f_-(x) \sim x^{-\nu}$ for $x \gg 1$. A similar form is also assumed in the density domain $\rho_+ = \langle\tau_{3L/4}\rangle$ using a particle-hole symmetry $\langle\tau_i\rangle = 1 - \langle\tau_{L-i+1}\rangle$, which is valid for $\rho = 1/2$. The scaling of density profiles according to the expression (4.16) is depicted in figure 4.8 for several values of parameters σ and L. The best overlapping of graphs is achieved if we presume $\nu = \sigma - 1$ for $\sigma < 2$ and $\nu = 1$ for $\sigma \geq 2$. As we see, in the shock phase the exponent of the power law becomes σ-dependent, while in the short-range limit for $\sigma > 2$ its value 1 equals to the exponent observed by Janowsky and Lebowitz in [59].

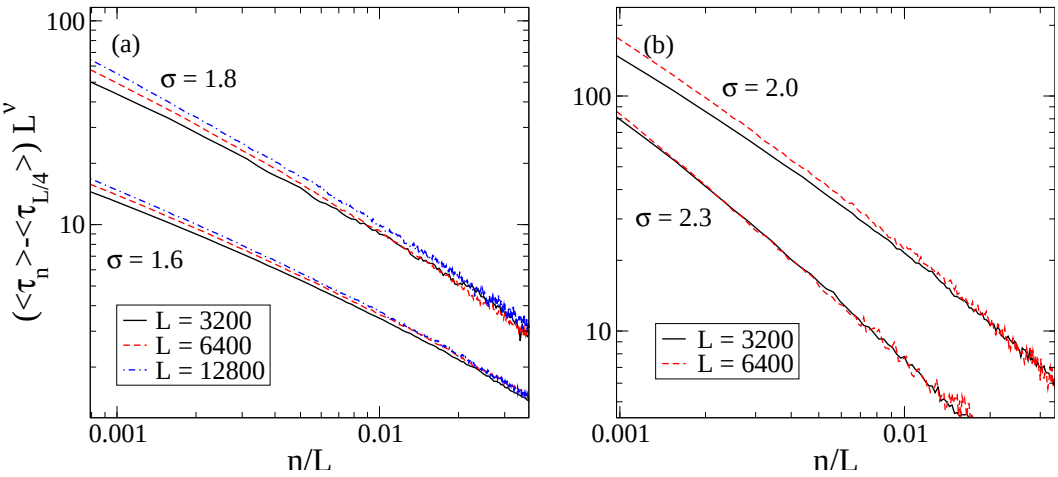

Figure 4.8: The deviation of density profile from $\rho_- = \langle\tau_{L/4}\rangle$ in the domain $1 \leq n \leq L/2$ for (a) $\sigma = 1.6$ and 1.8 and (b) $\sigma = 2$ and 2.3, for different system sizes $L = 3200$, 6400 and 12800. All profiles have been scaled in accordance with the expression (4.16) with (a) $\nu = \sigma - 1$ and (b) $\nu = 2$. The remaining parameters of the model are $\rho = 1/2$ and $t = 10^8$ MC steps/site.

The power law in density profile was also checked in the shock-free phase where $\rho_- = \rho_+ = 1/2$. Although the long-range correlations can still be observed, the density profile does not display simple scaling with a single exponent.

Finally, let us address the issue of the threshold σ_c. One should recall that in short-range model the threshold r_c is approximately (or at least) 0.8, close to the limit $r = 1$ of the pure system. Compared to the short-range model, the long-range one with an impurity undoubtedly points to the existence of a phase that has no domain wall. The difficulty of determining the threshold σ_c arises from

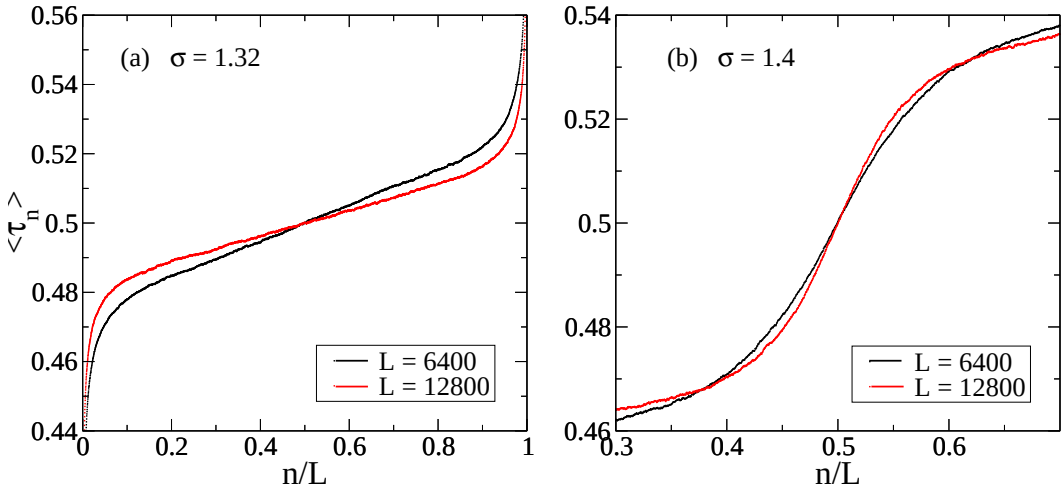

Figure 4.9: (a) The smallest and (b) the biggest σ for which the phases (a) without and (b) with a domain wall are persistent for all $L \leq L_{max} = 12800$. Other simulation parameters are $\rho = 1/2$ and $t = 10^8$ MC steps/site.

the fact that due to the long-range correlations and the finiteness of the system, the domain wall can be observed even for $\sigma < \sigma_c$. To bypass this problem, we shall give an estimate of the interval containing σ_c that is based on Monte Carlo simulations. The idea is, for the largest system size L_{max} available in simulations, to find the smallest (largest) $\sigma_c^-(L_{max})$ ($\sigma_c^+(L_{max})$), for which the slope in the density profile decreases (increases) as we increase $L < L_{max}$. In other words, for $\sigma < \sigma_c^-(L_{max})$, by increasing the system size $L < L_{max}$, the density profile approaches the homogeneous profile 1/2. On the other hand, by increasing the system size $L < L_{max}$ for $\sigma > \sigma_c^+(L_{max})$, the domain wall becomes steeper. For system size $L_{max} = 12800$ used in Monte Carlo simulations, we arrived to the estimate $1.32 < \sigma_c < 1.40$ (figure 4.9).

4.2.2 Density profiles in the mean-field approximation

The success of the mean-field approximation in the pure long-range model motivates us to use the same approximation in the model with impurity. Before we note the entire system of equations for densities $\langle \tau_n \rangle$ in the mean-field approximation $\langle \tau_n \tau_m \rangle \to \langle \tau_n \rangle \langle \tau_m \rangle$, $n \neq m$, we will try to determine the densities ρ_- and ρ_+ in a similar manner that was used in the short-range model i.e. presuming that the density profile assumes the shape of a sharp domain wall,

$$\langle \tau_n \rangle = \begin{cases} \rho_-, & 1 \leq n \leq L/2 \\ \rho_+, & L/2+1 \leq n \leq L, \end{cases} \tag{4.17}$$

and using the fact that the current is constant everywhere. One should recall that

in the model with long-range hopping the current is defined as the total sum of the current of all particles that jump over and from a site k,

$$j = \sum_{n=1}^{k} \sum_{l=k+1-n}^{L} p_l \langle \tau_n (1 - \tau_{n+l}) \rangle + \sum_{n=k+2}^{L} \sum_{l=L-n+k+2}^{L} p_l \langle \tau_n (1 - \tau_{n+l}) \rangle. \tag{4.18}$$

Inside the phase of density ρ_-, i.e. far away from both the impurity and the domain wall (e.g. site $k = L/4$), we expect the current of value $j = \lambda(\sigma)\rho_-(1 - \rho_-)$. The same current must be equal to the current over the impurity which is determined by inserting $k = L$ in to the expression (4.18). Together with the approximation (4.17), we have

$$j \approx \rho_+(1 - \rho_-)(p_2 + 2p_3 + 3p_4 + \dots) = [\lambda(\sigma) - 1]\rho_+(1 - \rho_-), \tag{4.19}$$

where we neglected the contributions arising from the jumps of length $l \geq L/2$, since they disappear in the limit $L \to \infty$. By equating these two expressions, in the limit $L \to \infty$ we arrive at ρ_- and ρ_+ as functions of λ,

$$\rho_- = \frac{1 - \lambda^{-1}}{2 - \lambda^{-1}}, \qquad \rho_+ = \frac{1}{2 - \lambda^{-1}}. \tag{4.20}$$

By substituting $r' = (\lambda - 1)/\lambda$, the upper expressions can be reduced to a known form of densities in the short-range model $\rho_- = r'/(1 + r')$ and $\rho_+ = 1/(1 + r')$, whereby we determined the effective strength of the impurity as function of σ. Unfortunately, such a simplified density profile (4.17) is useful for obtaining ρ_- and ρ_+ only for larger values of σ (e.g. for $\sigma \gtrsim 3$, as depicted in figure 4.10). It is therefore not surprising that our naive attempt to determine σ_c by equalling ρ_- and ρ_+ leads only to the trivial $\sigma_c = 1$ for which the current diverges and thus ignores the effect of the impurity completely.

In order to determine a non trivial σ_c and to explain the power law in the shock phase, we must talk into account the spatial dependence of the density profile. Let us start by marking the lattice sites with $n = -K, \dots, K$, $L = 2K$, so that the impurity resides on the site $n = 0$. The equations for density $\langle \tau_n \rangle(t)$ determined from the appropriate master equation in this new notation are,

$$\frac{d}{dt}\langle \tau_n \rangle = \sum_{\substack{l=1 \\ l \neq n}}^{L} p_l \langle \tau_{n-l}(1 - \tau_n) \rangle - \sum_{\substack{l=1 \\ l \neq L-n+1}}^{L} p_l \langle \tau_n (1 - \tau_{n+l}) \rangle, \quad n \neq 0, \tag{4.21}$$

where we assumed the periodical boundary conditions, $\tau_{K+n} = \tau_{-K+n-1}$. By applying the mean-field approximation, the aforementioned system of equations in the stationary limit $d\langle \tau_n \rangle/dt \to 0$ 0 is reduced to the problem of searching for root of nonlinear system of L equations with L unknowns. One should bear in mind that the of all L equations in (4.21), only $L - 1$ are independent, since their

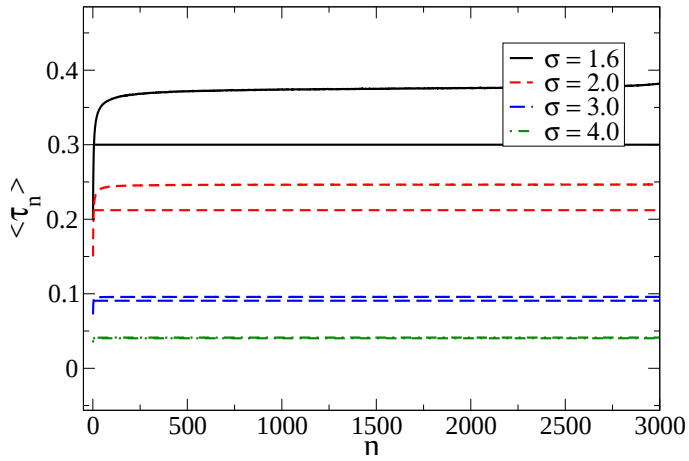

Figure 4.10: Density profiles in the shock phase determined by Monte Carlo simulations ($L = 6400$, $\rho = 1/2$ and $t = 10^8$ MC steps/site) and compared to the density $\rho_- = (1-\lambda^{-1})/(2-\lambda^{-1})$ for different values of the parameter σ.

total sum gives the total number of particles which is conserved by dynamics,

$$\frac{d}{dt}\sum_n \langle \tau_n \rangle = \frac{d}{dt} N = 0 \tag{4.22}$$

System consisting of $L-1$ equations (4.21) conditioned to $\sum_{n=1}^{L} \langle \tau_n \rangle = N$ is further being solved numerically using the HYBRD algorithm taken from the MINPACK library. The calculation was performed for several values of σ and L, and compared with the results of Monte Carlo simulations as depicted in figures 4.11 and 4.12.

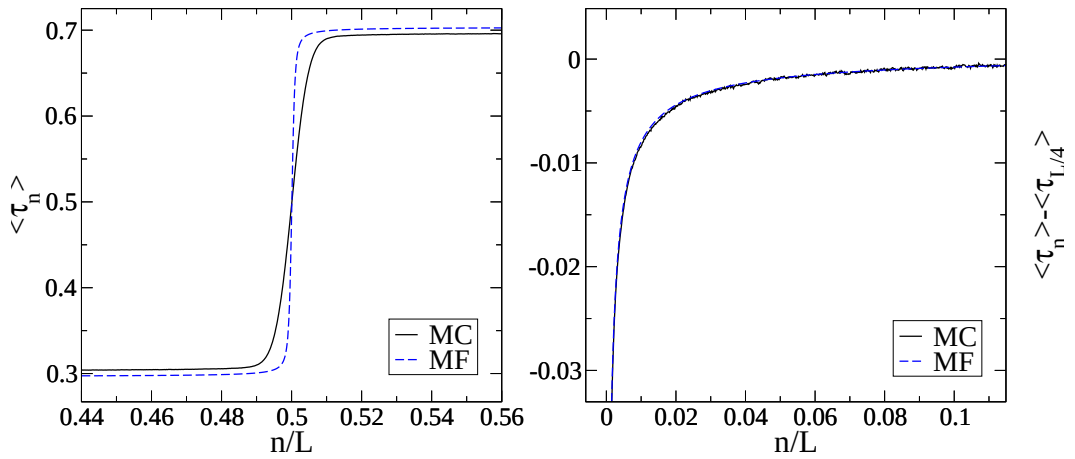

Figure 4.11: (a) The comparison of density profiles obtained from the mean-field approximation (MF) and Monte Carlo simulations (MC) for $\sigma = 1.8$ ($L = 6400$, $\rho = 1/2$ and $t = 10^8$ MC steps/site). (b) The respective spatially dependent deviations $\langle \tau_n \rangle - \langle \tau_{L/4} \rangle$ deduced from the mean-field approximation and Monte Carlo simulations.

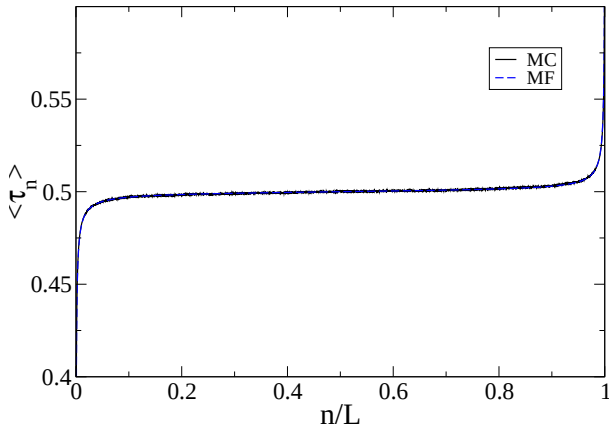

Figure 4.12: The comparison of density profiles obtained from the mean-field approximation (MF) and Monte Carlo simulations (MC) for $\sigma = 1.1$ ($L = 6400$, $\rho = 1/2$ and $t = 10^8$ MC steps/site).

In the shock phase, the numerical solution reproduces the results of Monte Carlo simulations but one finds a narrower smearing of the domain wall, and decreased and increased densities ρ_- and ρ_+, respectively, as well. The difference in the domain wall's shape is actually not surprising, as we now that it is the usual consequence of the mean-field approximation. A more detailed analysis of the domain wall indeed shows that in the mean-field approximation, the spreading of the domain wall is proportional to $L^{1-\sigma/2}$ instead $L^{1/3}$.

There is however, no explanation for the deviations of ρ_- and ρ_+. One can only note that they appear in the short-range model as well, probably due to neglecting of correlations in the close vicinity of the impurity where its influence on the correlations is the greatest. Still, an excellent agreement with Monte Carlo results appears when we subtract $\rho_- = \langle \tau_{L/4} \rangle$ from $\langle \tau_n \rangle$ (figure 4.11(b)). This is even more apparent in the shock-free phase in which mean-field approximation yields the exact values $\rho_- = \rho_+ = 1/2$ (figure 4.12).

The aforementioned agreement with the Monte Carlo simulations brings us to the conclusion already concluded in the pure model: no matter the impurity, the correlations between the particles yield higher-order terms in contrast to the lowest-terms yielded by the mean-field approximation. This leads us to the thought which we work out in the rest of this chapter, that it may actually be possible to use the estimate of the lowest-order terms to determine the power-law exponent of the shock phase.

Let us start with the equation (4.21) in the mean-field approximation in which we insert the density profile in the form of a domain wall with unknown spatially dependent corrections ϕ_n,

$$\langle \tau_n \rangle = \begin{cases} \rho_+ + \phi_n, & -K \le n < 0 \\ \rho_- + \phi_n, & 0 < n \le K. \end{cases} \tag{4.23}$$

For $0 < n \le K$, the right side of the equation (4.21) yields the following terms in the powers of ϕ_n:

$$\phi_n^0 : \quad -\rho_-(1-\rho_-)(p_n - p_{L-n+1}) + (\rho_+ - \rho_-)\left[(1-\rho_-)\sum_{l=n+1}^{n+K} p_l + \rho_- \sum_{K-n+1}^{L-n} p_l\right] \tag{4.24}$$

$$\phi_n^1 : \quad \left[\rho_- \sum_{\substack{l=1 \\ l\neq L-n+1}}^{L} p_l \Delta_l^+ \phi_n - (1-\rho_-)\sum_{\substack{l=1 \\ l\neq n}}^{L} p_l \Delta_l^- \phi_n\right] - \phi_n(1-2\rho_-)(p_n - p_{L-n+1}) + \\ + (\rho_+ - \rho_-)\phi_n\left[\sum_{l=K-n+1}^{L-n} p_l - \sum_{l=n+1}^{K+n} p_l\right] \tag{4.25}$$

$$\phi_n\phi_m : \quad \phi_n^2(p_n - p_{L-n+1}) + \phi_n\left[\sum_{\substack{l=1 \\ l\neq L-n+1}}^{L} p_l \Delta_l^+ \phi_n + \sum_{\substack{l=1 \\ l\neq n}}^{L} p_l \Delta_l^- \phi_n\right], \tag{4.26}$$

where we used the following notation: $\Delta_l^+ \phi_n \equiv \phi_{n+l} - \phi_n$ and $\Delta_l^- \phi_n \equiv \phi_n - \phi_{n-l}$. Since we wish to investigate the limit $a \to 0$ with $na = x < \infty$, the contribution of particular terms can be estimated by looking at their order in $a = 1/L$. The first term in ϕ_n^0 is of the order $O(a^{\sigma+1})$, because $p_n \sim L^{-(\sigma+1)} x^{-(\sigma+1)}$. For $0 < n < L/4$, the second term in ϕ_n^0 is positive and of the order $O(a^\sigma)$. To estimate the ϕ_n^1 terms, we assume the scaling form $\phi_n = L^{-\nu} f_-(n/L)$, where ν is unknown exponent and $f_-(n/L) < 0$ for $0 < n < L/4$. The second and third third terms in ϕ_n^1 are then of the order $O(a^{\nu+\sigma+1})$ and $-O(a^{\nu+\sigma})$, respectively. Neglecting the higher-order (nonlinear) terms $\phi_n\phi_m$, we are left with the following nontrivial terms to estimate

$$\frac{1}{2}\left[\sum_{\substack{l=1 \\ l\neq L-n+1}}^{L} p_l \Delta_l^+ \phi_n - \sum_{\substack{l=1 \\ l\neq n}}^{L} p_l \Delta_l^- \phi_n\right] - \Delta\rho_- \left[\sum_{\substack{l=1 \\ l\neq L-n+1}}^{L} p_l \Delta_l^+ \phi_n + \sum_{\substack{l=1 \\ l\neq n}}^{L} p_l \Delta_l^- \phi_n\right], \tag{4.27}$$

where we introduced $\Delta\rho_- = 1/2 - \rho_-$ to distinguish two cases, $\rho_- = 1/2$ ($\Delta\rho_- = 0$) and $\rho_- \neq 1/2$ ($\Delta\rho_- \neq 0$). These terms reminds us of sums replaced in the pure long-range model with

$$\frac{1}{2}\left[\sum_{l>0} p_l \Delta_l^+ \phi_n - \sum_{l>0} p_l \Delta_l^- \phi_n\right] \to \begin{cases} a^\sigma D_\sigma \Delta_\sigma \phi(x) + O(a^2), & 1 < \sigma < 2 \\ a^2 D_2 \Delta \phi(x) + O(a^{min\{\sigma,3\}}), & \sigma > 2, \end{cases} \tag{4.28}$$

$$\Delta\rho \left[\sum_{l>0} p_l \Delta_l^+ \phi_n + \sum_{l>0} p_l \Delta_l^- \phi_n\right] \to -a(1-2\rho)\lambda(\sigma)\frac{\partial \phi}{\partial x} + O(a^\sigma), \tag{4.29}$$

where $D_\sigma = -\Gamma(-\sigma)cos(\pi\sigma/2)/\zeta(\sigma+1)$, $D_2 = \zeta(\sigma-1)/(2\zeta(\sigma+1))$ and Δ_σ is fractional Laplacian, the difference being that by introducing the impurity we have lost the translational invariance. If we assume that the terms of the order a in the expression (4.27) are correctly described with (4.28) and (4.29), then for the estimate of terms (4.28) and (4.29) we get $O(a^{\sigma+\nu})$ and -$O(a^{\nu+1})$, respectively. At last, if we compare the two lowest-order terms having opposite signs, the result is $\nu = \sigma - 1$ for all σ corresponding to the shock phase (i.e. for $\sigma > \sigma_c$). The result is obviously not completely valid because for $\sigma > 2$ it does not produce $\nu = 1$, but we know by now that the mean-field approximation does not excel in describing the short-range limit. It should also be noted, the reason the exponent ν is not $(\sigma-1)/2$, as it is in the maximum-current phase in the pure long-range model with open boundary conditions, comes from the fact that the long-range correlations appear in the domains with densities $\rho_\pm \neq 1/2$ as well and so the term $\partial\phi/\partial x$ is of lower order in a then the nonlinear term $\phi\partial\phi/\partial x$.

However, if we insert $\rho_- = \rho_+ = 1/2$ in (4.24)-(4.26), we get only four terms,

$$\begin{aligned} 0 \;=\; & \frac{1}{4}(p_n - p_{L-n+1}) + \frac{1}{2}\left[\sum_{\substack{l=1 \\ l\neq L-n+1}}^{L} p_l \Delta_l^+ \phi_n - \sum_{\substack{l=1 \\ l\neq n}}^{L} p_l \Delta_l^- \phi_n\right] + \\ & + \phi_n^2(p_n - p_{L-n+1}) + \phi_n \left[\sum_{\substack{l=1 \\ l\neq L-n+1}}^{L} p_l \Delta_l^+ \phi_n + \sum_{\substack{l=1 \\ l\neq n}}^{L} p_l \Delta_l^- \phi_n\right], \end{aligned} \tag{4.30}$$

which points to the fact that nonlinear terms are becoming important. As result, the density profile no longer satisfies a simple scaling relation.

4.2.3 Calculation for the threshold σ_c

Knowing the dependence of the exponent $\nu(\sigma)$ in shock phase allows us to indirectly i.e. without knowing ρ_- and ρ_+ explicitely, determine the threshold σ_c. The idea is to show that the exponent ν on the threshold σ_c assumes the same value $\nu(\sigma_c) = 1/3$ as in the short-range model in the shock-free phase [143]. If we assume that the function $\nu(\sigma)$ is continuous at the point σ_c, then σ_c easily follows

from

$$\nu(\sigma_c) = \sigma_c - 1 = 1/3 \quad \Rightarrow \quad \sigma_c = \frac{4}{3}, \tag{4.31}$$

and is also within the limits of the earlier numerical estimate $1.32 < \sigma_c = 1.333... < 1.4$.

Essentially, the argument for $\nu(\sigma_c) = 1/3$ is same as the argument of Ha *et al.* for $\nu = 1/3$ in the short-range model [143]. Let us consider local density fluctuations that spontaneously appear in the system. Far away from the boundaries, they propagate with the speed $v_g = \delta j \delta\rho = \lambda_L(1 - 2\rho)$ which equals zero in the shock-free phase. The impurity, however, slows down the propagation of positive density fluctuations, and speeds up the negative ones. This results in increased local density just before the impurity and lowered just after. If the centre of mass of fluctuation propagates faster than the fluctuation dissipates in space, then the surplus of particles close to the impurity can be estimated with the total sum of fluctuations present in the system. This number, however, cannot be greater than the time t_f necessary for the fluctuation to circulate the entire system. Considering that the process of creation of fluctuations is a series of independent and random events, and that the number of positive and negative fluctuations is on average equal, the number of fluctuations in a system and thereby the surplus of particles near the boundaries can be estimated with $\delta N \propto t_f^{1/2}$, meaning that δN can be estimated by estimating t_f. Here Ha *et al.* assume that $v_g = \delta j/\delta\rho$ is satisfied *locally*, i.e. that close to the impurity the speed of spreading of fluctuations becomes spatially dependent and of the form $v_g \approx \lambda_L[1 - 2\rho(x)] \propto x^{-\nu}$, what can be justified only if the spatial variation of local density is slow enough. The position of the centre of mass is then evolving in time as $x_{\mathrm{CM}} \propto t^{1/(1+\nu)}$, yielding $t_f \propto L^{1+\nu}$. The surplus of particles then scales with L as $\delta N \propto t_f^{1/2} = L^{(\nu+1)/2}$ yielding $\nu = 1/3$ by equating δN with $\delta N \propto \int dx x^{-\nu}$.

The key assumption in the aforementioned argumentation is that the fluctuations propagate faster than they dissipate. It means that the characteristic length of spreading $\xi \propto t^{1/z}$ has to be smaller than $x_{\mathrm{CM}} \propto t^{1/(\nu+1)}$, i.e. that $\nu < z - 1$, where z is the dynamic exponent. Considering that in the long-range model $z = \min\{\sigma, 3/2\}$ and $\sigma_c < 3/2$, this means that σ_c is also a border value of σ for which that still applies. This may also account for the inability to apply the simple scaling to the profiles in the shock-free phase.

Throughout the chapter 4.1 we stated a number of arguments for and against the existence of a shock-free phase in TASEP with a static defect. In that sense we would like to stress that the results of the long-range model in chapter 4.2 are not biased in any way. The suggested model primarily points to the fact that at least in one driven diffusive system in one dimension, albeit with the fractional diffusive term, it is possible to determine such a transition and in particular to find its exact transition point.

As to the short-range problem, we feel that due to lack of the exact solution, the problem of static defect in TASEP will have to wait a bit more for a final conclusion. This problem additionally stresses the need for additional methods of studying phase transitions far away from equilibrium. A promising method is the one similar to the Yang-Lee theory [144, 145] not for the zeroes of partition function, but for the zeroes of the normalization constant $Z = \sum_C f(C)$, where sum runs over all states C, $f(C)$ being the solution of the master equation [146].

5

Phase separation induced by quenched disorder

From the experimental point of view, numerous real systems in the realm of driven diffusive systems are commonly subjected to some kind of disorder. Car speeds are certainly dependent of individual characteristics of both driver and car respectively, and of non-homogenous conditions on the road as well (e.g. construction works, accidents, speed limit). In the first case the disorder is assigned to the particles while in the latter case the disorder stems from the environment. The latter example can be found in the biosynthesis of proteins, in which certain triplets of nucleotides in interaction with transfer RNA slow down the process of translation [60] (figure 5.1). Translated into the language of TASEP, disorder from environment can be described with inhomogeneities in hopping probabilities on particular sites. Once selected, the hopping probabilities do not change in time, hence the name "quenched".

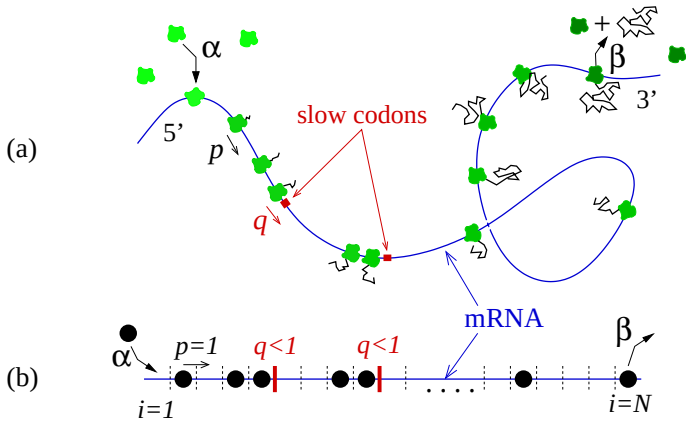

Figure 5.1: (a) Shematic picture of protein biosynthesis. Ribosomes (green) propagate along mRNA chain aided by the specific amino acids delivered by tRNA (not shown). Some codons (red) attract less tRNA resulting in slower propagation of ribosomes. (b) Corresponding TASEP with reduced hopping probability $q < 1$ at certain sites. The picture is taken from [60].

From a fundamental viewpoint, we are interested into how the stationary state

of the pure system and its characteristic properties, e.g. different phases, change in the presence of disorder. The next chapter shall present the argument by Tripathy and Barma [103], which states that the phase coexistence in the short-range TASEP occurs in the *finite* interval of densities $\rho_c < \rho < 1 - \rho_c$ irrespective of the choice of disorder distribution $\mathcal{P}(r_i)$, the threshold ρ_c being dependent of $\mathcal{P}$ but always less than 1/2. In the chapters 5.2 and 5.3 we have investigated whether the same result is valid in both theoretically and experimentally motivated generalizations of TASEP.

5.1 Short-range ASEP with quenched disorder

TASEP with site-wise disorder (disordered TASEP or dTASEP) was first considered by Tripathy and Barma [102,103] in a system with periodical boundary conditions. Like in the homogenous TASEP, $N = \rho L$ particles are distributed on L sites and each site is occupied by at most one particle. For the distribution $\mathcal{P}(r_i)$ of hopping probabilities r_i Tripathy and Barma have used the Bernoulli distribution

$$\mathcal{P}(r_i) = \begin{cases} c & r_i = r \\ 1 - c & r_i = 1, \end{cases} \tag{5.1}$$

where c is the concentration of defects. In other words, we randomly select $N_d = cL$ defects from which the particles move to the right with the probability $r < 1$ while from other sites they move with the probability 1.

Typical density profiles are depicted in figure 5.2. Depending on the density ρ, there are two distinct regimes. In the first regime the density is homogeneous on the macroscopic scale and approximately equal to ρ. The small variations can be discerned only at a microscopic scale equalling several lengths of lattice constant (figure 5.2(a)). In this regime the current has a similar functional dependence on density like in the pure model (region A in figure 5.3). The second regime is characterized by macroscopic areas with densities different than ρ, which are separated by domain walls (figures 5.2(b) and (c)). Such regime is characterized by a plateau in the current-density relation $j(\rho)$ of width 2Δ, centred around the density $\rho = 1/2$ (region B in figure 5.3). In figures 5.2 and 5.3 are also depicted the results obtained in the mean-field approximation by solving the equations

$$j = r_i \rho_i (1 - \rho_{i+1}), \quad i = 1, \ldots, L \tag{5.2}$$

that surprisingly excel at describing densities even at the microscopic scale (figures 5.2(d), (e) and (f)). The main trouble is that the solution can be found only numerically, which denies us further insight in the mechanism of phase separation.

In order to explain the separation, Tripathy and Barma start with the fact that disorder in a large system always creates clusters of "fast" and "slow" sites i.e. the

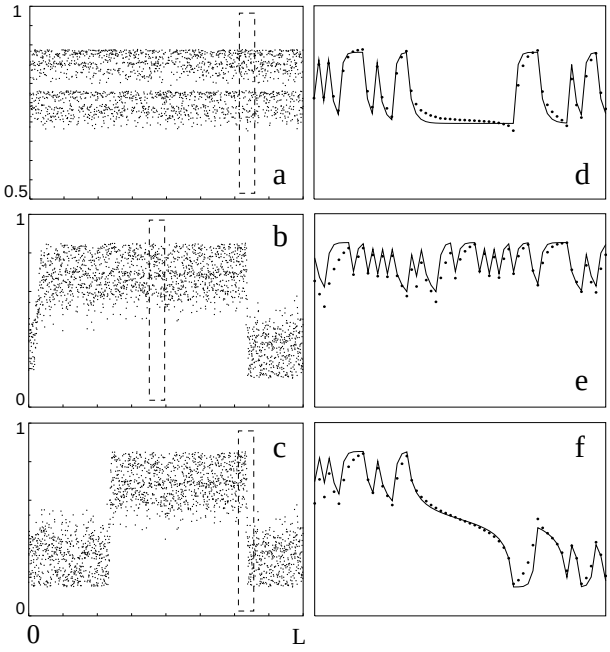

Figure 5.2: Density profiles of TASEP for a single disorder configuration at the densities: (a) $\rho = 0.8$, (b) $\rho = 0.6$ and (c) $\rho = 0.5$. Figures (d), (e) and (f) depict enlarged parts of the corresponding figures to the left, where symbols represent the results of Monte Carlo simulations, and lines the results of the mean-field approximation. The picture is taken from [103].

domains in which all hopping probabilities are either 1 or r. Let us suppose that the domains are large enough so that a homogeneous density can be established (the justification of this assumption shall be provided later on). Then for a certain current j_0 and density $\rho \leq 1/2 - \Delta$ (or $\rho \geq 1/2 + \Delta$), the possible bulk densities that are the solutions of the equation $j_0 = \rho_{1,4}(1-\rho_{1,4}) = r\rho_{2,3}(1-\rho_{2,3})$ are ρ_1 and ρ_2 (or ρ_3 and ρ_4 for $\rho \geq 1/2 + \Delta$), as depicted in figure 5.4. In a regime without phase separation, these densities correspond to bands of similar densities as shown in figure 5.2(a). If we increase the density ρ close enough to $\rho = 1/2$, the current will eventually achieve the maximum value equal to the maximum current in the domain of "slow" sites, $r/4$. Further increasing of ρ will not affect the current so that domains with densities $\rho_{1,2}$ will be replaced by domains with densities $\rho_{3,4}$, marking the onset of phase separation.

The key assumption in the above argument is that the disorder always creates large clusters of slow sites, so that the maximal current in the system is always limited to $r/4$. Tripathy and Barma justify this assumption with the fact that the average length of the *largest* cluster of slow sites, which is $\propto \ln L$, diverges in thermodynamic limit $L \to \infty$. This result stems from the mathematical theory of extreme values (for an introduction, see e.g. [148]) and was rigorously derived in [149] for an equivalent problem of the statistics of the longest sequence of consecutive "heads" in L coin tosses with $P(\text{"head"}) = c$,

$$\{l_{\max}\} = \frac{\gamma + \ln[L(1-c)]}{\ln(1/c)} - \frac{1}{2}, \tag{5.3}$$

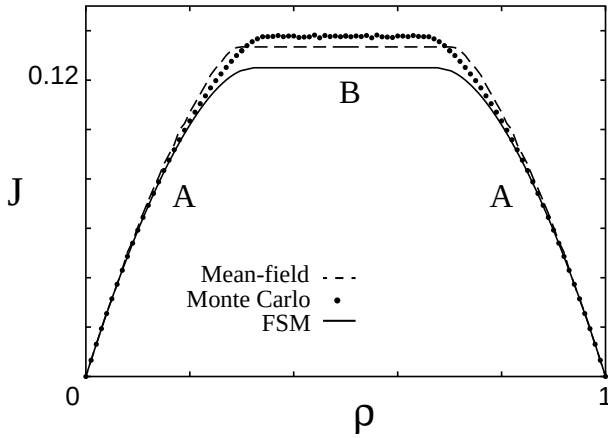

Figure 5.3: The current-density relation in dTASEP for a single disorder configuration and system size $L = 8000$ with $r = c = 1/2$. The dashed line corresponds to the current calculated by application of the mean-field approximation, while the full line corresponds to the current in a fully segregated model in which all impurities form a single cluster of length $N_d = cL$. The picture is taken from [103].

where $\{\dots\}$ denotes averaging over disorder configurations, and $\gamma = 0.5772\dots$ is the so-called Euler-Mascheroni constant. A short introduction to the theory of extreme values, which we will be used later on, can be found in A.

In order to extend the qualitative explanation of phase separation, Tripathy and Barma start with a simplified, fully segregated model in which all impurities make up a single cluster of length $N_d = cL$. Studying such a model can be justified by assuming that the current decreases with the length of the domain of "slow" sites, so that the greatest influence of disorder is expected when all disordered sites are in the consecutive order. If ρ_x and ρ_y denote the densities in domain of "fast" sites X and "slow" sites Y, respectively, then the conservation of current leads to the expression

$$j_0 = \rho_x(1-\rho_x) = r\rho_y(1-\rho_y). \tag{5.4}$$

To the above expression one should add the conservation of particles,

$$(1-c)\rho_x + c\rho_y = \rho. \tag{5.5}$$

which is enough to determine ρ_x, ρ_y and j_0 for a given ρ. We are specifically interested in the density ρ_c for which ρ_y equals $1/2$, i.e. for which the current in the domain of "slow" sites reaches the maximum value $r/4$. Inserting $\rho_y = 1/2$ in (5.4) and (5.5) yields the following ρ_c,

$$\rho_c = \frac{1-(1-c)\sqrt{1-r}}{2}, \tag{5.6}$$

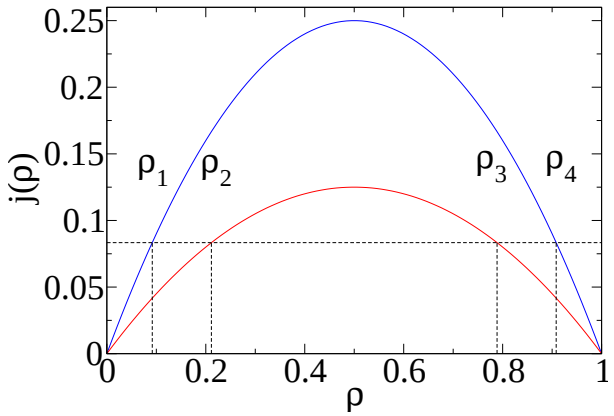

Figure 5.4: Mechanism of phase separation in dTASEP. The two parabolas correspond to the currents in the "slow" and "fast" domains, $j(\rho) = r\rho(1-\rho)$ and $j(\rho) = \rho(1-\rho)$ respectively. The picture is taken from [103].

which enables us to determine the width of the interval in ρ for which phase coexistence occurs, $\Delta = 1 - 2\rho_c$. Returning to the main issue, the expression (5.6) actually provides the upper limit on ρ_c, considering that the influence of disorder is in that case the greatest [147]. The lower limit is determined from a trivial fact that the maximal possible current in a system is $r/4$, which gives

$$\rho_c \geq \frac{1-\sqrt{1-r}}{2}. \tag{5.7}$$

It should be also pointed out that the phase separation cannot be avoided even in the limit $c \to 0$ in which $\rho_c = (1-\sqrt{1-r})/2$, i.e. $\Delta \neq 0$. That case should not be mistaken with TASEP with a single defect, in which density profiles can be optimized so that the maximal current equals $1/4$ instead of $r/4$.

The qualitative conclusions of Tripathy and Barma can be applied to arbitrary disorder distribution $\mathcal{P}(r_i)$ where the "slow" sites can be defined as sites with r_i smaller than a certain prescribed value $r_0 < \{r_i\}$ [147]. With such a definition the result $\{l_{\max}\} \propto \ln L$ still applies, but c in the expression (5.3) should be replaced with $P(r_i < r_0)$.

Another approach to the problem of disorder in TASEP can be found in the work of Harris and Stinchcombe [104], who studied the distribution $w(\rho')$ of densities $\langle\tau_i\rangle$ defined in the following way

$$w(\rho')\Delta\rho' = \frac{\text{number of sites where } |\langle\tau_i\rangle - \rho'| \leq \Delta\rho'/2}{L} \tag{5.8}$$

Using the mean-field approximation, Harris and Stinchcombe have determined the integral equation for $w(\rho')$ and solved it for several particular disorder distributions $\mathcal{P}(r_i)$, thereby showing that the width of plateau 2Δ never disappears and is

proportional to the distribution width.

* * *

Basically, the mechanism of phase separations in TASEP is of geometrical nature - any distribution $\mathcal{P}(r_i)$ of finite width will generate, in an infinite system, an infinite cluster of "slow" sites limiting the current. The next question is whether similar disorder-induced macroscopic structures can occur in a situation in which we allow the particles to *avoid* defect sites? To answer this question, we shall introduce two generalizations of TASEP [150]. In chapter 5.2 we first study a disordered TASEP with long-range jumps of length $l \geq 1$ taken from the probability distribution $p_l \propto l^{-(1+\sigma)}$ with $\sigma > 1$. Our motivation stems from the fact that the introduction of long-range jumps can lead to the absence of phase separation in the model with only one impurity (see chapter 4.2). From the technical side, we are motivated by the fact that the pure[1] model with long-range jumps retains most of the characteristics of the short-range model, but is at the same time well-describable by the mean-field approximation.

The second generalization, presented in chapter 5.3, deals with the generalization of TASEP to two dimensions, symmetric in the transverse direction and totally asymmetric in the longitudinal direction, where disorder occurs only in the latter. Unlike the previous model, this one can be easily imagined in a broader context of transport through disordered media, some examples being the flow of a fluid through a porous material [151, 152], traffic (whether of car or pedestrians) in the presence of obstacles [153] and the microfluidic systems in various geometries [154]. Common to all the aforementioned examples is the nontrivial interplay of driving, mutual interactions and the underlying geometry, which altogether may reduce the conductivity, in some cases even completely [151].

5.2 Generalization to long-range hopping

In this chapter we study an one-dimensional TASEP with random-sequential dynamics on a lattice of L sites and $N = \rho L$ particles, subjected to periodic boundary conditions. The particles move on a lattice with long-range jumps of length $1 \leq l \leq L-1$, which is selected from the power-law probability distribution $p_l \propto l^{-(1+\sigma)}$ with $\sigma > 1$. The disorder is introduced by selecting $N_d = cL$ sites randomly, *from which and to which*[2] the particles jump with the probability reduced by the factor $r < 1$ (figure 5.5).

[1] i.e. without disorder

[2] In this way we have retained the particle-hole symmetry, which is in fact not essential to our conclusions, but makes later analysis of our results easier.

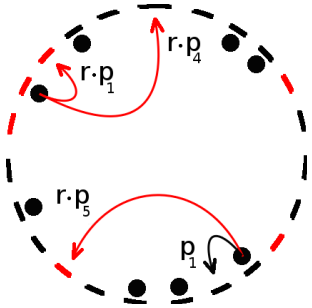

Figure 5.5: Schematic picture of $1d$ disordered TASEP with long-range hopping. Hopping probabilities are reduced by factor a $r < 1$ whenever particle moves either to or from the defect site (denoted in red). Note that not all possible jumps have been displayed, but only those that demonstrate the implementation of disorder.

5.2.1 Typical results of Monte Carlo simulations

Initially, we are interested in the stationary density profile $\langle \tau_i \rangle$, $i = 1, \ldots, L$, which we calculate by Monte Carlo simulations. Similar to the short-range model with Bernoulli distribution of disorder, the results of simulations reveal two typical behaviours depicted in figure 5.6a. Figure 5.6a depicts a density profile for lower values of ρ where only microscopic domain walls occur resulting in two bands of similar densities on the macroscopic scale. On the other hand, by increasing the density ρ above the threshold ρ_c[3] a macroscopic domain wall is induced, as depicted in figure 5.6b.

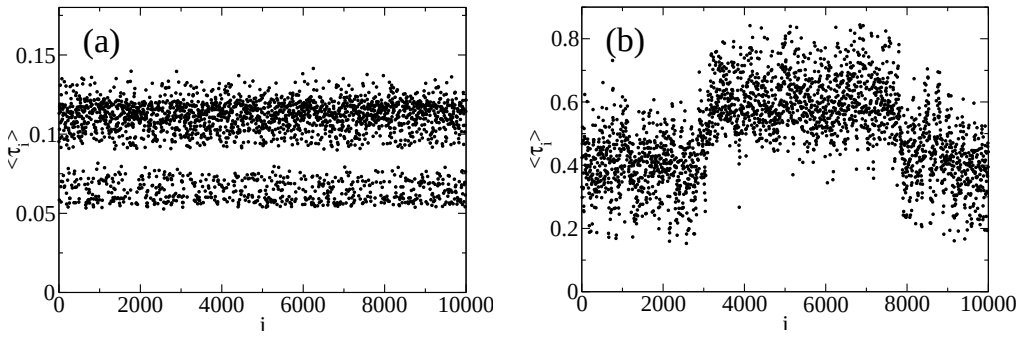

Figure 5.6: Density profiles for (a) $\rho = 0.1$ and (b) $\rho = 0.5$ in a system of size $L = 10^4$ and $r = 0.5$, $c = 0.5$ and $\sigma = 1.8$, obtained by Monte Carlo simulations ($t = 10^7$ MC steps/site) for a single disorder configuration.

The upper profiles are remarkably similar to the profiles found in the short-range dTASEP as depicted in 5.2, the main difference being that ρ_c now depends

[3]Due to the particle-hole symmetry, the same applies to reducing the density below the threshold $1 - \rho_c$

on the parameter of range σ. Recalling the results of the long-range model with a single impurity, this immediately poses a question whether by varying $\sigma > 1$ we can achieve $\rho_c = 1/2$ corresponding to the absence of phase separation[4] The figure 5.7a depicts a density profile for one particular set of parameters for which the absence of phase separation is observable (i.e. for σ small enough). The corresponding normalized density histogram $w(\langle\tau_i\rangle)$, $i = 1\ldots, L$, showing only one maximum, is depicted in figure 5.7b. The absence of phase separation can be observed in the current-density relation as well, which displays the usual plateau (figure 5.8).

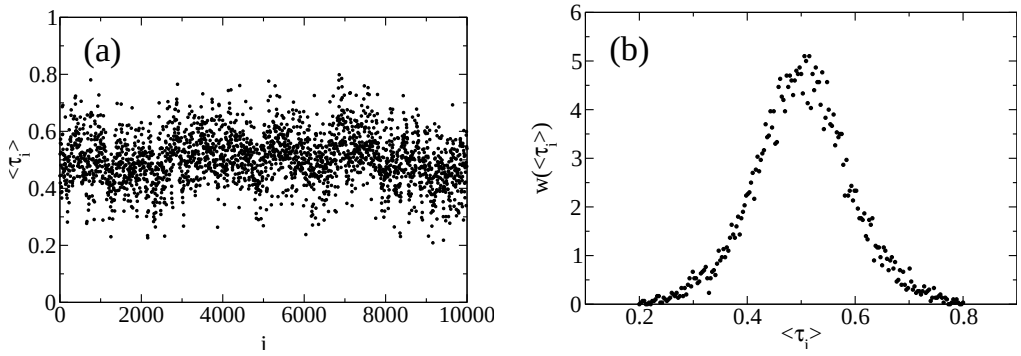

Figure 5.7: (a) Density profile in a system of size $L = 10^4$ and density $\rho = 0.5$ with $r = 0.5$, $c = 0.5$ and $\sigma = 1.2$, obtained by Monte Carlo simulations ($t = 10^7$ MC steps/site) for a single disorder configuration; (b) the corresponding normalized density histogram $\langle\tau_i\rangle$, $i = 1\ldots, L$ showing only one maximum around $\rho = 0.5$.

Due to the finiteness of the system, the aforementioned result has to be taken with a great care, especially when we take into account that the characteristic scale $\{l_{\max}\}$, generated by disorder in one dimension, is logarithmic in L. We shall therefore proceed to the analysis of the segregated model in which all defects are in the consecutive order in the same way that led Tripathy and Barma to estimate the value of ρ_c.

5.2.2 Fully segregated model in the mean-field approximation

Remember the mechanism of phase separation, described in detail in chapter 5.1, where a consecutive sequence of "slow" sites of the length $N_d = cL$ limits the maximum possible current to $j(\rho_c) = r/4$. We know that in a macroscopic domain of homogeneous density ρ, the introduction of long-range hopping leads to the same form of current $j(\rho) \propto \rho(1-\rho)$, different from the short-range one only

[4]Recall that the absence of phase separation is not possible in the short-range dTASEP which sets the upper limit on the threshold value ρ_c that is always smaller than 1/2.

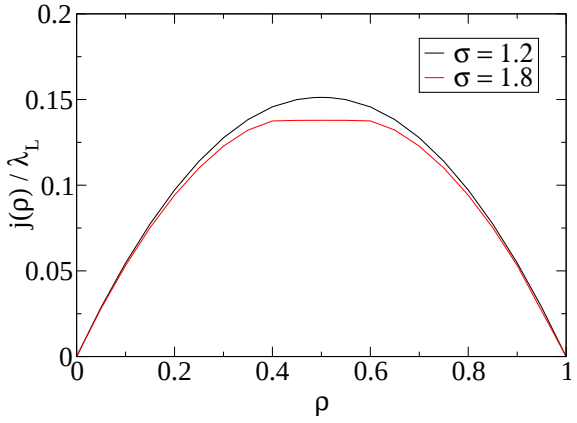

Figure 5.8: Current-density relation for two values of σ ($L = 10^4$, $c = 0.5$ i $r = 0.5$), obtained by Monte Carlo simulations for a single disorder configuration. For a better comparison, the current was divided by the average hopping length $\lambda_{L-1}(\sigma) = \sum_{i=1}^{L-1} l p_l$.

by factor $\lambda = \sum_i i p_i$. That factor, naturally, has no effect on the equation (5.4), suggesting the same ρ_c as in the short-range model. At the same time, this means that the absence of phase separation from figure 5.8 is actually a *finite-size effect* and not a possible (phase) transition. For the particular choice of parameters in figure 5.8 this is not surprising, considering that in that case $l_{\max} \approx 13$, obviously not long enough for the asymptotic current $\lambda r/4$ to be established. How long $l_{\max}$ is necessary for the asymptotic regime to be established is not easy to determine. Instead, we can imagine a segregated model with l "slow" sites where l is a *free* parameter and by varying l try to observe the change of the regime. The results of Monte Carlo simulations for such a model are depicted in figures 5.9a and 5.9b for various choices of l and σ. The figure 5.9a shows the absence of the domain wall for $l = 10$, while for $l = 1000$ the domain wall nearly approaches both the upper (5.6) and the lower (5.7) estimates. Curiously, the figure 5.9b, obtained for $\sigma = 1.05$, displays the change of regime only for $50 < l < 100$, which in dTASEP would be noticeable only for system sizes of $\ln L \sim O(10^2)$, obviously unattainable by Monte Carlo simulations[5].

The reason for such a slow approach to the asymptotic limit can be explained in a following manner. If we denote the "slow" sites with $i = L - l + 1, \ldots, L$, the expression for the current in the long-range model reads

$$j_i = \sum_{m=0}^{L-1} \sum_{m+n<L} p_{m+n} \langle \tau_{i-m}(1 - \tau_{i+n}) \rangle \delta^r_{i-m,i+n}, \tag{5.9}$$

where $\tau_{j\pm L} = \tau_j$, $j = 1, \ldots, L$ and the value of $\delta^r_{k,l}$ depends on whether a pair

[5]Such a slow approach to the thermodynamic limit was found in some other processes in driven diffusive systems [155].

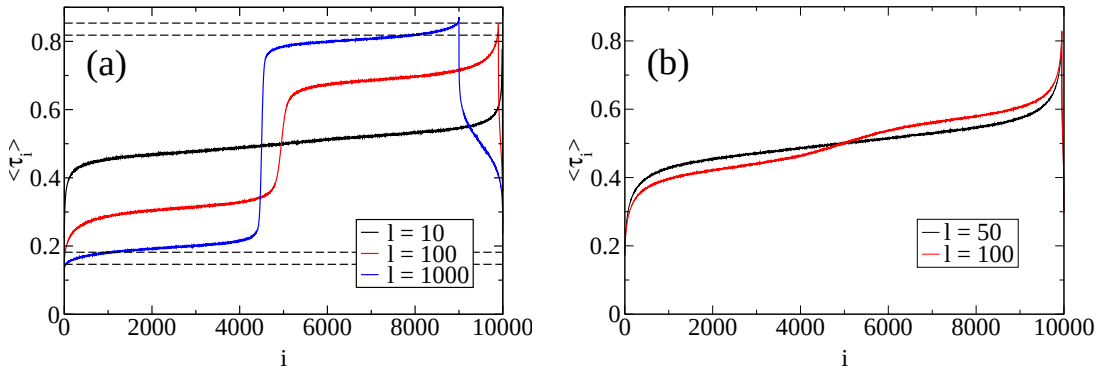

Figure 5.9: Density profiles in the segregated model for various l ($L = 10^4$, $r = 0.5$), obtained by Monte Carlo simulations ($t = 10^7$ MC steps/site) for a single disorder configuration at the density $\rho = 1/2$ and for (a) $\sigma = 1.2$ and (b) $\sigma = 1.05$. Dashed lines in (a) correspond to the upper and to the lower limit given by the expressions (5.6) and (5.7), respectively, with $c = l/L$ and $l = 1000$. Figure (b) shows the emergence of phase separation for some $50 < l < 100$, unattainable by Monte Carlo simulations in dTASEP due to the fact that $l \propto \ln L$.

of sites (k, l) contain at least one defect ($\delta^r_{k,l} = r$) or none ($\delta^r_{k,l} = 1$). In order to estimate the current, we will pick out a site exactly in the middle of a "slow" domain ($i = L - l/2 + 1$) and apply the mean-field approximation in the expression for the current. Let us presume the density profile in the shape of a domain wall,

$$\langle \tau_i \rangle = \begin{cases} \rho_i^x, & 1 \leq i \leq L - l \\ \rho_i^x, & L - l + 1 \leq i \leq L, \end{cases} \tag{5.10}$$

where x and y denote the local densities in the domains of "fast" (X) i "slow" (Y) sites. If we insert (5.10) into the expression for current (5.9), we get four different contributions to the current, j_{xx}, j_{xy}, j_{yx} and j_{yy}, that stem from the exchange of particles between X and Y domains. Since we are only interested in how fast the current decreases with l, we can use the fact that $\rho_i^{\mathrm{x,y}} \leq 1$, from where it follows

$$j_{\mathrm{xx}} < r(1 \cdot p_1 + 2 \cdot p_2 + \cdots + (l/2)p_{l/2}) \sim O(1) \tag{5.11a}$$

$$j_{\mathrm{xy}}, j_{\mathrm{yx}} < r(1 \cdot p_{l/2+1} + 2 \cdot p_{l/2+2} + \cdots + (l/2)p_l) \sim O(l^{-(\sigma-1)}) \tag{5.11b}$$

$$j_{\mathrm{yy}} < 1 \cdot p_{l+1} + 2 \cdot p_{l+2} + \cdots + l p_l \sim O(l^{-(\sigma-1)}), \tag{5.11c}$$

It is visible from these expressions that the corrections to the asymptotic value of current decrease slowly when σ is close to 1. This concludes that disorder in one dimension is always relevant, for it creates a "slow" domain of diverging length. Such a geometric condition is, however, limited to one dimension only, which is the reason why we turn to the two dimensional TASEP in the following chapter.

5.3 Generalization to two dimensions

We are studying TASEP in two dimensions on a lattice consisting of $L_x \times L_y$ sites and $N = \rho L_x L_y$ particles subjected to periodic boundary conditions in both directions. The system evolves in time with the random-sequential dynamics in the following manner: at a certain moment t a randomly selected particle moves to an empty neighbouring site either in the direction of the field or perpendicular to it with the probabilities $p_{\|} = p_x$ and $p_{\perp}$, respectively, where $p_x + 2p_y = 1$. In other words, the model corresponds to TASEP in the direction $\hat{x}$ and to SSEP in the direction $\hat{y}$. Disorder is introduced only in the direction of the field by banning the hops in the direction of the field from cL_xL_y randomly selected sites, what can be imagined as breaking the bonds between sites (i, j) and $(i + 1, j)$ (figure 5.10).

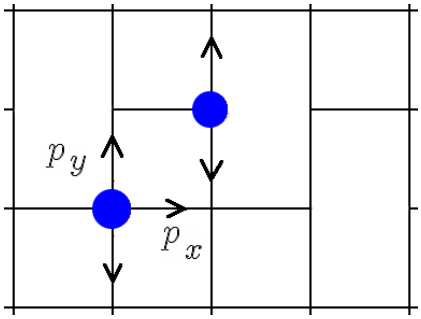

Figure 5.10: Schematic picture of two-dimensional TASEP with disorder. Disorder is introduced as the inability of particles to move to the right at certain sites, which is depicted as missing bonds.

Two-dimensional TASEP was investigated by several authors in different contexts. Ramaswamy and Barma [151, 152] studied ASEP with hopping probabilities $p_{\text{gore}} = p_{\text{udesno}} = w(1 + g)$ and $p_{\text{ulijevo}} = p_{\text{dolje}} = w(1 - g)$, where disorder was introduced by breaking bonds in $\hat{x}$ and $\hat{y}$ directions. The resulting lattice is qualitatively different from the one we use because it contains backbends along which particles propagate against the driving field, resulting in the current decaying exponentially with the length of the backbend. Saegusa *et al.* studied a multi-lane TASEP with static obstacles [153], where they found a plateau in the current-density relation, typical for the occurrence of phase separation. Alexander and Lebowitz investigated a symmetric model in $2d$ with a rod of length l orientated along the axis $\hat{y}$ and moving the same way as the other particles [156]. In the special case of the static rod of length $l = 1$, they calculated the density profile in the mean-field approximation and shown that a macroscopic domain of low density occurs behind the rod. Finally, large-scale inhomogeneities in $2d$ driven diffusive systems, although not induced by disorder but akin to phase coexistence, have been investigated in many works, e.g. in [157].

5.3.1 Typical results of Monte Carlo simulations

5.3.1.1 Current-density relation

First we must determine the dependence of current on density defined as

$$j_x(\rho,\alpha)/L_y = \frac{1}{L_y}\sum_{j=1}^{L_y} p_x\langle\tau_{ij}(1-\tau_{i+1,j})\rangle\cdot\omega_{ij}(\alpha), \quad i=1,\ldots,L_x, \tag{5.12}$$

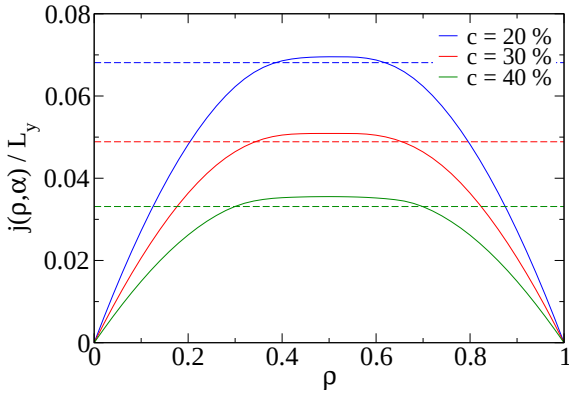

Figure 5.11: Current-density relation for several disorder concentrations c on a lattice 200×200 with $p_x = 2p_y = 1/2$, obtained from Monte Carlo simulations ($t = 10^6$ MCS/site) for a single disorder configuration. The dashed lines correspond to the best estimate of the maximum current provided by the expression (5.21).

where for a particular disorder configuration α, $\omega_{ij}(\alpha)$ equals 1 if the bond connecting the sites (i,j) and $(i+1,j)$ exists, and is 0 otherwise. Figure 5.11 depicts the current $j(\rho)$ obtained from Monte Carlo simulations for different disorder concentrations on a lattice 200×200 with $p_x = 2p_y = 1/2$. Compared to the current $j(\rho) = p_x\rho(1-\rho)$ in the pure system, we find the plateau around $\rho = 1/2$ and otherwise a parabolic form $j(\rho)\propto\rho(1-\rho)$ with a non trivial factor dependent on p_x and c. If we wish to estimate the maximal current, a naive attempt would be to say that the current is $(1-c)p_x/4$ where $1-c$ is the average number of existing bonds in a column. This, however, produces erroneous result at higher concentrations as denoted in the second column in table 5.1. Estimate can be improved by substituting $1-c$ with $\omega^*(\alpha)$, which corresponds to the smallest total number of bonds among all columns,

$$\omega^*(\alpha) \equiv \min_i\left\{\sum_{j=1}^{L_y}\omega_{ij}(\alpha)\right\} = L_y - \max_i\left\{\sum_{j=1}^{L_y}[1-\omega_{ij}(\alpha)]\right\}. \tag{5.13}$$

Table 5.1: Values of maximal current for various disorder concentrations obtained by Monte Carlo simulations ($L_x = L_y = 200$, $p_x = 2p_x = 1/2$, $t = 10^6$ MC steps/site) and compared: to the naive estimate $(1-c)p_x/4$, to the expression $\omega^*(\alpha)p_x/(4L_y)$ calculated by explicit counting of bonds for a given disorder configuration, to the expression $\overline{\omega}^* p_x/(4L_y)$ derived using the extreme-value theory and to the expression (5.21) that yields the best estimate.

c	Monte Carlo	$(1-c)p_x/4$	$\omega^*(\alpha)\cdot p_x/(4L_y)$	$\overline{\omega}^*\cdot p_x/(4L_y)$	expression (5.21)
0.1	0.09255(5)	0.1125	0.10507	0.10313	0.09154
0.2	0.06953(7)	0.1000	0.09063	0.09010	0.06812
0.3	0.05089(2)	0.0875	0.07688	0.07615	0.04887
0.4	0.03553(5)	0.0750	0.06000	0.06287	0.03312

Instead of explicit counting of bonds along the columns for a given disorder configuration, for $L_x \gg 1$ we can instead calculate the mean value $\overline{\omega}^*$ derived by averaging over all disorder configurations, using the mathematical theory of extreme values [148]. Considering that the calculation for $\overline{\omega}^*$ was, to the best of our knowledge, nowhere to be found in the literature, it is performed in Appendix A, with the final result noted below:

$$\overline{\omega}^* \approx L_y - a_{L_x}(c, L_y)\gamma - b_{L_x}(c, L_y), \tag{5.14}$$

where $a_{L_x}(c, L_y)$ and $b_{L_x}(c, L_y)$ are given by

$$a_{L_x}(c, L_y) = \frac{2\sqrt{2c(1-c)L_y}}{L_x} \cdot \exp\left\{\left[\mathrm{erf}^{-1}\left(1 - \frac{2}{L_x}\right)\right]^2\right\}, \tag{5.15}$$

$$b_{L_x}(c, L_y) = cL_y + \sqrt{2c(1-c)L_y} \cdot \mathrm{erf}^{-1}\left(1 - \frac{2}{L_x}\right). \tag{5.16}$$

For $L_x \gg 1$, the error function $\mathrm{erf}^{-1}(1 - 2/L_x)$ can be expanded around $L_x \to \infty$,

$$\mathrm{erf}^{-1}\left(1 - \frac{2}{x}\right) \approx \left\{\frac{1}{2}\ln\left[\frac{x^2/2\pi}{\ln(x^2/2\pi)}\right]\right\}^{1/2}, \tag{5.17}$$

which gives simplified expressions,

$$a_{L_x}(c, L_y) \approx \left[\frac{4c(1-c)L_y}{2\pi\ln L_x - \pi\ln 2\pi}\right]^{1/2}, \tag{5.18}$$

$$b_{L_x}(c, L_y) \approx cL_y + \left\{c(1-c)L_y\left[\ln\left(\frac{L_x^2}{2\pi}\right) - \ln\ln\left(\frac{L_x^2}{2\pi}\right)\right]\right\}^{1/2}. \tag{5.19}$$

$$\tag{5.20}$$

Although the comparison of $\omega^*(\alpha)$ and $\overline{\omega}^*$, depicted in table 5.1 for $L_x = L_y = 200$,

justifies replacing $\omega^*(\alpha)$ with its mean value, neither $\omega^*(\alpha)$ nor $\overline{\omega}^*$ yield a better estimate of the maximum current. The best estimate, displayed in the last column of the table 5.1, is derived if we recognize that the greatest contribution to the current stems from the sites that have both the inward and the outward bond. Considering that the probability of a site having both inward and outward bonds equals $(1-c)^2$ or $1-(1-c)^2 = 2c-c^2$ if at least one is lacking, we arrive to the following estimate of maximal current,

$$\begin{aligned} \max_{\rho}\{j_x(\rho,\alpha)\}/L_y &\approx \frac{1}{L_y}\min_i\left\{\sum_{j=1}^{L_y}\omega_{i-1,j}(\alpha)\omega_{ij}(\alpha)\right\}\cdot\frac{p_x}{4}\approx \\ &\approx [L_y - a_{L_x}(2c-c^2,L_y)\gamma - b_{L_x}(2c-c^2,L_y)]\cdot p_x/(4L_y). \end{aligned} \tag{5.21}$$

Here we must stress that the success of this estimate depends on p_x: the smaller it is (or the larger p_y is), there is a greater probability that the particle will exit the column at the different site (within a column). This can be confirmed by the following calculation. We select a column i and write down the equation for the stationary density $\rho_j^{(i)}$ in the mean-field approximation,

$$\frac{d\rho_j^{(i)}}{dt} = 0 = p_y(\rho_i^{(j+1)} + \rho_i^{(j-1)} - 2\rho_i^{(j)}) + \tag{5.22}$$

$$+ p_x\omega_j^{(i-1)}(\alpha)\rho_{i-1}^{(j)}(1-\rho_i^{(j)}) - p_x\omega_j^{(i)}(\alpha)\rho_i^{(j)}(1-\rho_{i+1}^{(j)}), \tag{5.23}$$

where instead of $\omega_{ij}(\alpha)$ we have introduced the notation $\omega_j^{(i)}$. We then notice that the equation written in such a manner corresponds to the mean-field equation of the one-dimensional simple symmetric exclusion process in which the system exchanges particles with the reservoir on randomly selected sites, the probabilities of absorption and desorption being $p_x\omega_j^{(i-1)}\rho_j^{(i-1)})$ and $p_x\omega_j^{(i)}(1-\rho_j^{(i+1)})$, respectively. Since the process is symmetric, the equation is linear in unknown local densities and can be written in the following matrix form,

$$T^{(i)}\rho^{(i)} = -p_x b^{(i-1)}, \tag{5.24}$$

where $b_j^{(i-1)} = -p_x\omega_j^{(i-1)}\rho_j^{(i-1)}$ and $T^{(i)}$ reads

$$T_{kl}^{(i)} = \begin{cases} d_k^{(i)} & k = l, \\ & k = l\pm 1, \\ p_y & k = 1, l = L, \\ & k = L, l = 1, \\ 0 & \text{other} \end{cases} \tag{5.25}$$

with

$$d_k^{(i)} = -[2p_y + p_x\omega_k^{(i-1)}\rho_k^{(i-1)} + p_x\omega_k^{(i)}(1-\rho_k^{(i+1)})]. \tag{5.26}$$

By formally expressing the solution $\rho^{(j)} = -p_x[T^{(i)}]^{-1}b^{(i-1)}$ of the matrix equation above, we arrive at the following expression for the current j

$$\begin{aligned} j &= \frac{1}{L_y}\sum_{j=1}^{L_y} p_x\omega_j^{(i)}\rho_j^{(i)}(1-\rho_j^{(i+1)}) = \\ &= -\frac{p_x}{L_y}\sum_{k=1}^{L_y}\rho_k^{(i-1)}[T_{kl}^{(i)}]^{-1}[1-\rho_l^{(i+1)}]\omega_k^{(i-1)}\omega_l^{(i)}, \end{aligned} \tag{5.27}$$

in which we recognize a bilinear form $\omega_k^{(i-1)}\omega_l^{(i)}$ in the variables of disorder. In order to estimate the weight of $\omega_k^{(i-1)}\omega_l^{(i)}$, we need to determine the inverse $[T^{(i)}]^{-1}$. Unfortunately this is not possible to achieve in a closed form unless we assume reflecting boundary conditions in $\hat{y}$ direction, meaning that $T_{1L}^{(i)} = T_{L1}^{(i)} = 0$. In that case the non-diagonal elements in $[T_{kl}^{(i)}]^{-1}$ decay exponentially with "distance" from the main diagonal [158],

$$[T_{kl}^{(i)}]^{-1} \propto p_y^{|k-l|} = e^{-|k-l|/(-1/\ln p_y)} \tag{5.28}$$

which for a given p_y gives the estimate of a typical distance between the sites at which particles are entering and leaving a column. For example, for $p_y = 0.25$ this gives $-1/\ln p_y \approx 0.72$, which means that the particles mostly exit at the same or at the neighbouring site, as it was assumed in the expression 5.21.

5.3.1.2 Density profiles

The previous chapter dealt with the influence of disorder on the current. This chapter turns to its influence on stationary density profiles. Figure 5.12 depicts the spatial distribution of local density, obtained from Monte Carlo simulations for various densities ρ, denoted by shades of blue ($\langle\tau_{ij}\rangle = 0$) and red ($\langle\tau_{ij}\rangle = 1$), where white represents the mean density ρ. The figure clearly represents how the increase of density ρ incites local inhomogeneities to appear, which grow to the size of the system at density around $\rho = 0.4$. That becomes even more obvious if we draw a local density histogram, which displays just one maximum at low/high densities (figure 5.13a) and two distinct maxima for densities around 1/2 (figure 5.13b). Whether the transition from one regime to the other is a consequence of the finite system size, or it exists in the thermodynamic limit as well, is not easily to determine solely from numeric simulations. We shall therefore investigate the anisotropic limit $p_x \to 0$, which can be analyzed analytically and which will reveal absence of such a transition for all values of disorder concentration.

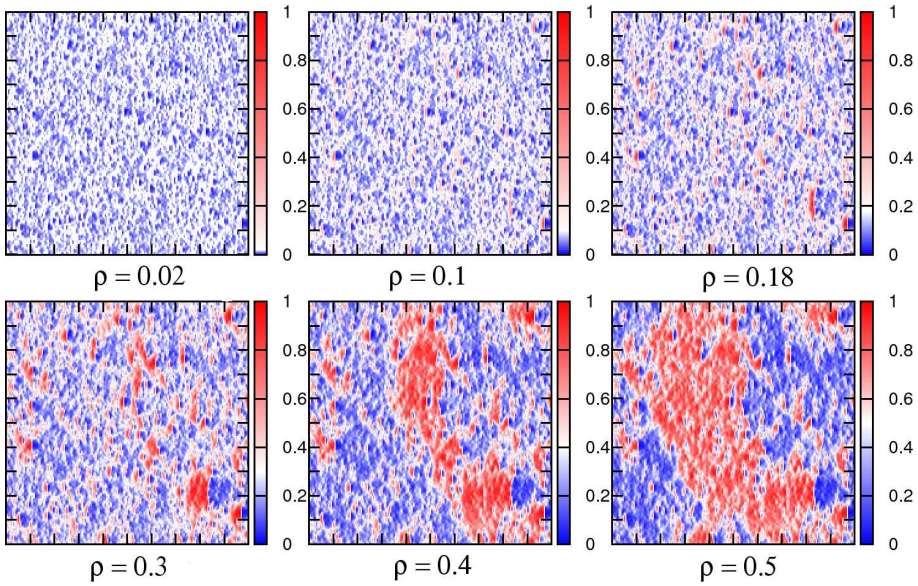

Figure 5.12: Density profiles for different ρ and concentration of disorder $c = 0.4$, obtained by Monte Carlo simulations ($L_x = L_y = 200$, $p_x = 2p_x = 1/2$, $t = 10^6$ MC steps/site) for a single disorder configuration. Blue denotes $\langle \tau_{ij} \rangle = 0$, white $\langle \tau_{ij} \rangle = \rho$ and red $\langle \tau_{ij} \rangle = 1$.

5.3.2 Mean-field approximation in the limit $p_x \to 0$

In the limit $p_x \to 0$, hops between the columns are so rare compared to the hops inside the columns that $n_i = \sum_{j=1}^{L_y}$ can be taken as slow variable. The system configuration can then be noted as $C = \{n_i | i = 1, \ldots, L_x\}$, and the time evolution of the system can be described with the master equation

$$\frac{d}{dt} P(C,t) = \sum_i \left[W(C_+^{i,i+1} \to C) P(C_+^{i,i+1}, t) - W(C \to C_-^{i,i+1}) P(C,t) \right], \quad (5.29)$$

where $C_\pm^{i,i+1} = \{n_1, \ldots, n_i \pm 1, n_{i+1} \mp 1, \ldots, n_{L_x}\}$. Considering the rareness of hops between the columns, we can assume that the particles within the column are always distributed homogeneously, thus the probability of a particle occupying a particular site equals n_i/L_y. That assumption taken, the transition rates W simply read

$$W(C \to C_-^{i,i+1}) = p_x \cdot \left(\sum_{j=1}^{L_y} \omega_{ij} \right) \cdot \frac{n_i}{L_y} \cdot \left(1 - \frac{n_{i+1}}{L_y} \right), \quad (5.30)$$

$$W(C_+^{i,i+1} \to C) = p_x \cdot \left(\sum_{j=1}^{L_y} \omega_{ij} \right) \cdot \frac{n_i + 1}{L_y} \cdot \left(1 - \frac{n_{i+1} - 1}{L_y} \right), \quad (5.31)$$

where $\omega_i \equiv \sum_{j=1}^{L_y} \omega_{ij}$. In this limit we have therefore reduced a two-dimensional

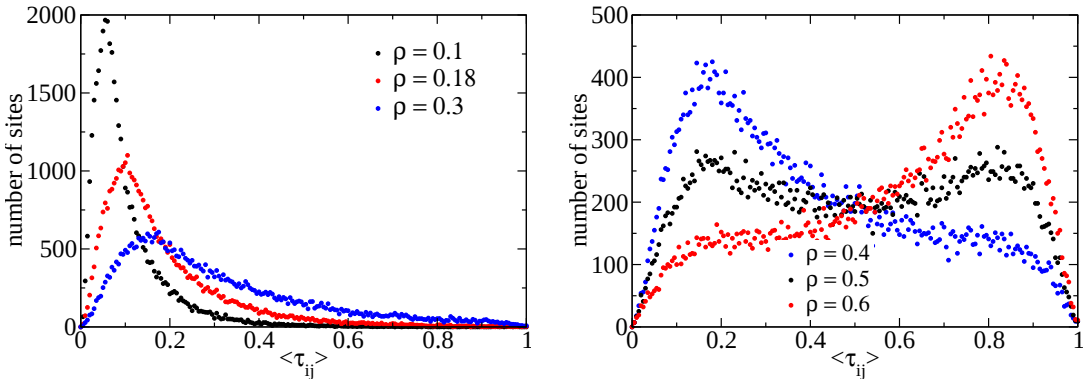

Figure 5.13: Histogram of local density $\langle \tau_{ij} \rangle$ obtained by Monte Carlo simulations for a single disorder configuration at disorder concentration $c = 0.4$ ($L_x = L_y = 200$, $p_x = 2p_x = 1/2$, $t = 10^6$ MC steps/site) which displays (a) a single maximum at low/high densities ρ and (b) two maxima for densities around $\rho = 1/2$.

problem to a one-dimensional one in which the disorder appears only through ω_i. A one-dimensional process that allows more than one particle per site and in which hopping probabilities depend on the number of particles on sites from which and to which the particle move is called a *misanthrope process* [159].

From (5.29) and (5.31) we can easily derive the equation for the mean number of particles n_i in column i,

$$\frac{d}{dt}\langle n_i(t)\rangle = p_x{\cdot}\omega_{i-1}{\cdot}\left\langle \frac{n_{i-1}}{L_y}\cdot\left(1-\frac{n_i}{L_y}\right)\right\rangle - p_x{\cdot}\omega_i{\cdot}\left\langle \frac{n_i}{L_y}\cdot\left(1-\frac{n_{i+1}}{L_y}\right)\right\rangle. \quad (5.32)$$

The upper equation is then transformed into the mean-field equation in $1d$ dTASEP if we further neglect the correlations, $\langle n_i n_{i+1}\rangle \approx \langle n_i\rangle\langle n_{i+1}\rangle$, and redefine $\langle n_i\rangle \to \langle n_i\rangle/L_y \equiv \rho_i$ and $\omega_i \to \omega_i/L_y \equiv r_i$, which gives

$$\frac{d\rho_i}{dt} = p_x \cdot r_{i-1}\rho_{i-1}(1-\rho_i) - p_x \cdot r_i\rho_i(1-\rho_{i+1}), \quad (5.33)$$

where r_i are chosen in accordance with binomial distribution

$$P(n = r_i \cdot L_y) = \binom{L_y}{n}(1-c)^n c^{L_y-n}, \quad (5.34)$$

$$\{r_i\} = 1-c, \qquad \{r_i^2\} - \{r_i\}^2 = c(1-c)/L_y. \quad (5.35)$$

The agreement of misanthrope process (5.29)-(5.31) with $2d$ TASEP was checked by constructing r_i for the given disorder configuration and choosing $p_x \ll 1$ in the Monte Carlo simulations. The results of simulations are depicted in images 5.14a and 5.14b for $p_x = 10^{-4}$ and $p_x = 10^{-2}$, respectively, to which were added the results of $1d$ dTASEP with the same r_i's. It is clearly visible that the misan-

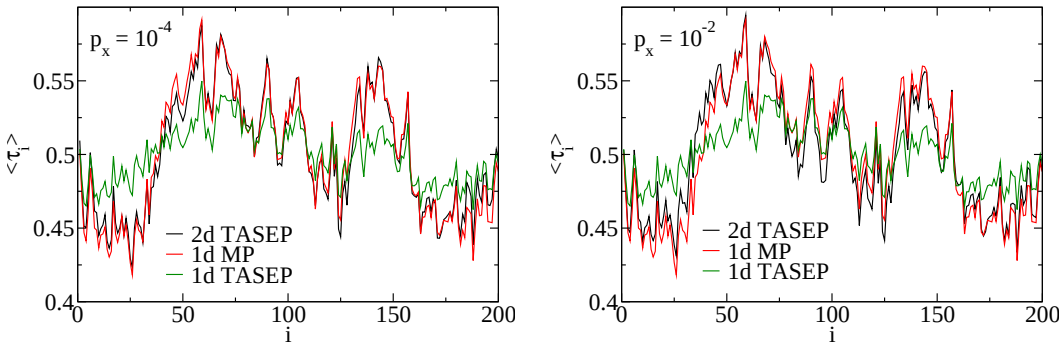

Figure 5.14: Comparison of stationary density profiles $\langle\tau_i\rangle \equiv \sum_{j=1}^{L_y}\langle\tau_{ij}\rangle/L_y$ obtained by Monte Carlo simulations of $2d$ TASEP for (a) $p_x = 10^{-4}$ and (b) $p_x = 10^{-2}$ ($L_x = L_y = 200$, $c = 0.2$, $\rho = 1/2$, $t = 10^6$ MC steps/site) with density profile in an equivalent $1d$ misanthrope process (MP) and in $1d$ dTASEP.

thrope process is very suitable for describing $2d$ TASEP in the limit of a small p_x, while that is not the case for $1d$ dTASEP. If we increase p_x, it is obvious that the image of homogeneous distribution of particles within the columns will cease to be applicable, and we are left with the question of how to estimate the limiting p_x. A rough estimate would consist of comparing the time $\sim L_y^z$ of relaxation of a symmetric $1d$ TASEP with the mean time $\sim 1/p_x$ the particle stays in the column. Since $z = 2$, this yields an estimate of $p_x \sim L_y^{-2}$, which for $L_y = 200$ gives a value $p_x \sim 10^{-5}$ much less than the one observed in simulations. The precise value of limiting p_x for which the conclusions of anisotropic limit still apply is left as an open issue and stands as a motivation for further research.

Once the original $2d$ problem is reduced to a $1d$ problem with site-wise disorder, we can invoke the theory of extreme values stating that in the limit of an infinite system there will always be an infinite cluster of sites on which all r_i's are smaller than some value r_0 below average (or above average), $r_0 < 1-c$ (or $r_0 > 1-c$). In other words, all we need to do now is to insert $p = P(r_i < r_0)$ into the expression (5.3),

$$p = P(x < r_0) = \frac{1}{2}\left[1 + \mathrm{erf}\left(\frac{r_0 - \mu}{\sqrt{2\sigma^2}}\right)\right], \tag{5.36}$$

where the binomial distribution was approximated by the Gaussian (according to Berry-Essen theorem the error is of order $1/\sqrt{L_y}$) with $\mu = 1 - c$ and $\sigma^2 = c(1-c)/L_y$. From this it follows that the size of a "slow" domain in a misanthrope process diverges as $\{l_{\max}\} \propto \ln L_x$, which considering that avoiding the defects is easiest within the limit of $p_x \to 0$ means that the phase separation in $2d$ TASEP occurs for *all* p_x. This conclusion is however correct only if the limit $L_x \to \infty$ is taken by keeping the L_y *finite* (e.g. in the TASEP with multiple lanes). However,

if we are interested in the true $2d$ problem i.e. in the limit $L_x \sim L_y \to \infty$, some precaution must be taken since $\sigma \to 0$. If we select $r_0 < \mu = 1 - c$, we can expand the error function around $-\infty$. For that purpose the expansion around ∞ can be used,

$$\mathrm{erf}(x) = 1 - \frac{e^{-x^2}}{\sqrt{\pi}x}\left[1 - \frac{1}{2x^2} + \dots\right], \quad x \to \infty. \tag{5.37}$$

together with the fact that the $\mathrm{erf}(x)$ is an odd function, $\mathrm{erf}(x) = -\mathrm{erf}(-x)$. The final result for the denominator in (5.3) is

$$\ln(1/p) = \ln\left[\frac{2\sqrt{\pi}|r_0 - 1 + c|}{\sqrt{c(1-c)}}\right] + \frac{1}{2}\ln L_y + 2\frac{(r_0 - 1 + c)^2}{c(1-c)}L_y, \tag{5.38}$$

while the numerator reads

$$\gamma + \ln[L_x(1-p)] \approx \gamma + \ln L_x + \sqrt{\frac{2}{\pi}}\frac{c(1-c)}{|r_0 - 1 + c|}\frac{1}{L_y}e^{-\frac{|r_0-1+c|^2}{2c(1-c)}L_y}. \tag{5.39}$$

This clearly shows that in the limit $L_y \to \infty$ the denominator grows faster than the numerator and therefore $\{l_{\max}\}$ disappears. We may say that in the limit $p_x \to 0$ the disorder "averages itself" and the argument for the phase separation due to the infinitely large domain of "slow" sites ceases to be valid. This can be proved by checking the current-density relation for a small p_x (figure 5.15a) as well as the histogram of the density profile for $\rho = 1/2$ (figure 5.15b). Indeed, the figure 5.15a does not show the usual plateau common to phase separation, while the current itself follows the parabolic shape $j(\rho) \propto \rho(1-\rho)$ with the proportionality constant close to $1 - c$. Also, the density profile histogram $\rho = 1/2$, depicted in figure 5.15b, shows only one maximum.

* * *

The presence of disorder in $1d$ ASEP has a universal consequence: for a current large enough disorder will always induce the phase separation, disregarding the microscopic details of disorder. Essentially, the reason for that is the fact that disorder will always result in a long sequence of sites having reduced hopping probabilities that will limit the current to a value smaller than the one which would be established if the disorder was not present. Once the maximum current is achieved the further increase of density must leave the current unchanged, and that results in the appearance of a macroscopic domain wall.

The universality of this result, which is valid no matter the details of disorder, is particular to one dimension. This has motivated us to investigate the possibility of avoiding phase separation by increasing the connectivity between the sites so

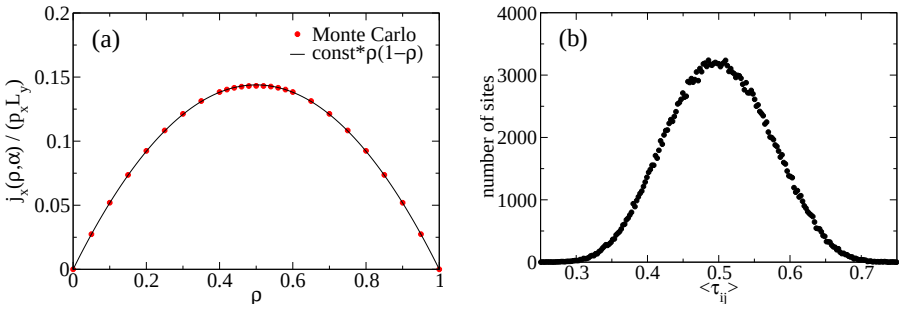

Figure 5.15: (a) Current–density relation obtained by Monte Carlo simulations of $2d$ TASEP for a single disorder configuration at $c = 0.4$ ($p_{\rm x} = 10^{-2}$, $L_{\rm x} = L_{\rm y} = 1000$ and $t = 10^5$ MC steps/site). The solid line is the best fit to the expression $j(\rho) = const. \times \rho(1-\rho)$ with $const. \approx 0.5756$ close to $1 - c = 0.6$. (b) The corresponding histogram of the density profile for $\rho = 1/2$.

that the particles can avoid the defect sites [150]. The avoidance of defect sites was incited in two ways: either by increasing the range of hopping or by increasing the dimensionality.

In a one-dimensional case we have shown that the long range jumps are not sufficient to avoid the phase separation, however, the separation was noted only in extremely large systems, $\ln L \approx 50$. In a two-dimensional case we have shown, by using a simple argument, a completely opposite thing, i.e. the absence of phase separation irrespective of the details of the disorder, but only in the strongly anisotropic limit in which the hopping rate in the direction of driving is much smaller than the one in the perpendicular direction. In this limit, the original $2d$ exclusion process reduces to the $1d$ misanthrope process, in which disorder enters only through the fraction of non-defect sites present in each column of the original $2d$ TASEP. By the central limit theorem, however, the probability distribution of this fraction has a variance which decays as $1/L_y$, so that in the limit $L_{\rm x} \sim L_{\rm y} \to \infty$ the otherwise diverging size of the largest 'bottleneck' vanishes resulting in the absence of a macroscopic phase separation.

To further strengthen the aforementioned arguments it would be interesting to look at the effect of adding disorder to the generalization of ASEP which includes several lanes that interchange particles. In that case our result claims that for a current strong enough the phase separation will always occur. Also the very same argument that excludes the possibility of phase separation in $2d$ in anisotropic limit can generally be applied to $3d$ as well, if we assume that disorder hinders the transport of particles only in the direction of the driving field. The unresolved issue remains to determine a regime of parameters in which the assumption of fast relaxation of density fluctuations in the directions perpendicular to the direction of the driving field ceases to be valid.

6 Conclusion

The vast number of the degrees of freedom which underlies everything that surrounds us poses a great challenge: how by inspecting the microscopic degrees of freedom to deduce the macroscopic observations. That program, at least in principle, is possible for systems in thermodynamic equilibrium, while the equivalent theory for systems out of equilibrium, at least in this generality is lacking.

One of the simplest nonequilibrium states are the stationary states which are maintained far from equilibrium, either by external force, or/and by imposing nonequilibrium boundary conditions. The lack of the systematic theory, even for stationary states, pushes us back to microscopic models that are designed to fulfil two roles. One role is achieved by constructing complex models with a potentially great number of parameters in order to accurately describe a particular physical phenomenon. The other role is achieved by setting up the so called minimal models containing only a few parameters which are believed to be essential for qualitative understanding of general principles.

In this dissertation we have dealt with asymmetric simple exclusion process (ASEP) as a minimal model of transport of (classical) particles driven by the external field and interacting only through the exclusion principle that prevents them to come too close to each other. Although simplified, this interaction describes several real situations, ranging from mobile ions in superionic conductors to self-propelled particles in mesoscopic (ribosomes) and macroscopic (pedestrians, cars) systems. From the theoretical viewpoint ASEP has become a paradigmatic model of boundary-induced phase transitions that are present even in one dimension.

In chapter 2 we gave an overview of the most important results for phase transition in ASEP with open boundary conditions. The local diffusive character of ASEP was replaced in chapter 3 with long-range jumps of length l which is taken from the probability distribution following the power law $p_l \sim l^{-(1+\sigma)}$, where σ is the range parameter [107]. By changing the diffusive character of transport we aimed to investigate the universality of phase transitions in ASEP which proved their robustness to various generalizations [78–82]. In the case of a single particle, such movement corresponds to Levy random walk and leads to a so-called anomalous diffusion [117].

The short-range model has shown how much one can deduce solely from a hydrodynamic equation, further improved by including e.g. the domain-wall dynamics. This provided the motivation to find the hydrodynamic equation in the long-range case, which was non-rigorously derived from the discrete mean-field equations on a infinite lattice [108]. The final result yielded the same hydrodynamic (Burgers) equation, but contained a non-local (fractional) diffusive term for $1 < \sigma < 2$ and the usual local diffusive term for $\sigma > 2$.

This provided us with the insight into several matters. Firstly, the change of regime at $\sigma = 2$ suggests that the short-range limit of the model arises for $\sigma > 2$, which was confirmed for all later calculations. Secondly, we expect the discrete model to inherit the well-known dynamical properties of the fractional-viscous equation, e.g. the dynamical exponent describing the late-time relaxation towards the stationary state. Indeed, the dynamical exponent $z = \min\{\sigma, 3/2\}$, obtained from the autocorrelation function for density fluctuations, $C(0,t) = \langle \delta\rho(0,0)\delta\rho(0,t)\rangle \sim t^{-1/z}$, agrees with the one already obtained using the renormalization group methods [126].

By introducing the long-range jumps into the finite system demanded the redefinition of boundary conditions, so as to make the movement of particles qualitatively same to the movement close to the boundary. The new boundary conditions, consistent with the long-range jumps, follow naturally if we imagine the reservoirs extending to the length of the system. A similar problem arises in the definition of boundary conditions when solving the differential equations with fractional derivations on finite intervals. The main novelty of such boundary conditions lies in the fact that the exchange of particles takes place at all sites sharing similarities with another generalization of TASEP that includes the Langmuir kinetics [96].

Regarding phase transitions, the Monte Carlo simulations on a finite system with open boundary conditions have shown the same phase diagram as in the short-range case. This was also hinted by the similarity of hydrodynamic equations, the difference being found in the first-order transition and in the maximum-current phase. The first-order transition differs in the phase separation for $1 < \sigma < 2$, which arises due to the localization of the domain wall's motion. In the approach that describes the domain wall as a random walker, the localization turns out to be induced by the external potential arising due to the non-local boundary conditions and having a global minimum which captures the domain wall for $1 < \sigma < 2$. A similar mechanism of phase separation was observed in ASEP with Langmuir kinetics [96]. In the maximum-current phase one still observes the power law decay away from boundaries but with an exponent of $(\sigma - 1)/2$ for $1 < \sigma < 2$ and $1/2$ for $\sigma > 2$. The σ-dependent exponent obtained from the Monte Carlo simulations can be also derived from the hydrodynamic equation, which suggests that in the long-range case the mean-field approximation, unlike the short-range case, is sufficient both for the phase diagram description and for the description

of the phase transitions as well.

A non-trivial stationary state does not appear only in contact with the reservoirs. ASEP with periodic boundary conditions and one defect site from which the particles move with a probability reduced by a factor r, is a well known, unsolved problem [59, 132] which evades the exact solution for almost 20 years. Defect in ASEP induces a global macroscopic phase separation, but the unsolved issue remains of whether the global shift occurs consistently for all defect "strengths" [143]. Our contribution to this problem is an explicit analytical proof of a regime change from separated to a homogeneous phase in a modified long-range model in which the defect is introduced as an impurity on a lattice which does not take part in the dynamics, but slows them down by forcing them to jump over it [131]. By this example we have demonstrated that such a transition is in principle possible, although the result was calculated from a model in many aspects similar to the short-range one but essentially a long-ranged one. More recent results seem to confirm the existence of a non-trivial transition in a related model of surface growth in the presence of a line defect [134].

Unlike the *single* defect, Tripathy and Barma [102] have shown that for a current large enough the presence of a *full* of disorder in the short-range ASEP in one dimension always induces phase separation, disregarding its microscopic details (shape of the distribution of hopping probability, concentration etc.) The reason for this stems from the fact that the disorder always generates a long domain of *equal*, but reduced hopping probabilities that will delimit the current to a maximum that can be established in a said domain. Once this maximum value is reached the further increase in density must leave the current unchanged, which results in the creation of a macroscopic domain wall. The universality of this result, applicable disregarding the details of disorder, is essentially of an geometrical nature: the disorder in $1d$ always creates long domains of slowly permeable sites. In chapter 5 we investigated the robustness of this result in the case of increased connectivity between the sites facilitating the faster movement of particles around the defect sites [150]. We observed specifically two such geometries: a $1d$ lattice with long-range hopping and a $2d$ lattice with short range hopping. In the $2d$ case the disorder is set only in the direction of the field so that the particles can move around the defect sites by moving perpendicularly to the direction of the field. We concluded: despite of the long-range of hopping the geometric reason always prevails in $1d$ but not necessarily in $2d$. In anisotropic limit in which the particle hopping rate in the direction of the field is much smaller than the one perpendicular to the field, the transport of the particles in a $2d$ disordered matrix becomes effectively one-dimensional. The reason for this is the fact that in this limit the particles are distributed much faster through the column (perpendicular to the direction of the field) than they move between different columns. The configuration of a $2d$ system is then completely describable by the total amount

of particles in every column, as if they were boxes. The probability of particle hopping from one box to another will then depend only on the total amount of defect sites in every column but not of their particular distribution within the column. This does not go to say that once the problem is reduced to $1d$, the phase separation will always occur. According to the central limit theorem the fluctuations in the total number of defect sites scaled with the column length L_y, have a standard deviation of $\sim L_y^{-1/2}$, so for $L_y \to \infty$ it is impossible to observe a long domain of "slow" columns. In this limit we arrived at the opposite result: the phase separation is not possible disregarding the details of disorder! Open issue remains of whether we can find the range of hopping probabilities for which the anisotropic limit ceases to apply, as well as the mechanism of phase separation in the true $2d$ case. Interesting may also seem the possibility of an experimental check of these results through recently studied microfluidics in $2d$ geometries [154].

A

Extreme-value theory: von Mises' conditions

If X_i designates the total number of broken bonds in the i-th column, $X_i = \sum_{j=1}^{L_y}(1-\omega_{ij})$, then the corresponding probability distribution is the binomial distribution

$$P(X_i = n) = \binom{L_y}{n} c^n (1-c)^{L_y - n}, \tag{A.1}$$

where c is the probability of finding a broken bond at site (i,j). Let $F(x) = P(x < X)$ be the corresponding cumulative distribution and x^* its right endpoint, $x^* = sup\{x : F(x) < 1\}$. We are interested in obtaining the maximum value of $\{X_1, \ldots, X_{L_x}\}$ as $L_x \to \infty$,

$$max\{X_1, \ldots, X_{L_x}\} \xrightarrow{P} x^*, \tag{A.2}$$

where $\to^P$ means convergence in probability, since $P(max\{X_1, \ldots, X_m\} \leq x) = F^m(x)$ is degenerate in the limit $m \to \infty$ as it converges either to 0 for $x < x^*$ or to 1 for $x \geq x^*$. We therefore seek a sequence of positive a_m and real b_m such that $lim_{m\to\infty} F^m(a_m x + b_m) = G(x)$ exists, where $G(x)$ is called extreme value distribution. A sufficient condition for that is von Mises' condition [148], which states that if $F''(x)$ exists and $F'(x) > 0$ for $x < x^*$ then

$$\lim_{m\to\infty} F^m(a_m x + b_m) = \exp\left[-(1+\gamma' x)^{-1/\gamma'}\right], \quad 1 + \gamma' x > 0, \tag{A.3}$$

where γ' is given by

$$\lim_{t\to x^{*+}} \left(\frac{[1-F(t)]F''(t)}{[F'(t)]^2} \right) = -\gamma' - 1. \tag{A.4}$$

Moreover, $b_m = U(m)$ and $a_m = mU'(m)$, where $U(m)$ is the inverse function of $1/(1-F(x))$. For $\gamma' = 0$, the right-hand side of (A.3) should read $\exp(-e^{-x})$. To apply this condition, we approximate binomial distribution with the normal $N(\mu, \sigma^2)$, where $\mu = cL_y$ and $\sigma^2 = L_y c(1-c)$. Numerical error in doing so need not to worry us since for cumulative distribution it is of the order of $1/\sqrt{L_y}$ (Berry-Essen theorem) and L_y is large. Then it is an easy exercise to show that

the cumulative distribution $F(x)$ and its inverse $U(x)$ are given by, respectively,

$$F(x) = \frac{1}{2}\left[1 + \mathrm{erf}\left(\frac{x-\mu}{\sqrt{2\sigma^2}}\right)\right], \tag{A.5}$$

$$U(x) = \mu + \sqrt{2\sigma^2}\cdot \mathrm{erf}^{-1}\left(1 - \frac{2}{x}\right), \quad x \geq 1, \tag{A.6}$$

where $\mathrm{erf}(x)$ and $\mathrm{erf}^{-1}(x)$ are the error function and its inverse, respectively. Inserting $F(x)$ and its derivatives in (A.4) we obtain $\gamma' = 0$, i.e. $G(x) = \exp(-e^{-x})$ (Gumbel distribution). The mean and the variance of the Gumbel distribution are given by Euler-Mascheroni constant $\gamma = 0.5772\ldots$ and $\pi^2/6$, respectively, which gives the mean and the variance of x^*

$$\langle x^* \rangle = a_{L_x}\gamma + b_{L_x}, \tag{A.7}$$

$$\langle x^{*2} \rangle - \langle x^* \rangle^2 = \frac{a_{L_x}^2 \pi^2}{6}, \tag{A.8}$$

where a_{L_x} and b_{L_x} are given by

$$a_{L_x}(c, L_y) = \frac{2\sqrt{2c(1-c)L_y}}{L_x}\cdot \exp\left\{\left[\mathrm{erf}^{-1}\left(1 - \frac{2}{L_x}\right)\right]^2\right\}, \tag{A.9}$$

$$b_{L_x}(c, L_y) = cL_y + \sqrt{2c(1-c)L_y}\cdot \mathrm{erf}^{-1}\left(1 - \frac{2}{L_x}\right). \tag{A.10}$$

For $L_x \gg 1$, $\mathrm{erf}^{-1}(1 - 2/L_x)$ can be expanded around $L_x \to \infty$, which gives

$$a_{L_x}(c, L_y) \approx \left[\frac{4c(1-c)L_y}{2\pi \ln L_x - \pi \ln 2\pi}\right]^{1/2}, \tag{A.11}$$

$$b_{L_x}(c, L_y) \approx cL_y + \left\{c(1-c)L_y\left[\ln\left(\frac{L_x^2}{2\pi}\right) - \mathrm{lnln}\left(\frac{L_x^2}{2\pi}\right)\right]\right\}^{1/2}. \tag{A.12}$$

Bibliography

[1] B. Schmittmann and R.K.P. Zia, *Statistical mechanics of driven diffusive systems* in *Phase Transtions and Critical Phenomena*, Ed. C. Domb and J.L. Lebowitz (Academic Press, San Diego, 1995)

[2] G.M. Schütz, *Exactly Solvable Models for Many-Body Systems Far From Equilibrium* in *Phase Transtions and Critical Phenomena*, Ed. C. Domb and J.L. Lebowitz (Academic Press, San Diego, 2001)

[3] B. Derrida, E. Domany and D. Mukamel, *J. Stat. Phys.* **69**, 667 (1992)

[4] G.M. Schütz and E. Domany, *J. Stat. Phys.* **72**, 109 (1993)

[5] B. Derrida, M.R. Evans, V. Hakim and V. Pasquier, *J. Phys. A* **26**, 1493 (1993)

[6] L.E. Reichl, *A Modern Course in Statistical Physics* (Wiley, New York, 1998)

[7] S.R. de Groot and P. Mazur, *Non-Equilibrium Thermodynamics* (Dover, New York, 1984)

[8] G. Gallavotti, *Statistical Mechanics: A Short Treatise* (Springer-Verlag, Berlin, 1999)

[9] G. Ódor, *Rev. Mod. Phys.* **76**, 663 (2004)

[10] H. E. Stanley, *Introduction to Phase Transitions and Critical Phenomena* (Oxford University Press, New York, 1987)

[11] K.G. Wilson, *Phys. Rev. B* **4**, 3174-3183 (1971)

[12] L. Onsager, *Phys. Rev.* **65**, 117-149 (1944)

[13] J. Krug, *Phys. Rev. Lett.* **67**, 1882 (1991)

[14] R. Peierls, *Proc. Cambridge Phil. Soc.* **32**, 477 (1936)

[15] S. Katz, J.L. Lebowitz and H. Spohn, *J. Stat. Phys.* **34**, 497-537 (1984)

[16] W. Dietrich, P. Fulde, and I. Peschel, *Adv. Phys.* **29**, 527 (1980)

[17] D.P. Landau and K. Binder, *Monte Carlo Simulations in Statistical Physics* (Cambridge University press, New York, 2000)

[18] A. Schadschneider, D. Chowdhury and K. Nishinari, *Stochastic Transport in Complex Systems: From Molecules to Vehicles* (Elsevier, Amsterdam, 2010)

[19] I. Prigogine, *The arrow of Time* in *The Chaotic Universe: Proceedings of the Second ICRA Network Workshop*, Advanced Series in Astrophysics and Cosmology, vol.10, Ed. V. G. Gurzadyan and R. Ruffini (World Scientific, Singapur, 2000)

[20] J.L. Lebowitz, *Rev. Mod. Phys.* **71**, S346-S357 (1999)

[21] D.J. Evans, E.G.D. Cohen and G.P. Morriss, *Phys. Rev. Lett.* **71**, 2401 (1993)

[22] D. Evans and D. Searles, *Phys. Rev. E* **50**, 1645 (1994)

[23] G. Gallavotti and E.G.D. Cohen, *Phys. Rev. Lett.* **74**, 2694 (1995); G. Gallavotti and E.G.D. Cohen, *J. Stat. Phys.* **80**, 931 (1995)

[24] J. Kurchan, *J. Phys. A* **31**, 3719 (1998)

[25] J.L. Lebowitz and H. Spohn, *J. Stat. Phys.* **95**, 333 (1999)

[26] E.D.G Cohen and G. Gallavotti, *J. Stat. Phys.* **96**, 1343-1349 (1999)

[27] O.G. Jepps and L. Rondoni, *J. Phys. A: Math. Theor.* **43** 133001 (2010)

[28] O. Penrose, *The Direction of Time* in *Chance in Physics: Foundations and Perspectives*, Ed. J. Bricmont, D. Dürr, M.C. Galavotti, G. Ghirardi, F. Petruccione and N. Zanghi (Springer-Verlag, Berlin, 2002)

[29] C. Jarzynski, *Phys. Rev. Lett.* **78**, 2690-2693 (1997)

[30] R.J. Harris and G.M. Schütz, *J. Stat. Mech.* P07020 (2007)

[31] L.D. Landau and E.M. Lifshitz, *Statistical Physics* (Pergamon Press, Oxford, 1990)

[32] C. Bustamante, J. Liphardt and F. Ritort, *Physics Today* **58**, 43-48 (2005)

[33] D. Ruelle, *Physics Today* **57**, 48-53 (2004)

[34] A. Einstein, *Ann. d. Phys.* **17**, 549 (1905)

[35] P. Langevin, *C. R. Acad. Sci. Paris* **146**, 530 (1908)

[36] L. Onsager, *Phys. Rev.* **37**, 405-426 (1931)

[37] L. Onsager and S. Machlup, *Phys. Rev.* **91**, 1505-1512 (1953)

[38] H.B. Callen and T.A. Welton, *Phys. Rev.* **83**, 34 (1951)

[39] H.B. Callen and R.F. Greene, *Phys. Rev.* **86**, 702 (1952)

[40] R. Kubo, *Rep. Prog. Phys.* **29**, 255 (1966)

[41] M. Baiesi, C. Maes and B. Wynants, *Phys. Rev. Lett.* **103**, 010602 (2009)

[42] B. Schmittmann and R.K.P Zia, *Phys. Rep.* **301**, 45-64 (1998)

[43] J. Marro, *Nonequilibrium Phase Transitions in Lattice Models* (Cambridge University Press, Cambridge, 1999)

[44] G. Grinstein, *J. App. Phys.* **69**, 5441 (1991)

[45] C.T. MacDonald, J.H. Gibbs and Pipkin, *Biopolymers* **6**, 1 (1968)

[46] C.T. MacDonald and J.H. Gibbs, *Biopolymers* **7**, 707 (1969)

[47] F. Spitzer, *Adv. Math* **5**, 246 (1970)

[48] L. Bertini, A. De Sole, D. Gabrielli, G. Jona-Lasinio and C. Landim, *J. Stat. Phys.* **135** 857-72 (2009)

[49] V.B. Priezzhev, *Phys. Rev. Lett.* **91**, 050601 (2003)

[50] L-H. Gwa and H. Spohn, *Phys. Rev. A* **46**, 844 (1992)

[51] J. de Gier and F.H.L. Essler, *Phys. Rev. Lett.* **95**, 240601 (2005)

[52] J. de Gier and F.H.L. Essler, *J. Stat. Mech.* P12011 (2006)

[53] M.R. Evans and T. Hanney, *J. Phys. A: Math. Gen.* 38, R195 (2005)

[54] D. van der Meer, K. van der Weele and D. Lohse, *Phys. Rev. Lett.* **88**, 174302 (2002)

[55] K. Nagel and M. Schreckenberg, *J. Phys. I* **2**, 2221 (1992)

[56] D. Chowdhury, L. Santen and A. Schadschneider, *Phys. Rep.* **329**, 199-329 (2000)

[57] V. Popkov, L. Santen, A. Schadschneider and G.M. Schütz, *J. Phys. A:Math. Gen.* **34**, L45 (2001)

[58] N. H. Barton *et al.*, *Evolution* (Cold Spring Harbor Laboratory Press, 2007)

[59] S.A. Janowsky and J.L. Lebowitz, *Phys. Rev. A* **45**, 618 (1992)

[60] T. Chou and G. Lakatos, *Phys. Rev. Lett.* **93**, 198101 (2004)

[61] J.J. Dong, B. Schmittmann and R.K.P. Zia, *Phys. Rev. E* **76**, 051113 (2007)

[62] J.J. Dong, B. Schmittmann and R.K.P. Zia, *J. Stat. Phys.* **128**, 21 (2007)

[63] J.J. Dong, R.K.P. Zia and B. Schmittmann, *J. Phys. A: Math. Gen.* **42**, 015002 (2009)

[64] M. Ebrahim Foulaadvand, A.B. Kolomeisky and H. Teymouri, *Phys. Rev. E 78*, 061116 (2008)

[65] R.K.P. Zia, J.J. Dong and B. Schmittmann, *J. Stat. Phys.* **128**, 21 (2007)

[66] P. Meakin, P. Ramanlal, L.M. Sander and R.C. Ball, *Phys. Rev. A* **34**, 5091 (1986)

[67] S.-C. Park, D. Kim and J.-M. Park, *Phys. Rev. E* **65**, 015102 (2002)

[68] M. Kardar, G. Parisi Y.-C. Zhang, *Phys. Rev. Lett* **56**, 889 (1986)

[69] M.J. Lighthill and G.B. Whitham, *Proc. R. Soc. London* Ser. A **229**, 281 (1955)

[70] P. D. Lax, *Hyperbolic Systems of Conservation Laws and the Mathematical Theory of Shock Waves* (SIAM, New York, 1973)

[71] P.G. Drazin and R.S. Johnson, *Solitons: An Introduction* (Cambridge University Press, New York, 1989)

[72] A.B. Kolomeisky, G.M. Schütz, E.B. Kolomeisky and J.P. Straley, *J. Phys. A: Math. Gen.* **31**, 6911 (1998)

[73] L. Santen and C. Appert, *J. Stat. Phys.* **106**, 187 (2002)

[74] B. Derrida, S. A. Janowsky, J. L. Lebowitz and E. R. Speer, *J. Stat. Phys.* **73**, 813-842 (1993)

[75] J.S. Hager, J. Krug, V. Popkov and G.M. Schütz, *Phys. Rev. E* **63**, 056110 (2001)

[76] J. Krug *Advances in Physics* **46**, 139 (1997)

[77] H.K. Janssen and K. Oerding, *Phys. Rev. E* **53**, 4544 (1996)

[78] T. Sasamoto, *J. Phys. Soc. Jpn.*, **69**, 1055 (2000)

[79] M.R. Evans, N. Rajewski and E.R. Speer, *J. Stat. Phys.* **95**, 45 (1999)

[80] J. de Gier and B. Nienhuis, *Phys. Rev. E* **59**, 4899 (1999)

[81] R. Juhász and L. Santen, *J. Phys. A: Math. Gen.* **37**, 3933 (2004)

[82] M. Bengrine et al., *J. Phys. A: Math. Gen.* **32**, 2527 (1999)

[83] V. Popkov and G.M. Schütz, *J. Stat. Phys.* **112**, 523-540 (2003)

[84] V. Popkov, *J. Phys. A: Math. Gen.* **37**, 1545 (2004)

[85] E. Pronina and A.B. Kolomeisky, *J. Phys. A: Math. Gen.* **37**, 9907 (2004)

[86] J. Brankov, N. Pesheva and N. Bunzarova, *Phys. Rev. E* **69**, 066128 (2004)

[87] E. Pronina and A.B. Kolomeisky, *J. Stat. Mech.* P07010 (2005)

[88] K. Mallick, *J. Phys. A: Math. Gen.* **29**, 5375 (1996)

[89] H.-W. Lee, V. Popkov and D. Kim, *J. Phys. A: Math. Gen.* **30** 8497 (1997)

[90] M.R. Evans, *Europhys. Lett.* **36**, 13 (1996)

[91] J. Krug and P.A. Ferrari, *J. Phys. A: Math. Gen.* **29**, L465-71 (1996)

[92] V. Karimipour, *Europhys. Lett.* **47**, 304 (1999)

[93] T. Antal and G.M. Schütz, *Phys. Rev. E* **62**, 83-93 (2000)

[94] G. Lakatos and T. Chou, *J. Phys. A: Math. Gen.* **36**, 2027 (2003)

[95] L.B. Shaw, R.K.P. Zia and K.H. Lee, *Phys. Rev. E* **68**, 021910 (2003)

[96] A. Parmeggiani, T. Franosch and E. Frey, *Phys. Rev. Lett.* **90**, 086601 (2003)

[97] T. Reichenbach, T. Franosch and E. Frey, *Phys. Rev. Lett.* **97**, 050603 (2006)

[98] A. Alberts et al. *The Molecular Biology of the Cell* (Garland, New York, 1994)

[99] M.R. Evans, R. Juhász and L. Santen, *Phys. Rev. E* **68**, 026117 (2003)

[100] A. Rakoś, M. Paessens and G.M. Schütz, *Phys. Rev. Lett.* **91**, 238302 (2003)

[101] D.E. Wolf and L.-H. Tang, *Phys. Rev. Lett.* **65**, 1591-1594 (1990)

[102] G. Tripathy M. Barma, *Phys. Rev. Lett.* **78**, 3039-42 (1997)

[103] G. Tripathy and M. Barma, *Phys. Rev. E.* **58**, 1911–26 (1998)

[104] R. J. Harris and R.B. Stinchcombe, *Phys. Rev. E.* **70**, 016108 (2004)

[105] P. Pfeuty and G. Toulouse, *Introduction to the Renormalization Group and to Critical Phenomena* (John Wiley & Sons, Inc., New York, 1977)

[106] F. J. Dyson, *Commun. Math. Phys.* **12**, 91 (1969)

[107] J. Szavits-Nossan and K. Uzelac, *Phys. Rev. E* **74**, 051104 (2006)

[108] J. Szavits-Nossan and K. Uzelac, *Phys. Rev. E* **77**, 051116 (2008)

[109] B. Derrida, *J. Stat. Mech.* P07023 (2007)

[110] G.M. Schütz, R. Ramaswamy and M. Barma, *J. Phys. A: Math. Gen.* **29** 837 (1996)

[111] A. Benassi and J.-P. Fouque, *Ann. Prob.*, **15** 546 (1987)

[112] F. Rezakhanlou, *Comm. Math. Phys.* **140**, 417 (1991)

[113] M. D. Jara, *Comm. Pure Appl. Math.* **62**, 198-214 (2009)

[114] S.G. Samko, A.A. Kilbas and O.I. Marichev, *Fractional Integrals and Derivatives* (Yverdon, Switzerland, Gordon and Breach, 1993)

[115] P.L. Butzer and U. Westphal, *An Introduction to Fractional Calculus* u *Applications of fractional calculus*, Ed. R. Hilfer (World Scientific, Singapore, 2000)

[116] K. Miller and B. Ross, *An Introduction to the Fractional Calculus and Fractional Differential Equations* (John Wiley & Sons, Inc., New York, 1993)

[117] R. Metzler and J. Klafter, *J. Phys. A* **37**, R161-R208 (2004)

[118] R. Hilfer (Ed.), *Applications of fractional calculus*, (World Scientific, Singapore, 2000)

[119] L. Debnath, *Int. J. Math. Math. Sci.* **2003**(54), 3413-3442 (2003)

[120] V.E. Tarasov, *J. Phys. A: Math. Gen.* **39**, 14895 (2006)

[121] J.E. Robinson, *Phys. Rev.* **83**, 678 (1951)

[122] J. Droniou, *Electronic Journal of Differential Equations* **117**, 1 (2003)

[123] D. Kim, *Phys. Rev. E* **52**, 3512 (1995)

[124] M. Henkel and G. Schütz, *Physica A* **206**, 187-195 (1994)

[125] J.A. Mann and W.A. Woyczynski, *Physica A* **291**, 159 (2001)

[126] E. Katzav, *Phys. Rev. E* **68**, 031607 (2003)

[127] A.D. Riggs, S. Bourgeois and M. Cohn, *J. Mol. Biol.* **53** 401-17 (1970)

[128] L. Mirny et al., *J. Phys. A: Math. Gen.* **42** 434013 (2009)

[129] M.A. Lomholt, T. Ambjörnsson and R. Metzler, *Phys. Rev. Lett.* **95**, 260603 (2005)

[130] B. Duplantier, *J. Stat. Phys.* **54**, 581 (1989)

[131] J. Szavits-Nossan and K. Uzelac, *J. Stat. Mech.* P12019 (2009)

[132] S.A. Janowsky and J.L. Lebowitz, *J. Stat. Phys.* **77**, 35 (1994)

[133] D. Kandel and D. Mukamel *Europhys. Lett.* **20**, 325 (1992)

[134] V. Beffara, V. Sidoravicius and M. Eulalia Vares, *Probab. Th. Rel. Fields* **147**, 565-581 (2009)

[135] D.A. Huse, C. Henley and D.S. Fisher, *Phys. Rev. Lett.* **55**, 2924-2924 (1985)

[136] L.H. Tang and I.F. Lyuksyutov, *Phys. Rev. Lett.* **71**, 2745 (1993)

[137] L. Balents and M. Kardar, *Europhys. Lett.* **23**, 503 (1993)

[138] L. Balents and M. Kardar, *Phys. Rev. B* **49**, 13030 (1994)

[139] T. Hwa and T. Nattermann, *Phys. Rev. B* **51**, 455 (1994)

[140] H. Kinzelbach and M. Lassig, *J. Phys. A: Math. Gen.* **28**, 6535 (1995)

[141] J.H. Lee and J.M. Kim, *Phys. Rev. E* **79**, 051127 (2009)

[142] G.M. Schütz, *J. Stat. Phys.* **71**, 471-505 (1993)

[143] M. Ha, J. Timonen and M. den Nijs, *Phys. Rev. E* **68**, 056122 (2003)

[144] C. N. Yang and T. D. Lee, *Phys. Rev.* **87**, 404 (1952)

[145] T. D. Lee and C. N. Yang, *Phys. Rev.* **87**, 410 (1952)

[146] R. A. Blythe and M. R. Evans, *Phys. Rev. Lett.* **89**, 080601 (2002)

[147] J. Krug J, *Braz. J. Phys.* **30**, 97-104 (2000)

[148] L. de Haan and A. Ferreira, *Extreme Value Theory: An Introduction* (Springer, New York, 2006)

[149] L. Gordon, M.F. Schilling and M.S. Waterman, *Probab. Th. Rel. Fields* **72**, 279-87 (1986)

[150] J. Szavits-Nossan and K. Uzelac, *J. Stat. Mech.* P05030 (2011)

[151] R. Ramaswamy and M. Barma, *J. Phys. A: Math. Gen.* **20**, 2973-87 (1987)

[152] M. Barma and R. Ramaswamy, *Field-induced transport in random media* in *Non-linearity and Breakdown of Soft Condensed Matter*, Ed. K. K. Bardhan *et al.* (Springer, Berlin, 1993) str. 309

[153] T. Saegusa, T. Mashiko and T. Nagatani, *Physica A* **387**, 4119-32 (2008)

[154] N. Champagne, R. Vasseur, A. Montourcy and D. Bartolo, *Phys. Rev. Lett.* **105**, 044502 (2010)

[155] Y. Kafri, E. Levine, D. Mukamel, G.M. Schütz and J. Török, *Phys. Rev. Lett.* **89**, 035702 (2002)

[156] F.J. Alexander and J.L. Lebowitz, *J. Phys. A: Math. Gen.* **27**, 683-96 (1994)

[157] B. Schmittmann B, K. Hwang and R.K.P. Zia, *Europhys. Lett.* **19**, (1) 19-25 (1992)

[158] R. Usmani, *Linear Algebra Appl.* **212-213**, 413 (1994)

[159] C. Cocozza-Thivent,*Z. Wahrsch. Verw. Gebiete* **70** 509-523 (1985)

Curriculum Vitae

Juraj Szavits-Nossan was born on 28th December 1980 in Zagreb, Croatia, where he attended elementary and high school. In high school he participated in various competitions in mathematics and physics on the national level and also in the XXX International Physics Olympiad in Padua, Italy in 1999. In the same year he started undergraduate studies in physics at the Faculty of Science at University of Zagreb, where he graduated in 2005 under supervision of Dr. Katarina Uzelac from the Institute of Physics. He is recipient of the University of Zagreb Rector's Award for the best student work in physics in 2004, shared with Ivan Balog.

From 2005 he is a postgraduate student in Condensed matter physics at the Faculty of Science at University of Zagreb and a research assistant at the Institute of Physics, under the supervision of Dr. Katarina Uzelac. His field of interest is nonequilibrium statistical physics and, more specifically, phase transitions far from the equilibrium. His is author of four papers and a teaching assistant on the undergraduate course "Advanced statistical physics" at Faculty of Science at University of Zagreb.

List of publications

4. **J. Szavits-Nossan** i K. Uzelac, Absence of phase coexistence in disordered exclusion processes with bypassing, *J. Stat. Mech.* P05030 (2011), arXiv:1105.5076

3. **J. Szavits-Nossan** i K. Uzelac, Impurity-induced shocks in the asymmetric exclusion process with long-range hopping, *J. Stat. Mech.* P12019 (2009), arXiv:0911.5280

2. **J. Szavits-Nossan** i K. Uzelac, Scaling properties of the asymmetric exclusion process with long-range hopping, *Phys. Rev. E* **77**, 051116 (2008), arXiv:0804.4094

1. **J. Szavits-Nossan** i K. Uzelac, Totally asymmetric exclusion process with long-range hopping, *Phys. Rev. E* **74**, 051104 (2006), arXiv:cond-mat/0610510

Sadržaj

1 Uvod

U ovom radu bavimo se klasom tzv. vođenih difuzijskih sustava [1, 2], čiji je tipični predstavnik slikovito prikazan na slici 1.1. Općenito, radi se o makroskopskim sustavima klasičnih čestica koji su u kontaktu s dva spremnika različitih gustoća (slika 1.1) ili temperatura, s kojima izmjenjuju čestice ili energiju. Pritom nas zanima situacija u kojoj na sustav djeluje vanjsko polje $\vec{E}$, npr. električno ili gravitacijsko, koje "tjera" (vodi) čestice u jednom smjeru, pri čemu se u sustavu uspostavlja tok mase i/ili energije. Zbog razlike u gustoći/temperaturi spremnika i proizvoljno jakog vanjskog polja, ovako zadan sustav s vremenom će postići stacionarno, ali neravnotežno stanje koje nije opisano (ravnotežnom) Gibbs-Boltzmannovom raspodjelom.

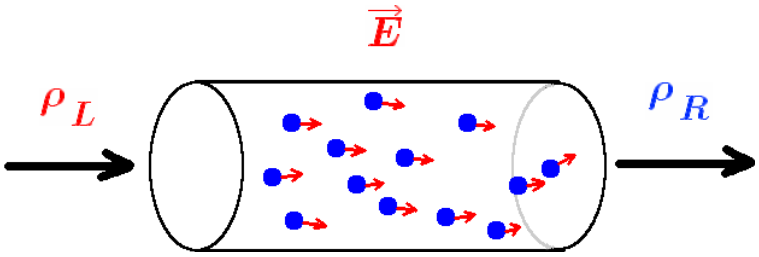

Slika 1.1: Simbolični prikaz vođenih difuzijskih sustava u kontaktu s dva spremnika različitih gustoća. Na sustav djeluje i vanjsko polje $\vec{E}$ koje određuje smjer kretanja čestica.

Osim u nekim jednodimenzionalnim modelima iz ove klase sustava [3–5], koje ćemo izložiti u poglavlju 2 , neravnotežna stacionarna raspodjela općenito nije poznata, što onemogućuje jednostavno računanje očekivanih vrijednosti makroskopskih veličina i njihovih fluktuacija, za što bi u ravnotežnom stanju u načelu dostatno bilo izračunati particijsku funkciju [6]. Na koji način iz mikroskopskih jednadžbi gibanja izvesti vremensku evoluciju makroskopskih, termodinamičkih varijabli (dostupnih eksperimentu) u sustavima izvan ravnoteže, središnji je problem neravnotežne statističke fizike. Obzirom da se taj problem, osim u slučaju kada se nalazimo blizu ravnoteže [7], tradicionalno ne pojavljuje u standardnim udžbenicima iz statističke fizike (kao iznimku vidi [8]), u poglavlju 1.1 pokušati

ćemo dati kratki, povijesni pregled glavnih pristupa ovom problemu, unaprijed se ograđujući od iluzije da u tome možemo biti iscrpni i potpuni.

Nepoznavanje stacionarne raspodjele dovodi nas do prvog motiva za istraživanjem vođenih difuzijskih sustava, koji se temelji na ideji da se, u nedostatku jedinstvenog pristupa problemu neravnoteže, proučavanjem jednostavnih neravnotežnih sustava izgradi svojevrsni katalog općenitih principa. Povijesno, sličnu ideju nalazimo u istraživanju faznih prijelaza, koje je prije [10] otkrića renormalizacijske grupe [11] mnoge zaključke crpila iz egzaktnih rješenja konkretnih mikroskopskih modela, poput Isingovog modela u dvije dimenzije [12]. Slijedeći tu ideju, u poglavlju 1.2 kratko ćemo predstaviti, a u poglavlju 2 detaljno proučiti tzv. jednostavni asimetrični proces isključenja (eng. *Asymmetric Simple Exclusion Process, ASEP*) [3–5], čije su razne generalizacije središnja tema ovog rada, prezentirane u poglavljima 3, 4 i 5.

Fazni prijelazi ujedno nas dovode do drugog motiva za istraživanjem vođenih difuzijskih sustava na primjeru ASEP-a. ASEP u kontaktu sa spremnicima čestica različitih gustoća primjer je sustava u kojem se u stacionarnom stanju variranjem rubnih uvjeta javljaju neravnotežni fazni prijelazi [13]. Posebnost i zanimljivost ovog prijelaza naglašena je činjenicom da se radi o faznom prijelazu s kratkodosežnim međudjelovanjem u jednoj dimenziji, čije je postojanje u ravnotežnim sustavima isključeno Peierlsovim argumentom [14]. S druge strane, jednom kad napustimo ravnotežu, ovakav rezultat nas ne bi trebao iznenaditi, obzirom da za sustave trajno daleko od ravnoteže važnu ulogu igra vremenska evolucija, o čijim detaljima čak može ovisiti hoće li se, i kakvo, stacionarno stanje uopće postići. Naravno, broj mogućih vremenskih evolucija koje neki sustav ne vode k ravnotežnom stanju može nam se na prvi pogled činiti ogromnim, posebno na razini matematičkih modela poput ASEP-a. U slučaju faznih prijelaza, nit vodilju daje nam iskustvo s ravnotežom u kojoj na karakter faznih prijelaza utječe tek nekoliko sastojaka (simetrija parametra reda, doseg međudjelovanja, dimenzija, itd.). Veliki napredak da se za neravnotežne sustave uspostave slične klase univerzalnosti već je postignut [9], ali neriješenih pitanja još ima. Primjere faznih prijelaza daleko od ravnoteže u vođenim difuzijskim sustavima predstaviti ćemo u poglavlju 1.2.

Naposljetku dolazimo i do posljednjeg, trećeg, jednako važnog motiva za istraživanjem vođenih difuzijskih sustava - primjene na realne sustave. Iako se iz perspektive matematičkih modela ovaj motiv često doima zanemarenim, proučavanjem pojednostavljenih mikroskopskih modela nastoji se prepoznati *nužne* (minimalne) sastojke potrebne da se objasni neka pojava, koji se u svrhu boljih kvantitativnih predviđanja kasnije nadopunjuju novima. Povijesno, prvi model iz klase vođenih difuzijskih sustava, tzv. KLS model (nazvan po njegovim autorima S. Katzu, J.L. Lebowitzu i H. Spohnu [15]), originalno je bio motiviran teorijom superionskih vodiča (npr. α-AgI) u kojima se pokretljivi ioni ponašaju

poput tekućine koja primjenom električnog polja teče kroz kristalnu rešetku statičkih iona [16]. S druge strane ASEP, kao njegova jednodimenzionalna inačica u granici jakog polja, našla je i brojne druge primjene, poput kvantnih spinskih lanaca, modeliranja rasta površina balističkim taloženjem, biosinteze proteina i automobilskog prometa, koje detaljnije opisujemo u poglavlju 2.2. Ovi primjeri nam ukazuju da "čestice" u mnogim makroskopskim sustavima možemo zamisliti u mnogo širem rasponu prostornih skala od onoga na koji smo navikli u fizici kondenzirane materije, od spinova u Heisenbergovom modelu, proteina u citoplazmi sve do automobila u prometu. U potonjem primjeru primorani smo tradicionalni pristup Hamiltonijanom zamijeniti stohastičkim pristupom, npr. master jednadžbom, pa nas i konceptualno malo toga zapravo veže za ravnotežu. Iz tog razloga svoje uporište u neravnotežnoj statističkoj fizici nalaze i mnogi "netermodinamički" primjeri makroskopskih sustava, koje nalazimo u biologiji i društvu[1]. Iz te nam se perspektive ne čini pretencioznim reći da je, u svijetu oko nas, ravnoteža zapravo više iznimka nego pravilo.

1.1 Sustavi izvan ravnoteže: kratki pregled

Unatoč brojnim naporima započetim još u pretprošlom stoljeću, razumijevanje makroskopskih sustava izvan ravnoteže još je uvijek daleko od zaokružene teorije. Razlog tome prije svega leži u činjenici da je neravnoteža *dinamički* problem, u smislu da je za njezin opis potrebno poznavati način na koji sustav evoluira u vremenu. Ključni problem koji se pritom javlja je što u općenitom slučaju vremensku evoluciju makroskopskih, termodinamičkih varijabli (dostupnih eksperimentu) ne znamo izvesti iz odgovarajućih mikroskopskih jednadžbi gibanja.

Povijesno, prvi korak u tom smjeru napravio je sam Boltzmann predloživši jednadžbu za vremensku evoluciju raspodjele čestica po položaju i brzini u razrijeđenom plinu, poznatu Boltzmannovu jednadžbu, kojom je uz pretpostavku molekularnog kaosa (njem. "Strosszahlansatz"), objasnio relaksaciju plina k ravnotežnoj, Maxwell-Boltzmannovoj raspodjeli (tzv. H-teorem). Jednadžba je u ono vrijeme doživjela velike kritike sadržane u tvrdnji da reverzibilne Newtonove jednadžbe ne mogu objasniti ireverzibilne makroskopske pojave. S druge strane, klasična mehanika je tvrdila da sve makroskopske pojave slijede iz mikroskopskih, Newtonovih jednadžbi, što je dovelo do tzv. Loschmidtovog paradoksa, nazvanog po Boltzmannovom kritičaru J. Loschmidtu. Ubrzo se, međutim, pokazalo da je ireverzibilnost zapravo već ugrađena u H-teorem pretpostavkom molekularnog kaosa, čime je pitanje porijekla ireverzibilnosti, kojega je britanski astronom A. Eddington popularno nazvao i pitanjem "strelice vremena", započelo svoju dugu

[1] Za općeniti pregled vidi poglavlje "Monte Carlo methods outside of physics" u [17]; u kontekstu difuzijskih sustava vidi [18].

povijest. Mišljenje koje danas prevladava[2], ireverzibilnost doživljava kao rezultat *tipičnog* ponašanja *makroskopskog* sustava, koje nije u kontradikciji s reverzibilnim *mikroskopskim* jednadžbama gibanja [20]. Tome u prilog idu i otkrića fluktuacijskih teorema (FT) [21–25], kolekcije srodnih[3] teorema koji otkrivaju asimetriju u fluktuacijama koje povećavaju ili smanjuju entropiju. Označimo s $\pi(\sigma_\tau)$ vjerojatnost da je u vremenskom intervalu τ prosječna brzina kontrakcije volumena faznog prostora jednaka σ_τ. Prema Liouvilleovom teoremu, ta je brzina identički jednaka nula u sustavima s konzervativnim silama, ali je različita od nule i jednaka brzini produkcije entropije u sustavima s disipacijom. Fluktuacijski teorem kaže da je u disipativnim sustavima

$$\frac{\pi(\sigma_\tau)}{\pi(-\sigma_\tau)} = e^{\tau\sigma_\tau}. \tag{1.1}$$

Drugim riječima, vremenska evolucija po onim putanjama koje smanjuju entropiju eksponencijalno je manje vjerojatna od vremenske evolucije po onim putanjama koje je povećavaju. Ali ne samo to: produkcija entropije je ekstenzivna veličina, pa gornji rezultat, primjenjen na makroskopske sustave, još više umanjuje vjerojatnost spontanog smanjenja entropije. Gornji teorem vrijedi vrlo općenito, a njegove brojne inačice razlikuju se po tome radi li se o determinističkom ili stohastičkom sustavu, te da li nas zanima prijelazno (kao u izrazu 1.1) ili stacionarno stanje (u granici $\tau \to \infty$). Na primjer, Gallavotti i Cohen su spomenuti teorem dokazali za tzv. termostatirane disipativne, ali *reverzibilne* sustave, matematičkoj idealizaciji realnih termostatiranih sustava (za noviji pregled vidi [27]). Iz perspektive drugog zakona termodinamike i pitanja "strelice vremena", ovi rezultati sugeriraju da intrinsične "strelice vremena" nema, ali da je možemo opaziti *lokalno*, u smjeru koji je određen predznakom produkcije entropije[4].

Uz fluktuacijske teoreme veže se još jedan iznenađujući i općeniti rezultat, jednakost Jarzynskog [29], za koju se pokazalo da je specijalni oblik fluktuacijskih teorema [30] (Štoviše, Harris i Schütz su pokazali da se svi fluktuacijski teoremi mogu izvesti iz fundamentalnih svojstava Markovljevih procesa obzirom na inverziju vremena, vidi [30].). Zamislimo neki sustav u kontaktnu s okolinom u kojem energija sustava ovisi o nekom parametru λ, kojeg variramo u vremenu. Ako parametar λ variramo *beskonačno sporo*, ukupni prosječni rad $\langle W \rangle$ obavljen na sustavu od vanjske sile jednak je razlici slobodnih energija konačnog (2) i početnog (1) ravnotežnog stanja, $\langle W \rangle = F_2 - F_1 = \Delta F$ [31]. Ukoliko parametar λ variramo konačnom brzinom općenito vrijedi $\langle W \rangle \geq \Delta F$, što je ekvivalentno

[2]Suprotnu ideju, da je ireverzibilnost intrinsična mikroskopskim dinamičkim sustavima, zagovarao je I. Prigogine, dobitnik Nobelove nagrade za kemiju 1977. godine (za neformalni uvod vidi [19]).

[3]Za raspravu o sličnostima i razlikama vidi npr. [26].

[4]U kontekstu kozmologije, ovaj način razmišljanja naposljetku vodi na pretpostavku o rođenju Svemira u jako uređenom stanju, vidi npr. [28]

drugom zakonu termodinamike. S druge strane, relacija Jarzynskog daje slijedeću *jednakost* za *proizvoljno brzu* promjenu parametra λ,

$$\langle exp(-\beta_1 W)\rangle_{1\to 2} = exp(-\beta\Delta F) \tag{1.2}$$

pri čemu konačno stanje 2 uopće ne mora biti ravnotežno, ali se usprkos tome, u relaciji ipak pojavljuje F_2! Iz gornje relacije, drugi zakon termodinamike slijedi primjenom Jensenove nejednakosti, $\langle exp(A)\rangle \geq exp(\langle A\rangle)$. Relacija 1.2 posebno je važna u eksperimentima, jer omogućuje da se promjena u slobodnoj energiji ravnotežnog sustava mjeri brzim, neravnotežnim mjerenjima. S eksperimentalnog stajališta, fluktuacijski teoremi svoju najveću primjenu nalaze u mezoskopskim sustavima, primjerice u biologiji, u kojima su, zbog manjeg broja stupnjeva slobode, odstupanja od klasične termodinamike neminovna (za pregled eksperimentalnih provjera fluktuacijskih teorema i jednakosti Jarzynskog vidi [32]). Fluktuacijski teoremi i jednakost Jarzynskog perjanica su tzv. dinamičkog pristupa problemu neravnoteže (vidi npr. [33]), koji polazi od (egzaktne) Liouvilleove jednadžbe i koristi svu "artiljeriju" teorije dinamičkih sustava, poput Lyapunovljevih eksponenata. Povijesno mnogo stariji od ovog pristupa je tzv. stohastički pristup, koji je u fiziku uveo Einstein još 1905. godine kako bi riješio problem Brownovog gibanja [34].

U osnovi, stohastički pristup temelji se na prepoznavanju tzv. brzih i sporih stupnjeva slobode, pri čemu su potonji najčešće posljedica zakona očuvanja ili npr. kritičnog usporavanja na prijelazu drugog reda. Na primjeru Brownovog gibanja, položaj i moment zrnca peluda predstavlja spore stupnjeve slobode, naspram položaja i momenata molekula vode koji predstavljaju brze stupnjeve slobode. Ta nam razlika u vremenskim skalama omogućuje da zapišemo mezoskopsku jednadžbu za vremensku evoluciju sporih stupnjeva slobode, tzv. Langevinovu jednadžbu [35], u kojoj se brzi stupnjevi slobode aproksimiraju stohastičkim članom $\vec{\eta}$,

$$m\frac{d\vec{v}}{dt} = -\lambda\vec{v} + \vec{\eta}, \tag{1.3}$$

gdje je

$$\langle \eta(\vec{x},t)\eta(\vec{x}',t')\rangle = 2\lambda k_B T\delta(\vec{x}-\vec{x}')\delta(t-t'). \tag{1.4}$$

Langevinova jednadžba, u općenitom obliku, temelj je tzv. linearne ireverzibilne termodinamike (vidi npr. [7]), koja opisuje male pomake sporih varijabli oko ravnoteže u granici linearnog odziva. Razvijana do sredine prošlog stoljeća, ova je teorija dala zaokruženi opis fluktuacija termodinamičkih varijabli blizu ravnoteže, kojima je kasnije, konceptom lokalne ravnoteže, dodana i prostorna ovisnost [7]. Središnja ideja linearne ireverzibilne termodinamike je Onsagerova hipoteza regresije fluktuacija [36], eksplicitno dokazana za Gaussove Markovljeve procese [37], koja kaže da relaksacija sustava perturbiranog vanjskom linearnom smetnjom slijedi *istu* vremensku evoluciju kao i spontane fluktuacije u ravnoteži. Drugim

riječima, u granici linearnog odziva sustav u prosjeku ne razlikuje način na koji je pripremljeno početno stanje. S praktične strane, to nam omogućuje da odziv sustava na vanjsku smetnju povežemo s ravnotežnim fluktuacijama, što vodi na fluktuacijsko-disipacijski (FD) teorem [38, 39] i Green-Kubo (GK) relacije [40]. Otada je bilo mnogo pokušaja da se FD teorem i GK relacije generaliziraju na nelinearni odziv i sustave daleko od ravnoteže, a značajni interes bilježi se posebno u posljednje vrijeme (vidi [41] i sadržane reference).

S druge strane, važan primjer sustava koji nisu nužno lokalno u ravnoteži su upravo sustavi kojima smo započeli poglavlje - vođeni difuzijski sustavi, čiji pregled donosimo u nastavku.

1.2 Vođeni difuzijski sustavi

Matematički model vođenih difuzijskih sustava je tzv. vođeni plin na rešetci (eng. *driven lattice gas*), kojega su predložili Katz, Lebowitz i Spohn (KLS) 1984. godine [15] kao jednostavno poopćenje Isingovog modela, u svrhu modeliranja vodljivosti u superionskim vodičima, npr. u anorganskim kristalima poput β-Al_2O_3, staklima poput AgI-Ag_2MoO_4 i polimerima poput (polietilen-oksid)-$NaBF_4$. Njihova je zajednička karakteristika nagli pad vodljivosti od nekoliko redova veličine na niskim temperaturama, koji se, obzirom da ovisi o vanjskom električnom polju, može smatrati i *neravnotežnim* faznim prijelazom.

Jedan od najjednostavnijih realizacija vođenog plina na rešetci je sustav (klasičnih) čestica koje zauzimaju mjesta na kubičnoj rešetci u d dimenzija, uz uvjet da je svaki čvor rešetke zauzet najviše jednom česticom ($\sigma_{\vec{r}} = 0, 1$). Osim interakcije "nultog" dosega, čestice još međudjeluju kratkodosežnom interakcijom, tako da je ukupna energija sustava (do na konstantu) oblika

$$\mathcal{H} = -4J \sum_{|\vec{r}-\vec{r}'|=1} \sigma_{\vec{r}}\sigma_{\vec{r}'}. \tag{1.5}$$

Uz to, na čestice djeluje i vanjsko polje $\vec{E}$, u kojem se one ponašaju kao pozitivno nabijeni ioni. U kontekstu superionskih vodiča, čestice predstavljaju "tekuću" fazu vodljivih iona koji difundiraju kroz kristalnu rešetku statičkih iona. Zbog zasjenjenja Coulombove interakcije, rezultantna interakcija modelira se principom isključenja na malim udaljenostima i kratkodosežnom interakcijom koja se u modelu zanemaruje izvan dosega prvih susjeda.

U kontaktu s toplinskim spremnikom na temperaturi T i vanjskim poljem $\vec{E}$, vođeni plin na rešetci evoluira u vremenu prema master jednadžbi

$$\frac{\partial P_E(\vec{\sigma}, t)}{\partial t} = \sum_{\vec{\sigma}^{\vec{r}\vec{r}'}} [c_E(\vec{\sigma}^{\vec{r}\vec{r}'}, \vec{r}, \vec{r}')P_E(\vec{\sigma}^{\vec{r}\vec{r}'}, t) - c_E(\vec{\sigma}, \vec{r}, \vec{r}')P_E(\vec{\sigma}, t)], \tag{1.6}$$

gdje je $\vec{\sigma}^{\vec{r}\vec{r}'}$ konfiguracija dobivena zamjenom varijabli okupiranosti čvorova na mjestima $\vec{r}$ i $\vec{r}'$, $P_E(\vec{\sigma}, t)$ je vjerojatnost nalaženja konfiguracije $\vec{\sigma}$ u trenutku t,

a $c_E(\vec{\sigma}, \vec{r}, \vec{r}')$ vjerojatnost promjene konfiguracije po jedinici vremena iz $\vec{\sigma}$ u $\vec{\sigma}^{\vec{r}\vec{r}'}$. Zamjena $\vec{r} \leftrightharpoons \vec{r}'$ odgovara pomaku čestice na susjednu šupljinu ako je $\sigma_{\vec{r}} - \sigma_{\vec{r}'} \neq 0$ i $|\vec{r} - \vec{r}'| = 1$, dok su ostali prijelazi među konfiguracijama zabranjeni. Vjerojatnosti $c_E(\vec{\sigma}, \vec{r}, \vec{r}')$ definirane su na slijedeći način,

$$c_E(\vec{\sigma}, \vec{r}, \vec{r}') = \phi(\beta\Delta\mathcal{H} - \epsilon\beta E), \tag{1.7}$$

gdje je $\Delta\mathcal{H} = \mathcal{H}(\vec{\sigma}^{\vec{r}\vec{r}'}) - \mathcal{H}(\vec{\sigma})$, a $-\epsilon E$ rad potreban da se čestica pomakne na susjedno mjesto (pretpostavljamo jedinični naboj i jediničnu konstantu rešetke), pri čemu je $\epsilon = -1, 0$ i 1 za pomake redom suprotno od smjera polja, okomito na smjer polja i u smjeru polja. Funkcija ϕ se bira tako da u odsutnosti vanjskog polja, $c_E(\vec{\sigma}, \vec{r}, \vec{r}')$ zadovoljava princip detaljne ravnoteže[5],

$$\phi(\beta\Delta\mathcal{H}) = e^{-\beta\Delta\mathcal{H}}\phi(-\beta\Delta\mathcal{H}). \tag{1.8}$$

što osigurava postizanje termodinamičke ravnoteže u kojoj je stacionarna vjerojatnost dana Gibbs-Boltzmannovom raspodjelom

$$P_{E=0}(\vec{\sigma}) = \frac{1}{Z} e^{-\beta\mathcal{H}(\vec{\sigma})}. \tag{1.9}$$

U tom slučaju javlja se uobičajeni kontinuirani feromagnetski fazni prijelaz na gustoći $\rho = 1/2$ i temperaturama 0, 2.27 J/k_B i 4.5 J/k_B, redom u jednoj, dvije i tri dimenzije.

U prisutnosti vanjskog polja, sustav pokazuje kontinuirani fazni prijelaz u uređenu fazu (u $d > 2$), ali na kritičnoj temperaturi koja ovisi o vanjskom polju, $T_c(E)$. Osim te sličnosti, razlike nalazimo u svim temperaturnim režimima (za potpuniji pregled vidi [1, 42, 43]). Od iznenađujućih razlika izdvajamo:

- dugodosežne korelacije u neuređenoj fazi, $T > T_c(E)$, $G(\vec{r}) \sim |\vec{r}|^{-d}$, za koje se može pokazati da su generička odlika *neravnotežnih* sustava u kojima vremenska evolucija čuva parametra reda [44], i

- činjenicu da $T_c(E)$ raste s E, te se saturira u $T_c(\infty) > T_c(0)$, suprotno očekivanju da će jako vanjsko polje unijeti nered i sniziti temperaturu prijelaza.

Ova i druga neočekivana svojstva vođenih difuzijskih sustava pobudila su interes za još jednostavnijim modelima, po mogućnosti dostupnijim analitičkim računima od KLS modela, čije je istraživanje u nedostatku egzaktnog rješenja ponajviše bilo ograničeno na Monte Carlo simulacije i metode renormalizacijske grupe. Primjer takvog modela je već spomenuti jednostavni asimetrični proces isključenja (ASEP) kao specijalni slučaj jednodimenzionalnog KLS modela bez kratkodosežnog međudjelovanja ($J = 0$).

[5] Na primjer, izbor $\phi(x) = \min\{1, e^{-x}\}$ odgovara Metropolisovoj izmjeni.

ASEP je prvi put promatran kao model za transport ribosoma na mRNA 1968. godine [45, 46], te 1970. godine kao čisto matematički model interagirajućih Markovljevih procesa [47]. U kontekstu vođenih difuzijskih sustava, ASEP je riješen egzaktno 1993. godine u slučaju otvorenih rubnih uvjeta [4, 5], koji predstavljaju izmjenu čestica sa spremnicima gustoća ρ_L i ρ_R. Egzaktno rješenje potaknulo je veliki interes za ovim modelom, a iz perspektive teorije neravnotežnih stacionarnih stanja uslijedilo je nekoliko važnih rezultata. Derrida, Lebowitz i Speer su iz egzaktnog rješenja izveli raspodjelu vjerojatnosti da se u stacionarnom stanju opazi fluktuacija gustoće proizvoljnog makroskopskog profila $\rho(x)$,

$$P_L(\rho(x)) \sim exp[-L\mathcal{F}(\{\rho(x)\})], \tag{1.10}$$

gdje se $\mathcal{F}(\{\rho(x)\})$ može protumačiti kao neravnotežna inačica slobodne energije. Izraz za funkcional $\mathcal{F}(\{\rho(x)\})$ je složen, a ovdje ćemo istaknuti njegove glavne značajke. Prvo, za razliku od ravnotežnog slučaja (obje gustoće jednake, nema struje), funkcional $\mathcal{F}(\{\rho(x)\})$ je *nelokalna* funkcija od $\rho(x)$. Drugo, ovisno o gustoćama na rubovima, nije više nužno konveksna funkcija. Treće, fluktuacije oko najvjerojatnijeg profila nisu nužno Gaussove.

Bertini *et al.* [48] su kasnije izveli gornji funkcional iz čisto hidrodinamičkih razmatranja za općenite vođene difuzijske sustave, čije se makroskopsko ponašanje može opisati gustoćom $\rho(x,t)$ i strujom $j(x,t)$ koje povezuje jednadžba kontinuiteta,

$$\frac{\partial \rho}{\partial t} = -\frac{\partial j}{\partial x}. \tag{1.11}$$

pri čemu se struja $j(x,t)$ sastoji od difuznog člana $-D\partial\rho/\partial x$ i člana koji je induciran vanjskim poljem (u linearnom odzivu),

$$j(x,t) = -D(\rho)\frac{\partial \rho}{\partial x} + \sigma(\rho)E. \tag{1.12}$$

(U poglavlju 2 ćemo pokazati da ASEP odgovara koeficijentima $D(\rho) = const.$ i $\chi(\rho) = \rho(1-\rho)$). Teorija Bertinija *et al.*, nazvana *makroskopskom teorijom fluktuacija*, osim stacionarnih fluktuacija opisuje i dinamičke fluktuacije, pa je u tom smislu generalizacija Onsager-Machlup teorije [37], koja za sustave u ravnoteži daje vjerojatnost opažanja neke zadane vremenske evolucije spontanih fluktuacija. U kontekstu mikroreverzibilnosti, na kojoj počiva Onsager-Machlup teorija, makroskopska teorija fluktuacija otkrila je asimetriju u vremenskim evolucijama spontanih fluktuacija i odgovarajućih relaksacija kao jednu od osnovnih značajki neravnotežnih sustava, koje izvan ravnoteže više nisu vremenski inverz jedna drugoj. U tom je smislu ASEP, na kojem su ovi principi prvi put otkriveni, opravdao svoju ulogu prozora u svijet neravnotežnih pojava.

2

Jednostavni asimetrični proces isključenja

S jedne strane, ASEP je zanimljiv jer ga se može povezati s modelima kojima se opisuju raznolike pojave poput rasta površina, sinteze proteina, automobilskog prometa i dr. S druge strane, taj model zauzima važno mjesto u statističkoj fizici kao egzaktno rješiv model za opis faznih prijelaza daleko od ravnoteže koji su inducirani rubnim uvjetima. Fazni dijagram u modelu s otvorenim rubnim uvjetima iz pedagoških razloga izlažemo prvo u aproksimaciji srednjeg polja, a zatim i kroz egzaktno rješenje, koje zbog svoje složenosti i mogućnosti prilagodbe na brojne generalizacije modela predstavlja svojevrsno teorijsko dostignuće. Povrh egzaktnog rješenja u nastavku dajemo i fenomenološki opis faznog prijelaza prvog reda u okviru slike dinamike domenskih zidova, koja se oslanja na svojstva tzv. Burgersove jednadžbe dobivene u hidrodinamičkoj granici modela. Zatim analiziramo fazni prijelaz drugog reda karakteriziran divergencijom prostorne skale, te navodimo pripadajući kritični eksponent. Naposljetku, raspravljamo o nekim poopćenjima modela, a koja će kasnije biti od koristi za bolje razumijevanje robustnosti ove slike faznih prijelaza.

2.1 Definicija modela

U jednostavnom asimetričnom procesu isključenja (ASEP), klasične čestice zauzimaju diskretna mjesta na jednodimenzionalnoj rešetci uz jednostavno pravilo da jedan čvor rešetke istovremeno može zauzeti najviše jedna čestica ($\tau_i = 0$ i 1 redom za nepopunjeni i popunjeni čvor). Vremenska evolucija se može definirati na više načina, ovisno o problemu koji se želi modelirati. Tako se za opis pojava u prometu uvodi tzv. *paralelna* dinamika, u kojoj se sve čestice pomiču za jedno mjesto istovremeno u diskretnim vremenskim koracima. Najčešće se ipak promatra tzv. *nasumično-sekvencijalna* dinamika, u kojoj se u nekom vremenskom intervalu $[t, t + dt]$ pomiče samo jedna, nasumično odabrana čestica. Takva je vremenska evolucija opisana master jednadžbom

$$\frac{d}{dt}P(C,t) = \sum_{C'} \left[W(C' \to C)P(C',t) - W(C \to C')P(C,t)\right], \qquad (2.1)$$

gdje je $P(C,t)$ vjerojatnost da je sustav u trenutku t u konfiguraciji C, pri čemu je konfiguracija C potpuno određena zaposjednućima čvorova, $C = \{\tau_1, \tau_2, \dots\}$. U jednoj dimenziji, vjerojatnosti prijelaza $W(C \to C')$ su dane s

$$W(C \to C') = \begin{cases} p, & C = \{\dots, \tau_i = 1, \tau_{i+1} = 0, \dots,\}, \\ & C' = \{\dots, \tau_i = 0, \tau_{i+1} = 1, \dots,\}, \\ q = 1 - p, & C = \{\dots, \tau_i = 0, \tau_{i+1} = 1, \dots,\}, \\ & C' = \{\dots, \tau_i = 1, \tau_{i+1} = 0, \dots,\}, \\ 0, & \textit{ostalo}. \end{cases} \tag{2.2}$$

Ovisno o iznosu p odnosno q govorimo o potpuno asimetričnom procesu ($p = 1$, $q = 0$) u kojem se čestice pomiču samo udesno, o djelomično asimetričnom procesu ($p \neq q \neq 0$) u kojem se čestice pomiču i ulijevo ili o simetričnom procesu ($p = q$) u kojem se čestice jednako učestalo pomiču ulijevo i udesno. Fizikalne veličine od interesa su lokalna gustoća $\langle \tau_i \rangle$ i lokalna struja $j_i = \langle \tau_i(1 - \tau_{i+1}) \rangle$, pri čemu $\langle \dots \rangle$ označava usrednjavanje po raspodjeli $P(C,t)$, $\langle \dots \rangle = \sum_C (\dots) P(C,t)$. Lokalnu gustoću i struju povezuje jednadžba kontinuiteta,

$$\frac{d}{dt}\langle \tau_i \rangle = j_{i-1} - j_i, \tag{2.3}$$

odakle trivijalno slijedi da je u stacionarnoj granici u kojoj je $d\langle \tau_i \rangle / dt = 0$, struja konstantna kroz lanac, $j_i \equiv j$. Na konačnoj rešetci od L čvorova potrebno je definirati i rubne uvjete, koji mogu biti periodički ($\tau_1 = \tau_{L+1}$) ili otvoreni (slika 2.1). Potonji fizikalno znače da sustav izmjenjuje čestice sa (beskonačnim) spremnicima konstantih gustoća, pri čemu se neravnotežno stanje postiže nejednakim gustoćama.

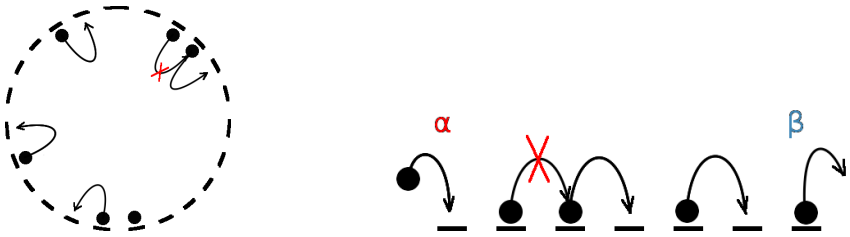

Slika 2.1: Slikoviti prikaz jednostavnog potpuno asimetričnog procesa isključenja s periodičkim (lijevo) i otvorenim rubnim uvjetima (desno).

2.1.1 Periodički rubni uvjeti

Rješenje master jednadžbe za ovaj model u općenitom, nestacionarnom stanju pronađeno je tek nedavno koristeći Bethe ansatz [49]. Nas zanima stacionarna granica u kojoj je lako vidjeti da su sve konfiguracije jednako vjerojatne, što daje

$$P(C) = \frac{1}{\binom{L}{N}}, \tag{2.4}$$

gdje je $N = \rho L$ broj čestica, a ρ gustoća. Sukladno tome, profil gustoće je konstantan, a korelacijska funkcija se faktorizira,

$$\langle \tau_i \rangle = \frac{N}{L} = \rho, \quad \langle \tau_i \tau_j \rangle = \frac{(N-1)N}{(L-1)L} \approx \rho^2, \tag{2.5}$$

što vodi na slijedeći oblik struje

$$j = \frac{N}{L}\frac{L-N}{L-1} = \rho(1-\rho) + O(L^{-1}), \tag{2.6}$$

Sa slike 2.2 vidimo da struja postiže maksimum na gustoći 1/2, što je posljedica međudjelovanja putem principa isključenja. U zajednici koja se bavi modeliranjem prometa, ovisnost struje o gustoći često se naziva se i *fundamentalnim dijagramom.*

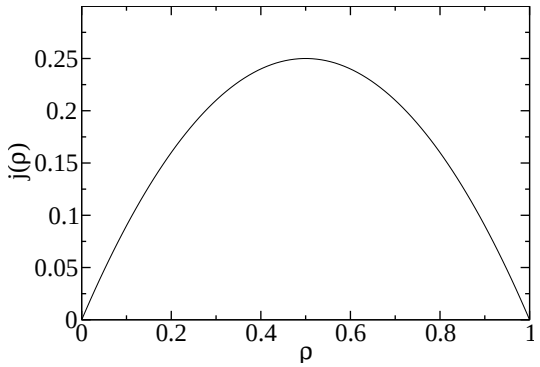

Slika 2.2: Ovisnost struje j o gustoće ρ u TASEPu s periodičkim rubnim uvjetima.

2.1.2 Otvoreni rubni uvjeti

U slučaju otvorenih rubnih uvjeta, sustav izmjenjuje čestice na rubovima na način da čestice ulaze i izlaze iz sustava s određenom vjerojatnošću. Na primjer, u potpuno asimetričnom procesu, čestice ulaze u lanac na mjesto $i = 1$ s vjerojatnošću α, ako je to mjesto prazno, a izlaze iz lanca s mjesta $i = L$ s vjerojatnošću β, ako je to mjesto popunjeno. U master jednadžbi (2.1), vjerojatnosti prijelaza (2.2) treba dakle nadopuniti s

$$W(C \to C') = \begin{cases} \alpha, & C = \{\tau_1 = 0, \dots\}, C' = \{\tau_1 = 1, \dots\}, \\ \beta, & C = \{\dots, \tau_L = 1\}, C' = \{\dots, \tau_L = 0\}, \\ 0, & \textit{ostalo.} \end{cases} \tag{2.7}$$

Kako je na rubovima struja j jednaka $j = \alpha(1 - \langle\tau_1\rangle) = \beta\langle\tau_L\rangle$, rubove možemo interpretirati kao spremnike čestica gustoća $\rho_L = \alpha$ i $\rho_R = 1-\beta$. Za izbor gustoća $\rho_L = \rho_R$, što odgovara $\alpha = 1-\beta$, lako je pokazati da je stacionarno rješenje slično onome za periodičke rubne uvjete u smislu da je profil gustoće konstantan i bez korelacija

$$\langle\tau_i\rangle = \alpha, \quad \langle\tau_i\tau_j\rangle = \alpha^2, \quad \alpha = 1 - \beta. \tag{2.8}$$

Netrivijalno ponašanje dobiva se za $\rho_L \neq \rho_R$, a zanimljivo je po tome što se variranjem α i β javljaju različite faze u sustavu koje su razlikuju u profilima gustoće i iznosima struje, a koje razdvajaju fazni prijelazi. Kako ćemo vidjeti u poglavlju 2.3, ti fazni prijelazi imaju velike sličnosti s faznim prijelazima u ravnotežnim sustavima.

2.2 Preslikavanje na druge modele i primjene

2.2.1 Rast površina

ASEP se može preslikati na diskretni model rasta površine [66], u kojem se površina izlaže snopu atoma koji se na površinu vežu (odnosno od površine odvajaju) samo na mjestima lokalnog minimuma, $h_i - h_{i\pm1} = -1$ (odnosno maksimuma, $h_i - h_{i\pm1} = 1$), a h_i je visina površine na mjestu i. Preslikavanje konfiguracije površine $\{h_i|i = 1, \ldots, L\}$ u konfiguraciju čestica $\{\tau_i|i = 1, \ldots, L\}$ u ASEP-u dano je relacijom

$$h_{i+1} - h_i = 1 - 2\tau_i, \tag{2.9}$$

tako da jedan pomak čestice udesno (ulijevo) odgovara porastu (smanjenju) površine $h_i \to h_i + 2$ ($h_i \to h_i - 2$), kao što je prikazano na slici 2.3. Ovim procesom površina raste srednjom brzinom $v = 2j$, gdje je $j = (p - q)\rho(1 - \rho)$ stacionarna struja u ASEP-u,

$$\bar{h} = \frac{1}{L}\sum_{i=1}^{L} h_i \approx vt, \quad t \to \infty. \tag{2.10}$$

Površina je pritom hrapava u smislu da je

$$\xi = \left[\frac{1}{L}\sum_{i=1}^{L}(h_i - \bar{h})^2\right]^{1/2} \propto L^{\chi}, \quad t \to \infty. \tag{2.11}$$

U kontinuiranoj granici u kojoj $h_i \to h(x, t)$ [67], diskretni model rasta u simetričnom slučaju $p = q$ opisan je tzv. Edwards-Wilkinsonovom (EW) jednadžbom,

$$\frac{\partial}{\partial t}h(x,t) = \nu\nabla^2 h(x,t) + \eta(x,t) \tag{2.12}$$

a u asimetričnom slučaju $p \neq q$ tzv. Kardar-Parisi-Zhang (KPZ) jednadžbom,

$$\frac{\partial}{\partial t}h(x,t) = \nu\nabla^2 h(x,t) + \frac{\lambda}{2}(\nabla h)^2 + \eta(x,t) \tag{2.13}$$

gdje je $\eta(x,t)$ bijeli šum s kovarijancom oblika

$$\langle \eta(x,t)\eta(x',t')\rangle = D\delta(x-x')\delta(t-t'). \tag{2.14}$$

Karakteristična dužina hrapavosti površine ξ pritom zadovoljava relaciju homogenosti,

$$\xi(\bar{h}, L) = L^{\chi} f(\bar{h}L^{-z}), \tag{2.15}$$

gdje je $f(x) \approx$ const. za $x \to \infty$ i $f(x) \propto x^{\chi/z}$ za $x \to 0$. Drugim riječima, za konačna vremena t, ξ raste s $\bar{h}$ kao $\xi \propto \bar{h}^{\chi/z}$, te se saturira u $\xi \propto L^{\chi}$ u $t \to \infty$. Za EW jednadžbu, obzirom da je linearna, lako je pokazati da je $\chi = 1/2$ i $z = 2$, dok je to znatno složenije za KPZ jednadžbu, za koju je metodom dinamičke renormalizacijske grupe [68] pokazano da je $\chi = 1/2$ i $z = 3/2$.

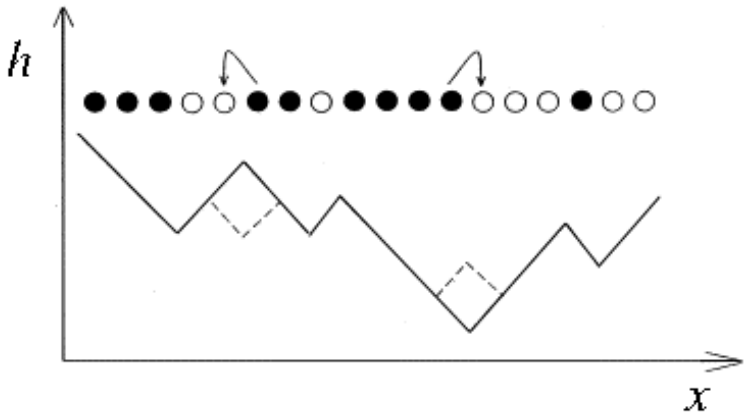

Slika 2.3: Preslikavanje ASEP-a na model rasta površine balističkim taloženjem. Pomak čestice na i-tom čvoru udesno (ulijevo) u ASEP-u odgovara porastu (smanjenju) površine $h_i \to h_i + 2$ ($h_i \to h_i + 2$).

2.2.2 Kvantni spinski lanci

Formalna sličnost stohastičkog i kvantnog sustava počiva na činjenici da su i master jednadžba i Schrödingerova jednadžba linearne u vremenu. Da bismo

zapisali master jednadžbu u kvantnom formalizmu, krenimo od općenitog zapisa master jednadžbe,

$$\frac{d}{dt}P(C,t) = \sum_{C'} \left[W(C' \to C)P(C',t) - W(C \to C')P(C,t)\right], \tag{2.16}$$

te pridružimo svakoj konfiguraciji C vektor $|C\rangle$. Ako definiramo vektor $|P(t)\rangle \equiv \sum_C P(C,t)|C\rangle$, tada master jednadžba prelazi u jednadžbu za $|P(t)\rangle$,

$$\frac{\partial}{\partial t}|P(t)\rangle = -H|P(t)\rangle, \tag{2.17}$$

gdje je H "Hamiltonijan" zadan matričnim elementima,

$$\langle C|H|C'\rangle = \begin{cases} -W(C' \to C) & C \neq C' \\ \sum_{C'' \neq C} W(C \to C'') & C = C'. \end{cases} \tag{2.18}$$

Odavde odmah slijede dva općenita svojstva "Hamiltonijana" H. Ako uvedemo vektor $\langle S| \equiv \sum_C \langle C|$, tada prvo svojstvo slijedi iz činjenice da je zbroj svih vjerojatnosti $\sum_C P(C,t) = 1$,

$$\langle S|P(t)\rangle = \sum_C P(C,t) = 1 \quad \forall t, \tag{2.19}$$

što dalje vodi na

$$\langle S|H = 0. \tag{2.20}$$

Drugo svojstvo tiče se stacionarnog stanja (ukoliko postoji), koje u kvantnom formalizmu odgovara osnovnom stanju "Hamiltonijana",

$$\frac{d}{dt}|P(t)\rangle = 0 \quad \Rightarrow \quad H|P^*\rangle = 0. \tag{2.21}$$

Sličnost s kvantnim formalizmom se može razvijati dalje, pa tako observablu F možemo zapisati dijagonalnom matricom $F(t) = \sum_C F(C)|C\rangle\langle C|$, što za očekivanu vrijednost daje $\langle F(t)\rangle = \sum_C F(C)P(C,t) = \langle S|F|P(t)\rangle$. Ubacimo li u izraz za $\langle F(t)\rangle$ jedinični operator zapisan u bazi svojstvenih vektora $|\epsilon\rangle$ "energije" ϵ, $\hat{1} = \sum_\epsilon |\epsilon\rangle\langle\epsilon|$, tada očekivanu vrijednost možemo zapisati kao

$$\langle F(t)\rangle_{P_0} = \sum_\epsilon \langle S|F|\epsilon\rangle\langle\epsilon|P_0\rangle e^{-\epsilon t}, \tag{2.22}$$

gdje $|P_0\rangle$ označava neko početno stanje. Za jako velika vremena t, očekujemo da je gornja suma određena najmanjom energijom pobuđenja ϵ_1, što vodi na

$$\langle F(t)\rangle_{P_0} \to \langle F\rangle^* + \langle S|F\epsilon_1\rangle\langle\epsilon_1|P_0\rangle e^{-\epsilon_1 t}, \quad t \to \infty \tag{2.23}$$

gdje je $\langle F\rangle^*$ očekivana vrijednost observable F u stacionarnom stanju. Ova korespondencija je jako važna jer omogućuje da se iz spektra odgovarajućeg kvantnog sustava odredi karakteristična skala τ relaksacije stohastičkog sustava, $\tau \sim 1/|\mathrm{Re}(\epsilon_1)|$.

Razlog zbog kojeg smo "Hamiltonijan" napisali s navodnicima je u tome što da bi opravdao naziv kvantnog Hamiltonijana, H mora biti Hermitska matrica, a svojstvene vrijednosti od H realne i pozitivne. To je, međutim, tako samo ukoliko za stacionarno rješenje master jednadžbe $P^*(C)$ vrijedi princip detaljne ravnoteže[1],

$$P^*(C)W(C \to C') = P^*(C')W(C' \to C), \tag{2.24}$$

dok je u protivnom "Hamiltonijan" *nehermitski*.

U konkretnom slučaju jednostavnog procesa isključenja, konfiguracija C zadana je brojevima zauzeća $C = \{\tau_1, \ldots, \tau_L\}$, pa je vektor $|C\rangle$ jednak

$$|C\rangle = |\tau_1 \ldots \tau_L\rangle \equiv |\tau_i\rangle \otimes \cdots \otimes |\tau_L\rangle. \tag{2.25}$$

U kvantom sustavu s dva stanja, prirodna reprezentacija operatora su Paulijeve matrice

$$\sigma^x = \begin{pmatrix} 0 & 1 \\ 1 & 0 \end{pmatrix}, \qquad \sigma^y = \begin{pmatrix} 0 & -i \\ i & 0 \end{pmatrix}, \qquad \sigma^z = \begin{pmatrix} 1 & 0 \\ 0 & -1 \end{pmatrix}, \tag{2.26}$$

od kojih se mogu konstruirati operatori $s^{\pm}$ i n,

$$s^+ = \begin{pmatrix} 0 & 1 \\ 0 & 0 \end{pmatrix}, \qquad s^- = \begin{pmatrix} 0 & 0 \\ 1 & 0 \end{pmatrix}, \qquad n = \begin{pmatrix} 0 & 0 \\ 0 & 1 \end{pmatrix}, \tag{2.27}$$

takvi da je

$$s^+|0\rangle = 0, \quad s^+|1\rangle = |0\rangle \tag{2.28}$$

$$s^-|0\rangle = |1\rangle, \quad s^-|1\rangle = 0 \tag{2.29}$$

$$n|0\rangle = 0, \quad n|1\rangle = |1\rangle. \tag{2.30}$$

Prisjetimo se sada prijelaza među stanjima u ASEP-u koji odgovaraju pomicanju čestica udesno odnosno ulijevo,

$$1_i 0_{i+1} \xrightarrow{p} 0_i 1_{i+1}, \tag{2.31}$$

$$0_i 1_{i+1} \xrightarrow{q} 1_i 0_{i+1}. \tag{2.32}$$

[1]Dokaz je elementaran, ali nešto duži, pa čitatelja upućujemo na npr. [2].

U zapisu preko operatora $s^{\pm}$, gornji procesi vode na nedijagonalne članove u H oblika $-ps_i^- s_{i+1}^+$ i $-qs_i^+ s_{i+1}^-$. Dijagonalne članove lako dobijemo prepoznamo li da je

$$\langle S|s_i^+ = \langle S|n_i \quad \text{i} \quad \langle S|s_i^- = \langle S|(1-n_i). \tag{2.33}$$

Kako bi ispunili uvjet $\langle S|H = 0$, to znači da za svaki nedijagonalni član trebamo dodati isti takav dijagonalni član, ali u kojem smo zamijenili s_i^- s n_i, te s_i^+ s $1-n_i$. To naposljetku daje

$$H_{\text{ASEP}} = \sum_{i=1}^{L} [pn_i(1-n_{i+1}) + q(1-n_i)n_{i+1} - ps_i^- s_{i+1}^+ - qs_i^+ s_{i+1}^-]. \tag{2.34}$$

Iz gornjeg izraza se transformacijom sličnosti $H \to BH_{\text{ASEP}}B^{-1}$ dobiva Hamiltonijan Heisenbergovog XXZ lanca zajedno s nehermitskim članovima proizašlim iz rubnih uvjeta [2],

$$H_{XXZ} = -J\sum_i [\sigma_i^x\sigma_{i+1}^x + \sigma_i^y\sigma_{i+1}^y + \Delta(\sigma_i^z\sigma_{i+1}^z - 1)] + \text{r.u.}, \tag{2.35}$$

gdje su

$$J = \frac{\sqrt{pq}}{2}, \quad \Delta = \frac{\sqrt{p/q} + \sqrt{q/p}}{2} \quad \text{i} \quad B = e^{\ln(p/q)\sum_i i\sigma_i^z}. \tag{2.36}$$

Spektar gornjeg Hamiltonijana se može dalje tražiti Betheovim ansatzom. U slučaju periodičkih rubnih uvjeta, za prvo pobuđeno stanje ϵ_1 se dobiva kompleksna "energija" [50],

$$\epsilon_1 = -2\sqrt{\rho(1-\rho)}\frac{6.509189...}{L^{3/2}} + \pm\frac{2i\pi(2\rho-1)}{L}. \tag{2.37}$$

Realni dio pritom opisuje relaksaciju k stacionarnom stanju iz koje slijedi da je dinamički eksponent $z = 3/2$, dok imaginarni dio daje oscilatorno ponašanje, a odgovara kinematičkim valovima koji putuju grupnom brzinom $v_g = 1-2\rho$. Sličan račun može se provesti i za otvorene rubne uvjete [51,52]. U fazama niske i visoke gustoće to daje konstantni ϵ_1, tj. relaksaciju koja trne eksponencijalno u vremenu, dok se na liniji $\alpha = \beta < 1/2$ i u fazi maksimalne struje dobiva redom $\epsilon_1 \propto L^{-2}$ i $\epsilon_1 \propto L^{-3/2}$.

2.2.3 Proces nultog dosega

Proces nultog dosega (eng. *zero-range process*, ZRP) još je jedan primjer vođenog difuzijskog sustava, a od ASEP-a se razlikuje po tome što čestice zauzimaju čvorove na rešetci bez principa isključenja ($n_i = 0, 1, 2, \dots$), te se pomiču udesno

s vjerojatnošću $u(n_i)$ koja ovisi o broju čestica na tom čvoru. ZRP je zanimljiv zbog pojave kondenzacije u stacionarnom stanju (za pregled vidi [53] i sadržane reference), u smislu da se makroskopski broj čestica ($\propto N$) nalazi na samo jednom čvoru, za što je nužno da vjerojatnosti preskoka $u(i)$ opadaju sporije od

$$u(i) \simeq \beta\left(1+\frac{2}{i}\right), \quad i \gg 1. \tag{2.38}$$

Primjeri sustava koje je moguće opisati ZRP-om uključuju granularne "plinove" (npr. zrnca pijeska ili plastične kuglice) izloženi vibraciji, kao i prometne gužve. Eksperiment u [54] je pokazao da se granularni "plin" raspoređen u L spojenih posuda i izložen vibraciji u jednom trenutku kondenzira u jednoj od posuda (slika 2.4). S prometom ZRP povezuje činjenica da se ZRP može preslikati na TASEP na način da čvorovi i čestice u ZRP-u postaju redom čestice i šupljine u TASEP-u (slika 2.5). Kondenzacija u ZRP-u u tom slučaju odgovara makroskopskoj domeni nepopunjenih čvorova ispred jedne čestice, tj. makroskopskoj koloni iza te čestice.

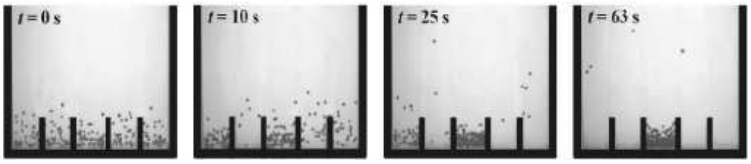

Slika 2.4: Vremenska evolucija granularnog "plina" izloženoga vertikalnoj vibraciji amplitude $a = 1$ mm i frekvencije $f = 21$ Hz. Preuzeto iz [54].

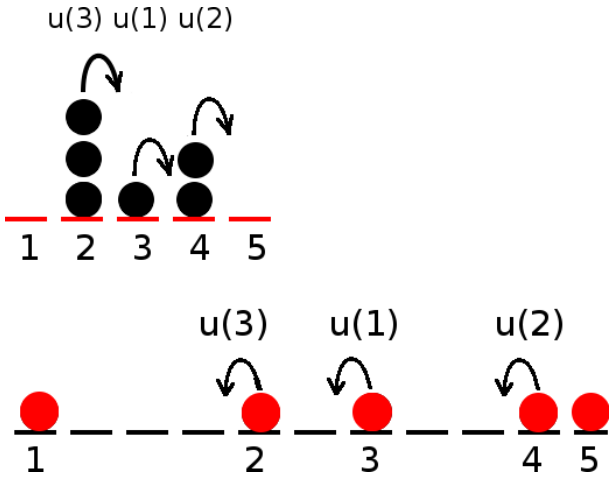

Slika 2.5: Preslikavanje ZRP-a na TASEP. Čvorovi u ZRP-u (označeni brojevima) preslikavaju se u čestice u TASEP-u, a broj čestica na nekom čvoru $i = 1, \ldots, L$ u ZRP-u odgovara broju čestica u TASEP-u ispred i-te čestice.

2.2.4 Automobilski promet

Slika 2.6(a) prikazuje putanje automobila snimljenih iz zraka, pri čemu svaka linija označava putanju jednog automobila. Na slici je zanimljivo uočiti tzv. "fantomski" prometni čep, koji se kreće u *suprotnom* smjeru od smjera kretanja automobila. Naziv "fantomski" znači da usporavanje automobila nije uzrokovano vanjskom smetnjom (npr. radovima na cesti, prometnom nesrećom, itd.), već se radi o spontanoj perturbaciji (uzrokovanoj npr. nespretnom ili pretjeranom reakcijom jednog vozača), koja se dalje prenosi na druga vozila. Da li će do "fantomskog" prometnog čepa doći ili ne, ovisi o tzv. fundamentalnom dijagramu, tj. o ovisnosti struje o gustoći. Primjer takvog dijagrama izmjerenog u stvarnom prometu prikazan je na slici 2.6(b), a sastoji se tzv. slobodnog režima u kojem struja raste linearno s gustoćom i tzv. zakrčenog režima u kojem struja opada s gustoćom.

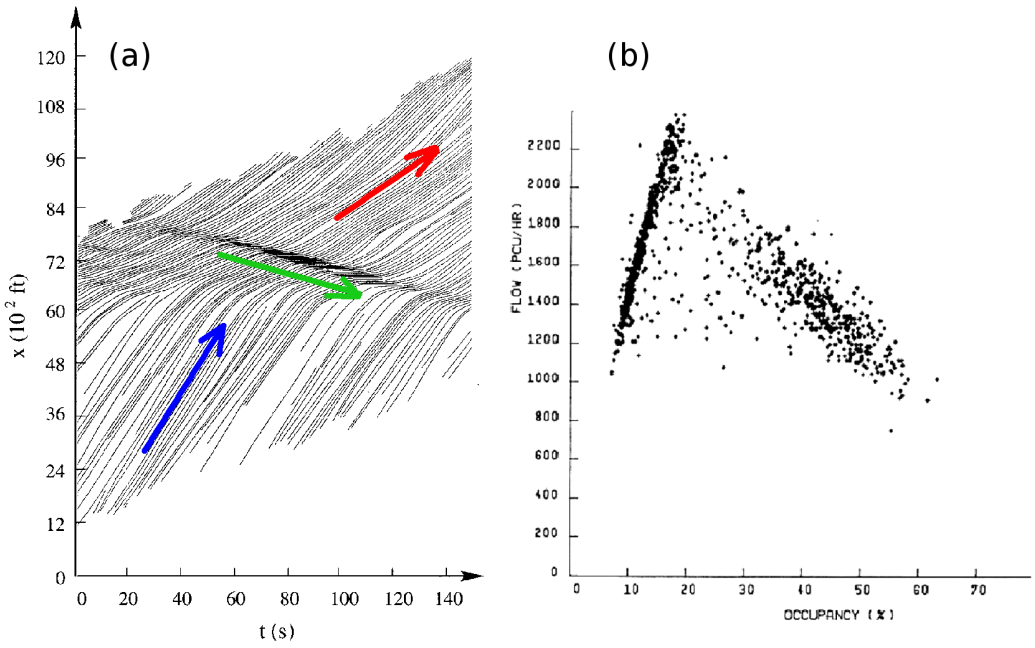

Slika 2.6: (a) Putanje automobila snimljenih iz zraka s pripadnim vektorima brzine (crvena i plava strelica) i tzv. "fantomski" prometni čep koji putuje unazad (zelena strelica). (b) Fundamentalni dijagram stvarnog prometa. Preuzeto iz [55].

Fundamentalni dijagram na slici 2.6(a) podsjeća na ovisnost struje o gustoći u TASEP-u, prikazanoj na slici 2.2. Doista, TASEP s paralelnom dinamikom se može preslikati na tzv. Nagel-Schreckenbergov (NG) model prometa [55] u granici $v_{\max} = 1$. NG model je jednodimenzionalni model na rešetci s periodičkim ili otvorenim rubnim uvjetima u kojem je svakom automobilu pridružena diskretna

varijabla brzine $v_i = 0, 1, \ldots, v_{\max}$. Automobili se u diskretnim vremenskim koracima istovremeno (paralelno) pomiču u istom smjeru prema slijedećim pravilima:

1. **ubrzanje**: ako je $v_i < v_{\max}$, onda $v_i \to v_i + 1$
2. **kočenje**: ako je udaljenost $d_i = x_{i+1} - x_i$ do automobila ispred manja od v_i, onda $v_i \to d_i - 1$
3. **fluktuacije u brzini**: $v_i \to v_i - 1$ s vjerojatnošću p
4. **kretanje**: i-ti automobil se pomiče za v_i mjesta

NG model je minimalni model za opis prometa u smislu da su sva četiri koraka nužna za opis stvarnog prometa. Prvi korak odražava namjeru vozača da vozi najbržom dozvoljenom brzinom. Drugim korakom vozači izbjegavaju sudare. Treći korak odražava individualne karakteristike vozača (npr. pretjeranu reakciju koja rezultira kočenjem) i važan je upravo za formiranje "fantomskih" prometnih čepova. NS model je doživio brojne generalizacije koje odgovaraju realnim uvjetima na prometnicama (za noviji pregled vidi [56] i [18]).

S praktične strane, modeliranje automobilskog prometa važno je radi boljeg razumijevanja (a s ciljem izbjegavanja) nastanka zakrčene faze, u kojoj protok vozila pada s porastom gustoće. Zanimljivo je da iz te problematike dolazi i prvi eksperimentalni dokaz faznog prijelaza prvog reda induciranog rubnim uvjetima, eksperimentalno opažen na prometnicama Kölna [57].

2.2.5 Biosinteza proteina

Biosinteza proteina jedan je od najvažnijih procesa u stanici kojim se genetski kod zapisan u DNK pretvara u proteine kao nosioce specifičnih zadaća. Proces započinje transkripcijom, tj. stvaranjem informacijske RNK (mRNA) u staničnoj jezgri iz DNK pomoću enzima RNK polimeraze (slika 2.7). mRNA zatim napušta jezgru kroz jezgrine pore, te dolazi u citoplazmu. Tu se odvija proces translacije, koji započinje vezanjem ribosoma za mRNA. Ribosom se zatim kreće duž mRNA lanca tražeći tzv. start kodon. Kada ga pronađe, na njega se veže transportna RNK (tRNA), čiji je triplet nukleotida (tzv. antikodon) komplementaran tripletu (kodonu) na mjestu vezanja ribosoma i mRNA. tRNA na sebi nosi jednu aminokiselinu, koja se otpušta i dodaje polipeptidnom lancu (budućem proteinu). Ribosom se pritom pomiče za jedan kodon, na koji se opet veže odgovarajuća tRNA i tako dalje. Proces se ponavlja sve dok ribosom ne "pročita" tzv. stop kodon, nakon čega se protein otpušta s ribosoma.

Ideja MacDonalda *et al.* [45] je bila proces translacije modelirati TASEP-om s otvorenim rubnim uvjetima, u kojem rubovi odgovaraju start i stop kodonima, a čestice ribosomima. TASEP su zatim generalizirali na tzv. l-TASEP [46], u kojem

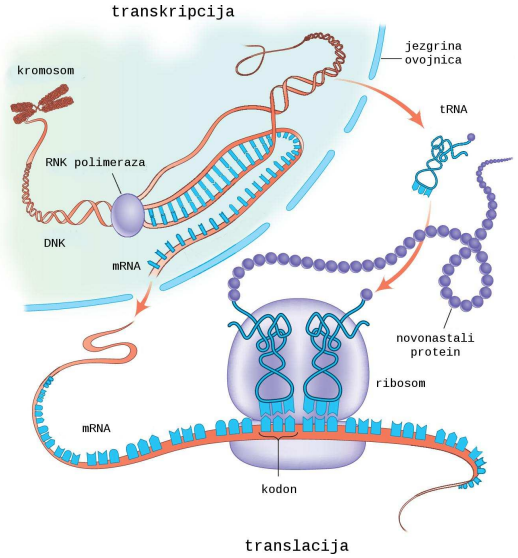

Slika 2.7: Slikoviti prikaz biosinteze proteina koja se sastoji od transkripcije u staničnoj jezgri (stvaranja mRNA iz DNK) i translacije (kretanja ribosoma duž mRNA) u citoplazmi. Preuzeto iz [58].

svaka čestica zauzima l čvorova na rešetci ($l \approx 12$), obzirom da se ribosomi ne vežu samo za jedan kodon. Za potpuniji opis važno je uzeti u obzir i prostorno ovisne vjerojatnosti preskoka, kojima se modelira nejednako vezanje tRNA na pojedinim kodonima na mRNA. U sustavu s periodičkim rubnim uvjetima, pokazuje se da već jedan takav defekt drastično mijenja stacionarno stanje [59]. U slučaju otvorenih rubnih uvjeta, TASEP s jednim i više defekata u kontekstu biosinteze proteina promatralo je nekoliko autora [60–62, 64], a pokazuje se da struja u TASEP-u, a time i brzina sinteze proteina, drastično ovisi o međusobnom položaju defekata, kao i o udaljenosti defekata od rubova lanca.

2.3 Fazni prijelazi u modelu s otvorenim rubnim uvjetima

2.3.1 Fazni dijagram u aproksimaciji srednjeg polja

Vratimo se sada na TASEP s otvorenim rubnim uvjetima. Uvrstimo li izraz za struju u jednadžbu kontinuiteta (2.3), dobivamo jednadžbu oblika

$$\frac{d}{dt}\langle\tau_i\rangle = \langle\tau_{i-1}(1-\tau_i)\rangle - \langle\tau_i(1-\tau_{i+1})\rangle. \tag{2.39}$$

Problem s gornjom jednadžbom za $\langle\tau_i\rangle$ je što sadrži nepoznate korelacijske funkcije višeg reda, $\langle\tau_{i-1}\tau_i\rangle$ i $\langle\tau_i\tau_{i+1}\rangle$, analogno Bogoliubov-Born-Green-Kirkwood-Yvon hi-

jerarhiji. Uobičajena aproksimacija za takav problem je tzv. aproksimacija srednjeg polja, koja aproksimira $\langle\tau_i\tau_{i+1}\rangle \approx \langle\tau_i\rangle\langle\tau_{i+1}\rangle$. Označimo li $\langle\tau_i\rangle$ u aproksimaciji srednjeg polja s ρ_i, u stacionarnoj granici $d\rho_i/dt = 0$ dobivamo rekurziju oblika

$$\rho_{i+1} = 1 - \frac{C}{\rho_i}, \quad i = 1, \ldots, L-1 \tag{2.40}$$

gdje je $C = \alpha(1-\rho_1) = \beta\rho_L$ zapravo struja. Gornja rekurzija rješava se [3] prepoznavanjem da je desna strana od (2.40) homografska funkcija [2] oblika $f(x) = (x-C)/x$, što znači da se iz rješenja kvadratne jednadžbe $f(x) = x$,

$$\rho_\pm = \frac{1 \pm \sqrt{1-4C}}{2}, \quad 1-4C > 0 \tag{2.41}$$

može konstruirati novi niz b_i, koji se, ovisno o tome da li kvadratna jednadžba (2.41) ima jedno ili dva realna rješenja, definira kao $b_i = \rho_i - 1/2$ u prvom slučaju, te $b_i = (\rho_i - \rho_-)/(\rho_i - \rho_+)$ u drugom slučaju. Uvrštavanjem rekurzije (2.40) u definiciju za b_i, lako je pokazati da je u prvom slučaju niz b_i aritmetički, a u drugom geometrijski, što olakšava rješavanje. Konačno rješenje za ρ_i je oblika

$$\rho_i = \frac{-\rho_+\rho_-(\rho_+^{i-1} - \rho_-^{i-1}) + (\rho_+^i - \rho_-^i)\rho_1}{-\rho_+\rho_-(\rho_+^{i-2} - \rho_-^{i-2}) + (\rho_+^{i-1} - \rho_-^{i-1})\rho_1}. \tag{2.42}$$

gdje je $\rho_1 = 1 - C/\alpha$, a struja C je rješenje implicitne jednadžbe $\rho_L = C/\beta$. Ovisno o α i β, moguće su 4 vrste rješenja, koje izlažemo u nastavku.

Faza niske gustoće (A). U ovoj fazi je $\rho_1 = \rho_- + 0^\pm$, što daje struju $C = \alpha(1-\alpha)$. Iteracijom rekurzije dobiva se gotovo konstantan profil $\rho_i \approx \alpha$ u cijelom lancu (slika 2.8a), osim blizu $i = L$, pri čemu je $\rho_L = \alpha(1-\alpha)/\beta < \rho_+$. Takvi ρ_1 i ρ_L odgovaraju slijedećim α i β,

$$\alpha \leq 1/2, \qquad \beta > \alpha. \tag{2.43}$$

Faza visoke gustoće (B). U ovoj fazi je $\rho_L = \rho_+ + 0^\pm$, što daje struju $C = \beta(1-\beta)$ i $\rho_L = 1-\beta$. Iteracijom rekurzije dobiva se gotovo konstantan profil $\rho_i \approx 1-\beta$ u cijelom lancu (slika 2.8b), osim blizu $i = 1$, pri čemu je $\rho_1 = 1-\beta(1-\beta)/\alpha < \rho_+$. Takvi ρ_1 i ρ_L odgovaraju slijedećim α i β,

$$\beta \leq 1/2, \qquad \beta < \alpha. \tag{2.44}$$

Ove dvije faze veže simetrija modela na istovremenu zamjenu čestica sa šupljinama ($\tau_i \leftrightarrow 1-\tau_i$) i promjenu smjera kretanja ($i \leftrightarrow L-i+1$ i $\alpha \leftrightarrow \beta$)

$$\langle\tau_i\rangle(\alpha,\beta) = 1 - \langle\tau_{L-i+1}\rangle(\beta,\alpha). \tag{2.45}$$

[2] Specijalni oblik racionalne funkcije

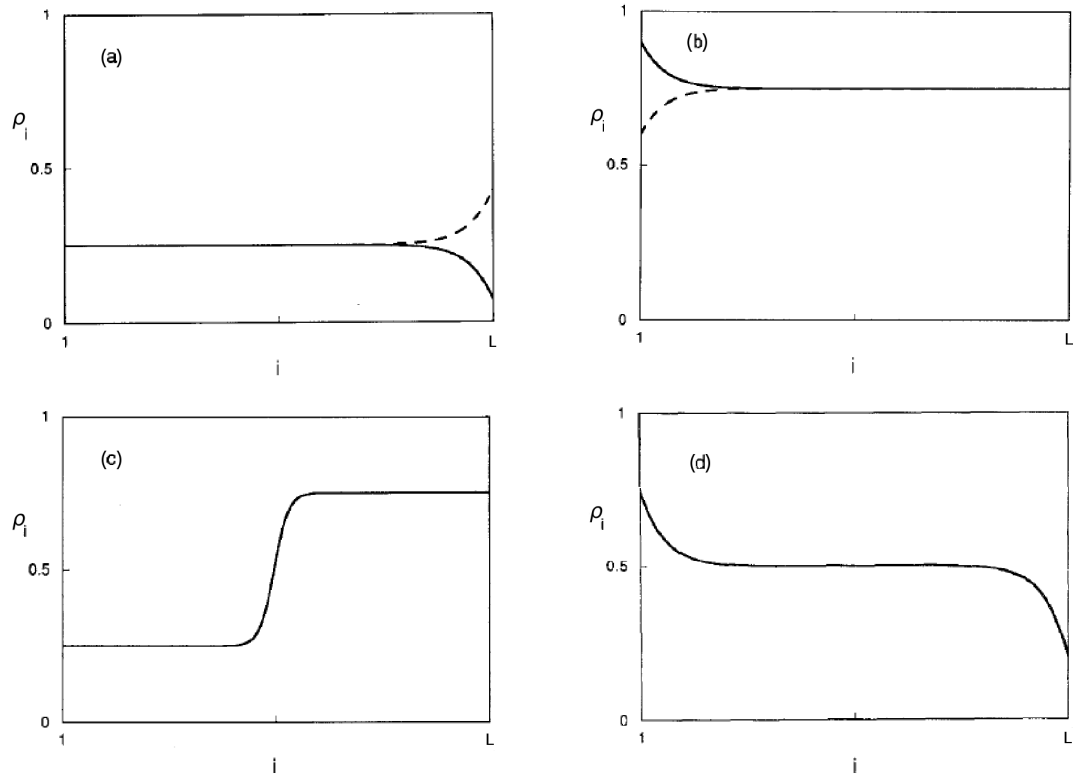

Slika 2.8: Profili gustoće u jednostavnom potpuno asimetričnom procesu isključenja dobiveni u aproksimaciji srednjeg polja u (a) fazi niske gustoće A ($\alpha \leq 1/2$, $\beta > \alpha$), (b) fazi visoke gustoće B ($\beta \leq 1/2$, $\beta < \alpha$), (c) na liniji koegzistencije faza A i B ($\alpha = \beta < 1/2$) i (d) u fazi maksimalne struje ($\alpha > 1/2$, $\beta > 1/2$).

Linija koegzistencije faza. Na granici faza A i B rekurzija započinje s ρ_1 infinitezimalno ispod ρ_-, a završava s ρ_L infinitezimalno iznad ρ_+, što daje struju $C = \alpha(1-\alpha)$. Profil gustoće ima izgled domenskog zida (slika 2.8c), a javlja se za slijedeće α i β,

$$\alpha = \beta < 1/2. \tag{2.46}$$

Faza maksimalne struje (C). Naposljetku, kada su $\rho_1 > 1/2$ i $\rho_L < 1/2$, struja poprima najveću moguću vrijednost, $C = 1/4$, što se javlja za

$$\alpha > 1/2, \qquad \beta > 1/2, \tag{2.47}$$

Profil gustoće poprima vrijednost 1/2 u unutrašnjosti lanca (slika 2.8d), dok odstupanja blizu rubova prate potencijski zakon s eksponentom 1. Blizu lijevog ruba profil gustoće je oblika

$$\rho_i - \frac{1}{2} \sim \frac{1}{2i}, \tag{2.48}$$

a slično ponašanje se dobiva i blizu desnog ruba korištenjem simetrije (2.45).

Sumarno, fazni dijagram ASEPa u aproksimaciji srednjeg polja prikazan je na slici 2.9. Kako ćemo u nastavku vidjeti iz egzaktnog rješenja, aproksimacija srednjeg polja daje općenito točan fazni dijagram u smislu svih faza koje se pojavljuju, ali daje krive profile gustoće na liniji koegzistencije faza i u fazi maksimalne struje, tj. na granicama faza.

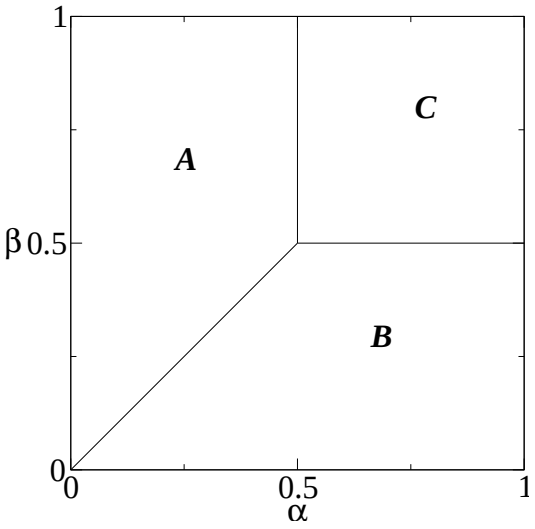

Slika 2.9: Fazni dijagram jednostavnog potpuno asimetričnog procesa isključenja, dobiven u aproksimaciji srednjeg polja, a koji se sastoji od faze niske gustoće (A), faze visoke gustoće (B) i faze maksimalne struje (C).

2.3.2 Egzaktno rješenje

Egzaktno rješenje potpuno asimetričnog procesa s otvorenim rubnim uvjetima prvi su ponudili Derrida, Domany i Mukamel 1992. godine [3], prepoznavši da se nenormirana težina $f_L(\tau_1, \ldots, \tau_L)$, koja je rješenje stacionarne master jednadžbe (2.1), može rekurzivno povezati s $f_{L-1}(\tau_1, \ldots, \tau_{L-1})$ na slijedeći način. Promotrimo li neku konfiguraciju $C = \{\tau_i | i = 1, \ldots, L\}$, tada za svaki par susjednih čvorova u kojima su $\tau_i = 1$ i $\tau_{i+1} = 0$ vrijedi

$$\begin{aligned} f_L(\tau_1, \ldots, \tau_{i-1}, 1, 0, \tau_{i+2}, \ldots, \tau_L) &= f_{L-1}(\tau_1, \ldots, \tau_{i-1}, 1, \tau_{i+2}, \ldots, \tau_L) + \\ &+ f_{L-1}(\tau_1, \ldots, \tau_{i-1}, 0, \tau_{i+2}, \ldots, \tau_L). \end{aligned} \quad (2.49)$$

Također, ako je na rubovima $\tau_1 = 0$ ili $\tau_L = 1$, još vrijedi

$$f_L(0, \tau_2, \ldots, \tau_L) = \frac{1}{\alpha} f_{L-1}(\tau_2, \ldots, \tau_L) \quad (2.50)$$

$$f_L(\tau_1, \ldots, \tau_{L-1}, 1) = \frac{1}{\beta} f_{L-1}(\tau_1, \ldots, \tau_{L-1}). \quad (2.51)$$

Ove su rekurzivne relacije dovoljne da se odredi $f_L(\tau_1, \ldots, \tau_L)$ polazeći od rješenja master jednadžbe za $L = 1$, $f_1(0) = 1/\alpha$ i $f_L(1) = 1/\beta$. Problem je, međutim, bio naći analitički izraz za proizvoljni L, kojeg su Derrida, Domany i Mukamel dobili samo za $\alpha = \beta = 1$, a iduće godine generalizirali na proizvoljni α i β Schütz i Domany [4]. Kako je postupak u tim rješenjima vrlo kompliciran, ovdje izlažemo elegantnije rješenje Derride, Evansa, Hakima i Pasquiera iz 1993. godine [5] pomoću vrlo korisne postavke u obliku umnoška matrica (*matrix-product Ansatz*, MPA).

Ideja iza rekurzija (2.49) i (2.51) je da se nenormalizirana težina $f_L(\tau_1, \ldots, \tau_L)$ zapiše kao umnožak matrica D i E te vektora $\langle W|$ i $|V\rangle$,

$$f_L(\tau_1, \ldots, \tau_L) = \langle W| \prod_{i=1}^{L} [\tau_i D + (1 - \tau_i)E] |V\rangle, \tag{2.52}$$

što rekurzivne relacije (2.49) i (2.51) svodi na jednadžbe za D, E, $\langle W|$ i $|V\rangle$,

$$DE = D + E \tag{2.53}$$

$$\langle W|E = \frac{1}{\alpha}\langle W| \tag{2.54}$$

$$D|V\rangle = \frac{1}{\beta}|V\rangle. \tag{2.55}$$

Skup jednadžbi (2.53)-(2.55) često se naziva i DEHP algebrom po njezinim autorima (Derrida, Evans, Hakim i Pasquier). U [5] je pokazano da su matrice D i E općenito beskonačno dimenzionalne, osim za $\alpha + \beta = 1$, kada su skalari. Jedan mogući izbor (reprezentacija) matrica D i E, te vektora $\langle W|$ i $|V\rangle$ dan je s

$$D = \begin{pmatrix} 1 & 1 & 0 & 0 & \cdots \\ 0 & 1 & 1 & 0 & \\ 0 & 0 & 1 & 1 & \\ 0 & 0 & 0 & 1 & \\ \vdots & & & & \ddots \end{pmatrix}, \qquad E = \begin{pmatrix} 1 & 0 & 0 & 0 & \cdots \\ 1 & 1 & 0 & 0 & \\ 0 & 1 & 1 & 0 & \\ 0 & 0 & 1 & 1 & \\ \vdots & & & & \ddots \end{pmatrix}, \tag{2.56}$$

$$\langle W| = \kappa \left(1, \left(\frac{1-\alpha}{\alpha}\right), \left(\frac{1-\alpha}{\alpha}\right)^2, \ldots, \right), \quad |V\rangle = \kappa \begin{pmatrix} 1 \\ \left(\frac{1-\beta}{\beta}\right) \\ \left(\frac{1-\beta}{\beta}\right)^2 \\ \vdots \end{pmatrix}, \tag{2.57}$$

gdje je $\kappa = \sqrt{(\alpha + \beta - 1)/\alpha\beta}$ izabran kako bi vrijedilo $\langle W|V\rangle = 1$.

Jednom kada su nađene matrice D i E, te vektori $\langle W|$ i $|V\rangle$, lako je pokazati da je normalizacija $Z_L = \sum_{\{\tau_i\}} f_L(\{\tau_i\})$ jednaka $\langle W|C^L|V\rangle$, gdje je $C = D + E$.

Tada su srednja lokalna gustoća $\langle\tau_i\rangle_L$ i struja $j_L = \langle\tau_i(1-\tau_i)\rangle$ dane slijedećim izrazima,

$$\langle\tau_i\rangle = \frac{\langle W|C^{i-1}DC^{L-i}|V\rangle}{\langle W|C^L|V\rangle}, \tag{2.58}$$

$$j = \frac{Z_{L-1}}{Z_L}. \tag{2.59}$$

Izračunamo li profil gustoće i struju iz gornjih izraza koristeći svojstva DEHP algebre (2.53)-(2.55) [5], uočavamo isti fazni dijagram kao i u aproksimaciji srednjeg polja, u smislu da su srednje vrijednosti gustoće is truje struje u pojedinoj fazi jednake onima dobivenim u aproksimaciji srednjeg polja. Iznimku čini linija koegzistencije faza za $\alpha = \beta < 1/2$, gdje se umjesto domenskog zida dobiva linearni profil oblika

$$\langle\tau_{Lx}\rangle_L \simeq \alpha + x(1-2\alpha), \quad 0 < x < 1, \quad \alpha = \beta < 1/2. \tag{2.60}$$

Drugu iznimku čini ponašanje profila gustoće blizu rubova. U fazi niske gustoće tako razlikujemo tri slučaja ovisno o vrijednosti β, u kojima u granici $L \to \infty$ odstupanje od srednje gustoće α trne eksponencijalno s udaljenošću $i \gg 1$ od desnog ruba,

$$\langle\tau_{L-i}\rangle_L = \alpha + \begin{cases} \left(\frac{\alpha(1-\alpha)}{\beta(1-\beta)}\right)^{i+1}(1-2\beta) & \beta < 1/2 \\ \frac{[4\alpha(1-\alpha)]^{i+1}}{2\sqrt{\pi}i^{1/2}} & \beta = 1/2 \\ \frac{[4\alpha(1-\alpha)]^{i+1}}{\sqrt{\pi}i^{3/2}}\frac{(\alpha-\beta)(1-\alpha-\beta)}{(1-2\alpha)^2(1-2\beta)^2} & \beta > 1/2. \end{cases} \tag{2.61}$$

Promotrimo li izraze u (2.61), primjećujemo da se javljaju dvije karakteristične dužine,

$$\xi_\alpha^{-1} = -\ln[4\alpha(1-\alpha)] \quad \text{i} \tag{2.62}$$

$$\xi_\beta^{-1} = -\ln[4\beta(1-\beta)]. \tag{2.63}$$

Tako u području $\alpha < \beta < 1/2$ odstupanje od ruba određuje karakteristična dužina $1/\xi = |1/\xi_\alpha - 1/\xi_\beta|$, dok je za $\beta \geq 1/2$, $\xi = \xi_\alpha$, jer $\xi_\beta \to \infty$. Činjenica da ξ_β divergira odražava se u profilu gustoće javljanjem potencijskog opadanja s udaljenošću od ruba, pri čemu su odgovarajući eksponent jednaki $1/2$ za $\beta = 1/2$ i $3/2$ za $\beta > 1/2$. Vidimo dakle da egzaktno rješenje otkriva dva različita oblika profila gustoće unutar faze A, jedan u kojem se javlja čisto eksponencijalno opadanje s udaljenošću (faza AI) i drugi u kojem se osim eksponencijalnog, javlja još i potencijsko opadanje (faza AII). Slični izrazi i zaključci dobivaju se i za fazu visoke gustoće, uzimajući u obzirom već ranije spomenutu simetriju (2.45).

Naposljetku, u fazi maksimalne struje odstupanje od srednje gustoće $1/2$ slijedi potencijski zakon, ali s eksponenentom $1/2$, koji se razlikuje od eksponenta 1

dobivenog u aproksimaciji srednjeg polja. Blizu lijevog ruba profil gustoće ima oblik

$$\langle \tau_i \rangle_L \simeq \frac{1}{2} + \frac{1}{2\sqrt{\pi} i^{1/2}} + \mathrm{O}(i^{-3/2}), \tag{2.64}$$

a slično se ponašanje dobiva blizu desnog ruba korištenjem simetrije (2.45). Sumarno, fazni dijagram kojeg daje egzaktno rješenje prikazan je na slici 2.10.

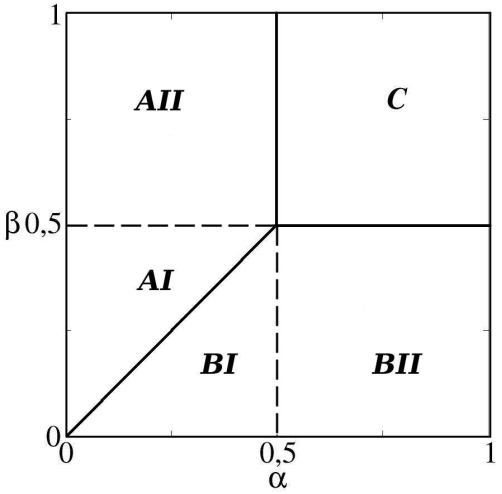

Slika 2.10: Fazni dijagram jednostavnog potpuno asimetričnog procesa isključenja, koji se sastoji od faze niske gustoće (AI i AII), faze visoke gustoće (BI i BII) i faze maksimalne struje (C).

Činjenica da aproksimacija srednjeg polja ne opisuje dobro profil gustoće na granici faza A i B ($\alpha = \beta < 1/2$), kao ni u fazi maksimalne struje (C), nije slučajna. Iskustvo iz ravnotežnih faznih prijelaza govori nam da su upravo fazni prijelazi situacije gdje aproksimacija srednjeg polja često ne daje dobar opis iz razloga što zanemaruje fluktuacije. U nastavku ćemo pokazati da faze A i B dijeli prijelaz koji se zbog prekida u prvoj derivaciji struje po α može okarakterizirati kao prijelaz prvog reda, dok se prijelaz iz faza A ili B u fazu C zbog prekida u drugoj derivaciji može okarakterizirati kao prijelaz drugog reda. Sličnost s ravnotežnim prijelazima utoliko je veća, što se na prijelazu prvog reda javlja koegzistencija faza, dok na prijelazu drugog reda (ali i u cijeloj fazi C) karakteristična dužina ξ divergira.

2.3.3 Prijelaz prvog reda i dinamika domenskih zidova

Prisjetimo se izraza za struju u fazama A, B i C,

$$j(\alpha,\beta) = \begin{cases} \alpha(1-\alpha), & \alpha < 1/2, \alpha \leq \beta \quad \text{(faza A)} \\ \beta(1-\beta), & \beta < 1/2, \beta \leq \alpha \quad \text{(faza B)} \\ 1/4 & \alpha \geq 1/2, \beta \geq 1/2 \quad \text{(faza C).} \end{cases} \tag{2.65}$$

Iz gornjeg izraza je lako vidjeti da za fiksni $\beta < 1/2$, prva derivacija struje po α ima prekid na $\alpha = \beta < 1/2$,

$$\lim_{\alpha\to\beta^+} \frac{\partial J(\alpha,\beta)}{\partial\alpha} = 0 \tag{2.66}$$

$$\lim_{\alpha\to\beta^-} \frac{\partial J(\alpha,\beta)}{\partial\alpha} = 1-2\beta, \tag{2.67}$$

pa po uzoru na ravnotežne fazne prijelaze možemo govoriti o faznom prijelazu prvog reda. S druge strane, prijelaz prvog reda uvijek je povezan s koegzistencijom faza i konačnom korelacijskom dužinom, pa se možemo pitati postoji li takva slika i ovdje.

Odgovor na to pitanje možemo pronaći polazeći od aproksimacije srednjeg polja i odgovarajućeg profila gustoće za $\alpha = \beta < 1/2$ (slika 2.8c), u kojem domenski zid razdvaja područje niske gustoće α od područja visoke gustoće $1-\alpha$. Takav oblik stacionarnog rješenja lakše je razumijeti promotrimo li jednadžbu za $\rho_i(t)$,

$$\frac{d\rho_i}{dt} = \rho_{i-1}(1-\rho_i) - \rho_i(1-\rho_{i+1}), \tag{2.68}$$

u kontinuiranoj (hidrodinamičkoj) granici u kojoj konstanta rešetke $a = 1/L \to 0$, uz $i \to x = ia$, $t \to ta$ i $\rho_i(t) \to \rho(x,t)$. Pritom gornja jednadžba za ρ_i prelazi u tzv. neviskoznu Burgersovu jednadžbu za $\rho(x,t)$ na intervalu $[0,1]$,

$$\frac{\partial\rho}{\partial t} = -(1-2\rho)\frac{\partial\rho}{\partial x}, \tag{2.69}$$

uz rubne uvjete $\rho(0,t) = \alpha$ i $\rho(1,t) = 1-\beta$ i neki početni uvjet $\rho_0(x,0)$. Burgersova jednadžba je kao nelinearna jednadžba poznata po tome što njezina rješenja mogu evoluirati u vremenu u tzv. udarne valove [69]. Da bismo to vidjeli, korisno je definirati tzv. karakteristične krivulje $x = X(t)$ na kojima je gustoća $\rho(X(t),t)$ konstanta [69],

$$\rho(X(t),t) = \rho(X(0),0) = \rho_0(X(0)). \tag{2.70}$$

Deriviranjem gornjeg izraza po t dobiva se

$$\frac{d}{dt}\rho(X(t),t) = \frac{\partial\rho}{\partial t} + \frac{dX}{dt}\frac{\partial\rho}{\partial x} = 0, \tag{2.71}$$

odakle uspoređivanjem s Burgersovom jednadžbom slijedi da je

$$\frac{dX}{dt} = 1 - 2\rho \equiv c(\rho). \tag{2.72}$$

Zanemarimo li na trenutak konačnost sistema, dobivamo da su karakteristične krivulje pravci oblika

$$x = X(t) = x_0 + c(\rho_0(x_0))t, \quad -\infty < x_0 < \infty. \tag{2.73}$$

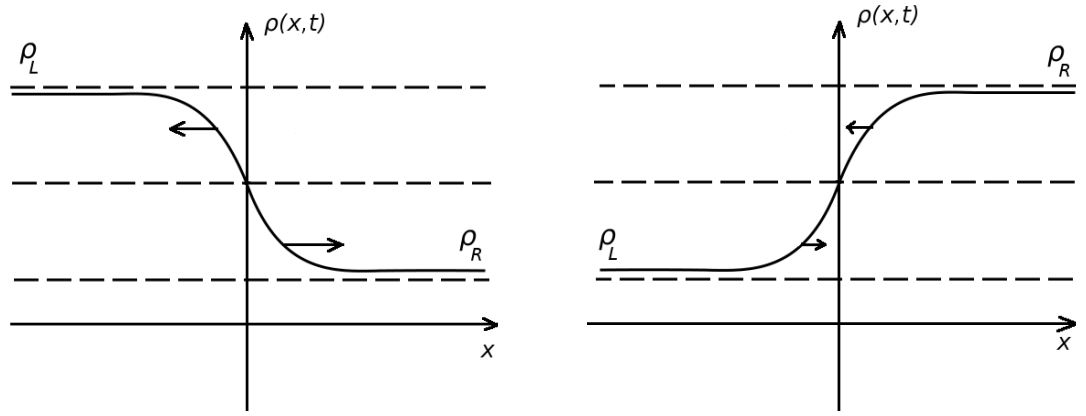

Slika 2.11: Vremenska evolucija profila gustoće u neviskoznoj Burgersovoj jednadžbi (2.69) za početne uvjete koji vode na val razrjeđenja (lijevo) i udarni val (desno).

Pogledajmo sad što se događa s vremenskom evolucijom početnog profila $\rho_0(x)$ koji ima oblik "silazne" stepenice (slika 2.11a) uz $\rho_0(-\infty) = \rho_L$ i $\rho_0(\infty) = \rho_R < \rho_L$, pri čemu smo ishodište izabrali tako da je $\rho_0(0) = 1/2$. Tada je lako vidjeti da je $c(\rho_0(x)) < 0$ za svaki $x < 0$ i $c(\rho_0(x)) > 0$ za svaki $x > 0$. Drugim riječima, za neku izabranu gustoću $\rho_1 > 1/2$ (tj. za koju je početni $x_0 < 0$, gdje je x_0 definiran s $\rho(x_0) = \rho_1$), položaj x za koji je $\rho(x,t) = \rho_1$ postaje s vremenom sve negativniji, dok za fiksnu gustoću $\rho < 1/2$ (tj. za početni $x_0 > 0$), $x > 0$ u karakterističnoj krivulji (2.73) postaje s vremenom sve pozitivniji. Kao rezultat se dobiva "razvlačenje" početne stepenice, što se naziva valom razrjeđivanja.

S druge strane, ako profil ima oblik "uzlazne" stepenice, tj. za $\rho_L < \rho_R$, kao na slici 2.11b, tada se događa obrnuti efekt - profil se "skuplja", što se naziva udarnim valom. Tu, međutim, postoji problem, koji se sastoji u tome da će se u jednom trenutku val "prebaciti" preko sebe, što odgovara trenutku u kojem se dvije karakteristične krivulje sijeku. Kako svaka karakteristična krivulja odgovara drugoj gustoći, to bi značilo da gustoća $\rho(x,t)$ može poprimiti dvije različite vrijednosti za isti x i t, tj. $\rho(x,t)$ nije dobro definirana. Naravno, to se ne može dogoditi u diskretnom modelu, gdje $\langle \tau_i \rangle$ označava prosječnu posjećenost nekog čvora na rešetci. Problem je, dakle, u granici $a = 1/L \to 0$, u kojoj se profili gustoće promatraju na prostornim skalama koje ne uključuju mikroskopske udarne valove

širine a. Ideja je stoga u razvoju $\rho_{i\pm1}$ zadržati članove višeg reda u a, što vodi na viskoznu Burgersovu jednadžbu,

$$\frac{\partial \rho}{\partial t} = -(1-2\rho)\frac{\partial \rho}{\partial x} + a\frac{\partial^2 \rho}{\partial x^2}, \tag{2.74}$$

u kojoj se još javlja difuzijski/viskozni član s konstantom difuzije/viskoznosti jednakoj a. Pokazuje se da dodavanje upravo difuzijskog člana, što se u matematici zove paraboličk regularizacija (vidi npr. [70]), regularizira rješenja Burgersove jednadžbe, u smislu da je domenski zid stabilan i uzak. Polazeći od jednadžbe kontinuiteta, tada se može pokazati da je njegova brzina jednaka

$$V = \frac{j(\rho_L) - j(\rho_R)}{\rho_L - \rho_R}. \tag{2.75}$$

Stabilnost udarnog vala u prisustvu disipacije intuitivno je lako za shvatiti, obzirom da difuzijski član nastoji disipirati ("rastegnuti") udarni val, čime se nadoknadi nastojanje vala da se "prebaci" preko sebe. Međusobno poništavanje efekata nelinearnosti i disipacije, koje se javlja u viskoznoj Burgersovoj jednadžbi, ali i u nekim drugim nelinearnim parcijalnim diferencijalnim jednadžbama, ključno je za pojavu *solitona* - stabilnih valova koji u vremenu ne mijenjaju oblik (vidi neki od uvodnih knjiga, npr. [71]).

Postavimo li gornju raspravu u okvir opisa linije koegzistencije faza u aproksimaciji srednjeg polja, pokazali smo kako se u vremenskoj evoluciji Burgersove jednadžbe javlja stabilni domenski zid koji povezuje domene niske i visoke gustoće nametnute rubnim uvjetima. S druge strane, vidjeli smo da egzaktno rješenje (2.60) za $\alpha = \beta < 1/2$ pokazuje linearni profil gustoće. Nadogradnju slike udarnih valova na način da se uključe fluktuacije, koje aproksimacija srednjeg polja očito zanemaruje, predložili su Kolomeisky *et al.* u [72]. Oni polaze od ideje da se u sistemu, koji još nije dosegao stacionarno stanje, domenski zid pojavljuje kao *metastabilno* stanje koje povezuje dva moguća stacionarna stanja nametnuta rubnim uvjetima, pri čemu je $\rho_L = \alpha$ i $\rho_R = 1 - \beta$. Da bi takav zid bio stabilan, očito mora biti $\rho_L < 1/2$ i $\rho_R > 1/2$, tj. $\alpha < 1/2$ i $\beta < 1/2$ (faze AI i BI). Prema izrazu (2.75), brzina domenskog zida je tada

$$V = \beta - \alpha, \qquad \alpha < 1/2, \beta < 1/2. \tag{2.76}$$

Za $\alpha < \beta$ (faza AI), domenski zid putuje prema desnom rubu, pa je gustoća u sistemu jednaka $\rho_L = \alpha$. S druge strane, za $\alpha > \beta$, domenski zid putuje prema lijevom rubu, pa je gustoća u sistemu jednaka $\rho_R = 1 - \beta$. Za točno $\alpha = \beta < 1/2$, brzina domenskog zida iščezava, ali zbog fluktuacija nije realno očekivati da će domenski zid ostati na mjestu. Na primjer, čestica koja skoči u lanac iz lijevog spremnika će se zbog niske gustoće $\alpha < 1/2$ brzo propagirati kroz lanac sve dok ne dođe do domenskog zida. Priključivanjem čestice domenskom zidu faza visoke

gustoće se povećava, čime se domenski zid pomiče ulijevo. S druge strane, čestica koja napusti lanac ostavlja iza sebe šupljinu koja se zbog visoke gustoće kreće brzo kroz lanac, sve dok ne dođe do domenskog zida. Priključivanjem šupljine domenskom zidu faza visoke gustoće se smanjuje, čime se domenski zid pomiče udesno. Obzirom da su ulasci i izlasci čestica u i iz lanca nekorelirani i nasumični, ovako opisani domenski zid ponaša se kao nasumični šetač, koji se kreće brzinama D_L ulijevo i D_R udesno,

$$D_L = \frac{j(\rho_L)}{\rho_L - \rho_R}, \qquad D_R = \frac{j(\rho_R)}{\rho_L - \rho_R}, \tag{2.77}$$

uz refleksiju na rubovima (slika 2.12).

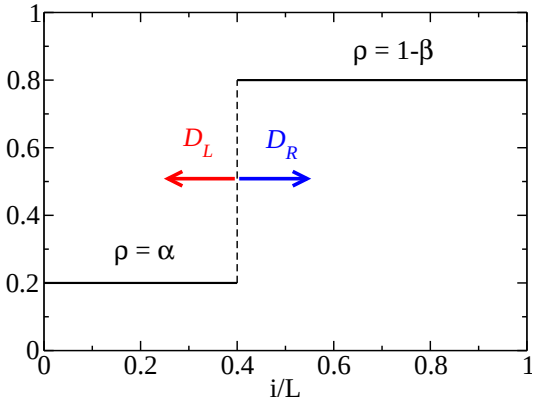

Slika 2.12: Domenski zid u slici Kolomeiskyog *et al.* kao nasumični šetač koji se kreće brzinama D_L ulijevo i D_R udesno.

Pretpostavimo da je širina domenskog zida jednaka a[3], tako da za položaj domenskog zida možemo odabrati kariku koja spaja čvorove i i $i+1$. Tada je vjerojatnost $P_i(t)$ da se domenski zid u trenutku t nalazi na karici $(i, i+1)$ zadovoljava master jednadžbu

$$\frac{dP_i}{dt} = D_R P_{i-1} + D_L P_{i+1} - (D_L + D_R) P_i, \quad i = 1, \ldots, L-1, \tag{2.78}$$

dok na rubovima vrijedi

$$\frac{dP_0}{dt} = D_L P_1 - D_R P_0, \tag{2.79}$$

$$\frac{dP_L}{dt} = D_R P_{L-1} - D_L P_L, \tag{2.80}$$

[3]Da su udarni valovi u TASEP-u mikroskopskih dimenzija, rigorozno je dokazano (vidi npr. [74] i reference unutra).

pri čemu smo uzeli u obzir da homogeni profili gustoće $\langle\tau_j\rangle = \rho_L$ i $\langle\tau_j\rangle = \rho_R$, $j = 1, \ldots, L$, odgovaraju položajima $i = 0$ i $i = L$ domenskog zida. Ukoliko je rješenje $P_i(t)$ jednadžbi (2.78) i (2.80) poznato, profil gustoće u slici domenskih zidova ρ_i^{DW} dobiva se iz izraza

$$\rho_i^{DW}(t) = \sum_{j=0}^{i} P_j(t)\rho_L + \sum_{j=i+1}^{L} P_j(t)\rho_R. \tag{2.81}$$

Rješenje jednadžbe (2.78) i (2.80) moguće je odrediti za proizvoljni t [73]. Nas zanima samo stacionarna granica $dP_i/dt = 0$, koja se rješava pretpostavkom na P_i, $P_i = exp(-ki)/\mathcal{N}$, što daje $k = \ln(D_L/D_R)$ te P_i oblika

$$P_i = \begin{cases} \frac{e^{-(L-i)/\xi}}{\mathcal{N}} & \alpha < \beta < 1/2 \\ \frac{e^{-i)/\xi}}{\mathcal{N}} & \beta < \alpha < 1/2, \end{cases} \qquad \mathcal{N} = \frac{1 - e^{-(L+1)/\xi}}{1 - e^{-1/\xi}}, \tag{2.82}$$

gdje je ξ karakteristična dužina oblika

$$\xi^{-1} = \left| \ln\left(\frac{\alpha(1-\alpha)}{\beta(1-\beta)}\right) \right|. \tag{2.83}$$

Vidimo, dakle, da dinamika domenskih zidova u slici Kolomeiskyog *et al.* daje istu karakterističnu dužinu kao i egzaktno rješenje. Također, izračunamo li stacionarni profil na liniji koegzistencije faza $\alpha = \beta < 1/2$ u slici dinamike domenskog zida, dobivamo točno egzaktno rješenje (2.60), koje predviđa linearni profil. To je intuitivno jasno, jer $\alpha = \beta < 1/2$ odgovara $D_L = D_R$, tj. simetričnom nasumičnom šetaču, pa je vjerojatnost P_i jednaka u cijelom lancu što vodi na linearni profil gustoće.

Naposljetku, kažimo nešto i o granici primjene ove slike. Kad smo opisivali dinamiku domenskog zida, pretpostavili smo da je domenski zid oštar. To je istina samo za $\alpha < 1/2$ i $\beta < 1/2$, što se može razumjeti promatrajući brzinu $c(\rho)$, koju iz prethodne rasprave o karakterističnim krivuljama možemo shvatiti kao brzinu kojom se lokalne perturbacije gustoće propagiraju kroz sustav. Shvatimo li malu promjenu u rubnoj gustoći α kao jednu takvu perturbaciju (uz fiksni $\beta < 1/2$), vidimo da je za $\alpha < 1/2$ brzina $c(\alpha) > 0$, pa se perturbacija u α širi kroz sistem. S druge strane, za $\alpha > 1/2$ je brzina $c(\alpha) < 0$, pa perturbacija ostaje lokalizirana uz rub. Prisjetimo li se egzaktnog rješenja i karakterističnih dužina ξ_α i ξ_β, vidimo da ovaj prijelaz u ponašanju koincidira s divergencijom karakteristične dužine ξ_α u fazi AII. ($\alpha \geq 1/2$). To naravno nije slučajnost - slika dinamike domenskih zidova Kolomeiskyog *et al.* daje mikroskopski opis prijelaza (ne faznog!) iz faze AI u fazu AII upravo kroz činjenicu da tada ξ ovisi samo o β, jer se daljnja promjena u $\alpha \geq 1/2$ više ne propagira kroz sistem. No, kako se za $\alpha > 1/2$ i $\beta < 1/2$ perturbacija ulaskom čestice u lanac više ne propagira do domenskog zida, slika

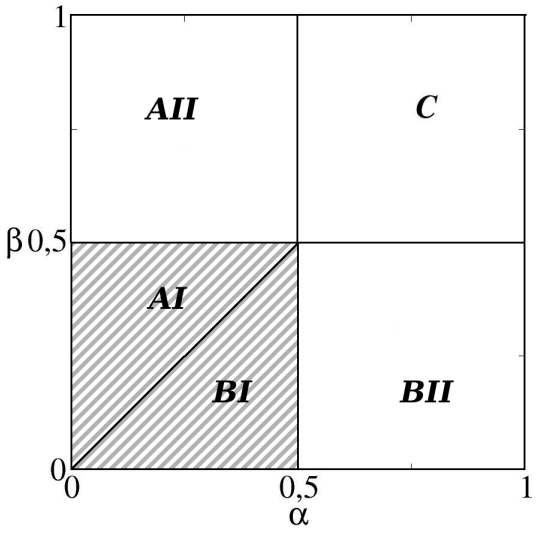

Slika 2.13: Područje primjene slike dinamike domenskog zida Kolomeiskyog *et al.* u faznom dijagramu TASEPa.

nasumičnog šetača prestaje vrijediti. Područje primjene slike dinamike domenskih zidova prikazano je slikovito na slici 2.13.

Obzirom da je jednostavni potpuno asimetrični proces isključenja riješen egzaktno, rasprava u ovom poglavlju mogla bi se činiti suvišnom, barem u ovom opsegu. Važnost ove slike postaje, međutim, očitija kada se u model uvedu poopćenja takva da egzaktno rješenje modela više nije poznato, kao u poglavlju 3.

2.3.4 Prijelaz drugog reda i kritični eksponenti

Za razliku od linije $\alpha = \beta < 1/2$, prva derivacija struje (2.65) na linijama $\alpha = 1/2$, $\beta > 1/2$ i $\alpha > 1/2$, $\beta = 1/2$, koje dijele faze niske i visoke gustoće A i B od faze maksimalne struje C, je neprekidna, ali zato postoji prekid u drugoj derivaciji

$$\lim_{\alpha \to 1/2^+} \frac{\partial^2 J(\alpha, \beta)}{\partial \alpha^2} = 0 \tag{2.84}$$

$$\lim_{\alpha \to 1/2^-} \frac{\partial^2 J(\alpha, \beta)}{\partial \alpha^2} = -2. \tag{2.85}$$

Iz egzaktnog rješenja vidimo da ovaj prijelaz prati divergencija karakteristične dužine ξ, što je u profilu gustoće popraćeno potencijskim zakonom s eksponentom 1/2 danim u jednadžbi (2.64). Kako je taj eksponent različit od eksponenta koji se dobiva u aproksimaciji srednjeg polja, pitamo se postoji li način da se aproksimacija srednjeg polja nadogradi uključivanjem fluktuacija, što bi, slično

kao i na prijelazu prvog reda, dalo dobar opis faznog prijelaza i točan eksponent potencijskog zakona.

Potvrdan odgovor na to pitanje dali su Hager *et al.* [75] polazeći od stohastičke (viskozne) Burgersove jednadžbe za odstupanje lokalne gustoće od srednje gustoće, $\phi(x,t) \equiv \rho(x,t) - \overline{\rho}$,

$$\frac{\partial \phi}{\partial t} = -c(\overline{\rho})\frac{\partial \phi}{\partial x} - \kappa\phi\frac{\partial \phi}{\partial x} + \nu\frac{\partial^2 \phi}{\partial x^2} - \frac{\partial \eta}{\partial x}, \tag{2.86}$$

gdje su $c(\overline{\rho})$ i κ dani izrazima,

$$c(\overline{\rho}) = \left.\frac{dj(\rho)}{d\rho}\right|_{\rho=\bar{\rho}} = 1 - 2\bar{\rho}, \tag{2.87}$$

$$\kappa = \left.\frac{d^2 j(\rho)}{d\rho^2}\right|_{\rho=\bar{\rho}} = -2. \tag{2.88}$$

Stohastički član u jednadžbi (2.86) predstavlja fluktuacije u gustoći uzrokovane fluktuacijama u struji, a obzirom da je struja lokalno sačuvana, javlja se kao gradijent struje $\eta(x,t)$. Pritom se pretpostavlja da je raspodjela nasumične struje $\eta(x,t)$ dana Gaussovom raspodjelom s kovarijancom oblika

$$\langle \eta(x,t)\eta(x',t')\rangle = D\delta(x-x')\delta(t-t'). \tag{2.89}$$

Prelaskom u koordinatni sustav koji se giba brzinom $c(\overline{\rho})$ (ili u posebnom slučaju $\overline{\rho} = 1/2$), te transformacijom $\phi = \partial h/\partial t$, gornja jednadžba prelazi u ranije spomenutu Kardar-Parisi-Zhang (KPZ) jednadžbu oblika

$$\frac{\partial h}{\partial t} = \nu\frac{\partial^2 h}{\partial x^2} + \frac{|\kappa|}{2}\left(\frac{\partial h}{\partial x}\right)^2 + \eta. \tag{2.90}$$

U translacijski invarijantnom sistemu u jednoj dimenziji, KPZ jednadžba ima važno svojstvo da su konstante D/ν i $|\kappa|$ invarijantne na renormalizaciju (transformaciju prostorne i vremenske skale) [76]. To omogućuje da se dimenzionalnom analizom povežu karakteristične skale prostornih i vremenskih fluktuacija [76], što daje

$$\xi(t) \sim [(D/\nu)^{1/2} \cdot |\kappa| \cdot t]^{2/3}, \tag{2.91}$$

gdje prepoznajemo dinamički eksponent $z = 3/2$. Kako bi primijenili gornji rezultat na sistem s otvorenim rubnim uvjetima u fazi maksimalne struje, Hager *et al.* polaze od beskonačnog sistema na pozitivnoj realnoj osi ($x > 0$) uz rubni uvjet $\rho(0) = \rho_L$. Zatim pokazuju da u stacionarnom stanju, jedina kombinacija parametara D, ν, $|\kappa|$ i $\Delta\rho \equiv \rho_L - 1/2$ koja ima dimenziju dužine mora biti oblika

$$l = (D/\nu)(\Delta\rho)^{-2}. \tag{2.92}$$

Pretpostavivši da srednje odstupanje profila gustoće $\langle\phi(x)\rangle = \rho(x) - 1/2$ u stacionarnom stanju ima oblik [13]

$$\langle\phi(x)\rangle = \Delta\rho\mathcal{F}(x/l), \tag{2.93}$$

uz $\mathcal{F}(0) = 1$, te da se u fazi maksimalne struje zbog $c(1/2) = 0$ informacija o ρ_L ne prenosi u unutrašnjost lanca, Hager *et al.* zaključuju da funkcija $\mathcal{F}$ mora imati slijedeće asimptotsko ponašanje

$$\mathcal{F}(x) \sim x^{-1/2}, \quad x \to \infty, \tag{2.94}$$

što daje traženi eksponent 1/2. Spomenimo i da je isti eksponent, kao i asimptotski oblik funkcije $\mathcal{F}(x)$, dobiven ranije u [77] primjenom $2 - \epsilon$ razvoja na odgovarajući Martin-Siggia-Rose funkcional koji opisuje prostorno-vremenske fluktuacije u viskoznoj Burgersovoj jednadžbi (2.86).

Gornji se eksponent pokazao univerzalnim u smislu da ostaje nepromijenjen u raznim poopćenjima modela, kao što su djelomično asimetrične brzine preskoka ($p \neq q$) [78], paralelna dinamika [79,80], nesačuvanje čestica u unutrašnjosti lanca (tzv. Langmuirova kinetika) [81] i nehomogene brzine preskoka pridružene česticama [82]. U duhu "potrage" za univerzalnošću, možemo se stoga pitati koji su ključni "sastojci" koji vode na takvu "univerzalnost". Odgovor na to pitanje ostavljamo za poglavlje 3.

2.4 Poopćenja

Prisjetimo li se fizikalnih pojava koje smo naveli na početku poglavlja kao najvažnije primjene ASEPa, jasno je da je za njihov opis ASEP znatno pojednostavljeni model. Većina postojećih poopćenja predložena je stoga u svrhu realističnijeg modeliranja tih pojava, najčešće onih u prometu i u biologiji. Neke od generalizacija motiviranih prometom uključuju više prometnih traka [83–85], raskrižja [86, 87], više vrsta automobila [88, 90–92], prilagodbu brzine uvjetima na cesti [93] itd. U biološkim procesima, neke od generalizacija uključuju čestice koje zauzimaju više od jednog mjesta [94, 95], nehomogenosti u vjerojatnostima preskoka [60], desorpciju i apsorpciju čestica u lancu (tzv. Langmuirovu kinetiku) [96], interna stanja čestica [97], itd.

S teorijske pak strane, dio tih poopćenja, od kojih neka navodimo u nastavku, pomažu "katalogizirati" ponašanje vođenih difuzijskih sustava u smislu da se nastoje u njima prepoznati one elemente koji vode na slično ili bitno različito ponašanje.

2.4.1 Langmuirova kinetika

Po uzoru na Langmuirov proces apsorpcije i desorpcije atoma, iona ili molekula na površini, Parmeggiani, Franosch i Frey su predložili poopćenje ASEPa u kojem sustav izmjenjuje čestice s okolinom na svakom čvoru rešetke, poštujući pritom i dalje princip isključenja [96]. Takvo poopćenje inspirirano je kretanjem raznih molekularnih motora - proteina koji pretvaraju kemijsku energiju u mehaničku - po staničnom kosturu (citoskeletu), koji se mogu odvojiti od citoskeleta te se na njega kasnije ponovo vezati [98]. Shematski prikaz modela prikazan je na slici 2.14, pri čemu smo s ω_A i ω_D označili vjerojatnosti apsorpcije i desorpcije u procesima

$$\text{apsorpcija} \quad 0 \overset{\omega_A}{\to} 1 \tag{2.95}$$

$$\text{desorpcija} \quad 1 \overset{\omega_D}{\to} 0 \tag{2.96}$$

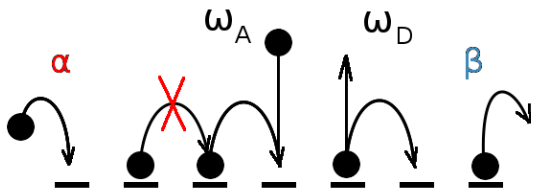

Slika 2.14: Slikoviti prikaz TASEPa s otvorenim rubnim uvjetima i Langmuirovom kinetikom.

Zanimljiva svojstva ovog modela dobivaju se za izbor vjerojatnosti apsorpcije i desorpcije koje su obrnuto proporcionalne veličini sustava, $\omega_A \equiv \Omega_A/L$ i $\omega_D \equiv \Omega_D/L$, jer se tada procesi preskoka i Langmuirove kinetike odvijaju na istoj vremenskoj skali. Parmeggiani, Franosch i Frey pokazali su da u tom slučaju u granici $L \to \infty$ dolazi do lokalizacije domenskog zida (tj. koegzistencije faza) u smislu da njegova širina ξ_{DW} divergira sporije od L, $\xi_{DW} \propto L^{1/2}$. Ovaj eksponent, koji ne odgovara eksponentu kojeg bi dala teorija srednjeg polja, protumačili su Evans, Juhaśz i Santen [99] pokazavši da se kretanje domenskog zida može opisati slučajnim hodom, slično kao i u originalnom TASEPu, ali sada s prostorno ovisnim vjerojatnostima preskoka $D_L(x)$ i $D_R(x)$ (prostorno ovisne vjerojatnosti kretanja domenskog zida promatrali su nezavisno od [99] i Rakós, Paessens i Schütz u [100])

$$D_L(x) = \frac{j_L(x)}{\rho_R(x) - \rho_L(x)}, \qquad D_R(x) = \frac{j_R(x)}{\rho_R(x) - \rho_L(x)}. \tag{2.97}$$

Prostorna ovisnost u $D_L(x)$ i $D_R(x)$ se pritom javlja zbog netrivijalnog profila domenskog zida $\rho_s(x)$, koji je u aproksimaciji srednjeg polja rješenje jednadžbe

$$(1 - 2\rho_s)\frac{\partial \rho_s}{\partial x} - \Omega_A(1 - \rho_s) + \Omega_D \rho_s = 0, \tag{2.98}$$

a koji ulazi u izraz za ukupnu ulaznu struju u domenu niske odnosno visoke gustoće,

$$j_L(x) = \sum_{y<x} \Omega_A[1-\rho_s(y)] - \sum_{y<x} \Omega_D \rho_s(y) \tag{2.99}$$

$$j_R(x) = \sum_{y>x} \Omega_D \rho_s(y) - \sum_{y>x} \Omega_A[1-\rho_s(y)]. \tag{2.100}$$

Stacionarna vjerojatnost $P(x)$ nalaženja domenskog zida na mjestu x može se naći eksplicitno, jer zadovoljava detaljnu ravnotežu

$$D_R(x)P(x) = D_L(x+a)P(x+a), \tag{2.101}$$

gdje je $a = 1/L$ jedinični korak kretanja domenskog zida. Iz detaljne ravnoteže slijedi da je $P(x) \propto exp(-E(x))$, gdje je $E(x+a) - E(x) = D_L(x+a)/D_R(x)$. Profil domenskog zida može se eksplicitno odrediti iz jednadžbe (2.98) u slučaju $\Omega_A = \Omega_D = \Omega$, što daje minimum u $E(x)$ na položaju x_s gdje iščezava brzina domenskog zida $V = D_R(x) - D_L(x)$. Razvojem $P(x)$ oko x_s do kvadratnog člana lako se odredi standardna devijacija, za koju se dobiva da je proporcionalna $\propto L^{1/2}$. Ovaj račun koristiti ćemo u poglavlju 3 u generalizaciji ASEPa na dugodosežne preskoke.

Spomenimo i to da prostorno ovisne vjerojatnosti preskoka domenskog zida mogu u nekim procesima voditi na bitno drugačiji oblik funkcije $E(x)$. Na primjer, Rakós, Paessens i Schütz modificiraju Langmuirovu kinetiku na način da se apsorpcija ili desorpcija na nekom čvoru odvija samo u slučaju kada su okolni čvorovi već popunjeni [100]. U tom slučaju može se pokazati da $E(x)$ ima globalni maksimum čija visina raste s veličinom sustava, što u granici beskonačnog sustava vodi na zanimljiva svojstva poput spontanoga loma ergodičnosti i histereze.

2.4.2 Nehomogenosti u vjerojatnostima preskoka

Osim lokalizacije domenskog zida u sustavu s otvorenim rubnim uvjetima i Langmuirovom kinetikom, separaciju faza možemo inducirati ukoliko nekim česticama ili čvorovima pridružimo vjerojatnosti preskoka koje su drugačije od ostalih. Problem jedne spore čestice, koja se kreće brzinom $\alpha < 1$, a koju pritom druge čestice mogu prestići s vjerojatnošću β, egzaktnu su riješili Mallick [88] i Kim *et al.* [89]. Pritom je pokazao da se u sustavu spore čestice, za neki izbor parametara, opaža makroskopski domenski zid. Ako je u sustavu pak više sporih čestica s različitim vjerojatnostima preskoka, ali se zabranjuje pretjecanje ($\beta = 0$), problem se može riješiti preslikavanjem na model nultog dosega [90, 91], te se pokazuje da separaciju fazu pritom izaziva najsporija čestica u sustavu, iza koje se gomila makroskopski broj čestica. Modeli u kojima se različite vjerojatnosti pridružuju čestica svoju primjenu najčešće nalaze u prometu, u kojem "sporije" čestice odgovaraju, primjerice, kamionima kojima je maksimalna dozvoljena brzina obično manja od one za automobile.

S druge strane, stacionarno rješenje modela s nehomogenostima koje su pridružene čvorovima najčešće nije poznato. Janowsky i Lebowitz [59] su u najjednostavnijem slučaju TASEP-a s jednim, lokaliziranim defektom s kojeg se čestice pomiču s vjerojatnošću $r < 1$, pokazali da defekt inducira separaciju faza. U kontekstu rasta površina opisanog KPZ jednadžbom, sličan problem promatrali su Wolf i Tang [101], pri čemu se lokalizirani defekt preslikava na linijski defekt duž kojeg površina raste sporije. Usprkos brojnim nastojanjima, uz oba problema veže se do danas otvoreno pitanje postoji li režima u r takav da defekt ne inducira separaciju faza. Povijest tog problema kao i naš doprinos njegovom boljem razumijevanju donosimo u poglavlju 4. Osim lokaliziranih defekata, zanimljivo je, i opravdano u biološkim sustavima, promatrati problem punog nereda. U tom slučaju svakom se čvoru pridruži jedna vjerojatnost preskoka, koja se bira iz neke zadane raspodjele. Jednom izabrane vjerojatnosti ne mijenjaju se u vremenu, pa govorimo i o *zamrznutom* neredu. ASEP sa zamrznutim neredom razlikuje se od ASEP-a s lokaliziranim defektima u tome što je mehanizam separacije faza drugačiji, što ćemo detaljno objasniti u poglavlju 5.

3

Fazni prijelazi u modelu s dugodosežnim skokovima

U prethodnom poglavlju pokazali smo da se uz fazne prijelaze u ASEP-u vežu pojave karakteristične za ravnotežne fazne prijelaze, poput pojave domenskog zida na prijelazu prvog reda ili beskonačne korelacijske dužine na prijelazu drugog reda. Prijelaz drugog reda u ASEP-u dijeli pritom barem dvije sličnosti s ravnotežnim faznim prijelazima. Prvo, isti potencijski zakon $\langle \tau_i \rangle - 1/2 \propto i^{-1/2}$ nalazimo i u drugim generalizacijama modela [78–82], što nas prirodno vodi na koncept *univerzalnosti* (za iscrpni pregled koncepta univerzalnosti daleko od ravnoteže vidi [9]). Također, primjena teorije srednjeg polja pokazuje se na samom prijelazu neadekvatnom, jer pritom zanemaruje relevantni doprinos koji potječe od fluktuacija.

Jedan od (rijetkih) načina na koji možemo direktno utjecati na fluktuacije sastoji se od povećanja dosega međudjelovanja. Uvedemo li međudjelovanje koje potencijski opada s duljinom l kao $l^{-(\sigma+1)}$, tada variranjem parametra dosega σ možemo interpolirati između dva rubna slučaja, kratkodosežnog slučaja za $\sigma \to \infty$ i efektivno beskonačno dimenzionalnog slučaja $\sigma = -1$. U ravnotežnim sustavima, ovisno o konkretnom modelu i vrijednosti parametra σ, kao rezultat možemo očekivati npr. promjenu klase univerzalnosti (vidi npr. [105]), fazni prijelaz u jednoj dimenziji [106] ili bolje slaganje s teorijom srednjeg polja (vidi npr. [10]).

U ovom ćemo poglavlju izložiti generalizaciju kratkodosežnog procesa isključenja, koju smo predložili u radovima [107, 108]. Poopćenje se odnosi na doseg čestica, koje se propagiraju dugodosežnim preskocima čija se duljina bira iz raspodjele $p_l \propto l^{-(1+\sigma)}$. Osim navedene, općenite motivacije, dodatna motivacija potječe i od nelokalnih korelacija koje se javljaju u kratkodosežnom modelu (vidi [109] i sadržane reference), a koje se pokazuju generičkom karakteristikom brojnih sustava daleko od ravnoteže. U tom kontekstu, opravdanim se čini uvesti nelokalne korelacije *izravno*, te ispitati njihov utjecaj na fazni dijagram u smislu univerzalnosti. U poglavlju 3.3 također prikazujemo i moguću primjenu na opis transporta DNK regulatornih proteina.

3.1 Definicija modela

Umjesto kratkodosežnih preskoka, generalizacijom na dugodosežne preskoke česticama dopuštamo preskoke proizvoljne duljine $1 \leq l \leq L$, pri čemu zadržavamo princip isključenja. Duljinu preskoka l pritom biramo iz raspodjele

$$p_l \propto \frac{1}{l^{\sigma+1}}, \tag{3.1}$$

gdje je σ parametar dosega. Ograničimo li se na nasumično-sekvencijalnu dinamiku, to znači da se u svakom infinitezimalnom intervalu vremena $[t, t+dt]$ nasumično izabrana čestica na čvoru i pomiče za l mjesta bilo ulijevo na čvor $i-l$ (s vjerojatnošću $q \cdot p_l$), bilo udesno na čvor $i+l$ (s vjerojatnošću $p \cdot p_l$), ali pod uvjetom da je čvor na koji čestica skače prazan. Kao i u kratkodosežnom slučaju, za $p = 1$ i $q = 0$ govorimo o potpuno asimetričnom, za $p \neq q \neq 0$ o djelomično asimetričnom, a za $p = q$ o simetričnom procesu.

U ovom konkretnom modelu, izbor parametra dosega σ pritom nije posve proizvoljan. Naime, kasnije ćemo pokazati da je struja u dugodosežnom modelu jednaka struji u kratkodosežnom uvećanoj za faktor $\lambda_{L-1}(\sigma) = \langle l \rangle = \sum_{l=1}^{L-1} l \cdot p_l$, koji u granici $L \to \infty$ divergira za $\sigma \leq 1$. S druge strane, u granici $\sigma \to \infty$ vjerojatnost (3.1) postaje Kroneckerova delta funkcija $\delta_{l,1}$, pa se dobiva standardni, kratkodosežni ASEP. Područje u σ koje nas zanima je stoga $1 < \sigma < \infty$.

3.1.1 Periodički rubni uvjeti

U slučaju periodičkih rubnih uvjeta za koje vrijedi $\tau_{i+L} = \tau_i$, vjerojatnost nalaženja sustava u nekoj konfiguraciji $C = \{\tau_i | i = 1, \ldots, L\}$ zadovoljava slijedeću master jednadžbu,

$$\frac{d}{dt}P(C,t) = \sum_{C'} W(C' \to C)P(C',t) - \sum_{C'} W(C \to C')P(C,t), \tag{3.2}$$

gdje su za svaki $i = 1, \ldots, L$ i $l = 1, \ldots, L-1$, vjerojatnosti prijelaza u jedinici vremena iz C u C' jednake

$$W(C \to C') = \begin{cases} p \cdot p_l, & C = \{\ldots, \tau_i = 1, \tau_{i+l} = 0, \ldots,\}, \\ & C' = \{\ldots, \tau_i = 0, \tau_{i+l} = 1, \ldots,\}, \\ q \cdot p_l, & C = \{\ldots, \tau_i = 0, \tau_{i+1} = 1, \ldots,\}, \\ & C' = \{\ldots, \tau_i = 1, \tau_{i+1} = 0, \ldots,\}, \\ 0, & ostalo, \end{cases} \tag{3.3}$$

pri čemu je $p_l = l^{-(1+\sigma)}/\zeta_{L-1}(\sigma+1)$, a $\zeta_{L-1}(\sigma+1) = \sum_{l=1}^{L-1} l^{-(1+\sigma)}$ je parcijalna suma Riemannove zeta funkcije. Iz gornjeg izraza dobivamo jednadžbu za srednju lokalnu gustoću $\langle \tau_i \rangle$, koja zapisana u obliku jednadžbe kontinuiteta,

$$\frac{d}{dt}\langle\tau_i\rangle = j_{i-1} - j_i, \tag{3.4}$$

definira struju j_i kao ukupnu struju svih čestica koje preskaču mjesto i, kao i onih koje skaču s njega,

$$j_i = \sum_{l=1}^{L-1} \sum_{k=i-l+1}^{i} p_l \langle \tau_k (1 - \tau_{k+l}) \rangle. \tag{3.5}$$

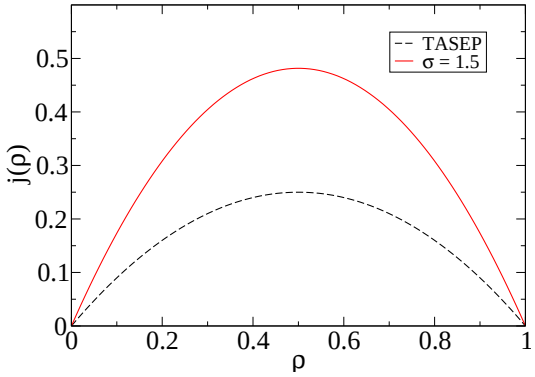

Slika 3.1: Fundamentalni dijagram jednostavnog potpuno asimetričnog procesa isključenja s kratkodosežnim (isprekidana linija) i dugodosežnim preskocima (puna linija) za $\sigma = 1.5$.

Kao i u kratkodosežnom modelu (za detaljnije objašnjenje vidi [110]), u stacionarnom stanju su sve vjerojatnosti $P(C)$ jednake, što daje konstantni profil gustoće i struju oblika

$$\langle\tau_i\rangle = \frac{N}{L} = \rho, \quad j = \frac{\zeta_{L-1}(\sigma)}{\zeta_{L-1}(\sigma+1)} \frac{N(N-1)}{L(L-1)} = \lambda_{L-1}(\sigma)\rho(1-\rho) + O(L^{-1}). \tag{3.6}$$

Vidimo, dakle, da u dugodosežnom modelu fundamentalni dijagram $j(\rho)$ poprima isti oblik $\propto \rho(1-\rho)$ kao i u kratkodosežnom modelu, ali uvećan za faktor $\lambda_{L-1}(\sigma)$ (slika 3.1), koji odgovara srednjoj duljini preskoka obzirom na raspodjelu p_l, $\lambda_{L-1}(\sigma) = \langle l \rangle$. U termodinamičkoj granici u kojoj $L \to \infty$, srednja duljina preskoka je jednaka omjeru dviju zeta funkcija, $\zeta(\sigma)/\zeta(\sigma+1)$, pri čemu je $\zeta(\sigma) < \infty$ samo za $\sigma > 1$. Drugim riječima, zanima nas područje parametra $\sigma > 1$ za koje je ukupna struja konačna.

3.1.2 Otvoreni rubni uvjeti

Za razliku od kratkodosežnog modela, dugodosežni preskoci općenito vode na nelokalne "rubne uvjete". Da bismo to vidjeli, promotrimo situaciju u kojoj neka

česticu u sustavu izabere takav l da je mjesto $i+l$ na koje treba skočiti izvan sustava. Ako zabranimo taj preskok zahtijevajući da čestica napusti sustav samo s mjesta $i = L$, u model ćemo uvesti ponašanje na rubovima koje se drastično razlikuje od onoga u unutrašnjosti. Prirodniji izbor rubnih uvjeta bio bi dopustiti čestici da u tom slučaju napusti sustav, ali s dodatnom vjerojatnošću β koja ovisi o gustoći izlaznog spremnika. Slično možemo zaključiti za svaki l za koji je $i+l > L$, što vodi na ukupnu vjerojatnosti β_i da čestica koja se nalazi na mjestu i napusti sustav,

$$\beta_i = \frac{\beta}{\zeta_L(\sigma+1)} \sum_{j=L-i+1}^{L} \frac{1}{j^{\sigma+1}}. \tag{3.7}$$

Na sličan način dolazimo i do lijevog "rubnog uvjeta", pri čemu definiramo vjerojatnost α_i da čestica skoči iz lijevog spremnika na prazno mjesto i u lancu, ali samo s onih mjesta u spremniku koja su udaljena od mjesta i najviše L mjesta,

$$\alpha_i = \frac{\alpha}{\zeta_L(\sigma+1)} \sum_{j=i}^{L} \frac{1}{j^{\sigma+1}}. \tag{3.8}$$

Za slikoviti prikaz rubnih uvjeta upućujemo na sliku 3.2. Primijetimo, također, da izbor rubnih uvjeta (3.7) i (3.8) zadržava simetriju na istovremenu zamjenu $\alpha \leftrightarrow \beta$ i $\tau_i \leftrightarrow 1 - \tau_{L-i+1}$.

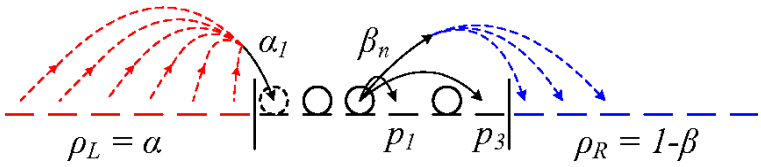

Slika 3.2: Slikoviti prikaz jednostavnog potpuno asimetričnog procesa isključenja s dugodosežnim preskocima i otvorenim rubnim uvjetima.

Izborom rubnih uvjetima (3.7) i (3.8) smo propagiranju čestica unutar lanca dodali izmjenu čestica sa spremnicima na svakom čvoru rešetke. U vremenskoj evoluciji profila gustoće to se očituje vezanjem lokalne gustoće $\langle \tau_i \rangle$, $1 \leq i \leq L$, na "vanjsko polje" α_i i β_i,

$$\frac{d}{dt}\langle \tau_i \rangle = \alpha_i(1 - \langle \tau_i \rangle) + \sum_{j=1}^{i-1} p_{i-j} \langle \tau_j(1-\tau_i) \rangle - \\ - \sum_{j=i+1}^{L} p_{j-i} \langle \tau_i(1-\tau_j) \rangle - \beta_i \langle \tau_i \rangle, \tag{3.9a}$$

$$\frac{d}{dt}\langle\tau_1\rangle = \alpha_1(1-\langle\tau_1\rangle) - \sum_{j=2}^{L} p_{j-1}\langle\tau_1(1-\tau_j)\rangle - \beta_1\langle\tau_1\rangle, \tag{3.9b}$$

$$\frac{d}{dt}\langle\tau_L\rangle = \alpha_L(1-\langle\tau_L\rangle) + \sum_{j=1}^{L-1} p_{L-j}\langle\tau_j(1-\tau_L)\rangle - \beta_L\langle\tau_L\rangle, \tag{3.9c}$$

Gornje jednadžbe mogu se sažetije zapisati u obliku lokalne jednadžbe kontinuiteta,

$$\frac{d}{dt}\langle\tau_i(t)\rangle = j_i - j_{i+1}, \tag{3.10}$$

gdje je struja j_i definirana kao ukupna struja svih čestica koje ili skaču s čvora i ili ga preskaču,

$$j_i = \sum_{k=i+1}^{L} \alpha_k(1-\langle\tau_k\rangle) + \sum_{k=1}^{i}\sum_{l=i+1}^{L} p_{l-k}\langle\tau_k(1-\tau_l)\rangle + \sum_{k=1}^{i}\beta_k\langle\tau_k\rangle. \tag{3.11}$$

Gornji izraz za struju možemo proširiti na mjesta $i = 0$ i $i = L+1$, što daje ukupnu struju čestica koje ulaze ili izlaze iz lanca,

$$j_{\text{in}} = \sum_{i=1}^{L} \alpha_i(1-\langle\tau_i\rangle) \tag{3.12}$$

$$j_{\text{out}} = \sum_{i=1}^{L} \beta_i\langle\tau_i\rangle \tag{3.13}$$

U stacionarnom stanju, naravno, vrijedi $j_{\text{in}} = j_1 = \cdots = j_L = j_{\text{out}}$.

Jedan od načina da interpretiramo jednadžbe (3.9a)-(3.9c) je da zamislimo spremnike duljine L i konstantnih gustoća $\rho_L = \alpha$ i $\rho_R = 1-\beta$. U posebnom slučaju kada je $\rho_L = \rho_R$ ($\alpha = 1-\beta$), sustav efektivno postaje translacijski invarijantan što daje konstantan profil gustoće $\langle\tau_i\rangle = \alpha$ i struju $j = \alpha(1-\alpha)$. Netrivijalno ponašanje očekuje se za $\rho_L \neq \rho_R$, a obzirom na dugodosežne preskoke, nije za očekivati da se stacionarno stanje može zapisati pomoću umnoška matrica. Kao prirodni put istraživanja ovog modela nameću se stoga numeričke Monte Carlo simulacije i analitički pristup u aproksimaciji srednjeg polja. Kao što smo pokazali u prethodnom poglavlju, polazište analitičkog pristupa je parcijalna diferencijalna jednadžba za lokalnu gustoću dobivena iz jednadžbe kontinuiteta u kontinuiranoj granici. U izvodu te jednadžbe problem bi nam mogli predstavljati nelokalni rubni uvjeti, pa se za sada ograničavamo na beskonačan sustav bez spremnika, dok uvođenje rubnih uvjeta ostavljamo za kasnije.

3.2 Hidrodinamički pristup u aproksimaciji srednjeg polja

Promotrimo proces na beskonačnoj rešetci za proizvoljni p i q uz vjerojatnosti preskoka $p_l = l^{-(1+\sigma)}/\zeta(\sigma+1)$. Polazeći od master jednadžbe, za vremensku evoluciju srednje lokalne gustoće $\langle\tau_n\rangle$ dobiva se jednadžba oblika

$$\frac{d}{dt}\langle\tau_n\rangle(t) = \langle K_n^{(1)}\rangle, \tag{3.14}$$

gdje je

$$K_n^{(1)} = \sum_{r>0} p_r(\Delta_r^+\tau_n - \Delta_r^-\tau_n) - (p-q)\sum_{r>0} p_r\left[(1-\tau_n)\Delta_r^+\tau_n + \tau_n\Delta_r^-\tau_n\right], \tag{3.15}$$

pri čemu smo uveli slijedeću notaciju, $\Delta_r^+\tau_n \equiv \tau_{n+r} - \tau_n$ i $\Delta_r^-\tau_n \equiv \tau_n - \tau_{n-r}$. U osnovi, zanima nas gornja jednadžba u tzv. hidrodinamičkoj granici u kojoj su mikroskopski detalji usrednjeni preko prikladnih prostornih i vremenskih skala. U matematici, ta je procedura rigorozno definirana, a provedena je dosad za proizvoljni p u kratkodosežnom slučaju [111, 112], te nedavno za $p = q$ u dugodosežnom slučaju [113]. U kratkodosežnom slučaju rezultat je Burgersova jednadžba za $p \neq q$,

$$\frac{\partial\rho}{\partial t} = -(p-q)\frac{\partial}{\partial x}[\rho(1-\rho)], \tag{3.16}$$

te difuzijska jednadžba za $p = q$,

$$\frac{\partial\rho}{\partial t} = \frac{1}{2}\frac{\partial^2\rho}{\partial x^2}. \tag{3.17}$$

U gornjim jednadžbama lokalna gustoća $\rho(x,t)$ predstavlja mikroskopsku lokalnu gustoću $\langle\tau_n\rangle$ usrednjenu na tzv. Eulerovoj skali ($t \to t/a$, $x \to x/a$) za $p \neq q$ i difuzijskoj skali ($t \to t/a^2$, $x \to x/a$) za $p = q$. Razlog zbog kojeg se na taj način dobiva isti rezultat kao i "naivnim" razvojem u red po konstanti rešetke a leži u tome što je stacionarno rješenje master jednadžbe $P(C)$ uniformno na prostoru stanja, što se može zapisati u faktoriziranom obliku do na korekcije koje nestaju u hidrodinamičkoj granici.

U dugodosežnom slučaju, rigorozni račun u simetričnom slučaju $p = q$ [113] daje tzv. frakcionalnu difuzijsku jednadžbu oblika

$$\frac{\partial\phi}{\partial t} = \nu_\sigma\Delta_\sigma\phi(x,t), \quad 1 < \sigma < 2, \tag{3.18}$$

gdje je $\nu_\sigma = -2p\Gamma(-\sigma)cos(\pi\sigma/2)/\zeta(\sigma+1) > 0$, a Δ_σ frakcionalni Laplacian sa svojstvom da je za neku prikladno izabranu funkciju $f(x)$, Fourierov transformat od $\Delta_\sigma f(x)$ jednak

$$\mathcal{F}\{\Delta_\sigma f(x)\} = -|k|^\sigma \hat{f}(k). \tag{3.19}$$

U realnom prostoru, frakcionalni Laplacian (poznat još kao i Rieszova frakcionalna derivacija, vidi [114,115]) definira se kao linearna kombinacija Weylovih frakcionalnih derivacija,

$$\Delta_\sigma f(x) \equiv -\frac{{}_{-\infty}\mathcal{D}_x^\sigma + {}_x\mathcal{D}_\infty^\sigma}{2cos(\pi\sigma/2)}, \tag{3.20}$$

$${}_{-\infty}\mathcal{D}_x^\sigma f(x) = \frac{1}{\Gamma(n-\sigma)}\frac{d^n}{dx^n}\int_{-\infty}^{x} f(\xi)(x-\xi)^{n-\sigma-1}, \tag{3.21a}$$

$${}_x\mathcal{D}_\infty^\sigma f(x) = \frac{(-1)^n}{\Gamma(n-\sigma)}\frac{d^n}{dx^n}\int_{x}^{\infty} f(\xi)(\xi-x)^{n-\sigma-1}, \tag{3.21b}$$

koje imaju slijedeće svojstvo obzirom na Fourierovu transformaciju,

$$\mathcal{F}\{{}_{-\infty}\mathcal{D}_x^\sigma f(x)\} = (-ik)^\sigma \hat{f}(k), \tag{3.22a}$$

$$\mathcal{F}\{{}_x\mathcal{D}_\infty^\sigma f(x)\} = (ik)^\sigma \hat{f}(k). \tag{3.22b}$$

Derivacije necjelobrojnog reda spominju se prvi put u radovima Leibnitza, Eulera, Laplacea, Fouriera i drugih, a sistematsku teoriju postavljaju nezavisno Riemann i Liouville u 19. stoljeću (vidi npr. [116]). U fizici, frakcionalne derivacije javljaju se u matematičkoj teoriji koja opisuje pojavu *subdifuzijskog* ($\mu < 2$) i *superdifuzijskog* ($\mu > 2$) transporta, u kojem srednje kvadratno odstupanje položaja ne slijedi linearni oblik u vremenu, već potencijski zakon s necjelobrojnim eksponentom μ (vidi npr. [117]),

$$\langle(\Delta\vec{r})^2\rangle = \langle(\vec{r} - \langle\vec{r}\rangle)^2\rangle \propto t^\mu. \tag{3.23}$$

Primjenu frakcionalnih derivacija nalazimo u biofizici (gore spomenuta anomalna difuzija), fizici polimera (Levyjev nasumični hod), teoriji kaosa, reologiji, u opisu relaksacije u neuređenim sustavima (amorfni metali, spinska stakla, feroelektrični kristali, itd.), elektrotehnici (sklopovi impendancije $|Z| \propto \omega^{-1/2}$) - da spomenemo samo neke (za kompletniji pregled primjena u fizici i inženjerstvu vidi redom [118] i [119]).

Vratimo li se na jednadžbu (3.14), primjenom aproksimacije srednjeg polja $\langle\tau_n\tau_m\rangle \to \langle\tau_n\rangle\langle\tau_m\rangle$, $n \neq m$, dobivamo jednadžbu oblika

$$\frac{d\phi_n}{dt} = \sum_{r>0}\frac{p_r}{2}(\Delta_r^+\phi_n - \Delta_r^-\phi_n) + (\Delta\rho + \phi_n)(p-q)\sum_{r>0} p_r(\Delta_r^+\phi_n + \Delta_r^-\phi_n), \tag{3.24}$$

gdje smo s ϕ_n označili odstupanje lokalne gustoće od srednje gustoće $\bar{\rho}$, te smo uveli $\Delta\rho = \rho - 1/2$ kako bi razlikovali dva bitna slučaja, $\rho \neq 1/2$ i $\bar{\rho} = 1/2$. Da bismo dobili jednadžbu za $\phi(x,t)$ u granici $a \to 0$, koristimo proceduru opisanu u [120]. Ideja se sastoji u tome da $\phi_n(t)$ shvatimo kao koeficijente Fourierovog reda neke funkcije $\phi(\hat{k},t)$ definirane na intervalu $[-K/2, K/2]$,

$$\hat{\phi}(k,t) = \sum_{n=-\infty}^{\infty} \phi_n(t) e^{-ikx_n}, \tag{3.25a}$$

$$\phi_n(t) = \frac{1}{K} \int_{-K/2}^{K/2} \hat{\phi}(k,t) e^{ikx_n} dk, \tag{3.25b}$$

gdje je $x_n = na$ i $K = 2\pi/a$. Koristeći (3.25a) i (3.25b), jednadžbu (3.24) možemo zapisati u inverznom prostoru u slijedećem obliku,

$$\frac{d}{dt}\hat{\phi}(k,t) = \hat{\phi}(k,t)[D(ka) - D(0)] + \Delta\rho\hat{\phi}(k,t)B(ka) + \tag{3.26}$$

$$+ \frac{1}{K^2} \int_{-K/2}^{K/2} dk_1 \int_{-K/2}^{K/2} dk_2 \hat{\phi}(k_1,t)\hat{\phi}(k_2,t) \sum_{n=-\infty}^{\infty} e^{i(k_1+k_2-k)na} B(ka), \tag{3.27}$$

gdje su $D(ka)$ i $B(ka)$ dani s

$$D(ka) = \frac{1}{2}\left[Li_{\sigma+1}(e^{ika}) + Li_{\sigma+1}(e^{-ika})\right], \tag{3.28a}$$

$$B(ka) = (p-q)[Li_{\sigma+1}(e^{ika}) - Li_{\sigma+1}(e^{-ika})]. \tag{3.28b}$$

U gornjim izrazima, $Li_s(z)$ je tzv. polilogaritamska funkcija definirana slijedećim redom

$$Li_s(z) = \sum_{n=1}^{\infty} \frac{z^n}{n^s}, \tag{3.29}$$

a javlja se, između ostalog, i kao integral Bose-Einstenove i Fermi-Diracove raspodjele [121],

$$Li_s(z) = \frac{1}{\Gamma(s)} \int_0^{\infty} \frac{t^{s-1}}{e^t/z - 1} dt \tag{3.30a}$$

$$-Li_s(-z) = \frac{1}{\Gamma(s)} \int_0^{\infty} \frac{t^{s-1}}{e^t/z + 1} dt. \tag{3.30b}$$

Koristeći razvoj polilogaritamske funkcije $Li_s(e^z)$ oko $z = 0$ [121],

$$Li_s(e^z) = \Gamma(1-s)(-z)^{s-1} + \sum_{k=0}^{\infty} \frac{\xi(s-k)}{k!} z^k, \quad |z| < 2\pi, \quad s \neq 1, 2, 3, \ldots, \tag{3.31}$$

dobivamo slijedeći razvoj $D(ka)$ i $B(ka)$ u ka,

$$D(ka) - D(0) = \frac{1}{2\zeta(\sigma+1)} \left[2\Gamma(-\sigma) cos\frac{\pi\sigma}{2} |k|^\sigma a^\sigma + \right. \\ \left. + 2\sum_{n=1}^{\infty} \frac{\zeta(\sigma+1-2n)}{(2n)!} (ik)^{2n} a^{2n} \right], \tag{3.32a}$$

$$B(ka) = \frac{p-q}{\zeta(\sigma+1)} \left[-2i\Gamma(-\sigma) sin\frac{\pi\sigma}{2} sgn(k)|k|^\sigma a^\sigma + \right. \\ \left. + 2\sum_{n=1}^{\infty} \frac{\zeta(\sigma+2-2n)}{(2n-1)!} (ik)^{2n-1} a^{2n-1} \right]. \tag{3.32b}$$

Naposljetku, zanima nas granica $a \to 0$ u kojoj suma u (3.25a) prelazi u integral,

$$\hat{\phi}(k,t) = \sum_{n=-\infty}^{\infty} \phi_n(t) e^{-ikx_n} = \frac{1}{a} \sum_{n=-\infty}^{\infty} \phi_n(t) e^{-ikx_n} \overbrace{\Delta x_n}^{a} \tag{3.33}$$

$$\Rightarrow \quad lim_{a\to 0}[a\hat{\phi}(k,t)] = \int_{-\infty}^{\infty} \phi(x,t) e^{-ikx} dk \equiv \tilde{\phi}(k,t), \tag{3.34}$$

$$\phi(x,t) = \frac{1}{2\pi} \int_{-\infty}^{\infty} \tilde{\phi}(k,t) e^{ikx} dk, \tag{3.35}$$

gdje smo s $\tilde{\phi}(k,t)$ i $\phi(k,t)$ označili $\hat{\phi}(k,t)$ i $\phi_n(t)$ u kontinuiranoj granici. Pritom moramo transformirati vremensku skalu, $t \to t/a^z$, gdje je z najmanji eksponent u a (3.32a) i (3.32b). Obzirom na p i q, razlikujemo simetrični ($p = q$) i asimetrični slučaj ($p \neq q$).

3.2.1 Simetrični slučaj $p = q$

U slučaju $p = q$, $B(ka)$ je identički 0, dok iz (3.32a) slijedi da je $z = \min\{\sigma, 2\}$. Za $\sigma > 2$, dobiva se uobičajena difuzijska jednadžba oblika

$$\frac{\partial\phi}{\partial t} = \nu_2 \frac{\partial^2\phi}{\partial x^2}, \quad \sigma > 2, \tag{3.36}$$

s koeficijentom difuzije $\nu_2 = \zeta(\sigma-1)/2\zeta(\sigma+1) > 0$. S druge strane, za $1 < \sigma < 2$ se dobiva frakcionalna difuzijska jednadžba oblika

$$\frac{\partial\phi}{\partial t} = \nu_\sigma \Delta_\sigma \phi, \quad 1 < \sigma < 2, \tag{3.37}$$

gdje je $\nu_\sigma = -\Gamma(-\sigma) cos(\pi\sigma/2)/\zeta(\sigma+1) > 0$, identično rezultatu u [113].

3.2.2 Asimetrični slučaj $p \neq q$

U asimetričnom slučaju je $z = \min\{\sigma, 1\}$, što za $\sigma > 1$ daje neviskoznu Burgersovu jednadžbu s dodatnim članom $-v\partial/\partial x\phi(x,t)$,

$$\frac{\partial \phi}{\partial t} = -c(\bar{\rho})\frac{\partial \phi}{\partial x} - \kappa\phi\frac{\partial \phi}{\partial x}, \quad \sigma > 1, \tag{3.38}$$

uz slijedeće $c(\bar{\rho})$ i κ,

$$c(\bar{\rho}) = (p-q)(1-2\bar{\rho})\lambda(\sigma) = \left.\frac{dj(\rho)}{d\rho}\right|_{\rho=\bar{\rho}}, \tag{3.39}$$

$$\kappa = -2(p-q)\lambda(\sigma) = \left.\frac{d^2 j(\rho)}{d\rho^2}\right|_{\rho=\bar{\rho}}. \tag{3.40}$$

čime smo na prirodan način ponovo dobili struju $j(\sigma) = \lambda(\sigma)\rho(1-\rho)$ i srednju duljinu preskoka $\lambda(\sigma)$,

$$j(\rho) = (p-q)\lambda(\sigma)\rho(1-\rho), \quad \lambda(\sigma) = \frac{\zeta(\sigma)}{\zeta(\sigma+1)}. \tag{3.41}$$

Originalna Burgersova jednadžba (2.69) dobije se lako Galilejevom transformacijom prostorne skale $x \to x - c(\bar{\rho})t$, ili uvrštavanjem $\bar{\rho} = 1/2$, što odgovara $c = 0$.

S jedne strane, rezultat (3.38) je iznenađujući utoliko što na prvi pogled dugodosežni preskoci nemaju učinka na većim prostornim i vremenskih skalama. S druge strane, jednadžba (3.38) povlači iste one zaključke o kojima smo raspravljali u poglavlju (2.3), a koji se tiču pojave domenskih zidova i njihove nestabilnosti u neviskoznom slučaju. Opravdano je, stoga, pogledati članove višeg reda u a koje smo izostavili u strogoj granici $a \to 0$, a koji postaju relevantni ako želimo opisati ponašanje na manjim skalama. Za $1 < \sigma < 2$, prvi slijedeći članovi u (3.32a) i (3.32b su reda a^σ, a u realnom prostoru odgovaraju frakcionalnom Laplacianu $\Delta_\sigma\phi$ i nelinearnom članu $\phi H_\sigma\phi$, gdje je nelokalni operator H_σ dan slijedećom linearnom kombinacijom Weylovih frakcionalnih derivacija,

$$H_\sigma \equiv \frac{{}_{-\infty}\mathcal{D}_x^\sigma - {}_x\mathcal{D}_\infty^\sigma}{2sin(\pi\sigma/2)}, \tag{3.42}$$

te ima slijedeće svojstvo obzirom na Fourierovu transformaciju $\mathcal{F}$ i prikladno izabranu funkciju $f(x)$

$$\mathcal{F}\{H_\sigma f(x)\} = -isgn(k)|k|^\sigma \hat{f}(k), \quad \hat{f}(k,t) = \mathcal{F}\{f(x)\}. \tag{3.43}$$

Iako su oba člana nelokalna i istog reda u a, možemo pretpostaviti da će zbog nelinearnosti član $\phi H_\sigma\phi$ biti općenito višeg reda od difuzijskog člana. Zanemarivanjem nelinearnog člana dobiva se viskozna Burgersova jednadžba s frakcionalnim difuzijskim članom za $1 < \sigma < 2$, te uobičajenim difuzijskim članom za $\sigma > 2$,

$$\frac{\partial \phi^a}{\partial t} = a^{\sigma-1}\nu_\sigma \Delta_\sigma \phi^a - \kappa \phi^a \frac{\partial \phi^a}{\partial x}, \quad 1 < \sigma < 2, \tag{3.44}$$

$$\frac{\partial \phi^a}{\partial t} = a\nu_2 \Delta \phi^a - \kappa \phi^a \frac{\partial \phi^a}{\partial x}, \quad \sigma > 2, \tag{3.45}$$

gdje smo lokalno odstupanje gustoće označili s $\phi^a(x,t)$ da naglasimo ovisnost o a.

Gornje jednadžbe vode na dva važna zaključka. Prvi zaključak nam govori da se kratkodosežna granica *efektivno* javlja već za $\sigma > 2$, što je rezultat u koji ćemo se kasnije pri razmatranju otvorenih rubnih uvjeta više puta uvjeriti. Drugi važan rezultat tiče se regularnosti rješenja Burgersove jednadžbe s frakcionalnim difuzijskim članom. Jednadžbu oblika (3.44) razmatralo je nekoliko autora (vidi [122] i sadržane reference), koji su pokazali da frakcionalni difuzijski član ima sličan učinak kao i uobičajeni difuzijski član, u smislu da i u rješenjima jednadžbe (3.44) možemo očekivati stabilne domenske zidove.

3.2.3 Vremenska relaksacija k stacionarnom stanju

Prije nego što u prethodnu diskusiju uključimo rubne uvjete (3.8) i (3.7), zgodno je na neki način provjeriti koliko su zaključci prethodnog poglavlja, dobiveni u hidrodinamičkoj granici, relevantni za diskretni model. Pritom je jasno da se zbog numeričkih simulacija moramo ograničiti na konačni sustav, što nas, želimo li zadržati translacijsku invarijantnost, vodi na model s periodičkim rubnim uvjetima. Sada nas, međutim, umjesto (trivijalnog) stacionarnog stanja koje smo razmatrali u poglavlju 3.1.1, zanima relaksacija sustava ka stacionarnom stanju, točnije, najduže relaksacijsko vrijeme τ.

U poglavlju 2.2 pokazali smo kako je u kratkodosežnom slučaju τ obrnuto proporcionalno procjepu između osnovnog i prvog pobuđenog stanja XXZ spinskog lanca, koji se dobiva zapisom master jednadžbe u kvantnom formalizmu. Kvantni spinski lanac s kratkodosežnim međudjelovanjem u jednoj dimenziji može se dalje tretirati Betheovim Ansatzom. Kao rezultat se, ovisno o asimetriji u p i q i za fiksnu gustoću[1], dobiva difuzijska relaksacija za $p = q$ [50],

$$\tau \propto L^z, \quad z = 2, \quad p = q, \tag{3.46}$$

dok u asimetričnom slučaju, $p \neq q$, divergira kao $\tau \propto L^z$ uz $z = 3/2$ [50, 123]. Slično ponašanje dobiva se i u slučaju otvorenih rubnih uvjeta [51, 52] na linije egzistencije faza ($\tau \propto L^2$ zbog difuznog kretanja domenskog zida) i u fazi maksimalne struje ($\tau \propto L^{3/2}$), osim u fazama niske i visoke gustoće gdje je τ konačno.

Kao što smo spomenuli ranije u poglavlju 2.2, drugi način za odrediti τ sastoji se od ispitivanja invarijantnosti na promjenu vremenske i prostorne skale hidrodinamičkih jednadžbi, točnije, njihovih stohastičkih inačica. Transformacijom

[1] Ako umjesto gustoće fiksiramo broj čestica, tada se procjep skalira kao L^2, vidi [124]

$\phi(x,t) = \partial h(x,t)/\partial x$, difuzijska jednadžba u simetričnom ($p = q$) i Burgersova jednadžba u asimetričnom ($p \neq q$) slučaju prelaze redom u Edwards-Wilkinsovu (EW) i Kardar-Parisi-Zhang (KPZ) jednadžbu,

$$\frac{\partial h}{\partial t} = \nu \Delta h + \eta, \tag{3.47}$$

$$\frac{\partial h}{\partial t} = \nu \Delta h + \frac{\lambda}{2}\left(\frac{\partial h}{\partial x}\right)^2 + \eta, \tag{3.48}$$

Za stohastičke procese opisane gornjim jednadžbama, vremenska korelacijska funkcija $\langle \phi(0,0)\phi(x,t)\rangle$ je homogena funkcija određena eksponentima χ i z,

$$C(\lambda x, \lambda^{1/z} t) = \lambda^{2\chi - 2} C(x,t), \tag{3.49}$$

gdje se usrednjavanje $\langle \dots \rangle$ vrši po svim mogućim vremenskim evolucijama šuma. Obzirom na linearnost EW jednadžbe, χ i z se mogu jednostavno odrediti dimenzionalnom analizom, što daje $\chi = 1/2$ i $z = 2$. U slučaju KPZ jednadžbe račun je kompliciraniji, a sastoji se u dokazivanju dviju važnih svojstava KPZ jednadžbe. Prvo svojstvo je relacija $\chi + z = 2$, koja slijedi iz invarijantnosti KPZ jednadžbe na jednu posebnu vrstu Galilejeve transformacije parametriziranu vektorom $\vec{v}$ [76],

$$h'(\vec{x},t) = h(\vec{x} - \vec{v}t) - \frac{1}{\lambda}\vec{v}\cdot\vec{x} + \frac{1}{2\lambda}\vec{v}^2 t \tag{3.50}$$

i vrijedi za proizvoljnu dimenziju prostora d. Drugo svojstvo karakteristično je samo za $d = 1$, a ogleda se u činjenici da stacionarna raspodjela vjerojatnosti visina $P[h(x,t)]$, kao i u EW jednadžbi, odgovara Gaussovoj raspodjeli [76],

$$P[h] \propto exp\left[-\frac{\nu}{D}\int dx (\nabla h)^2\right], \tag{3.51}$$

gdje je D definiran relacijom (2.89). To za posljedicu ima da je $\chi = 1/2$, što zajedno s prvim svojstvom daje $z = 3/2$.

Nelokalne inačice EW i KPZ jednadžbe promatrane su u [125, 126], pri čemu je lokalni difuzijski član $\Delta h(x,t)$ zamijenjen frakcionalnim $\Delta_\sigma h(x,t)$,

$$\frac{\partial h}{\partial t} = \nu \Delta_\sigma h + \eta, \quad 0 < \sigma \leq 2, \tag{3.52}$$

$$\frac{\partial h}{\partial t} = \nu \Delta_\sigma h + \frac{\lambda}{2}\left(\frac{\partial h}{\partial x}\right)^2 + \eta, \quad 0 < \sigma \leq 2. \tag{3.53}$$

U slučaju frakcionalne EW jednadžbe (FEW), $\chi = (\sigma - 1)/2$, a z poprima vrijednost σ, što također slijedi iz dimenzionalne analize [125]. S druge strane, frakcionalna KPZ jednadžba (FKPZ) pokazuje znatno kompleksnije ponašanje s nekoliko različitih režima, ovisno o vrijednosti parametra σ i o tome da li je šum $\eta(x,t)$

koreliran u prostoru ili ne [126]. Ukoliko je šum nekoreliran, račun pokazuje postojanje dva režima: prvi je frakcionalni EW režim za $\sigma < 3/2$ uz $\chi = (\sigma - 1)/2$ i $z = \sigma$, a drugi je standardni KPZ režim za $\sigma > 3/2$ uz $\chi = 1/2$ i $z = 3/2$. Promjena režima u $z(\sigma)$ na vrijednosti $3/2$ može se intuitivno shvatiti na način da se sustav uvijek nastoji relaksirati kroz svoju najbržu "komponentu", koja za $\sigma > 3/2$ prestaje biti frakcionalna difuzija, jer je tada $z_{FEW} < z_{FKPZ}$.

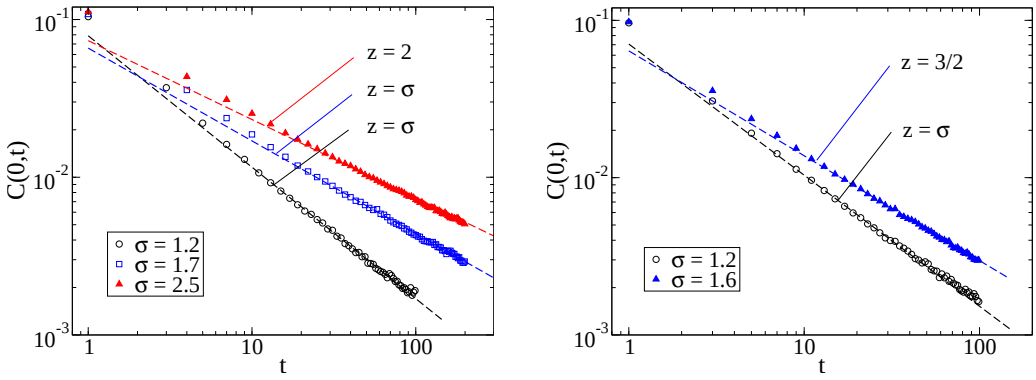

Slika 3.3: Ovisnost korelacijske funkcije $C(0,t)$ o t u jednostavnom simetričnom (lijevo) i asimetričnom (desno) procesu isključenja s dugodosežnim preskocima na periodičkoj rešetci duljine $L = 10^4$ i gustoće čestica $\rho = 1/2$. Korelacijska funkcija dobivena je usrednjavanjem po 10^7 nezavisnih Monte Carlo simulacija ukupne duljine $t = 100$ Monte Carlo koraka po čvoru. Isprekidane linije označavaju analitički oblik $C(0,t) \propto t^{-1/z}$ uz $z = \min\{\sigma, 2\}$ (lijevo) i $z = \min\{\sigma, 3/2\}$ (desno).

Gornja predviđanja provjerili smo u diskretnom modelu računanjem vremenske korelacijske funkcije $C(i-j,t)$ pomoću Monte Carlo simulacija. U tu svrhu promatramo simetrični i djelomično asimetrični model s dugodosežnim preskocima i periodičkim rubnim uvjetima na rešetci duljine $L = 10^4$ i gustoće $\rho = 1/2$, te računamo korelacijsku funkciju $\langle[\tau_i(0)-\rho][\tau_j(t)-\rho]\rangle$, usrednjenu po 10^7 nezavisnih Monte Carlo simulacija duljine $t = 100$ Monte Carlo koraka po čvoru. Ograničimo li se samo na računanje dinamičkog eksponenta z, z možemo odrediti iz $C(i-j,t)$ odabirom $ct = i - j$, obzirom da je

$$C(ct,t) \propto t^{-1/z}. \tag{3.54}$$

Ovisnost $C(0,t)$ o t (gdje smo uzeli u obzir da je $c = 0$ za $\rho = 1/2$) prikazana je u simetričnom slučaju na slici 3.3a, a u djelomično simetričnom na slici 3.3b. U oba slučaja se dobiva izvrsno slaganje s predviđenim vrijednostima $z = \min\{\sigma, 2\}$ za $p = q$ i $z = \min\{\sigma, 3/2\}$ za $p \neq q$ u slučaju prostorno nekoreliranog šuma.

3.3 Dugodosežni efekti u transportu DNK regulatornih proteina

DNK regulatorni proteini se vežu na molekulu DNK sudjelujući pritom u mnogim važnim procesima poput transkripcije gena ili kondenzacije DNK molekule u kromosome. Neki od njih, poput transkripcijskih faktora, vežu se samo na određena mjesta na DNK molekuli kontrolirajući pritom prijenos genetske informacije s DNK na glasničku RNK. Brzinu k_a reakcije proteina P sa specifičnim mjestom S na DNK molekuli,

$$P + S \leftrightharpoons PS, \tag{3.55}$$

moguće je pritom eksperimentalno izmjeriti [127] mjereći omjer

$$k_a = \frac{d[PS]/dt}{[P][S]} \tag{3.56}$$

U početku se smatralo da se proces traženja specifičnog mjesta na DNK molekuli odvija putem difuzije proteina u stanici. Teorijski to vodi na $k_{3D} = 4\pi D_{3D} b a \approx 10^8$ $\mathrm{M}^{-1}\mathrm{s}^{-1}$, gdje je D_{3D} konstanta difuzije, b udarni presjek reakcije, a a udio u površini proteina kojim se protein veže za DNK. Tako dobivena vrijednost, međutim, odstupa dva reda veličine od eksperimentalno utvrđenih vrijednosti, što je procesu donijelo ime *potpomognuta* difuzija. Danas je poznato da u traženju specifičnog mjesta DNK regulatorni protein naizmjence izvodi trodimenzionalnu difuziju u stanici i efektivno jednodimenzionalnu difuziju duž DNK molekule (za detaljniju povijest problema vidi [128]), što je slikovito prikazano na slici 3.4. Drugim riječima, protein se veže na DNK po kojoj se pomiče 1D difuzijom, a potom se odvoji i nastavlja se kretati 3D difuzijom do ponovnog vezanja s DNK.

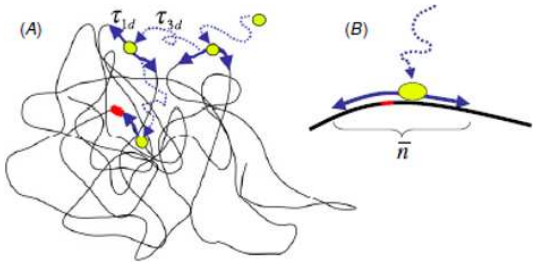

Slika 3.4: (A) Slikoviti prikaz potpomognute difuzije kojom DNK regulatroni protein (označen žutom bojom) traži specifično mjesto na DNK (označeno crvenom bojom). (B) Između apsorpcije i desorpcije protein prijeđe u prosjeku put od $\bar{n}$ bazičnih parova (bp) čime povećava udarni presjek b s 1 bp na $\bar{n}$. Preuzeto iz [128].

Ukoliko je DNK molekula dugačka i isprepletena, tada se može dogoditi da se dva dijela DNK lanca, od kojih je na jednom vezan protein, toliko približe da

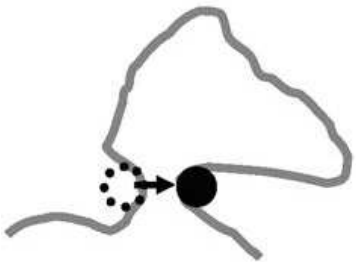

Slika 3.5: Slikoviti prikaz međusegmentnog prijenosa kao jednog od mehanizama potpomognute difuzije.

protein prijeđe s jednog dijela DNK lanca na drugi, što se naziva međusegmentnim prijenosom (slika 3.5). Lomholt *et al.* su predložili da se taj proces opiše frakcionalnom difuzijom proteina duž DNK molekule [129], obzirom da raspodjela duljina petlji l isprepletenog polimera slijedi potencijski zakon $p_l \propto l^{-1-\sigma}$, pri čemu je u dobrim otapalima $1 < \sigma < 2$ [130]. U tom kontekstu, dugodosežni preskoci u TASEP-u bi se mogli promatrati kao diskretna inačica frakcionalne difuzije kao predloženog mehanizma za traženje specifičnih mjesta na dugačkim lancima.

3.4 Fazni prijelazi u modelu s otvorenim rubnim uvjetima

Činjenica da se u hidrodinamičkoj granici beskonačnog sustava s dugodosežnim preskocima dobiva ista (Burgersova) jednadžba kao i u kratkodosežnom slučaju, a da su dugodosežni učinci opisani tek članovima višeg reda, sugerira fazni dijagram isti ili sličan dijagramu u kratkodosežnom modelu. Pritom, međutim, treba imati na umu da su rubni uvjeti nelokalni, u smislu da sustav izmjenjuje čestice sa spremnicima na svakom čvoru rešetke. U nastavku ćemo, prvo korištenjem Monte Carlo simulacija, a zatim i analitički, pokazati da ta činjenica ne mijenja fazni dijagram kratkodosežnog modela, ali da mijenja ponašanje sustava na linijama prijelaza.

3.4.1 Fazni dijagram

Da bismo odredili fazni dijagram, provodimo Monte Carlo (MC) simulacije s nasumično-sekvencijalnom dinamikom, na način da se u svakom diskretnom vremenskom koraku nasumično izabere jedan čvor $1 \leq i \leq L$ na rešetci (L takvih koraka definira jedan Monte Carlo korak po čvoru). Ako je čvor i prazan ($\tau_i = 0$), tada na to mjesto iz lijevog spremnika gustoće $\rho_L = \alpha$ skače čestica s vjerojatnošću α_i. Ako je čvor i popunjen, slučajna duljina $1 \leq l \leq L$ se bira iz raspodjele p_l, te su moguća dva slučaja. U prvom slučaju čestica skače za l mjesta na čvor $i + l$, pod uvjetom da je $i + l \leq L$ i da je čvor $i + l$ prazan. U slučaju da je $i + l > L$, čestica napušta sustav s vjerojatnošću β. Stacionarni profil gustoće $\langle \tau_i \rangle$ i struju j_i

računamo tek nakon što se sustav relaksirao t_0 MC koraka po čvoru, što osigurava da je postignuto stacionarno stanje.

Na slikama 3.6a do 3.6d prikazani su profili gustoća dobiveni za tipične α i β. U odnosu na kratkodosežni model, sa slika uočavamo nekoliko sličnosti i razlika. Prvo, faze niske i visoke gustoće i dalje su prisutne (slike 3.6a i 3.6b), ali je odstupanje od srednje gustoće blizu rubova veće. Drugo, na liniji $\alpha = \beta < 1/2$ primjećujemo netrivijalni profil, koji ne odgovara linearnom profilu iz kratkodosežnog modela (slika 3.6c). Naposljetku, u fazi maksimalne struje srednja gustoća je i dalje 1/2, ali uz znatno veća odstupanja blizu rubova (slika 3.6d).

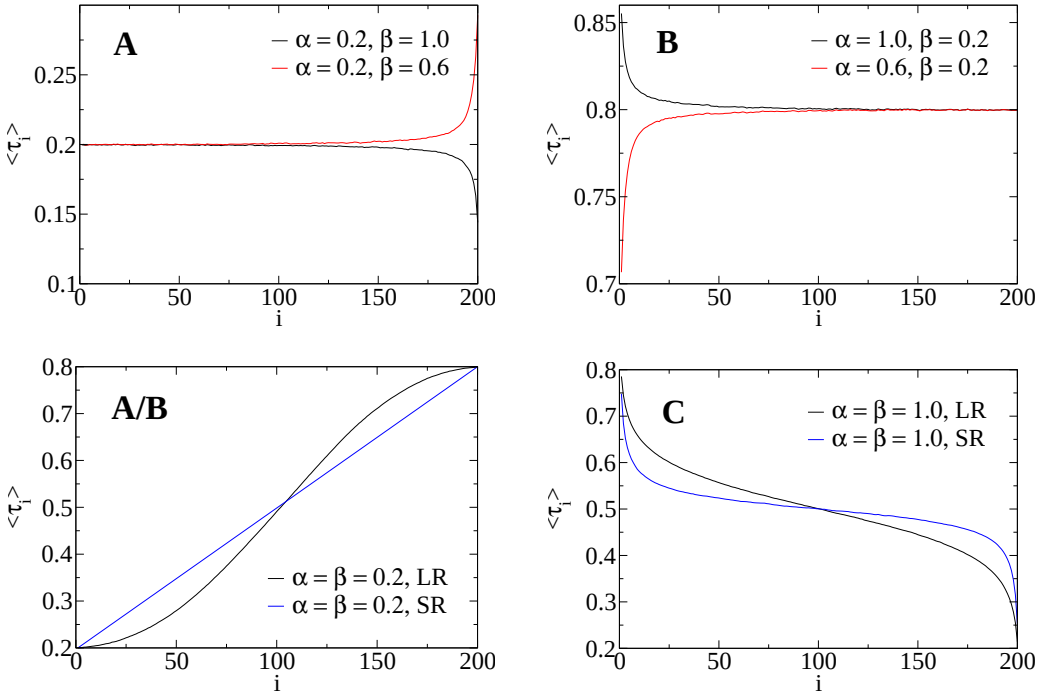

Slika 3.6: Profili gustoće u jednostavnom potpuno asimetričnom procesu isključenja s dugodosežnim preskocima za $\sigma = 1.5$ dobiveni Monte Carlo simulacijama u: (a) fazi niske gustoće A, (b) fazi visoke gustoće B, (c) na liniji koegzistencije faza A i B i (d) u fazi maksimalne struje. Radi lakše usporedbe, na slikama (c) i (d) prikazani su profili gustoća u kratkodosežnom modelu (SR) za iste α i β. Parametri svih simulacija su $L = 200$ i $t_0 = t = 10^7$ MC koraka po čvoru.

Da bismo odredili prirodu prijelaza između faza, promatramo srednju gustoću $\bar{\rho} = \langle N \rangle / L = \sum_{i=1}^{L} \langle \tau_i \rangle / L$ i struju j_L kao funkcije od α za dvije fiksne vrijednosti parametra β, $\beta < 1/2$ (slika 3.7a) i $\beta > 1/2$ (slika 3.7b) [Obzirom da je fazni dijagram simetričan na zamjenu $\alpha \leftrightarrow \beta$, sličnu provjeru nije potrebno provesti variranjem β uz fiksni α.] Sa slike 3.7a vidimo da srednja gustoća $\bar{\rho}$ ima skok na liniji $\alpha = \beta = 0.3 < 1/2$, kao i u kratkodosežnom modelu. Na slici 3.7b prikazana je ovisnost struje j_L/λ_L o α uz fiksni $\beta = 0.7 > 1/2$, koja prati poznatu ovisnost struje o gustoći $j_L = \alpha(1-\alpha)$ za $\alpha < 1/2$ i $j_L = 1/4$ za $\alpha > 1/2$ (slika 3.7b). Na

obje slike prikazali smo i rezultate za $\sigma < 1$, koji potvrđuju raniji zaključak da zbog divergencije struje nema faznih prijelaza.

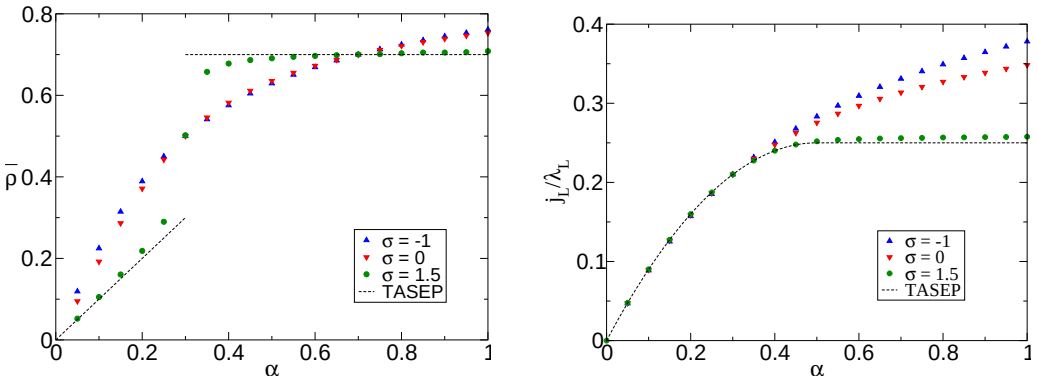

Slika 3.7: Ovisnost (a) srednje gustoće $\bar{\rho}$ o α za $\beta = 0.3$ i (b) struje j_L/λ_L o α za $\beta = 0.7$, za različite vrijednosti parametra σ. Parametri svih simulacija su $L = 200$ i $t_0 = t = 2 \cdot 10^6$ MC koraka po čvoru. Odgovarajuće ovisnosti u kratkodosežnom modelu (TASEP) prikazane su isprekidanim linijama.

Na osnovu Monte Carlo simulacija, zaključujemo da je fazni dijagram u dugodosežnom modelu ostao nepromijenjen. Razlike uočavamo na granici koegzistencije faza $\alpha = \beta < 1/2$ i u fazi maksimalne struje, čime se bavimo u nastavku.

3.4.2 Lokalizacija domenskog zida na prijelazu prvog reda

Netrivijalni profil gustoće na liniji koegzistencije faza $\alpha = \beta < 1/2$ može se objasniti pristupom preko dinamike domenskih zidova koji smo razradili u poglavlju 2.3.3. Opravdanje tog pristupa prije svega leži u činjenici da smo u hidrodinamičkoj granici dobili viskoznu Burgersovu jednadžbu s frakcionalnim difuzijskim članom koji stabilizira domenske zidove kao moguća rješenja. Kako je širina domenskog zida reda veličine konstante rešetke a, za trenutni profil domenskog zida možemo izabrati funkciju stepenice,

$$\rho_s(x) = \begin{cases} \alpha & x < x_s \\ 1-\beta & x > x_s. \end{cases} , \tag{3.57}$$

gdje je x_s trenutni položaj domenskog zida. Slično kao i u modelu s Langmuirovom kinetikom, kojeg smo opisali u poglavlju 2.4.1, vjerojatnosti preskoka domenskog zida na susjedne čvorove prostorno su ovisne, a razlog leži u prostornoj ovisnosti ukupne struje čestica koje ulaze lijevo ili izlaze desno od domenskog zida. Tako je, prema izrazu (2.97), vjerojatnost r_i preskoka domenskog zida s mjesta i na mjesto $i+1$ jednaka razlici ulazne i izlazne struje čestica u domenu gustoće $1-\beta$, podijeljenoj s visinom domenskog zida $1-\alpha-\beta$,

$$r_i = \frac{1}{1-\alpha-\beta}\left[\sum_{j=i}^{L}\beta_j(1-\beta) - \sum_{j=i}^{L}\alpha_j\beta\right], \quad i = 1, ..., L. \tag{3.58}$$

Slično, vjerojatnost l_i preskoka domenskog zida s mjesta i na mjesto $i-1$ jednaka je razlici ulazne i izlazne struje čestica u domenu gustoće α, podijeljenoj s visinom domenskog zida $1-\alpha-\beta$,

$$l_i = \frac{1}{1-\alpha-\beta}\left[\sum_{j=1}^{i-1}\alpha_j(1-\alpha) - \sum_{j=1}^{i-1}\beta_j\alpha\right], \quad i = 2, ..., L+1. \tag{3.59}$$

Pritom uzimamo da se domenski zid reflektira na rubovima, pa je $l_1 = r_{L+1} = 0$.

Izračunamo li iz relacija (3.58) i (3.59) brzinu domenskog zida $v_i = r_i - l_i$, možemo vidjeti da je za $\alpha < \beta$ brzina uvijek pozitivna, $v_i > 0$, pa se domenski zid zadržava blizu desnog ruba (faza niske gustoće). Za $\alpha > \beta$ je brzina pak uvijek negativna, $v_i < 0$, pa se domenski zid zadržava blizu lijevog ruba (faza visoke gustoće). Razliku u odnosu na kratkodosežni model čini linija $\alpha = \beta < 1/2$, na kojoj brzina ne iščezava (osim na mjestu $i = L/2+1$). Umjesto toga, brzina je pozitivna na mjestima $1 \leq i < L/2+1$ i negativna na mjestima $L/2+1 < i \leq L+1$, a njezina apsolutna vrijednost raste kako se zid približava rubovima. Drugim riječima, brzina domenskog zida je uvijek usmjerena prema središtu sustava i raste s udaljenošću od središta. Pitanje koje se uz to odmah nameće je da li je pritom nužna lokalizacija domenskog zida u središtu, u smislu da standardna devijacija njegovog položaja $\Delta_L = [\langle x_s^2\rangle - \langle x_s\rangle^2]^{1/2}$ raste sporije od L u granici beskonačnog sustava,

$$\lim_{L\to\infty} \Delta_L/L = 0 \quad \Leftrightarrow \quad \text{lokalizacija} \tag{3.60}$$

[U gornjem izrazu, termodinamička granica je nužna jer je konačni sustav uvijek ergodičan, pa je domenski zid moguće naći na svakom mjestu.]

Da bismo odgovorili na to pitanje, polazimo od stacionarnih jednadžbi za vjerojatnost P_i nalaženja domenskog zida na mjestu i

$$r_{i-1}P_{i-1} + l_{i+1}P_{i+1} - (r_i + l_i)P_i = 0, \quad i = 2, ..., L \tag{3.61}$$

$$l_2P_2 - r_1P_1 = 0 \tag{3.62}$$

$$r_LP_L + -l_{L+1}P_{L+1} = 0. \tag{3.63}$$

Rješenje gornjih jednadžbi moguće je naći u zatvorenom obliku [73],

$$P_i = \frac{1}{Z_L}\prod_{j=1}^{i-1}\frac{r_j}{l_{j+1}} \equiv \frac{1}{Z_L}e^{-V_i}, \tag{3.64}$$

gdje je Z_L normalizacijska konstanta, a V_i "potencijal" oblika

$$V_i = -\sum_{j=1}^{i-1} \ln \frac{r_j}{l_{j+1}}, \qquad q < i \leq L+1. \tag{3.65}$$

Jednom kad su vjerojatnosti P_i poznate, stacionarni profil gustoće slijedi iz izraza [73]

$$\langle \tau_i \rangle^{DW} = \left(\sum_{j=i+1}^{L+1} P_j \right) \alpha + \left(\sum_{j=1}^{i} P_j \right) (1-\beta). \tag{3.66}$$

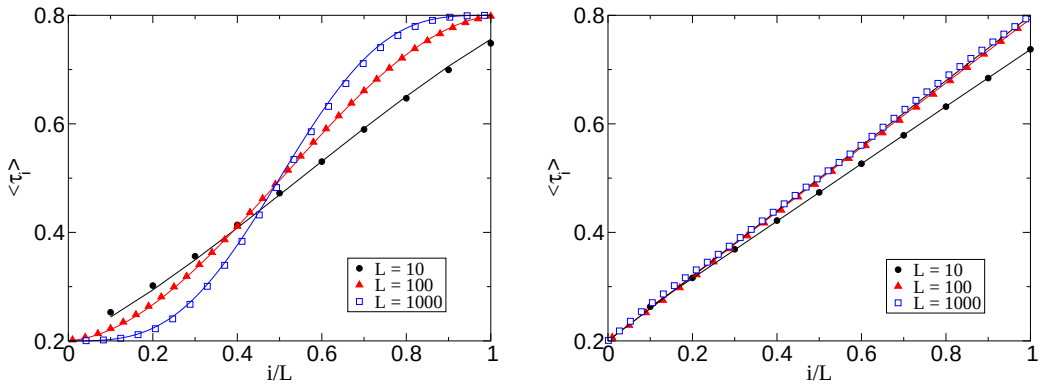

Slika 3.8: Usporedba profila gustoće dobivenih Monte Carlo simulacijama (simboli) i iz dinamike domenskih zidova (linije) za različite veličine sustava L i (a) $\sigma = 1.5$, te (b) $\sigma = 3$. U oba slučaja je $\alpha = \beta = 0.2$.

Gornji izraz može se izračunati numerički i usporediti s rezultatom Monte Carlo simulacija. Na slikama 3.8a i 3.8b prikazani su profili gustoće za $\sigma = 1.5$ i 3, za različite veličine sustava L. U svim slučajevima slaganje je izvrsno. Također vidimo da se za $\sigma = 1.5$ profil sužuje povećanjem veličine sustava L, što nije slučaj za $\sigma = 3$, za koji profili gustoće poprimaju linearni oblik istovjetan onome u kratkodosežnom modelu. Da bismo utvrdili postoji li lokalizacija domenskog zida, računamo standardnu devijaciju Δ_L u ovisnosti o L za nekoliko različitih vrijednosti σ. Rezultati prikazani na slici 3.9 u dobrom su slaganju s potencijskim zakonom oblika

$$\Delta_L \sim \begin{cases} L^{\frac{\sigma}{2}} & 1 < \sigma < 2 \\ L & \sigma > 2. \end{cases} \tag{3.67}$$

Drugim riječima, domenski zid je lokaliziran za $1 < \sigma < 2$, a delokaliziran za $\sigma > 2$.

Ovisnost Δ_L o L moguće je izvesti analitički. Ideja se sastoji od zamjene r_i, l_i, P_i i V_i kontinuiranim funkcijama $r(x)$, $l(x)$, $P(x)$ i $V(x)$ za konačni $x = i/L$ u granici $L \to \infty$, pri čemu

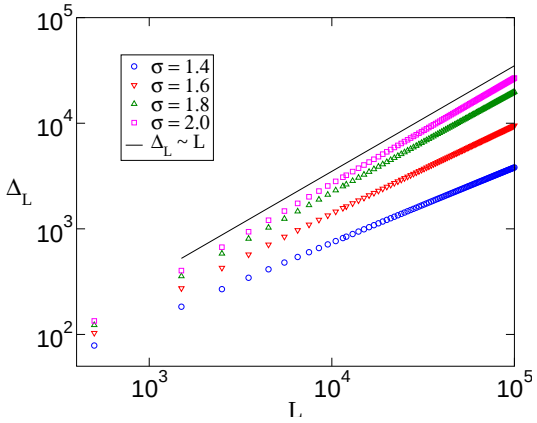

Slika 3.9: Standardna devijacija položaja domenskog zida Δ_L u ovisnosti o L za različite vrijednosti parametra σ i $\alpha = \beta = 0.1$.

$$L \cdot P_{i/L} \to P(x). \tag{3.68}$$

Uvedemo li diskretnu derivaciju potencijala V_i reda n na mjestu i, $\Delta_i^{(n)} \equiv \Delta_{i+1}^{(n-1)} - \Delta_i^{(n-1)}$, uz $\Delta_i^{(1)} = V_i - V_{i-1}$, tada u kontinuiranoj granici vrijedi

$$L^n \cdot \Delta_i^{(n)} \to \frac{d^n}{dx^n} V(x). \tag{3.69}$$

Na primjer, za prvu i drugu derivaciju se dobije

$$L \cdot \ln\left(\frac{r_{i-1}}{l_i}\right) \to \frac{d}{dx} V(x) \tag{3.70}$$

$$L^2 \cdot \ln\left(\frac{r_i \cdot l_i}{r_{i-1} \cdot l_{i+1}}\right) \to \frac{d^2}{dx^2} V(x). \tag{3.71}$$

Za $\alpha = \beta$ vrijedi $r_i = l_{L-i+2}$, pa se Taylorovim razvojem "potencijala" $V(x)$ oko minimuma u $x = 1/2 + 2/L$ dobiva red samo parnih potencija od $(x - 1/2)$,

$$V(x) = V(1/2) + \underbrace{\frac{1}{2!} \left.\frac{d^2V}{dx^2}\right|_{x=1/2}}_{c_2} \left(x - \frac{1}{2}\right)^2 + \underbrace{\frac{1}{4!} \left.\frac{d^4V}{dx^4}\right|_{x=1/2}}_{c_4} \left(x - \frac{1}{2}\right)^4 + \ldots \tag{3.72}$$

U najnižoj aproksimaciji odavde se dobiva Gaussova raspodjela, odakle slijedi da je standardna devijacija Δ_L proporcionalna $L/\sqrt{c_2}$. Time smo računanje Δ_L sveli na računanje c_2, tj. druge derivacije "potencijala" $V(x)$ u $x = 1/2$. Prostorna ovisnost potencijala V_i, koja opravdava aproksimaciju Gaussovom raspodjelom, prikazana je na slici 3.10.

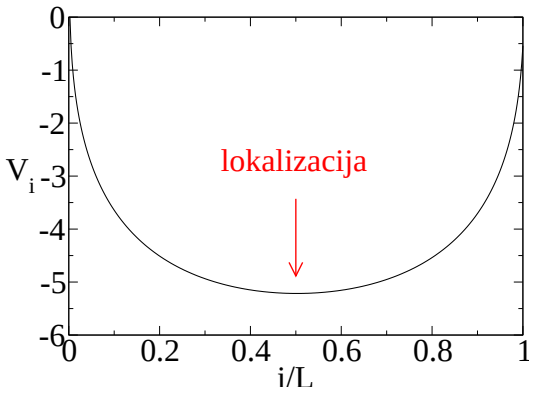

Slika 3.10: Prostorna ovisnosti "potencijala" V_i za $1 < \sigma < 2$. Minimum "potencijala" odgovara mjestu lokalizacije domenskog zida u granici $L \to \infty$.

Račun za c_2 polazi od kompaktnijeg zapisa suma koje se javljaju u izrazima (3.58) i (3.59) za r_i i l_i,

$$\sum_{j=1}^{i-1} \alpha_i = \alpha \left\{ \lambda_L \frac{\zeta_{i-1}(\sigma)}{\zeta_L(\sigma)} + (i-1) \left[1 - \frac{\zeta_{i-1}(\sigma+1)}{\zeta_L(\sigma+1)} \right] \right\}, \tag{3.73}$$

$$\sum_{j=i}^{L} \alpha_i = \alpha\lambda_L - \sum_{j=1}^{i-1} \alpha_i \tag{3.74}$$

$$\sum_{j=1}^{i-1} \beta_i = \beta \left\{ \lambda_L \left[1 - \frac{\zeta_{L-i}(\sigma)}{\zeta_L(\sigma)} \right] - (L-i+1) \left[1 - \frac{\zeta_{L-i}(\sigma+1)}{\zeta_L(\sigma+1)} \right] \right\}, \tag{3.75}$$

$$\sum_{j=i}^{L} \beta_i = \beta\lambda_L - \sum_{j=1}^{i-1} \beta_i \tag{3.76}$$

gdje smo s $\zeta_n(s)$ označili parcijalnu sumu zeta funkcije $\zeta(s)$,

$$\zeta_n(s) = \sum_{k=1}^{n} \frac{1}{k^s}. \tag{3.77}$$

Funkciju $\zeta_n(s)$ možemo ocijeniti integralom koristeći Euler-Maclaurinov razvoj, koji daje

$$\zeta_n(s) = \zeta(s) - \frac{1}{(s-1)} \frac{1}{n^{s-1}} + \int_n^{\infty} \frac{x - \lfloor x \rfloor}{x^{s+1}} dx, \tag{3.78}$$

pri čemu zadnji član možemo zanemariti jer je reda $O(n^{-s})$. Uvrštavanjem (3.78) u (3.58) i (3.59), te zamjenom $i \to x = i/L$ u granici $L \to \infty$ dobivamo

$$r(x) \simeq \frac{\beta(1-\beta)}{1-\alpha-\beta}\left[\lambda_L + \frac{f(x,\sigma,\alpha,\beta)}{L^{\sigma-1}}\right], \quad 0 \ll x \ll 1, \tag{3.79}$$

$$l(x) \simeq \frac{\alpha(1-\alpha)}{1-\alpha-\beta}\left[\lambda_L + \frac{f(1-x+2/L,\sigma,\beta,\alpha)}{L^{\sigma-1}}\right]., \quad 0 \ll x \ll 1, \tag{3.80}$$

gdje nam je za funkciju $f(x,\sigma,\alpha,\beta)$ jedino važno da je konačna i neprekidna za $0 < x < 1$. Uvrštavanjem gornjih izraza za $r(x)$ i $l(x)$ u izraze za $\Delta_i^{(2)}$ i $\Delta_i^{(4)}$ naposljetku se dobiva

$$c_2 = \frac{1}{2}\,\frac{d^2}{dx^2}V(x)\bigg|_{x=1/2} \simeq -\frac{2f'(1/2,\sigma,\alpha,\alpha)}{\lambda\alpha(1-\alpha)}L^{2-\sigma}, \tag{3.81}$$

$$c_4 = \frac{1}{24}\,\frac{d^4}{dx^4}V(x)\bigg|_{x=1/2} \simeq -\frac{2f'''(1/2,\sigma,\alpha,\alpha)}{\lambda\alpha(1-\alpha)}L^{2-\sigma}, \tag{3.82}$$

što daje traženu ovisnost Δ_L o L.

Za kraj spomenimo da se ovisnost $\Delta_L \propto L^{a/2}$ za $1 < a < 2$ javlja i u kratkodosežnom modelu s Langmuirovom kinetikom u kojem su brzine apsorpcije i desorpcije oblika [81],

$$\omega_A = \frac{\Omega_A}{L^a}, \quad \omega_D = \frac{\Omega_D}{L^a}. \tag{3.83}$$

Sličnost s dugodosežnim modelom otkriva se tek kada zapišemo α_i i β_i u kontinuiranoj granici,

$$\alpha_i \quad \to \quad \alpha(x) \simeq \frac{\alpha}{\zeta(\sigma+1)\sigma}\left[(x-1/L)^{-\sigma}-1\right]L^{-\sigma}, \tag{3.84}$$

$$\beta_i \quad \to \quad \beta(x) \simeq \frac{\beta}{\zeta(\sigma+1)\sigma}\left[(1-x)^{-\sigma}-1\right]L^{-\sigma}, \tag{3.85}$$

gdje prepoznajemo istu potencijsku ovisnost o veličini sustava L. Razlika je jedino u porijeklu te ovisnosti: u [81] je ona postulirana, dok u modelu s dugodosežnim preskocima prirodno slijedi iz nelokalnog transporta na konačnom segmentu.

3.4.3 Ovisnost kritičnog eksponenta o σna prijelazu drugog reda

Rezultati Monte Carlo simulacija, izloženi u poglavlju 3.4.1, pokazali su da se i u dugodosežnom modelu javlja kontinuirani fazni prijelaz iz faze niske ili visoke gustoće u fazu maksimalne struje. U kratkodosežnom modelu vidjeli smo da taj

prijelaz, kao i cijelu fazu maksimalne struje, karakteriziraju dugodosežne korelacije, što se očituje u potencijskom opadanju lokalne gustoće daleko od rubova s eksponentom 1/2. Obzirom na iskustvo iz ravnotežnih faznih prijelaza s dugodosežnim međudjelovanjem, za očekivati je da će dugodosežni preskoci promijeniti to ponašanje.

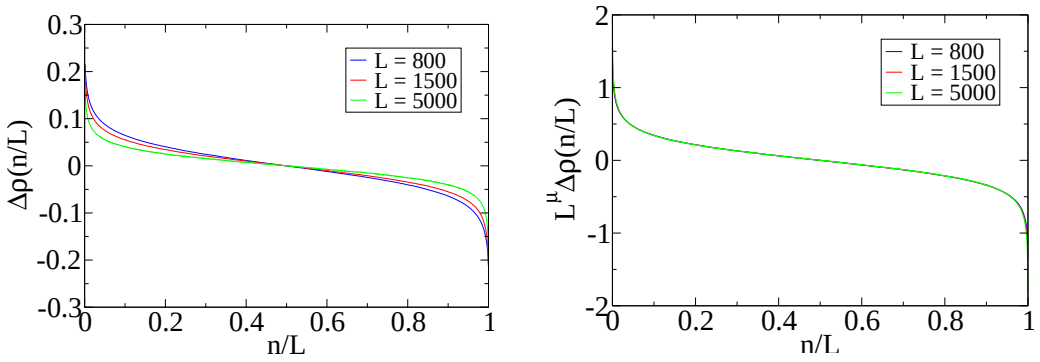

Slika 3.11: Prostorne ovisnosti odstupanja lokalne gustoće od srednje gustoće 1/2 za $\alpha = \beta = 0.8$, $\sigma = 1.5$ i različite veličine sustava L (a) prije primjene svojstva homogenosti (3.86) i (b) poslije.

Potencijsku ovisnost profila gustoće u fazi maksimalne struje provjeravamo Monte Carlo simulacijama. Ukoliko takva ovisnost postoji, tada za odstupanje lokalne gustoće od srednje gustoće 1/2, $\Delta\rho(n, L) \equiv |\langle\tau_n\rangle - 1/2|$, vrijedi svojstvo homogenosti,

$$\Delta\rho(n, L) = L^{-\mu} f(n/L), \tag{3.86}$$

gdje je $f(x) \propto x^{-\mu}$ za $0 \ll x \ll 1/2$, a μ odgovarajući kritični eksponent. Iz gornje relacije slijedi da za dvije različite veličine sustava, L_1 i L_2, vrijedi

$$\Delta\rho(n, L_1) = \left(\frac{L_2}{L_1}\right)^{\mu} \Delta\rho(n, L_1). \tag{3.87}$$

Slike 3.11a i 3.11b prikazuju redom $\Delta\rho(n, L)$ i $L^{\mu}\Delta\rho(n, L)$ za tri različite veličine sustava, $L = 800$, 1500 i 5000, te $\sigma = 1.5$, pri čemu se najbolje preklapanje krivulja dobiva za $\mu = 0.25$. Ista analiza je provedena na slici 3.12 za različite vrijednosti $\sigma = 1.2$, 1.5 i 1.8, na osnovu koje zaključujemo ovisnost $\mu(\sigma) = (\sigma - 1)/2$ za $1 < \sigma < 2$. Zajedno s $\mu = 1/2$, dobivenim u kratkodosežnoj granici $\sigma > 2$ u kojoj normalni difuzijski član zamjenjuje frakcionalni, na osnovu Monte Carlo simulacija zaključujemo da je $\mu(\sigma)$ oblika

$$\mu(\sigma) = \min\left\{\frac{\sigma - 1}{2}, \frac{1}{2}\right\}, \quad \sigma > 1. \tag{3.88}$$

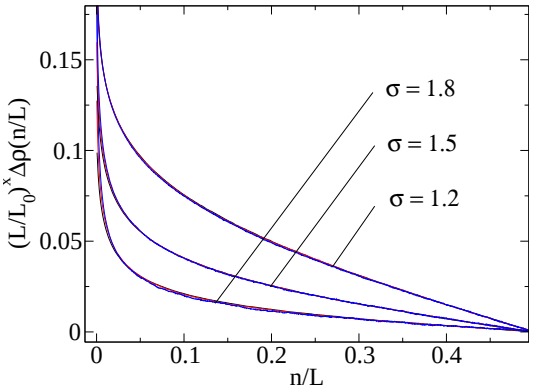

Slika 3.12: Prostorne ovisnosti odstupanja lokalne gustoće od srednje gustoće 1/2 za $\alpha = \beta = 0.8$ i različite vrijednosti parametra σ. Pritom su za isti σ, a različiti $L = 800$, 1500 i 5000, svi profili $\Delta\rho(n, L)$ skalirani na onaj s $L_0 = 5000$ prema izrazu (3.87).

U ostatku ovog poglavlja izvodimo pretpostavljeni izraz (3.88) za $\mu(\sigma)$. Pritom nas, nažalost, dugodosežnost u preskocima lišava brojnih analitičkih pristupa u rješavanju modela, a koji su uspješno primijenjeni na kratkodosežni model. U takvoj situaciji, kao gotovo jedini mogući pristup nudi se aproksimacija srednjeg polja, kojom se zanemaruju korelacije među čvorovima. Osim što se takav pristup logički nameće, motiviran je rezultatom Kruga [13], koji polazi od stacionarne viskozne Burgersove jednadžbe za rubne uvjete $\rho(0) = \rho_0$ i $\rho(L) = 0$, $L \to \infty$

$$D\frac{d\rho}{dx} = \rho(1-\rho) - j, \tag{3.89}$$

gdje je struja j javlja kao nepoznata konstanta. Za $\rho_0 > \rho^*$, gdje je $\rho^* = 1/2$ gustoća za koju $j(\rho)$ postiže maksimum, Krug je pokazao da se lokalna gustoća asimptotski približava konstantnoj gustoći ρ^* u unutrašnjosti sustava prema zakonu potencija,

$$\rho(x) \simeq \frac{1}{2} + \frac{D}{x}, \quad x \gtrsim D/(\rho_0 - \rho^*), \quad \rho_0 > \rho^*. \tag{3.90}$$

Iako je to, naravno, isti potencijski zakon (2.48) koji je dobiven eksplicitnim rješavanjem diskretnog modela u aproksimaciji srednjeg polja, gornji pristup dobiva na značaju onda kada egzaktno rješenje diskretnog problema nije poznato. U slučaju dugodosežnih preskoka, to nas vodi na glavnu ideju da za računanje eksponenta $\mu(\sigma)$ iskoristimo hidrodinamičke jednadžbe (3.44) i (3.45), ali prilagođene na rubne uvjete (3.7) i (3.8).

Polazimo, dakle, od jednadžbi za lokalnu gustoću ρ_n, $n = 1, \ldots, L$ u aproksimaciji srednjeg polja,

$$\frac{d}{dt}\rho_n = \alpha_n(1-\rho_n) + \sum_{m=1}^{n-1} p_{n-m}\rho_m(1-\rho_n) - \sum_{m=n+1}^{L} p_{m-n}\rho_n(1-\rho_m) - \beta_n\rho_n, \tag{3.91}$$

$$\frac{d}{dt}\rho_1 = \alpha_1(1-\rho_1) - \sum_{m=2}^{L} p_{m-1}\rho_1(1-\rho_m) - \beta_1\rho_1, \tag{3.92}$$

$$\frac{d}{dt}\rho_L = \alpha_L(1-\rho_L) + \sum_{m=1}^{L-1} p_{L-m}\rho_m(1-\rho_L) - \beta_L\rho_L, \tag{3.93}$$

Zatim prepoznajemo da se gornje jednadžbe mogu zapisati u sličnoj formi kao i u beskonačnom sustavu,

$$\frac{d}{dt}\rho_n(t) = \sum_{r=1}^{L} p_r(\Delta_r^+\rho_n - \Delta_r^-\rho_n) - \sum_{r=1}^{L} p_r\left[(1-\rho_n)\Delta_r^+\rho_n + \rho_n\Delta_r^-\rho_n\right], \tag{3.94}$$

pod uvjetom da pretpostavimo nelokalne "rubne" uvjete,

$$\rho_n = \begin{cases} \alpha, & -L < n \leq 0 \\ 1-\beta, & L < n \leq 2L, \end{cases} \tag{3.95}$$

Time smo sveli vezanje lokalne gustoće ρ_n i vanjskog polja α_n i β_n na rubni uvjet (3.95), čime smo otvorili put primjeni hidrodinamičkih jednadžbi na problem s otvorenim rubnim uvjetima. Obzirom da nas zanima samo eksponent potencijske ovisnosti, a ne puno rješenje u konačnom sustavu, možemo promatrati ekvivalentni beskonačni sustav za koji pretpostavljamo rješenje oblika,

$$\rho(x) = \begin{cases} \rho_0, & -\infty < x < 0 \\ \frac{1}{2} + \phi(x), & 0 < x < \infty \\ 1/2, & x \to \infty. \end{cases} \tag{3.96}$$

koje smo skicirali na slici 3.13. Za funkciju $\phi(x)$ pretpostavljamo asimptotski oblik $\phi(x) \propto (x/a)^{-\bar{\mu}} = n^{-\bar{\mu}}$, te uvrštavamo (3.96) u hidrodinamičke jednadžbe (3.44) i (3.45). Ideja je potom ocijeniti doprinose svakog pojedinog člana hidrodinamičke jednadžbe obzirom na to kojeg su reda u a. Za $1 < \sigma < 2$, to daje

$$-\kappa\phi(x)\frac{\partial\phi(x)}{\partial x} \simeq -\bar{\mu}|\kappa|a^{2\bar{\mu}}x^{-2\bar{\mu}-1}, \tag{3.97}$$

$$a^{\sigma-1}\nu_\sigma\Delta_\sigma\phi(x) \simeq \frac{\phi(0)}{\sigma\zeta(\sigma+1)}a^{\sigma-1}x^{-\sigma} + O(a^{\sigma-1+\bar{\mu}}x^{-\sigma-\bar{\mu}}), \tag{3.98}$$

gdje je $\phi(0) = \rho_0 - 1/2$. Primijetimo da član najnižeg reda u a u jednadžbi (3.98) dolazi upravo od konstantne gustoće za $x < 0$, tj. od vanjskog polja

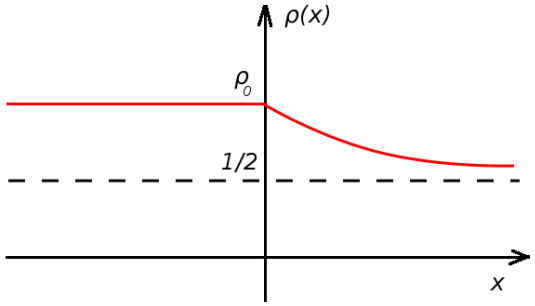

Slika 3.13: Skica rješenja $\rho(x)$ za $x > 0$ i rubnog uvjeta (3.96) za $x < 0$ koji je ekvivalentan vezanju lokalne gustoće $\rho(x)$ na vanjsko polje $\alpha(x)$.

α_i. [Napomenimo također da se za nelinearni član $a^{\sigma-1}\phi H\phi$, kojeg smo izostavili još ranije, može pokazati da smo ga opravdano izostavili jer je višeg reda, $O(a^{\sigma-1+\bar{\mu}}x^{-\sigma-\bar{\mu}})$.] Obzirom da u stacionarnoj granici lijeva strana jednadžbe (3.44) iščezava, $\partial\phi/\partial t = 0$, dva najniža doprinosa moraju biti istog reda (i suprotnog predznaka!), što daje,

$$2\bar{\mu} = \sigma - 1 \quad \Rightarrow \quad \bar{\mu} = \frac{\sigma-1}{2}, \quad 1 < \sigma < 2. \tag{3.99}$$

Na sličan način provodimo analizu za $\sigma > 2$, uz razliku da sada u hidrodinamičkoj jednadžbi moramo uključiti oba difuzijska doprinosa, $a\Delta\phi(x)$ i $a^{\sigma-1}\Delta_\sigma\phi$. U odnosu na članove (3.97) i (3.98), koji su ostali nepromijenjeni, treba još ocijeniti $a\Delta\phi(x)$,

$$a\nu_2\Delta\phi(x) \sim |\nu_2|\bar{\mu}(1+\bar{\mu})a^{1+\bar{\mu}}x^{-\bar{\mu}-2}. \tag{3.100}$$

Uspoređivanjem najnižih doprinosa dolazimo do jednadžbe $2\bar{\mu} = \min\{\sigma-1, 1+\bar{\mu}\}$, tj. eksponenta $\bar{\mu}$

$$\bar{\mu} = \begin{cases} \frac{\sigma-1}{2}, & 2 < \sigma < 3, \\ 1, & \sigma > 3 \end{cases} \tag{3.101}$$

Naposljetku, izraze (3.99) i (3.101) za $\bar{\mu}$ možemo objediniti u

$$\bar{\mu}(\sigma) = \min\left\{\frac{\sigma-1}{2}, 1\right\}. \tag{3.102}$$

Za $1 < \sigma < 2$, eksponent $\bar{\mu}$ identičan je eksponentu μ kojeg smo zaključili iz rezultata Monte Carlo simulacija. Razlika se, međutim, javlja u graničnom σ za koji nastupa kratkodosežna granica u kojoj je $\bar{\mu} = 1$: u (3.102) granični σ je 3 umjesto 2. Na osnovu toga zaključujemo da je u modelu s dugodosežnim preskocima, aproksimacija srednjeg polja primjenjiva za $1 < \sigma < 2$, dok je za $\sigma > 2$ doprinos koji potječe od nelokalni rubnih uvjeta precijenjen u odnosu na doprinos (zanemarenih) korelacija.

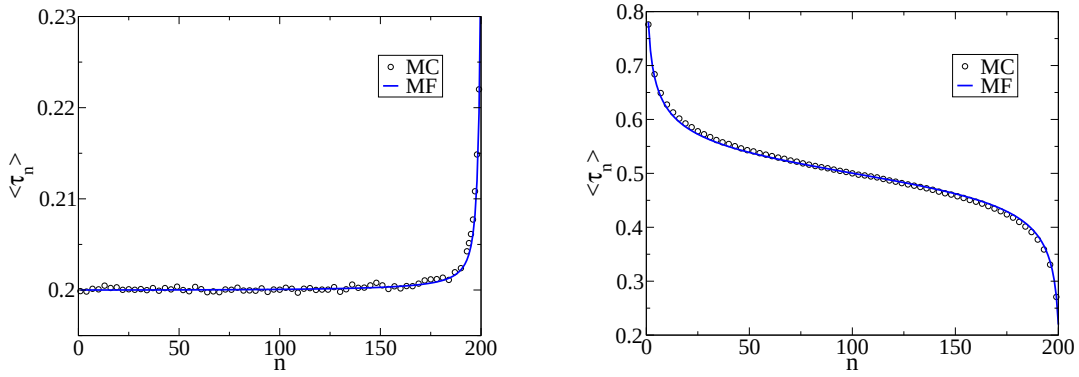

Slika 3.14: Usporedba profila gustoće u modelu s dugodosežnim preskocima (a) u fazi niske gustoće ($\alpha = 0.2$ i $\beta = 0.7$) i (b) u fazi maksimalne struje ($\alpha = 1.0$ i $\beta = 1.0$), dobivenih Monte Carlo simulacijama (simboli) i u aproksimaciji srednjeg polja (linija) za $\sigma = 1.8$.

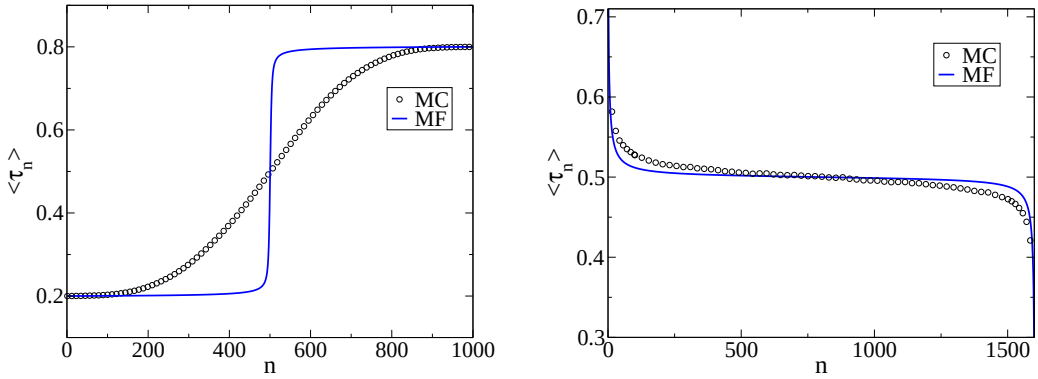

Slika 3.15: Usporedba profila gustoće u modelu s dugodosežnim preskocima (a) na granici faza niske i visoke gustoće ($\alpha = \beta = 0.2$, $\sigma = 1.8$) i (b) u fazi maksimalne struje ($\alpha = 1.0$ i $\beta = 1.0$, $\sigma = 2.5$), dobivenih Monte Carlo simulacijama (simboli) i u aproksimaciji srednjeg polja (linija).

3.4.3.1 Numeričko rješenje jednadžbi srednjeg polja

Iznesene zaključke možemo direktno provjeriti numeričkim rješavanjem jednadžbi (3.91) - (3.93) u stacionarnoj granici. Problem se tada svodi na traženje nultočke nelinearnog sustava L jednadžbi s L nepoznanica. Od mnogih programskih paketa predviđenih za taj problem, mi smo se odlučili za algoritam HYBRD dostupan unutar biblioteke MINPACK[2]. Na slikama (3.14a) i (3.14b) prikazana su numerička rješenja dobivena za $\sigma = 1.8$, te α i β koji odgovaraju fazi niske gustoće i fazi maksimalne struje (fazu visoke gustoće s fazom niske gustoće veže simetrija (2.45)). U oba slučaja slaganje je izvrsno. Razlika u rješenjima javlja se tek na granici koegzistencije faza $\alpha = \beta < 1/2$ (slika 3.15a), te u kratkodosežnoj granici za $\sigma > 2$ (slika 3.15b). U prvom slučaju profil gustoće ima oblik domenskog zida,

[2]http://www.netlib.org/minpack/

ali znatno više rastegnutog. Slaganje s rezultatima Monte Carlo simulacija postiže se tek kada se u obzir uzme dinamika domenskog zida, čemu smo posvetili cijelo prošlo poglavlje. U drugom slučaju pomoći nema - u kratkodosežnoj granici aproksimacija srednjeg polja zanemaruje ključni doprinos od korelacija i ne može točno opisati fazu maksimalne struje.

* * *

Dugodosežni model, zamišljen da ispita robustnost i univerzalnost faznih prijelaza u ASEP-u, u mnogome je ispunio naša početna očekivanja. Prije svega, pokazali smo da je fazni dijagram ostao nepromijenjen, osim na prijelazima prvog i drugog reda. Valjanost aproksimacije srednjeg polja, neiznenađujuća za dugodosežno međudjelovanje, omogućila nam je da karakter faznih prijelaza objasnimo iz odgovarajuće hidrodinamičke jednadžbe, iz koje je odmah uslijedilo nekoliko rezultata relevantnih za ASEP: (a) nelokalni karakter difuzije koji, među ostalim, stabilizira domenski zid, (b) dinamički eksponent $z = \min\{\sigma, 3/2\}$, koji opisuje relaksaciju k stacionarnom stanju u fazi maksimalne struje, te (c) postojanje kratkodosežne granice za $\sigma > 2$.

Primjenom jednadžbe na sustav s otvorenim rubnim uvjetima, dobiva se točan, σ-ovisni eksponent u dugodosežnom režimu $1 < \sigma < 2$ u fazi maksimalne struje, kao i domenski zid na liniji prijelaza prvog reda. U odnosu na profil gustoće dobiven Monte Carlo simulacijama, taj je zid preoštar, a točan profil se dobiva tek kada se u obzir uzme i dinamika domenskog zida, koja se opisuje nasumičnim hodom u potencijalu s globalnim minimumom, koji u termodinamičkoj granici zarobljava domenski zid i vodi na separaciju faza.

4

Separacija faza inducirana jednim defektom

U prethodna dva poglavlja, netrivijalno stacionarno stanje postigli smo dovođenjem sustava u kontakt sa spremnicima različitih gustoća. U ovom poglavlju ćemo opisati drugačiji problem, u kojem se netrivijalno stacionarno stanje postiže dodavanjem jednog lokaliziranog defekta (nečistoće) s kojeg se čestice pomiču s reduciranom vjerojatnošću $r < 1$. Posebnost modela leži i u tome što se uz njega i danas veže otvoreno pitanje da li će defekt pritom nužno izazvati separaciju faza bez obzira na iznos parametra r. Osim što egzaktno rješenje izmiče gotovo 20 godina, jedan od problema je i što aproksimacija srednjeg polja daje trivijalni rezultat $r_c = 1$, tj. homogenu granicu bez defekta. Imajući to na umu, u poglavlju 4.2 ćemo uvesti nečistoću u TASEP s dugodosežnim preskocima, te ćemo pokazati da je variranjem parametra dosega σ moguće postići prijelaz u režim bez separacije faza, pri čemu je točnu točku prijelaza moguće odrediti pomoću aproksimacije srednjeg polja [131].

4.1 Kratkodosežni model

Promatramo TASEP na rešetci od L čvorova i $N = \rho \cdot L$ čestica s periodičkim rubnim uvjetima, $\tau_{L+1} = \tau_1$, čija je propagacija na rešetci opisana nasumično-sekvencijalnom dinamikom s vjerojatnostima preskoka 1. Izuzetak čini jedan fiksni čvor, npr. $i = L$, s kojeg se čestica pomiče s vjerojatnošću r manjom od 1, $0 < r < 1$ (slika 4.1).

TASEP sa statičkim defektom i nasumično-sekvencijalnom dinamikom prvi su promatrali Janowsky i Lebowitz [59, 132]. Oni su u stacionarnom stanju opazili domenski zid koji odvaja makroskopske faze gustoća ρ_- i ρ_+ (slika 4.2). Gustoće ρ_- i ρ_+ odredili su u aproksimaciji srednjeg polja zanemarujući pritom bilo kakvu prostornu ovisnost gustoće $\langle \tau_i \rangle$,

$$\langle \tau_i \rangle \approx \begin{cases} \rho_- & 1 \leq i < i_s \\ \rho_+ & i_s \leq i \leq L \end{cases} . \tag{4.1}$$

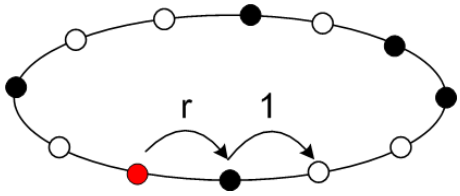

Slika 4.1: Slikoviti prikaz TASEP-a sa statičkom defektom s kojeg se čestica pomiče s reduciranom vjerojatnošću $0 < r < 1$. Vjerojatnost preskoka s ostalih čvorova je 1.

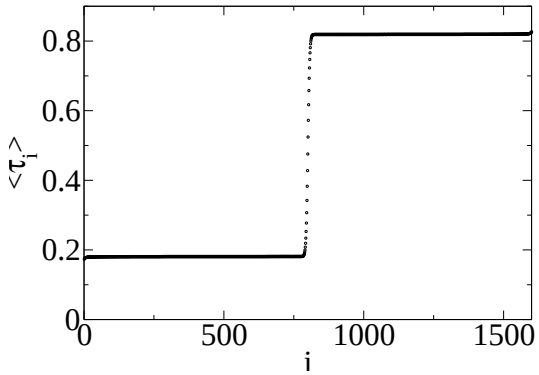

Slika 4.2: Profil gustoće u TASEP-u s jednim defektom na mjestu $i = L$ za $\rho = 1/2$ i $r = 0.2$ dobiven Monte Carlo simulacijom u sustavu veličine $L = 1600$.

gdje je i_s položaj domenskog zida. Obzirom da je gustoća daleko od defekta i domenskog zida homogena, a struja j svugdje očuvana, vrijedi

$$j = \rho_-(1-\rho_-) = \rho_+(1-\rho_+), \tag{4.2}$$

odakle slijedi $\rho_- = \rho_+$ ili $\rho_- = 1-\rho_+$. Zanemarujući korelacije blizu defekta, očuvanje struje dalje vodi na

$$j = r\rho_-(1-\rho_+), \tag{4.3}$$

odakle se dobiva

$$\rho_- = \frac{r}{1+r}, \quad \rho_+ = \frac{1}{1+r}. \tag{4.4}$$

Iskoristimo li još očuvanje ukupnog broja čestica, tada možemo odrediti položaj domenskog zida iz

$$\rho_- i_s + \rho_+(L-i_s) = \rho, \tag{4.5}$$

što daje

$$i_s = \frac{1-\rho(1+r)}{1-r}L. \tag{4.6}$$

Kako bi odredili stacionarne fluktuacije položaja domenskog zida, tj. njegovu širinu, Janowsky i Lebowitz koriste koncept čestice *druge klase*, koja se u međudjelovanju s drugim (običnim) česticama ponaša kao šupljina, a u međudjelovanju s šupljinama kao obična čestica. Tim je pravilom njezino kretanje usmjereno prema domenskom zidu, te se pokazuje da pritom neznatno odstupa od njegovog trenutačnog položaja, što daje jednostavni način da se u sustavu prati njegovo kretanje. Koristeći Monte Carlo simulacije, Janowsky i Lebowitz su pokazali da standardna devijacija ξ_L položaja čestice druge klase ovisi o veličini sustava L kao $\xi_L \propto L^{1/2}$ ako je $\rho \neq 1/2$ i $\xi_L \propto L^{1/3}$ ako je $\rho = 1/2$. Razlika u ponašanju za $\rho \neq 1/2$ i $\rho = 1/2$ može se protumačiti na slijedeći način [59]. Skok čestice s defektnog mjesta $i = L$ čine dva zavisna događaja - skok čestice udesno i skok šupljine ulijevo. Čestica se zatim kreće prema domenskom zidu prosječnom brzinom $1-\rho_-$, dok se šupljina kreće brzinom $-\rho_+ = -(1-\rho_-)$. Ukoliko je $\rho \neq 1/2$, položaj domenskog zida nije u sredini, pa su dolasci čestice i šupljine do domenskog zida nezavisni događaji. Fluktuacije položaja domenskog zida u tom su slučaju određene statistikom preskoka čestice preko defekta, tj. statistikom stvaranja para čestica/šupljina. S druge strane, za $\rho = 1/2$ domenski zid je u sredini, pa su dolasci čestica i šupljina u prosjeku istovremeni. Za razliku od prethodnog slučaja, fluktuacije položaja domenskog zida sada određuju lokalna odstupanja u brzini čestica i šupljina od srednjih brzina $1-\rho_-$ i $-\rho_+$.

4.1.1 Otvorena pitanja

Uz ovaj model veže se otvoreno pitanje da li postoji r_c takav da za $r_c < r < 1$ defekt ne dovodi do separacije faza ($\rho_- \neq \rho_+$), već da je lokalna gustoća svugdje $\langle\tau_i\rangle \approx \rho_- = \rho_+ = 1/2$. Povijest ovog problema je duga i seže u daleku 1990. godinu u kojoj su Wolf i Tang predložili tzv. RSOS model rasta površina u prisustvu linijskog defekta [101], koji se može preslikati na TASEP transformacijom $h_i - h_{i-1} = 1 - 2\tau_i$, gdje je h_i visina površine na mjestu i (vidi poglavlje 2.2.1). U tom modelu defekt odgovara linijskom defektu na pravcu $x = x_0$ duž kojeg površina raste sporije. Zapišemo li visinu površine na mjestu x i u trenutku t s $h(x,t)$, tada je odstupanje $h(x,t)$ od srednjeg nagiba površine $[h(0,t) - h(L,t)]/L$ jednako

$$\Delta\bar{h}(x) = \frac{1}{T}\int_0^T \left[h(x,t) - h(0,t) - x\frac{h(L,t)-h(0,t)}{L}\right] dt, \tag{4.7}$$

gdje se vremensko usrednjavanje radi po velikom vremenu $T \to \infty$. Uvođenjem defekta na mjestu x_0 dolazi do deformacija površine u smislu da je

$$d = \frac{1}{L}\sum_{x=0}^{L} \Delta\bar{h}(x) - \Delta\bar{h}(x_0) \neq 0 \tag{4.8}$$

što je slikovito prikazano na slici 4.3. Pritom kažemo da se površina deformira *slabo* ako $d \sim L^{\gamma}$ uz $\gamma < 1$, jer je tada $lim_{L\to\infty} d/L = 0$, dok jaku deformaciju nalazimo za $\gamma = 1$ za koji je $lim_{L\to\infty} d/L > 0$. U svom radu Wolf i Tang su računalnim simulacijama RSOS modela i analitičkim rješavanjem KPZ jednadžbe zaključili da je $\gamma = 1$, tj. da se površina uvijek jako deformira. U sličnom modelu rasta, ali koji se ne može izravno preslikati na TASEP, Kandel i Mukamel su dobili oba režima, ovisno o jačini defekta [133].

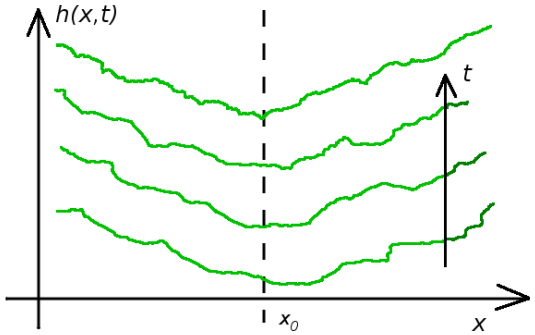

Slika 4.3: Skica rasta površine u tzv. RSOS modelu u prisustvu linijskog defekta na liniji $x = x_0$ duž kojeg je brzina rasta manja.

Preslikamo li problem deformacije površine natrag na TASEP, parametar reda d može se zapisati kao

$$d = \frac{2}{L}\sum_{i=1}^{L} i\left(\langle\tau_i\rangle - \frac{1}{2}\right) - \frac{L(L+1)\Delta}{2L^2}, \tag{4.9}$$

gdje je Δ srednji nagib površine, koji u TASEP-u odgovara $L - 2N$ i konstantan je u vremenu zbog periodičkih rubnih uvjeta. Odavde se lako uvjeriti da se npr. uvrštavanjem aproksimativnog rješenja (4.1) u izraz za d dobiva jaka deformacija, $d \propto L$. S druge strane, neka novija istraživanja ukazuju na mogućnost slabe deformacije.

Putem KPZ jednadžbe, TASEP se može povezati i s modelom usmjerenog polimera u neuređenom mediju. U ravnini, polimer možemo opisati usmjerenom putanjom od $(0, 0,)$ do (x, t) bez presijecanja. Model tada opisuje transverzalne fluktuacije polimera opisanog Hamiltonijanom

$$\mathcal{H}[x(t)] = \int dt' \left[\frac{\gamma}{2}\left(\frac{dx}{dt'}\right) + \eta(x', t') + V(x)\right] \tag{4.10}$$

gdje je γ napetost, $\eta(x,t)$ bijeli šum koji opisuje utjecaj medija, $\langle \eta(x,t)\eta(x',t')\rangle = 2D\delta(x-x')\delta(t-t')$, a $V(x) = -\epsilon\delta(x)$ privlačni potencijal lokaliziran na liniji $x = 0$ (slika 4.4). Označimo li sa $Z(x,t)$ particijsku funkciju,

$$Z(x,t) = \int_{(0,0)}^{(x,t)} \mathcal{D}x'(t')exp\{-\mathcal{H}/k_BT\}, \tag{4.11}$$

veza s rastom površina dobiva se preko slobodne energije $\mathcal{F}(x,t) = -k_BTZ(x,t)$ [135], koja u odsutnosti defekta $V(x) = 0$ zadovoljava KPZ jednadžbu,

$$\frac{\partial \mathcal{F}}{\partial t} = \nu\frac{\partial^2 \mathcal{F}}{\partial x^2} + \frac{\lambda}{2}\left(\frac{\partial \mathcal{F}}{\partial x}\right)^2 + \eta, \tag{4.12}$$

gdje je $\nu = k_BT/2\gamma$, a $\lambda = -1/\gamma$. Bez defekta, transverzalno odstupanje kraja polimera $\delta x = \langle [x(t)]^2\rangle^{1/2}$ se ponaša kao $\delta x \propto t^{1/z}$, gdje je $z = 3/2$ dinamički eksponent KPZ jednadžbe. S druge strane, uvedemo li linijski defekt putem potencijala $V(x) = -\epsilon\delta(x)$, tada se variranjem njegove jačine ϵ može postići saturacija $\delta x = \text{const.}$, tj. lokalizacija polimera koja u TASEP-u odgovara koegzistenciji faza. Netrivijalnim pitanjem pritom ostaje prag ϵ_c, takav da se lokalizacija gubi za $\epsilon < \epsilon_c$. Zbog nedostatka egzaktnog rješenja tim su se problemom bavili mnogi autori, često s oprečnim zaključcima ([136–141]).

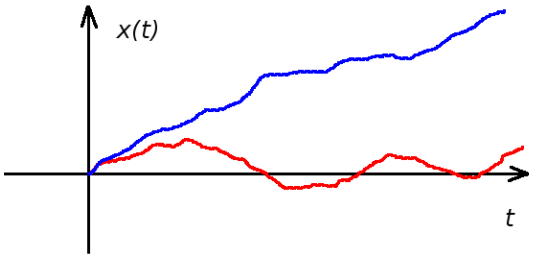

Slika 4.4: Skica delokaliziranog (plava linija) i lokaliziranog polimera (crvena linija) u prisustvu linijskog defekta na liniji $x = 0$.

U TASEP-u se problemom nestanka separacije faza bavilo nekoliko autora. Schütz je promatrao verziju TASEP-a u kojem se vremenska evolucija odvija u diskretnim vremenskim koracima koji su podijeljeni u dva podkoraka [142]. U prvom podkoraku se za jedno mjesto udesno propagiraju čestice na čvorovima $1, 3, \ldots$. Zatim se u drugom koraku ponovi isto, ali s česticama na čvorovima $2, 4, \ldots$. Izuzetak čini čestica na čvoru L, koja se u drugom podkoraku (L je paran!) propagira stohastički, tj. s vjerojatnošću $r < 1$. Ovako zadani model može se riješiti egzaktno [142] i daje $r_c = 1$. Pritom treba imati na umu da je vremenska evolucija gotovo deterministička, a korelacije među česticama veće nego u modelu s nasumično-sekvencijalnu dinamikom.

Pitanje praga r_c razmatrali su i Janowsky i Lebowitz u svojem kasnijem radu [132], u kojem su egzaktno riješili master jednadžbu za male sustave od tek nekoliko čvorova i otvorene rubne uvjete, te izračunali struju $j(r, \alpha = \beta = 1)$ za $\rho = 1/2$. Ukoliko prag postoji, na r_c trebala bi se opaziti promjena struje ovisne o r u struju $j = 1/4$, tj. neovisnu o r. Razvojem struje za mali r, Janowsky i Lebowitz su pokazali da se niži članovi reda ne mijenjaju povećanjem veličine sustava L, čime su zapravo dobili razvoj po r egzaktne struje $j_\infty(r, 1)$ u termodinamičkoj granici $L \to \infty$,

$$j_\infty(r, 1) = r - \frac{3}{2}r^2 + \frac{19}{16}r^3 - \frac{21535}{27648}r^4 + \dots . \tag{4.13}$$

Zatim su ekstrapolacijom te ovisnosti na veće vrijednosti r pokazali da nema promjene režima barem za $r \lesssim 0.8$.

Problem su ponovno "oživjeli" Ha et al. 2003. godine [143], koji su promatrali problem defekta na čvoru $L/2$ u TASEP-u s otvorenim rubnim uvjetima za $\alpha = 1-\beta$. Promatrajući kako se prikladno izabrani parametar reda $\rho_+(r, L) - \rho_-(r, L)$ skalira s L, Ha et al. su najbolje slaganje s potencijskim zakonom blizu prijelaza dobili za $r_c = 0.80(2)$, iznenađujuće blizu ocjene Janowskog i Lebowitza. Drugi zanimljiv rezultat Ha et al. tiče se profila gustoće. U fazi s domenskim zidom Ha et al. opažaju potencijsko opadanje gustoće s udaljenošću n od defekta

$$\langle \tau_n \rangle - \rho_- \sim -n^{-\nu}, \qquad \langle \tau_{L-n} \rangle - \rho_+ \sim n^{-\nu}, \quad 1 \ll n \ll L, \tag{4.14}$$

gdje je eksponent $\nu = 1/2$.[1] Slično potencijski zakon uz $\rho_- = \rho_+ = 1/2$ opaža se i u fazi bez domenskog zida, ali uz odgovarajući eksponent $\nu = 1/3$. U kontekstu rasta površina, takav oblik profila vodi na slabu deformaciju, u što se možemo uvjeriti uvrstimo li $\langle \tau_i \rangle - 1/2 = L^{-1/3} f(i/L)$ u izraz (4.8) za dubinu deformacije površine d,

$$d(\Delta = 0) = \frac{2}{L} \sum_{i=1}^{L} i \left(\langle \tau_i \rangle - \frac{1}{2} \right) \approx \frac{2}{L} L^2 \int_0^1 dx \cdot x \cdot f(x) L^{-1/3} \propto L^{2/3}, \tag{4.15}$$

odakle vidimo da je eksponent γ u $d \propto L^\gamma$ manji od 1.

U nastavku poglavlja 4 dajemo vlastiti doprinos problemu defekta u TASEP-u poopćenjem modela na dugodosežne preskoke. Pokazati ćemo da smo time zadržali glavne značajke kratkodosežnog modela, ali i da smo otvorili put primjeni aproksimacije srednjeg polja koja će nam omogućiti da analitički odredimo netrivijalnu točku prijelaza na kojoj nestaje separacija faza.

[1] Slično potencijsko ponašanje našli su Janowsky i Lebowitz u svojem prvom radu o TASEP-u s defektom [59], ali s eksponentom $\nu = 1$.

4.2 Izostanak separacije faza u modelu s dugodosežnim preskocima

Promatramo TASEP na jednodimenzionalnoj rešetci s $L+1$ čvorova i $N = \rho L$ čestica, te periodičkim rubnim uvjetima. Čvoru $L+1$ je pritom pridružen statički defekt tako da to mjesto ne može primiti niti jednu česticu i u modelu predstavlja nečistoću (slika 4.5). Čestice se propagiraju dugodosežnim preskocima i nasumično-sekvencijalnom dinamikom, pri čemu se duljina preskoka $1 \leq l \leq L$ bira iz raspodjele $p_l = l^{-(1+\sigma)}/\zeta_L(\sigma+1)$, gdje je $\zeta_L(\sigma+1)$ parcijalna suma zeta funkcije. Skok se prihvaća ako je čvor $i+l$ prazan, a u protivnom čestica ostaje na mjestu. Nečistoća na čvoru $L+1$ predstavlja prepreku utoliko što je čestice moraju preskočiti, što je moguće dokle god je $\sigma < \infty$. Prednost modela je što se za jačinu utjecaja nečistoće ne uvodi nikakav novi parametar, već se to postiže variranjem parametra σ. Stoga je svaka promjena režima u modelu, ako postoji, rezultat promjene parametra σ.

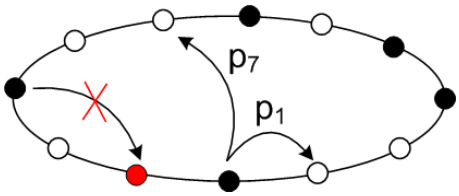

Slika 4.5: Slikoviti prikaz TASEP-a s dugodosežnim preskocima i statičkom nečistoćom na koju su skokovi čestica zabranjeni.

4.2.1 Rezultati Monte Carlo simulacija

Tipični rezultati Monte Carlo simulacija za $\rho = 1/2$ prikazani su na slici 4.6. Kao i kratkodosežnom modelu, uočavamo dva režima odvojena pragom σ_c: za $\sigma > \sigma_c$ nečistoća u sustavu inducira domenski zid koji razdvaja makroskopske domene gustoće ρ_+ lijevo i $\rho_- = 1 - \rho_+$ desno od nečistoće. S druge strane, za $1 < \sigma < \sigma_c$ profil gustoće se organizira tako da domenskog zida nema, pri čemu se postiže struja jednaka maksimalnoj struji u čistom dugodosežnom modelu, $\lambda_L(\sigma)/4$. Sličnost s kratkodosežnim modelom očituje se i u rastegnutosti profila gustoće, koji je rezultat fluktuacija trenutačnog položaja domenskog zida. Na slici 4.7 prikazana je ovisnost karakteristične duljine te rastegnutosti ξ_L o veličini sustava L, dobivena prilagodbom razlike $\langle \tau_{n+1} \rangle - \langle \tau_n \rangle$ na Gaussovu raspodjelu za dvije različite gustoće, $\rho = 0.5$ i $\rho = 0.55$. U oba slučaja rezultati su u suglasnosti s ranije spomenutim predviđanjem da je ξ_L proporcionalno s $L^{1/2}$ za $\rho \neq 1/2$ i $L^{1/3}$ za $\rho = 1/2$.

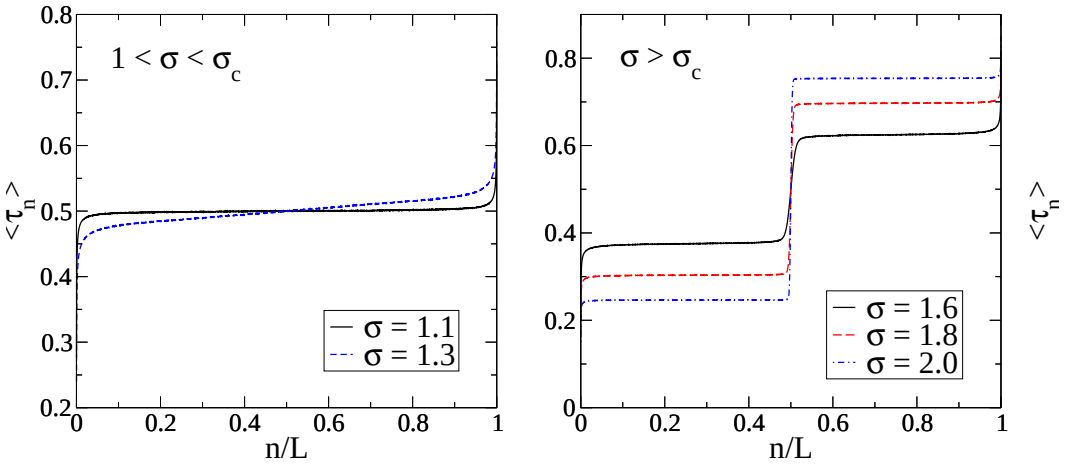

Slika 4.6: Profili gustoća u fazi bez domenskog zida za $\sigma = 1.1$ i 1.3 (lijevo) i u fazi s domenskim zidom za $\sigma = 1.6, 1.8$ i 2 (desno), dobiveni Monte Carlo simulacijama za sustav veličine $L = 6400$ i gustoće $\rho = 1/2$ usrednjavanjem po $t = 10^8$ MC koraka/čvoru.

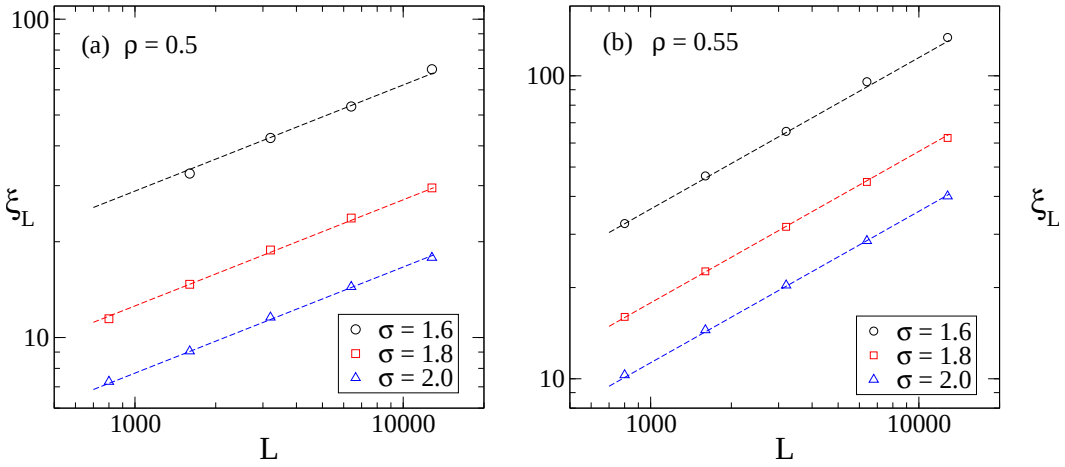

Slika 4.7: Karakteristična duljina rastegnutosti profila gustoće ξ_L u ovisnosti o veličini sustava za različite vrijednosti parametra σ i gustoće (a) $\rho = 1/2$ i (b) $\rho \neq 1/2$. Isprekidane linije predstavljaju orijentaciju za oko i imaju nagibe (a) 1/3 i (b) 1/2.

Imajući na umu rezultate Ha et al., zanimljivo je provjeriti odstupanje profila gustoće od srednjih gustoća ρ_- i ρ_+ u fazi s domenskim zidom, odnosno $\rho_- = \rho_+ = 1/2$ u fazi bez zida. Kako nam gustoće ρ_- i ρ_+ nisu poznate, promatramo odstupanje od gustoće $\langle\tau_{L/4}\rangle$ i $\langle\tau_{3L/4}\rangle$, obzirom da su čvorovi $L/4$ i $3L/4$ najviše udaljeni od domenskog zida i nečistoće. U domeni gustoće $\rho_- = \langle\tau_{L/4}\rangle$ pretpostavljamo profil gustoće oblika

$$\Delta\rho_-(n, L) \equiv \langle\tau_n\rangle - \langle\tau_{L/4}\rangle = L^{-\nu} f_-(n/L), \quad 1 \ll n \ll L/2, \tag{4.16}$$

gdje je $f_-(x) \sim x^{-\nu}$ za $x \gg 1$. Sličan oblik pretpostavljamo i u domeni gustoće $\rho_+ = \langle \tau_{3L/4} \rangle$ koristeći simetriju na zamjenu čestica i šupljina, $\langle \tau_i \rangle = 1 - \langle \tau_{L-i+1} \rangle$, koja vrijedi za $\rho = 1/2$. Skaliranje prema obliku (4.16) provedeno je na slici 4.8 za nekoliko vrijednosti parametra σ i L. Najbolje međusobno preklapanje krivulja dobiva se ukoliko se pretpostavi $\nu = \sigma - 1$ za $\sigma < 2$ i $\nu = 1$ za $\sigma \geq 2$. Drugim riječima, u fazi s domenskim zidom eksponent potencijskog zakona postaje ovisan o parametru σ, dok se u kratkodosežnoj granici za $\sigma > 2$ dobiva eksponent $\nu = 1$ jednak eksponentu kojeg su opazili Janowsky i Lebowitz u [59]. Potencijski oblik profila gustoće provjerili smo i u fazi bez domenskog zida gdje je $\rho_- = \rho_+ = 1/2$, ali iako opažamo dugodosežne korelacije, profil gustoće ne pokazuje jednostavno skaliranje s jednim eksponentom.

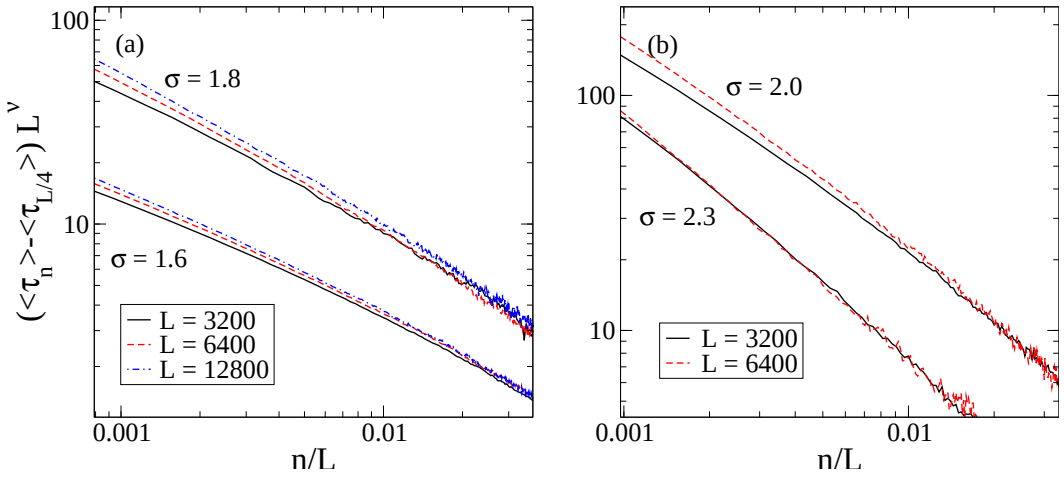

Slika 4.8: Odstupanje profila gustoće od $\rho_- = \langle \tau_{L/4} \rangle$ u domeni $1 \leq n \leq L/2$ za (a) $\sigma = 1.6$ i 1.8 i (b) $\sigma = 2$ i 2.3, za različite veličine sustava $L = 3200$, 6400 i 12800. Profili su pritom skalirani prema izrazu (4.16) uz (a) $\nu = \sigma - 1$ i (b) $\nu = 2$. Ostali parametri modela su $\rho = 1/2$ i $t = 10^8$ MC koraka/čvoru.

Naposljetku, dotaknimo se pitanja praga σ_c. Prisjetimo se da je u kratkodosežnom modelu prag r_c približno (ili barem) 0.8, što je blizu granice $r = 1$ čistog sustava. U usporedbi s kratkodosežnim modelom, dugodosežni model s nečistoćom nedvojbeno ukazuje na postojanje faze u kojoj nema domenskog zida. Numerički je pritom teško odrediti vrijednost praga σ_c, jer se zbog dugodosežnih korelacija i konačnosti sustava domenski zid može opaziti i za $\sigma < \sigma_c$. No, umjesto točne vrijednosti, na osnovu Monte Carlo simulacija možemo barem dati ocjenu intervala u kojem se nalazi σ_c. Ideja je za najveću u simulacijama dostupnu veličinu sustava L_{max} naći najmanji (najveći) $\sigma_c^-(L_{max})$ ($\sigma_c^+(L_{max})$) takav da se nagib u profilu gustoće smanjuje (povećava) kako povećavamo $L < L_{max}$. Drugim riječima, za $\sigma < \sigma_c^-(L_{max})$, povećanjem veličine sustava $L < L_{max}$ profil gustoće se sve više približava homogenom profilu 1/2. S druge strane, povećanjem veličine sustava

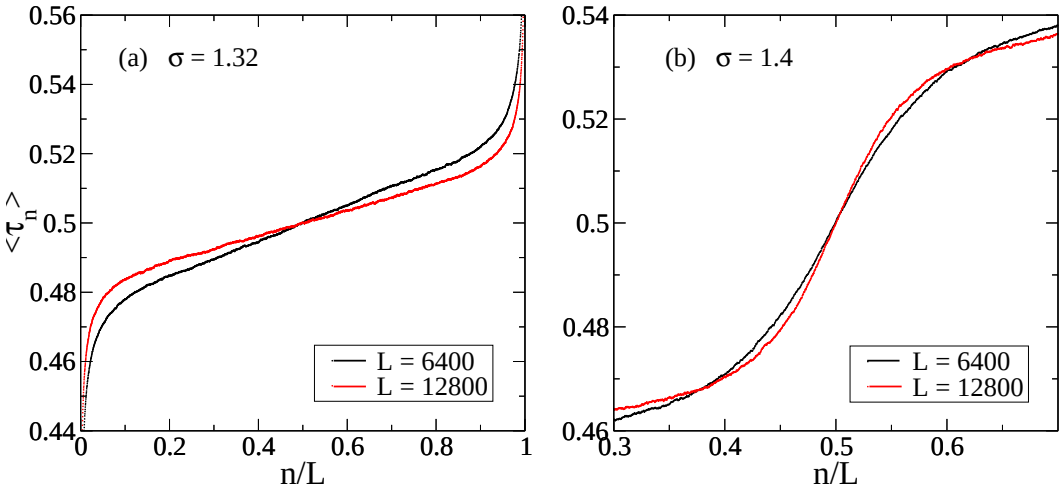

Slika 4.9: (a) Najmanji i (b) najveći σ pri kojima su faze (a) bez i (b) s domenskim zidom postojane za sve $L \leq L_{max} = 12800$. Ostali parametri simulacije su $\rho = 1/2$ i $t = 10^8$ MC koraka/čvoru.

$L < L_{max}$ za $\sigma > \sigma_c^+$ opaža se da domenski zid postaje sve "strmiji", tj. smanjuje mu se širina. Za veličinu sustava $L_{max} = 12800$ koju smo koristili u Monte Carlo simulacijama, na taj smo način došli do ocjene $1.32 < \sigma_c < 1.40$ (slika 4.9).

4.2.2 Profili gustoće u aproksimaciji srednjeg polja

Uspjeh aproksimacije srednjeg polja u čistom dugodosežnom modelu motivira nas da istu aproksimaciju primijenimo i u modelu s nečistoćom. Prije nego što zapišemo cijeli sustav jednadžbi za gustoće $\langle\tau_n\rangle$ u aproksimaciji srednjeg polja $\langle\tau_n\tau_m\rangle \to \langle\tau_n\rangle\langle\tau_m\rangle$, $n \neq m$, pogledajmo možemo li odrediti gustoće ρ_- i ρ_+ na sličan način kao i u kratkodosežnom modelu, tj. pretpostavljajući profil gustoće oblika oštrog domenskog zida,

$$\langle\tau_n\rangle = \begin{cases} \rho_-, & 1 \leq n \leq L/2 \\ \rho_+, & L/2+1 \leq n \leq L, \end{cases} \tag{4.17}$$

te koristeći činjenicu da je struja svugdje konstantna. Prisjetimo se da je u modelu s dugodosežnim preskocima struja definirana kao ukupna struja čestica koje skaču preko i s nekog čvora k,

$$j = \sum_{n=1}^{k} \sum_{l=k+1-n}^{L} p_l \langle\tau_n(1-\tau_{n+l})\rangle + \sum_{n=k+2}^{L} \sum_{l=L-n+k+2}^{L} p_l \langle\tau_n(1-\tau_{n+l})\rangle. \tag{4.18}$$

U unutrašnjosti faze gustoće ρ_-, tj. daleko od nečistoće i domenskog zida (npr. na čvoru $k = L/4$), očekujemo struju oblika $j = \lambda(\sigma)\rho_-(1-\rho_-)$. Ista ta struja

mora biti jednaka struji preko nečistoće, koju dobijemo ako u izraz za struju (4.18) uvrstimo $k = L$. Uz aproksimaciju (4.17), to daje

$$j \approx \rho_+(1-\rho_-)(p_2 + 2p_3 + 3p_4 + \dots) = [\lambda(\sigma) - 1]\rho_+(1-\rho_-), \tag{4.19}$$

gdje smo zanemarili doprinose struji od preskoka duljine $l \geq L/2$, obzirom da iščezavaju u granici $L \to \infty$. Izjednačavanjem ova dva izraza, u granici $L \to \infty$ dobivamo ρ_- i ρ_+ kao funkcije od λ,

$$\rho_- = \frac{1-\lambda^{-1}}{2-\lambda^{-1}}, \qquad \rho_+ = \frac{1}{2-\lambda^{-1}}. \tag{4.20}$$

Substitucijom $r' = (\lambda - 1)/\lambda$, gornje izraze možemo svesti na poznati oblik gustoća u kratkodosežnom modelu, $\rho_- = r'/(1+r')$ i $\rho_+ = 1/(1+r')$, čime smo, zapravo, dobili efektivnu jačinu nečistoće kao funkciju parametra σ. Nažalost, ovako pojednostavljeni profil gustoće (4.17) dobro opisuje ρ_- i ρ_+ samo za veće vrijednosti $\sigma \gtrsim 3$, što je vidljivo sa slike 4.10. Ne čudi stoga što naivni pokušaj da odredimo σ_c izjednačavajući ρ_- i ρ_+ vodi na trivijalni $\sigma_c = 1$ za koji struja divergira i samim time ne osjeća utjecaj nečistoće.

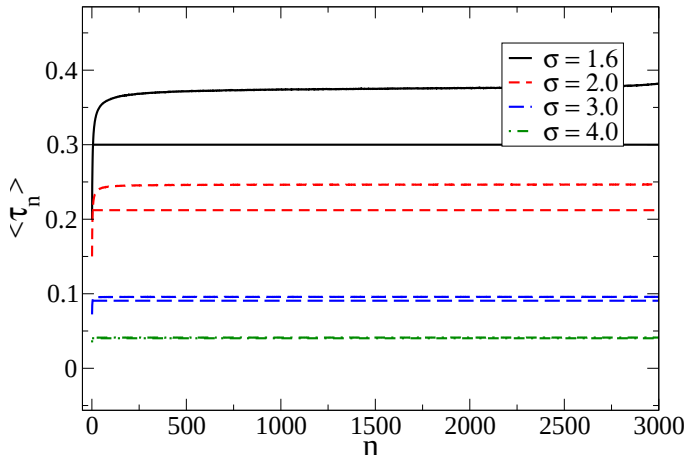

Slika 4.10: Profili gustoće u fazi s domenskim zidom dobiveni Monte Carlo simulacijama ($L = 6400$, $\rho = 1/2$ i $t = 10^8$ MC koraka/čvoru) i usporedba s gustoćom $\rho_- = (1-\lambda^{-1})/(2-\lambda^{-1})$ za različite vrijednosti parametra σ.

Da bismo odredili netrivijalni σ_c i objasnili potencijski zakon u fazi s domenskim zidom, moramo dakle uzeti u obzir i prostornu ovisnost profila gustoće. Označimo prvo čvorove rešetke s $n = -K, \dots, K$, $L = 2K$, tako da se nečistoća nalazi na čvoru $n = 0$. Jednadžbe za gustoću $\langle\tau_n\rangle(t)$ dobivene iz odgovarajuće master jednadžbe tada glase,

$$\frac{d}{dt}\langle\tau_n\rangle = \sum_{\substack{l=1\\l\neq n}}^{L} p_l\langle\tau_{n-l}(1-\tau_n)\rangle - \sum_{\substack{l=1\\l\neq L-n+1}}^{L} p_l\langle\tau_n(1-\tau_{n+l})\rangle, \quad n\neq 0, \tag{4.21}$$

gdje smo pretpostavili periodičke rubne uvjete, $\tau_{K+n} = \tau_{-K+n-1}$. Primjenom aproksimacije srednjeg polja gornji sustav jednadžbi u stacionarnoj granici $d\langle\tau_n\rangle/dt \to 0$ svodi se na problem traženja nultočke nelinearnog sustava od L jednadžbi s L nepoznanica. Pritom treba imati na umu da je od L jednadžbi (4.21) njih nezavisnih $L-1$, obzirom da njihov zbroj daje ukupni broj čestica,

$$\frac{d}{dt}\sum_n \langle\tau_n\rangle = \frac{d}{dt}N = 0 \tag{4.22}$$

Sustav od $L-1$ jednadžbi (4.21) i uvjetom $\sum_{n=1}^{L}\langle\tau_n\rangle = N$ rješavamo dalje numerički koristeći HYBRD algoritam iz biblioteke MINPACK. Račun smo proveli za nekoliko vrijednosti σ i L, a slaganje s rezultatima Monte Carlo simulacija prikazano je na slikama 4.11 i 4.12. U fazi s domenskim zidom nalazimo dobro slaganje s rezultatima Monte Carlo simulacija, ali primjećujemo uži domenski zid, te manju gustoću ρ_- (odnosno veću gustoću ρ_+). Razlika u rastegnutosti domenskog zida nije iznenađujuća i očekivana je posljedica aproksimacije srednjeg polja. Doista, detaljnija analiza domenskog zida pokazuje da je u aproksimaciji srednjeg polja karakteristična duljina te rastegnutosti proporcionalna $L^{1-\sigma/2}$ umjesto $L^{1/3}$.

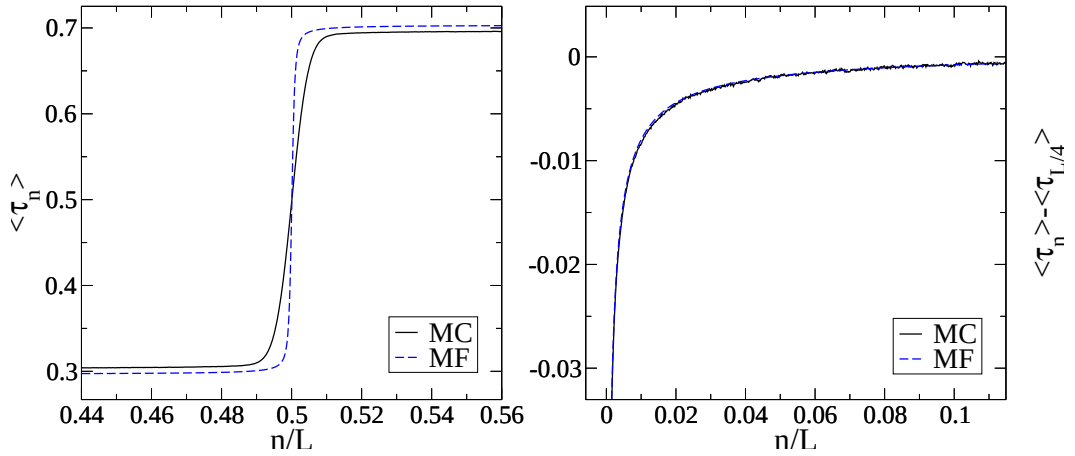

Slika 4.11: (a) Usporedba profila gustoće dobivenih u aproksimaciji srednjeg polja (MF) i Monte Carlo simulacijama (MC) za $\sigma = 1.8$ ($L = 6400$, $\rho = 1/2$ i $t = 10^8$ MC koraka/čvoru). (b) Odgovarajuća prostorno ovisna odstupanja $\langle\tau_n\rangle - \langle\tau_{L/4}\rangle$ dobivena u aproksimaciji srednjeg polja i Monte Carlo simulacijama.

S druge strane, za odstupanje od ρ_- i ρ_+ nemamo objašnjenje. Možemo jedino primijetiti da se ono javlja i u kratkodosežnom modelu, a najvjerojatnije

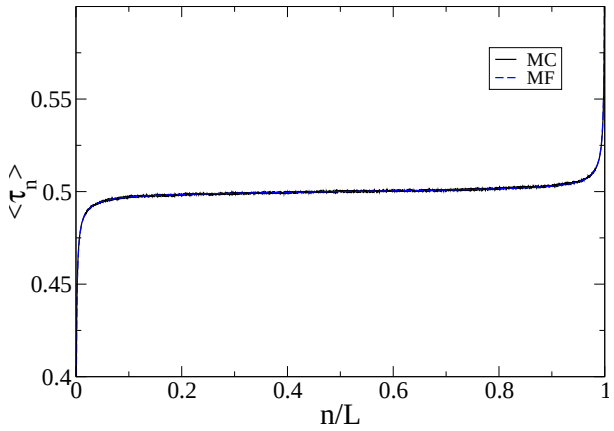

Slika 4.12: Usporedba profila gustoće dobivenih u aproksimaciji srednjeg polja (MF) i Monte Carlo simulacijama (MC) za $\sigma = 1.1$ ($L = 6400$, $\rho = 1/2$ i $t = 10^8$ MC koraka/čvoru).

je povezano sa zanemarivanjem korelacija u neposrednoj blizini nečistoće gdje je njezin utjecaj najveći. Usprkos tome, izvrsno slaganje s Monte Carlo rezultatima zato nalazimo ukoliko od $\langle\tau_n\rangle$ oduzmemo $\rho_- = \langle\tau_{L/4}\rangle$ (slika 4.11(b)). To je još očitije u fazi bez domenskog zida, u kojoj aproksimacija srednjeg polja daje točnu vrijednost $\rho_- = \rho_+ = 1/2$ (slika 4.12).

Gornje slaganje s rezultatima Monte Carlo simulacija dovodi nas do istog zaključka kao i čistom modelu: bez obzira na nečistoću, korelacije među česticama daju doprinose višeg reda u odnosu na najniže doprinose koje daje aproksimacija srednjeg polja. To nas dalje vodi na ideju, koju primjenjujemo u nastavku, da bismo ocjenom najnižih doprinosa mogli odrediti eksponent potencijskog zakona u fazi s domenskim zidom.

Polazimo od jednadžbi (4.21) u aproksimaciji srednjeg polja u koje uvrštavamo profil gustoće u obliku domenskog zida s nepoznatim prostorno ovisnim korekcijama ϕ_n,

$$\langle\tau_n\rangle = \begin{cases} \rho_+ + \phi_n, & -K \le n < 0 \\ \rho_- + \phi_n, & 0 < n \le K. \end{cases} \tag{4.23}$$

Za $0 < n \le K$, desna strana jednadžbe (4.21) daje slijedeće članove u potencijama od ϕ_n:

$$\phi_n^0: \quad -\rho_-(1-\rho_-)(p_n - p_{L-n+1}) + (\rho_+ - \rho_-)\left[(1-\rho_-)\sum_{l=n+1}^{n+K} p_l + \rho_- \sum_{K-n+1}^{L-n} p_l\right] \tag{4.24}$$

$$\phi_n^1: \quad \left[\rho_- \sum_{\substack{l=1\\ l\neq L-n+1}}^{L} p_l \Delta_l^+ \phi_n - (1-\rho_-) \sum_{\substack{l=1\\ l\neq n}}^{L} p_l \Delta_l^- \phi_n\right] - \phi_n(1-2\rho_-)(p_n - p_{L-n+1}) +$$
$$+ (\rho_+ - \rho_-)\phi_n \left[\sum_{l=K-n+1}^{L-n} p_l - \sum_{l=n+1}^{K+n} p_l\right] \tag{4.25}$$

$$\phi_n\phi_m: \quad \phi_n^2(p_n - p_{L-n+1}) + \phi_n \left[\sum_{\substack{l=1\\ l\neq L-n+1}}^{L} p_l \Delta_l^+ \phi_n + \sum_{\substack{l=1\\ l\neq n}}^{L} p_l \Delta_l^- \phi_n\right], \tag{4.26}$$

gdje smo upotrijebili slijedeću notaciju: $\Delta_l^+\phi_n \equiv \phi_{n+l} - \phi_n$ i $\Delta_l^-\phi_n \equiv \phi_n - \phi_{n-l}$. Doprinos pojedinih članova možemo ocijeniti tako da odredimo kojeg su reda u $a = 1/L$, pri čemu nas zanima granica $a \to 0$ uz $na = x < \infty$. Prvi član u ϕ_n^0 je reda $O(a^{\sigma+1})$, jer je $p_n \sim L^{-(\sigma+1)}x^{-(\sigma+1)}$. Za $0 < n < L/4$, drugi član u ϕ_n^0 je pozitivan i reda $O(a^\sigma)$. Za ocjenu članova ϕ_n^1, pretpostavljamo potencijski oblik $\phi_n = L^{-\nu} f_-(n/L)$, gdje je ν nepoznati eksponent, a $f_-(n/L) < 0$ za $0 < n < L/4$. Drugi i treći članovi u ϕ_n^1 su tada reda $O(a^{\nu+\sigma+1})$ i $-O(a^{\nu+\sigma})$. Zanemarimo li (nelinearne) članove višeg reda $\phi_n\phi_m$, preostaje nam ocijeniti

$$\frac{1}{2}\left[\sum_{\substack{l=1\\ l\neq L-n+1}}^{L} p_l \Delta_l^+ \phi_n - \sum_{\substack{l=1\\ l\neq n}}^{L} p_l \Delta_l^- \phi_n\right] - \Delta\rho_- \left[\sum_{\substack{l=1\\ l\neq L-n+1}}^{L} p_l \Delta_l^+ \phi_n + \sum_{\substack{l=1\\ l\neq n}}^{L} p_l \Delta_l^- \phi_n\right], \tag{4.27}$$

gdje smo uveli $\Delta\rho_- = 1/2 - \rho_-$ kako bi razlikovali dva slučaja, $\rho_- = 1/2$ ($\Delta\rho_- = 0$) i $\rho_- \neq 1/2$ ($\Delta\rho_- \neq 0$). Ti nas članovi podsjećaju na sume koje smo u čistom dugodosežnom slučaju zamijenili s

$$\frac{1}{2}\left[\sum_{l>0} p_l \Delta_l^+ \phi_n - \sum_{l>0} p_l \Delta_l^- \phi_n\right] \to \begin{cases} a^\sigma D_\sigma \Delta_\sigma \phi(x) + O(a^2), & 1 < \sigma < 2 \\ a^2 D_2 \Delta\phi(x) + O(a^{min\{\sigma,3\}}), & \sigma > 2, \end{cases} \tag{4.28}$$

$$\Delta\rho\left[\sum_{l>0} p_l \Delta_l^+ \phi_n + \sum_{l>0} p_l \Delta_l^- \phi_n\right] \to -a(1-2\rho)\lambda(\sigma)\frac{\partial\phi}{\partial x} + O(a^\sigma), \tag{4.29}$$

gdje je $D_\sigma = -\Gamma(-\sigma)cos(\pi\sigma/2)/\zeta(\sigma+1)$, $D_2 = \zeta(\sigma-1)/(2\zeta(\sigma+1))$, a Δ_σ frakcionalni Laplacian. Razlika je, međutim, u tome što smo uvođenjem nečistoće

izgubili translacijsku invarijantnost. Pretpostavimo li da je red veličine u a izraza (4.27) ipak točno opisan s (4.28) i (4.29), tada za ocjenu (4.28) i (4.29) dobivamo redom $O(a^{\sigma+\nu})$ i -$O(a^{\nu+1})$. Naposljetku, usporedimo li dva najniža člana u a suprotnih predznaka, dobivamo $\nu = \sigma - 1$ za sve σ za koje postoji domenski zid (tj. za $\sigma > \sigma_c$). Taj rezultat očito nije dobar jer za $\sigma > 2$ ne daje $\nu = 1$, no već otprije znamo da aproksimacija srednjeg polja ne opisuje dobro kratkodosežnu granicu. Napomenimo još da razlog zašto za eksponent ν nismo dobili $(\sigma - 1)/2$ kao u fazi maksimalne struje u čistom dugodosežnom modelu s otvorenim rubnim uvjetima, leži u činjenici da se dugodosežne korelacije javljaju u domenama gustoća $\rho_\pm \neq 1/2$, pa je samim time član $\partial\phi/\partial x$ nižeg reda u a od nelinearnog člana $\phi\partial\phi/\partial x$.

S druge strane, uvrstimo li u (4.24)-(4.26) $\rho_- = \rho_+ = 1/2$, dobivamo samo četiri člana,

$$\begin{aligned} 0 \;=\; & \frac{1}{4}(p_n - p_{L-n+1}) + \frac{1}{2}\left[\sum_{\substack{l=1 \\ l\neq L-n+1}}^{L} p_l \Delta_l^+ \phi_n - \sum_{\substack{l=1 \\ l\neq n}}^{L} p_l \Delta_l^- \phi_n\right] + \\ & + \phi_n^2 (p_n - p_{L-n+1}) + \phi_n \left[\sum_{\substack{l=1 \\ l\neq L-n+1}}^{L} p_l \Delta_l^+ \phi_n + \sum_{\substack{l=1 \\ l\neq n}}^{L} p_l \Delta_l^- \phi_n\right], \end{aligned} \tag{4.30}$$

odakle vidimo da nelinearni članovi postaju važni, a kao rezultat profil gustoće više ne zadovoljava jednostavnu relaciju skaliranja.

4.2.3 Račun za prag σ_c

Poznavanje ovisnosti eksponenta ν o σ u fazi s domenskim zidom omogućuje nam da na posredni način, tj. bez poznavanja ρ_- i ρ_+, odredimo prag σ_c. Ideja se sastoji u tome da pokažemo da eksponent ν na pragu σ_c poprima istu vrijednost kao i u kratkodosežnom modelu u fazi bez domenskog zida, $\nu(\sigma_c) = 1/3$ [143]. Ako pretpostavimo da je funkcija $\nu(\sigma)$ kontinuirana u točki σ_c, tada σ_c slijedi iz

$$\nu(\sigma_c) = \sigma_c - 1 = 1/3 \quad \Rightarrow \quad \sigma_c = \frac{4}{3}, \tag{4.31}$$

što je unutar granica ocjene $1.32 < \sigma_c = 1.333... < 1.4$ koju smo dobili na osnovu rezultata Monte Carlo simulacija.

U osnovi, argument za $\nu(\sigma_c) = 1/3$ isti je kao i argument od Ha et al. za $\nu = 1/3$ u kratkodosežnom modelu [143]. Promotrimo lokalne fluktuacije gustoće koje spontano nastaju u sustavu. Daleko od ruba, one se propagiraju brzinom $v_g = \delta j \delta\rho = \lambda_L(1-2\rho)$, koja je u fazi bez domenskog zida jednaka 0. Nečistoća, s druge strane, usporava propagaciju pozitivnih fluktuacija gustoće, a ubrzava propagaciju negativnih. Rezultat toga je povišena lokalna gustoća netom prije nečistoće, a

snižena netom poslije. Ukoliko se centar mase fluktuacije propagira brže nego što se fluktuacija rasipa u prostoru, tada višak čestica blizu nečistoće možemo ocijeniti ukupnim brojem fluktuacija prisutnih u sustavu. Taj broj, međutim, ne može biti veći od vremena t_f potrebnog da fluktuacija obiđe cijeli sustav. Obzirom da je proces stvaranja fluktuacija niz nezavisnih događaja, te da ih u prosjeku ima jednako i pozitivnih i negativnih, broj fluktuacija u sustavu, a time i višak čestica blizu rubova, možemo ocijeniti kao $\delta N \propto t_f^{1/2}$. Drugim riječima, δN možemo ocijeniti tako što ćemo ocijeniti t_f. Na ovom mjestu Ha et al pretpostavljaju da $v_g = \delta j/\delta\rho$ vrijedi *lokalno*, tj. da blizu nečistoće brzina širenja fluktuacija postaje prostorno ovisna i oblika $v_g \approx \lambda_L[1-2\rho(x)] \propto x^{-\nu}$, što se može opravdati ako je prostorna varijacija lokalne gustoće dovoljno spora. Položaj centra mase se tada mijenja u vremenu kao $x_{\mathrm{CM}} \propto t^{1/(1+\nu)}$, odakle slijedi da je $t_f \propto L^{1+\nu}$. Višak čestica blizu nečistoće skalira se s L kao $\delta N \propto t_f^{1/2} = L^{(\nu+1)/2}$, što izjednačavanjem s $\delta N \propto \int dx x^{-\nu}$ daje $\nu = 1/3$.

Ključna pretpostavka u gornjoj argumentaciji je da se fluktuacije propagiraju brže nego što se rasipaju. To znači da karakteristična duljina rasipanja, $\xi \propto t^{1/z}$, mora biti manja od $x_{\mathrm{CM}} \propto t^{1/(\nu+1)}$, tj. da je $\nu < z-1$, gdje je z dinamički eksponent. Obzirom da je u dugodosežnom modelu $z = \min\{\sigma, 3/2\}$, a $\sigma_c < 3/2$, to znači da je σ_c ujedno i granični σ za koji to još vrijedi. Time smo djelomično i objasnili nemogućnost prilagodbe profila u fazi bez domenskog zida na jednostavni potencijski oblik za $1 < \sigma < \sigma_c$.

U poglavlju 4.1 smo nabrojili pregršt argumenata za i protiv postojanja faze bez domenskog zida u TASEP-u sa statičkim defektom. U tom smislu želimo istaknuti da rezultati dugodosežnog modela u poglavlju 4.2 pritom ne zauzimaju stranu. Predloženi model prije svega ukazuje da je u barem jednom vođenom difuzijskom sustavu u jednoj dimenziji, u kojem je difuzijski član doduše frakcionalan, moguće nedvojbeno utvrditi takav tip prijelaza, te odrediti samu točku prijelaza.

Što se kratkodosežnog problema tiče, naš je dojam da će u nedostatku egzaktnog rješenja problem statičkog defekta u TASEP-u još pričekati konačni zaključak. Ovaj problem međutim i više nego ukazuje na potrebu za dodatnim metodama kojom bi se mogli sustavno istraživati fazni prijelazi daleko od ravnoteže, od kojih se obećavajućom čini metoda slična Yang-Lee teoriji [144, 145], ali ne za nultočke particijske funkcije, već za nultočke normalizacijske konstante $Z = \sum_C f(C)$, gdje suma ide po svim stanjima C, a $f(C)$ je rješenje master jednadžbe [146].

5

Separacija faza inducirana neredom

Seksperimentalne točke gledišta, brojni realni sustavi na koje se primjenjuju modeli vođenih difuzijskih sustava nerijetko su izloženi nekoj vrsti nereda. Brzine kojom se kreću automobili svakako ovise o individualnim karakteristikama kako vozača tako i vozila, kao i o "nehomogenim" uvjetima na cesti (npr. radovi, nesreće, ograničenje brzine). U prvom slučaju radi se o neredu koji je pridružen česticama, dok u drugom slučaju nered potječe iz okoliša. Primjer potonjeg nalazimo i u biosintezi proteina, u kojoj određeni tripleti nukleotida u interakciji s transferskom RNK usporavaju proces translacije [60] (5.1). Prebačeno u jezik TASEP-a, nered iz okoliša možemo opisati nehomogenostima u vjerojatnostima preskoka na pojedinim čvorovima, pri čemu se jednom izabrane vrijednosti ne mijenjaju u vremenu.

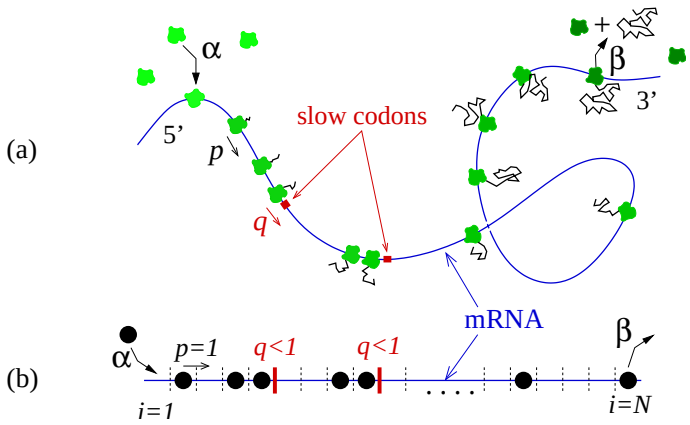

Slika 5.1: (a) Slikoviti prikaz sinteze proteina. Zelenim su označeni ribosomi koji se propagiraju na mRNK lancu na osnovu specifičnih aminokiselina koje na lanac donosi transferska RNK (nije prikazana na slici). Uz neke triplete (označene crvenom bojom) veže se manji broj transferske RNK, što rezultira sporijom propagacijom ribosoma. (b) Odgovarajući model TASEP-a s reduciranom vjerojatnošću preskoka $q < 1$ s određenih čvorova. Slika je preuzeta iz [60].

S fundamentalne točke gledišta, zanima nas kako se stacionarno stanje čistog sustava i njegova karakteristična svojstva, poput različitih faza, mijenjaju u prisustvu nereda. U slijedećem poglavlju prezentirati ćemo argument Tripathyja i

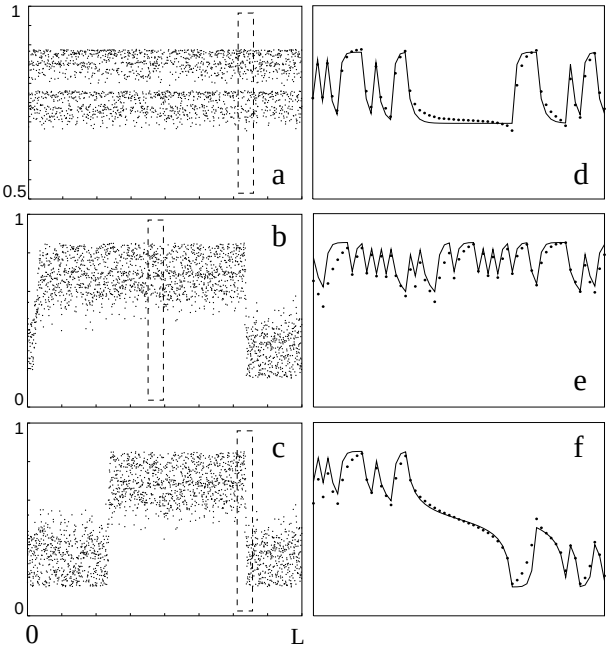

Slika 5.2: Profili gustoće u TASEP-u za jednu realizaciju nereda pri gustoćama: (a) $\rho = 0.8$, (b) $\rho = 0.6$ i (c) $\rho = 0.5$. Slike (d), (e) i (f) prikazuju uvećane dijelove odgovarajućih slika ulijevo, pri čemu simboli predstavljaju rezultate Monte Carlo simulacija, a krivulje rezultat dobiven primjenom aproksimacije srednjeg polja. Preuzeto iz [103].

Barme [103] koji kaže da se koegzistencija faza u kratkodosežnom TASEP-u javlja u *konačnom* intervalu gustoća $\rho_c < \rho < 1 - \rho_c$ bez obzira na izbor raspodjele nereda $\mathcal{P}(r_i)$, pri čemu prag ρ_c ovisi o detaljima raspodjele $\mathcal{P}$. U poglavljima 5.2 i 5.3 istražujemo vrijedi li isti rezultat kako u teorijski tako i u eksperimentalno motiviranim poopćenjima.

5.1 Kratkodosežni model

TASEP s neredom pridruženim čvorovima (u nastavku dTASEP, od eng. *disordered TASEP*) prvi su promatrali Tripathy i Barma [102,103] u sustavu s periodičkim rubnim uvjetima. Kao i u homogenom TASEP-u, $N = \rho L$ čestica raspoređeno je na L čvorova pri čemu je svaki čvor zauzet najviše jednom česticom. Za raspodjelu vjerojatnosti preskoka $\mathcal{P}(r_i)$ Tripathy i Barma uzimaju Bernoullijevu raspodjelu

$$\mathcal{P}(r_i) = \begin{cases} c & r_i = r \\ 1 - c & r_i = 1, \end{cases} \tag{5.1}$$

gdje je c koncentracija nečistoća. Drugim riječima, u sustavu se nasumično izabere $N_d = cL$ nečistoća s kojih se čestice pomiču s vjerojatnošću $r < 1$ udesno, dok se s ostalih mjesta pomiču s vjerojatnošću 1.

Tipični oblici profila gustoće prikazani su na slici 5.2. Ovisno o gustoći ρ, prepoznajemo dva režima. U prvom režimu gustoća je homogena na makroskopskoj skali i jednaka približno ρ, a male varijacije se uočavaju tek na mikroskopskoj

skali duljine nekoliko konstanti rešetke (slika 5.2(a)). U tom režimu struja ima sličnu funkcijsku ovisnost o gustoći kao i u čistom modelu (područje A na slici 5.3). Drugi režim karakterizira pojava makroskopskih domena gustoća različitih od ρ, koje su međusobno odvojene domenskim zidovima (slike 5.2(b) i (c)). Takav režim karakterizira zaravan u struji $j(\rho)$ širine 2Δ centrirane oko gustoće $\rho = 1/2$ (područje B na slici 5.3). Na slikama 5.2 i 5.3 također su prikazani i rezultati dobiveni u aproksimaciji srednjeg polja rješavanjem jednadžbi,

$$j = r_i \rho_i (1 - \rho_{i+1}), \quad i = 1, \ldots, L \tag{5.2}$$

koji zapravo jako dobro opisuju profile gustoće, čak i na mikroskopskoj skali (slike 5.2(d), (e) i (f)). Problem je, međutim, što je rješenje moguće naći samo numerički, pa ne daje uvid u mehanizam separacije.

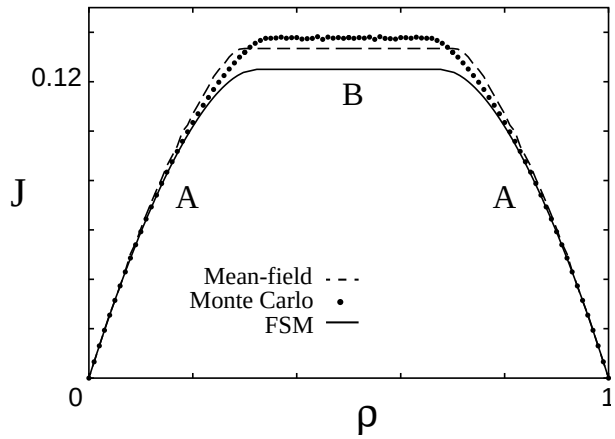

Slika 5.3: Ovisnost struje o gustoći u dTASEP-u za jednu realizaciju nereda i veličinu sustava $L = 8000$, te $r = c = 1/2$. Isprekidana linija odgovara struji dobivenoj primjenom aproksimacije srednjeg polja, dok puna linija odgovara struji u potpuno segregiranom modelu u kojem sve nečistoće čine jedan grozd duljine $N_d = cL$. Preuzeto iz [103].

Da bi objasnili separaciju, Tripathy i Barma polaze od činjenice da će nered u velikom sustavu uvijek stvoriti grozdove "brzih" i "sporih" čvorova, tj. domene u kojima su sve vjerojatnosti preskoka ili 1 ili r. Pretpostavimo da su te domene dovoljno velike da se u njima uspostavi homogena gustoća, što ćemo opravdati malo kasnije. Tada za neku zadanu struju j_0 i gustoću $\rho \leq 1/2 - \Delta$ (ili $\rho \geq 1/2 + \Delta$), moguće gustoće u domenama su ρ_1 i ρ_2 (ili ρ_3 i ρ_4 za $\rho \geq 1/2 + \Delta$), koja su rješenja jednadžbe $j_0 = \rho_{1,4}(1 - \rho_{1,4}) = r\rho_{2,3}(1 - \rho_{2,3})$ (slika 5.4). U režimu bez separacije, te gustoće odgovaraju vrpcama bliskih gustoća, kao primjerice na slici 5.2(a). Međutim, povećamo li gustoću ρ dovoljno blizu $\rho = 1/2$, struja će u jednom trenutku dostići maksimalnu vrijednost jednaku maksimalnoj struji u domeni "sporih" čvorova, $r/4$. Povećamo li ρ još više, struja ostaje ista, a u

sustavu se na uštrb domena s gustoćama $\rho_{1,2}$ stvaraju domene s gustoćama $\rho_{3,4}$, čime započinje separacija faza.

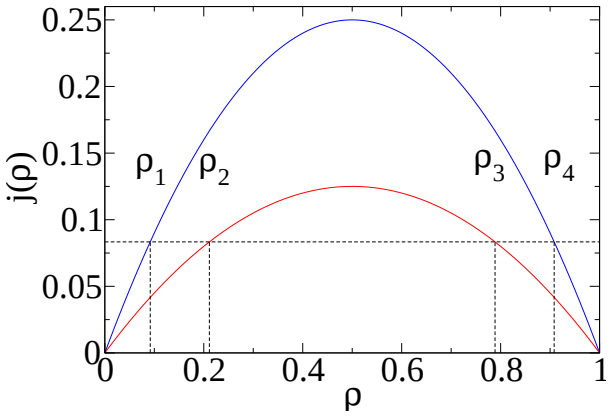

Slika 5.4: Mehanizam nastanka separacije faza u dTASEP-u. Dvije parabole odgovaraju strujama u "sporim" i "brzim" domenama u ovisnosti o gustoći u tim domenama, $j(\rho) = r\rho(1-\rho)$ i $j(\rho) = \rho(1-\rho)$. Preuzeto iz [103].

U gornjem argumentu ključna pretpostavka je da nered stvara dovoljno velike grozdove "sporih" čvorova, tako da je maksimalna struja u sustavu uvijek ograničena s $r/4$. Tu pretpostavku Tripathy i Barma opravdavaju činjenicom da je prosječna duljina *najdužeg* grozda "sporih" mjesta $\propto \ln L$, tj. divergira u termodinamičkoj granici $L \to \infty$. Taj rezultat slijedi iz matematičke teorije ekstremnih vrijednosti (za uvod vidi npr. [148]), a rigorozno je izveden u [149] za ekvivalentni problem statistike najdužeg niza uzastopno dobivenih "glava" u L bacanja novčića, pri čemu koncentraciju c zamjenjuje vjerojatnost $P(\text{"glava"}) = c$,

$$\{l_{\max}\} = \frac{\gamma + \ln[L(1-c)]}{\ln(1/c)} - \frac{1}{2}, \tag{5.3}$$

gdje $\{\dots\}$ označava usrednjavanje po narednim konfiguracijama, a $\gamma = 0.5772\dots$ je tzv. Euler-Mascheronijeva konstanta. Kratki uvod u teoriju ekstremnih vrijednosti, obzirom da će nam kasnije trebati, prilažemo u dodatku A.

Kako bi upotpunili kvalitativno objašnjenje nastanka separacije faza, Tripathy i Barma polaze od pojednostavljenoga tzv. potpuno segregiranog modela u kojem *sve* nečistoće u sustavu čine jedan veliki grozd duljine $N_d = cL$. Promatranje takvog modela može se opravdati pretpostavkom da struja opada s duljinom domene "sporih" čvorova, pa se za taj slučaj očekuje najveći utjecaj nereda. Označimo li gustoće u domeni "brzih" čvorova X s ρ_x, a u domeni "sporih" čvorova Y s ρ_y, tada očuvanje struje vodi na izraz

$$j_0 = \rho_x(1-\rho_x) = r\rho_y(1-\rho_y), \tag{5.4}$$

Gornjem izrazu treba još pribrojiti očuvanje broja čestica,

$$(1-c)\rho_x + c\rho_y = \rho. \tag{5.5}$$

što je dovoljno da se odrede ρ_x, ρ_y i j_0 za neki ρ. Konkretno, zanima nas gustoća ρ_c za koju ρ_y postaje $1/2$, tj. za koju struja u domeni "sporih" čvorova dostiže maksimalnu vrijednost $r/4$. Uvrštavanjem $\rho_y = 1/2$ u (5.4) i (5.5) za ρ_c se dobiva,

$$\rho_c = \frac{1-(1-c)\sqrt{1-r}}{2}. \tag{5.6}$$

odakle se lako odredi širina intervala u gustoći ρ za koje se javlja koegzistencija faza, $\Delta = 1 - 2\rho_c$. Vratimo li se na originalni problem, izraz (5.6) zapravo daje gornju granicu na ρ_c, obzirom da je tada utjecaj nereda najveći [147]. Donja granica slijedi iz trivijalne činjenice da je maksimalna moguća struja u sustavu $r/4$, što daje

$$\rho_c \geq \frac{1-\sqrt{1-r}}{2}. \tag{5.7}$$

Zanimljivo je pritom da se separacija faza ne može izbjeći čak ni u granici $c \to 0$, u kojoj je $\rho_c = (1-\sqrt{1-r})/2$, tj. $\Delta \neq 0$. Tu se granicu, međutim, ne smije zamijeniti s modelom *jedne* nečistoće u kojem se sustav može optimizirati tako da je maksimalna struja, umjesto $r/4$, jednaka $1/4$.

Kvalitativni zaključci Tripathyja i Barme se mogu primijeniti i na proizvoljnu raspodjelu $\mathcal{P}(r_i)$, pri čemu "spore" čvorove možemo definirati kao čvorove na kojima je r_i manje od neke zadane vrijednosti $r_0 < \{r_i\}$ [147]. Uz takvu definiciju i dalje vrijedi $\{l_{\max}\} \propto \ln L$, pri čemu u izrazu u (5.3) c zamjenjujemo s $P(r_i < r_0)$.

Drugi pristup problemu nereda U TASEP-u nalazimo u radu Harris i Stinchcombe-a [104], koji promatraju raspodjelu $w(\rho')$ gustoća $\langle\tau_i\rangle$ definiranu na slijedeći način,

$$w(\rho')\Delta\rho' = \frac{\text{broj čvorova na kojima je } |\langle\tau_i\rangle - \rho'| \leq \Delta\rho'/2}{L} \tag{5.8}$$

Koristeći aproksimaciju srednjeg polja, Harris i Stinchcombe su odredili integralnu jednadžbu za $w(\rho')$, koju su zatim riješili za neke specifične raspodjele $\mathcal{P}(r_i)$, pokazavši pritom da je širina zaravni 2Δ nikad ne iščezava, te da je proporcionalna širini raspodjele $\mathcal{P}(r_i)$.

* * *

U osnovi, mehanizam separacije faza u TASEP-u je geometrijske prirode - bilo koja raspodjela $\mathcal{P}(r_i)$ konačne širine u beskonačnom sustavu generirati će beskonačni grozd "sporih" čvorova koji ograničava struju. Možemo se stoga upitati da li ćemo slične makroskopske strukture inducirane neredom sresti i u situaciji u kojoj

česticama dozvolimo da *zaobilaze* defektne čvorove? Da bismo odgovorili na to pitanje, uvest ćemo dva poopćenja TASEP-a [150]. U poglavlju 5.2 promatramo TASEP s neredom i dugodosežnim preskocima čija vjerojatnost opada potencijski s duljinom preskoka l, $p_l \propto l^{-(1+\sigma)}$ uz $\sigma > 1$. Pritom nas, prije svega, motivira činjenica da dugodosežni preskoci u modelu s jednom nečistoćom mogu dovesti do izostanka separacije faza. S tehničke pak strane nas motivira činjenica da model s dugodosežnim preskocima u čistom slučaja zadržava većinu karakteristika svoje kratkodosežne inačice, ali se pritom vrlo dobro može opisati aproksimacijom srednjeg polja. Drugi model koji promatramo u poglavlju 5.3 je poopćenje TASEP-a na dvije dimenzije, simetričnog u transverzalnom i potpuno asimetričnog u longitudinalnom smjeru, pri čemu se nered javlja samo u longitudinalnom smjeru. Za razliku od prethodnog modela, ovaj je model lako zamisliti u širokom kontekstu transporta u neuređenom mediju, počevši od toka fluida kroz porozni materijal [151, 152], prometa (bilo automobilskog ili pješačkog) u prisutnosti prepreka [153], pa sve do mikrofluidičkih sustava u raznovrsnim geometrijama [154]. U navedenim primjerima zajedničko je netrivijalno ispreplitanje utjecaja vanjskog polja koje generira struju, međudjelovanja i geometrije medija, što u nekim situacijama može dovesti do iščezavajuće vodljivosti [151].

5.2 Poopćenje na dugodosežne skokove

U ovom poglavlju promatramo jednodimenzionalni TASEP s nasumično-sekvencijalnom dinamikom na rešetci od L čvorova i $N = \rho L$ čestica, te periodičkim rubnim uvjetima. čestice se na rešetci pomiču dugodosežnim preskocima duljine $1 \leq l \leq L-1$, koja se bira iz potencijske raspodjele $p_l \propto l^{-(1+\sigma)}$ uz $\sigma > 1$. Nered uvodimo tako što nasumično izaberemo $N_d = cL$ čvorova *s kojih i na koje*[1] čestice skaču s vjerojatnošću koja je reducirana za faktor $r < 1$ (slika 5.5).

5.2.1 Tipični rezultati Monte Carlo simulacija

Za početak, zanima nas stacionarni profil gustoće $\langle \tau_i \rangle$, $i = 1, \ldots, L$, kojeg računamo Monte Carlo simulacijama. Slično kao i u kratkodosežnom modelu s binarnim (Bernoullijevim) neredom, rezultati simulacija otkrivaju dva tipična ponašanja, prikazana na slici 5.6a. Slika 5.6a prikazuje profil gustoće pri niskoj gustoći ρ, gdje uočavamo samo mikroskopske domenske zidova, koji na makroskopskoj skali izgledaju kao dvije vrpce bliskih gustoća. S druge strane, povećanjem gustoće ρ iznad praga ${\rho_c}^2$ u sustavu se inducira makroskopski domenski zid, kao što je prikazano na slici 5.6b.

[1] Na taj način smo u modelu zadržali simetriju na zamjenu čestica i šupljina, što će nam kasnije olakšati analizu rezultata.

[2] Zbog simetrije na zamjenu čestica i šupljina isto vrijedi i za smanjivanje gustoće ispod praga $1 - \rho_c$

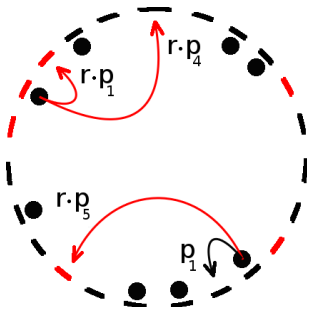

Slika 5.5: Slikoviti prikaz jednodimenzionalnog TASEP-a s dugodosežnim preskocima i neredom. Vjerojatnosti preskoka reducirane su za faktor $r < 1$ uvijek kada se čestica pomiče na defektni čvor ili s njega (označeno crvenom bojom). Slika ne prikazuje sve moguće preskoke, već samo one koji demonstriraju implementaciju nereda.

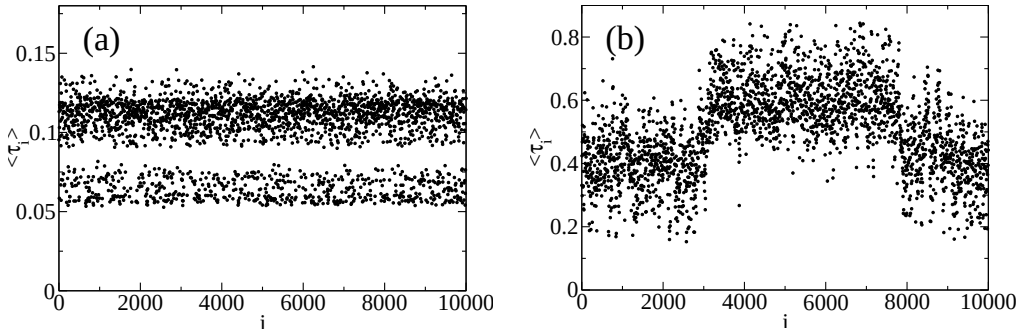

Slika 5.6: Profili gustoće za (a) $\rho = 0.1$ i (b) $\rho = 0.5$ u sustavu veličine $L = 10^4$ za $r = 0.5$, $c = 0.5$ i $\sigma = 1.8$, dobiveni Monte Carlo simulacijama ($t = 10^7$ MC koraka/čvoru) za jednu realizaciju nereda.

Gornji profili su vrlo slični profilima koje nalazimo u kratkodosežnom TASEP-u s neredom sa slike 5.2, uz glavnu razliku što ρ_c sada ovisi o parametru dosega σ. Imajući na umu rezultate dugodosežnog modela s jednom nečistoćom, to nas odmah vodi na pitanje možemo li variranjem $\sigma > 1$ postići $\rho_c = 1/2$, što odgovara izostanku separacije faza[3]. Na slici 5.7a je prikazan profil gustoće za jedan izbor parametara za koji je to moguće (i.e. za dovoljno mali $\sigma > 1$), te odgovarajući normirani histogram gustoća $w(\langle\tau_i\rangle)$, $i = 1 \ldots, L$ (slika 5.7b), koji ima samo jedan maksimum. Izostanak separacije faza može se također opaziti i u ovisnosti struje o gustoći, koja ne pokazuje uobičajenu zaravan (slika 5.8).

Zbog konačnosti sustava, s gornjim rezultatom ipak treba biti oprezan, posebno uzme li se u obzir da je karakteristična skala $\{l_{\max}\}$ koju generira nered u jednoj dimenziji logaritamska u L. U nastavku ćemo stoga provesti analizu segregiranog modela u kojem su svi defekti u nizu, po uzoru na model Tripathyja i Barme koji

[3]Prisjetimo se, to nije moguće postići u kratkodosežnom TASEP-u s neredom, u kojem postoji gornja granica na iznos praga ρ_c, koja je uvijek manja od 1/2.

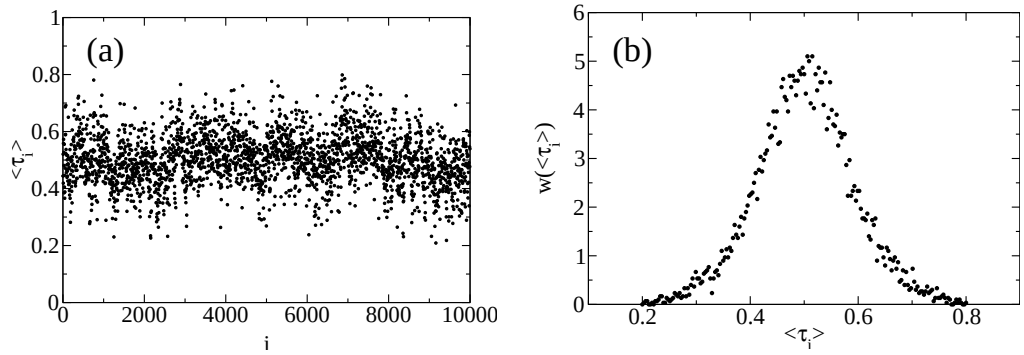

Slika 5.7: (a) Profil gustoće za sustav veličine $L = 10^4$, te $r = 0.5$, $c = 0.5$ i $\sigma = 1.2$, dobiven Monte Carlo simulacijama ($t = 10^7$ MC koraka/čvoru) za jednu realizaciju nereda pri gustoći $\rho = 0.5$; (b) odgovarajući normirani histogram gustoća $\langle \tau_i \rangle$, $i = 1 \ldots, L$ koji pokazuje samo jedan maksimum oko $\rho = 0.5$.

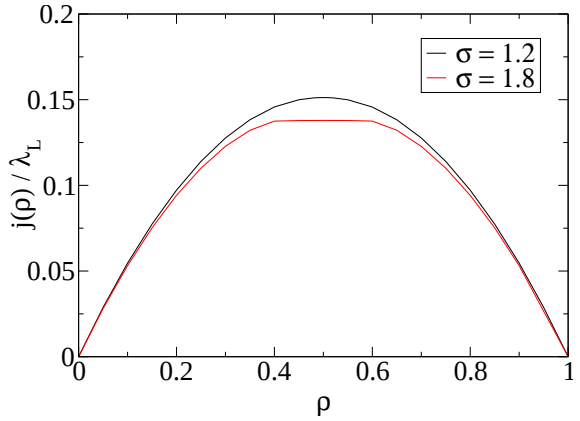

Slika 5.8: Ovisnost struje o gustoći za dvije različite vrijednosti parametra σ ($L = 10^4$, $c = 0.5$ i $r = 0.5$), dobivena Monte Carlo simulacijama za jednu realizaciju nereda. Radi lakše usporedbe, struja je podijeljena s prosječnom duljinom preskoka $\lambda_{L-1}(\sigma) = \sum_{i=1}^{L-1} l p_l$.

su na taj način analitički ocijenili ρ_c.

5.2.2 Segregirani model u aproksimaciji srednjeg polja

Prisjetimo se mehanizma separacije faza koji smo detaljno opisali u poglavlju 5.1, u kojem uzastopni niz "sporih" čvorova duljine $N_d = cL$ ograničava maksimalnu moguću struju na $j(\rho_c) = r/4$. Otprije znamo da u makroskopskoj domeni homogene gustoće ρ, uvođenje dugodosežnih preskoka vodi na isti oblik struje $j(\rho) \propto \rho(1-\rho)$, koja se od struje u kratkodosežnom modelu razlikuje jedino po faktoru $\lambda = \sum_i i p_i$. Taj faktor, jasno, nema nikakav učinak na jednadžbu (5.4), što sugerira isti ρ_c kao i u kratkodosežnom modelu. Istovremeno, to znači da je izostanak separacije faza sa slike 5.8 zapravo posljedica *konačnosti* sustava, a

ne možebitnog (faznog) prijelaza. Za parametre sa slike 5.8 to zapravo i ne čudi obzirom da je u tom slučaju $l_{\max} \approx 13$, što je premala duljina da se u toj domeni uspostavi asimptotski izraz za struju $\lambda r/4$. Koliki $l_{\max}$ je nužno pritom postići da se uspostavi asimptotski režim nije jednostavno odrediti. Umjesto toga možemo zamisliti segregirani model u kojem je duljina "spore" domene l *slobodni* parametar, te pokušati variranjem l "uhvatiti" promjenu režima. Rezultati Monte Carlo simulacija za takav model i različite l i σ prikazani su na slikama 5.9a i 5.9b. Na slici 5.9a se vidi da domenskog zida nema za $l = 10$, dok se za $l = 1000$ gotovo približio gornjoj i donjoj ocjeni (5.6) i (5.7). Zanimljivo je također da na slici 5.9b za $\sigma = 1.05$ promjenu režima uočavamo tek za $50 < l < 100$, što bi se u modelu s neredom opazilo tek za veličine sustava $\ln L \sim O(10^2)$, svakako nedostupne u Monte Carlo simulacijama[4].

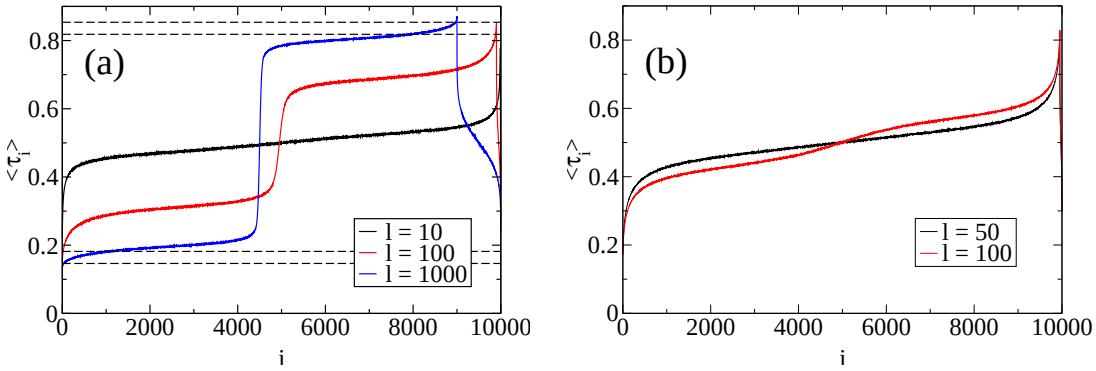

Slika 5.9: Profili gustoća u segregiranom modelu za različite l ($L = 10^4$, $r = 0.5$), dobiveni Monte Carlo simulacijama ($t = 10^7$ MC koraka/čvoru) za jednu realizaciju nereda pri gustoći $\rho = 1/2$ i (a) $\sigma = 1.2$ te (b) $\sigma = 1.05$. Isprekidane linije u (a) odgovaraju gornjoj i donjoj granici prema izrazima (5.6) i (5.7) uz $c = l/L$ i $l = 1000$. Slika (b) prikazuje nastanak separacija faza za neki $50 < l < 100$ koji je nemoguće postivći u Monte Carlo simulacijama modela s neredom zbog činjenice da je $l \propto \ln L$.

Razlog takvog sporog približavanja asimptotskoj granici možemo objasniti na slijedeći način. Označimo "spora" mjesta s $i = L - l + 1, \ldots, L$. U dugodosežnom modelu s neredom izraz za struju glasi

$$j_i = \sum_{m=0}^{L-1} \sum_{m+n<L} p_{m+n} \langle \tau_{i-m}(1 - \tau_{i+n}) \rangle \delta^r_{i-m,i+n}, \tag{5.9}$$

gdje je $\tau_{j\pm L} = \tau_j$, $j = 1, \ldots, L$, a $\delta^r_{k,l}$ ovisi o tome da li par čvorova (k, l) sadrži barem jedan defekt ($\delta^r_{k,l} = r$) ili niti jedan ($\delta^r_{k,l} = 1$). Da bismo ocijenili struju, izabrat ćemo mjesto točno u sredini "spore" domene ($i = L - l/2 + 1$), te u izrazu

[4]Sporo približavanje termodinamičkoj granici opaženo je i u nekim drugim vođenim difuzijskim sustavima [155]

za struju primijeniti aproksimaciju srednjeg polja. Pretpostavimo profil gustoće u obliku domenskog zida,

$$\langle \tau_i \rangle = \begin{cases} \rho_i^x, & 1 \le i \le L-l \\ \rho_i^x, & L-l+1 \le i \le L, \end{cases} \tag{5.10}$$

gdje smo s x i y označili redom lokalne gustoće u domenama "brzih" (X) i "sporih" (Y) čvorova. Uvrstimo li (5.10) u izraz za struju (5.9) dobivamo četiri različita doprinosa struji, j_{xx}, j_{xy}, j_{yx} i j_{yy}, koji dolaze od izmjene čestica između domena X i Y. Obzirom da nas zanima samo koliko brzo struja opada s l, možemo iskoristiti da su $\rho_i^{\mathrm{x,y}} \le 1$, odakle slijedi

$$j_{\mathrm{xx}} < r(1 \cdot p_1 + 2 \cdot p_2 + \cdots + (l/2)p_{l/2}) \sim O(1) \tag{5.11a}$$

$$j_{\mathrm{xy}}, j_{\mathrm{yx}} < r(1 \cdot p_{l/2+1} + 2 \cdot p_{l/2+2} + \cdots + (l/2)p_l) \sim O(l^{-(\sigma-1)}) \tag{5.11b}$$

$$j_{\mathrm{yy}} < 1 \cdot p_{l+1} + 2 \cdot p_{l+2} + \cdots + l p_l \sim O(l^{-(\sigma-1)}), \tag{5.11c}$$

Iz gornjih izraza vidimo da korekcije na asimptotski izraz za struju opadaju vrlo sporo ukoliko je σ blizu 1. Time smo potvrdili da je nered u jednoj dimenziji i u termodinamičkoj granici $L \to \infty$ uvijek relevantan, jer stvara "sporu" domenu divergirajuće duljine. Takav je geometrijski uvjet, međutim, ograničen na jednu dimenziju, zbog čega u nastavku promatramo TASEP u dvije dimenzije.

5.3 Poopćenje na dvije dimenzije

TASEP u dvije dimenzije promatramo na rešetci s $L_x \times L_y$ čvorova i $N = \rho L_x L_y$ čestica, te periodičkim rubnim uvjetima u oba smjera. Sustav evoluira u vremenu nasumično-sekvencijalnom dinamikom na slijedeći način: u nekom trenutku t, nasumično izabrana čestica se pomiče na prazni susjedni čvor ili u smjeru polja s vjerojatnošću $p_{\parallel} = p_x$ ili okomito na smjer polja s vjerojatnošću $p_{\perp}$, pri čemu je $p_x + 2p_y = 1$. Drugim riječima, model odgovara TASEP-u $\hat{x}$ i SSEP-u $\hat{y}$ smjeru. Nered pritom uvodimo samo u smjeru polja tako što na nasumično izabranih cL_xL_y mjesta zabranjujemo preskoke u smjeru polja, što možemo zamisliti kao da smo prekinuli "kariku" između čvorova (i, j) i $(i+1, j)$ (slika 5.10).

TASEP u dvije dimenzije promatralo je nekoliko autora u različitim kontekstima. Ramaswamy i Barma [151, 152] su proučavali ASEP s vjerojatnostima preskoka $p_{\mathrm{gore}} = p_{\mathrm{udesno}} = w(1+g)$ i $p_{\mathrm{ulijevo}} = p_{\mathrm{dolje}} = w(1-g)$, gdje se nered uvodi prekidanjem karika u $\hat{x}$ i $\hat{y}$ smjeru. Rešetka koja se tako dobije kvalitativno je drugačija od naše, jer sadrži "grane" po kojima se čestice propagiraju suprotno od smjera polja, zbog čega struja u takvoj "grani" trne eksponencijalno s duljinom "grane". Saegusa *et al.* su promatrali TASEP s više paralelnih lanaca i statičkim preprekama [153], u kojem su našli zaravan u struji u ovisnosti u gustoći, tipičnu

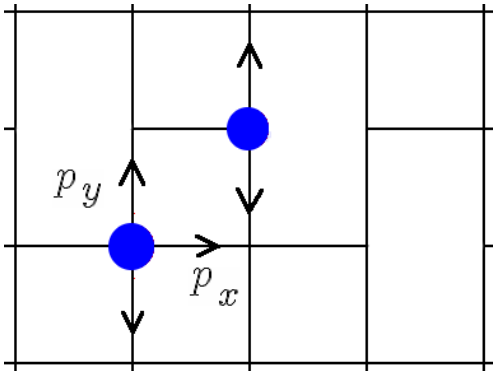

Slika 5.10: Slikoviti prikaz TASEP-a s neredom u dvije dimenzije. Nered je uveden kao nemogućnost čestica da se pomaknu udesno s nekih čvorova, što je na slici predstavljeno karikama koje nedostaju.

za pojavu separacije faza. Alexandar i Lebowitz su promatrali simetrični model u dvije dimenzije i jednim štapom duljine l usmjerenim duž $\hat{y}$ osi koji se kreće isto kao i druge čestice [156]. U slučaju štapa duljine $l = 1$ koji miruje oni su odredili profil gustoće u aproksimaciji srednjeg polje, te pokazali da se iza štapa stvara makroskopska domena niske gustoće. Naposljetku, slične makroskopske nehomogenosti u gustoći, ali koje nisu inducirane neredom, pronađene su i u drugim modelima vođenih difuzijskih sustava, npr. u [157].

5.3.1 Tipični rezultati Monte Carlo simulacija

5.3.1.1 Ovisnost struje o gustoći

Naš prvi zadatak je odrediti ovisnost struje o gustoći, koja se definira kao

$$j_x(\rho,\alpha)/L_y = \frac{1}{L_y}\sum_{j=1}^{L_y} p_x\langle\tau_{ij}(1-\tau_{i+1,j})\rangle\cdot\omega_{ij}(\alpha), \quad i=1,\ldots,L_x, \tag{5.12}$$

gdje je za neku konfiguraciju nereda α, $\omega_{ij}(\alpha) = 1$ ako karika koja spaja čvorove (i,j) i $(i+1,j)$ postoji, te $\omega_{ij}(\alpha) = 0$ ako ne postoji. Slika 5.11 prikazuje struju $j(\rho)$ dobivenu Monte Carlo simulacijama za različite koncentracije nereda c na 200×200 rešetci uz $p_x = 2p_y = 1/2$. Usporedimo li je sa strujom u čistom sustavu, $j(\rho) = p_x\rho(1-\rho)$, uočavamo zaravan oko $\rho = 1/2$, a u području bez zaravni paraboličnu ovisnost o ρ, $j(\rho) \propto \rho(1-\rho)$, s netrivijalnim faktorom koji ovisi o p_x i c. želimo li ocijeniti iznos maksimalne struje, naivni pokušaj bio bi $(1-c)p_x/4$, gdje je $1-c$ prosječni broj postojećih karika u stupcu. To, međutim, ne daje dobro slaganje pri većim koncentracijama, što se može vidjeti iz drugog stupca tablice 5.1. Ocjena se može popraviti ukoliko umjesto $1-c$ uvrstimo $\omega^*(\alpha)$, koji odgovara broju karika u stupcu s najmanje karika,

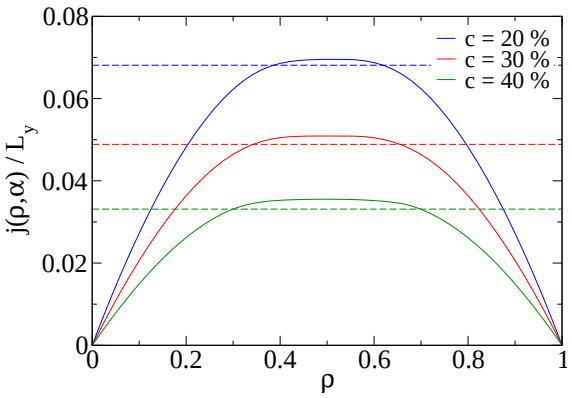

Slika 5.11: Ovisnost struje o gustoći za različite koncentracije nereda c na 200×200 rešetci i $p_x = 2p_x = 1/2$, dobivena Monte Carlo simulacijama ($t = 10^6$ MCS/site) za jednu realizaciju nereda. Isprekidane linije odgovaraju najboljoj ocjeni maksimalne struje danoj izrazom (5.21).

$$\omega^*(\alpha) \equiv \min_i \left\{ \sum_{j=1}^{L_y} \omega_{ij}(\alpha) \right\} = L_y - \max_i \left\{ \sum_{j=1}^{L_y} [1 - \omega_{ij}(\alpha)] \right\}, \tag{5.13}$$

Tablica 5.1: Iznosi maksimalne struje pri različitim koncentracijama nereda dobiveni Monte Carlo simulacijama ($L_x = L_y = 200$, $p_x = 2p_x = 1/2$, $t = 10^6$ MCS/site) i različitim ocjenama: naivnom ocjenom $(1-c)p_x/4$, iz izraza $\omega^*(\alpha)p_x/(4L_y)$ eksplicitnim brojanjem za zadanu konfiguraciju nereda, iz izraza $\overline{\omega}^* p_x/(4L_y)$ izračunatoga pomoću teorije ekstremnih vrijednosti i iz izraza (5.21), koji daje najbolju ocjenu.

c	Monte Carlo	$(1-c)p_x/4$	$\omega^*(\alpha)\cdot p_x/(4L_y)$	$\overline{\omega}^*\cdot p_x/(4L_y)$	izraz (5.21)
0.1	0.09255(5)	0.1125	0.10507	0.10313	0.09154
0.2	0.06953(7)	0.1000	0.09063	0.09010	0.06812
0.3	0.05089(2)	0.0875	0.07688	0.07615	0.04887
0.4	0.03553(5)	0.0750	0.06000	0.06287	0.03312

Umjesto eksplicitnog brojenja karika po stupcima za danu konfiguraciju nereda, za $L_x \gg 1$ umjesto ω^* možemo računati srednju vrijednost $\overline{\omega}^*$, koja se dobije usrednjavanjem po svim konfiguracijama nereda, koja se može izračunati iz matematičke teorije ekstremnih vrijednosti [148]. Obzirom da račun za $\overline{\omega}^*$ nismo uspjeli pronaći u literaturi, provodimo ga u dodatku A, a ovdje iznosimo samo konačni rezultat,

$$\overline{\omega}^* \approx L_y - a_{L_x}(c, L_y)\gamma - b_{L_x}(c, L_y), \tag{5.14}$$

gdje su $a_{L_x}(c, L_y)$ i $b_{L_x}(c, L_y)$ dani s

$$a_{L_x}(c, L_y) = \frac{2\sqrt{2c(1-c)L_y}}{L_x} \cdot \exp\left\{\left[\mathrm{erf}^{-1}\left(1 - \frac{2}{L_x}\right)\right]^2\right\}, \tag{5.15}$$

$$b_{L_x}(c, L_y) = cL_y + \sqrt{2c(1-c)L_y} \cdot \mathrm{erf}^{-1}\left(1 - \frac{2}{L_x}\right). \tag{5.16}$$

Za $L_x \gg 1$, Gaussova funkcija greške $\mathrm{erf}^{-1}(1-2/L_x)$ se može razviti oko $L_x \to \infty$,

$$\mathrm{erf}^{-1}\left(1 - \frac{2}{x}\right) \approx \left\{\frac{1}{2}\ln\left[\frac{x^2/2\pi}{\ln(x^2/2\pi)}\right]\right\}^{1/2}, \tag{5.17}$$

što daje pojednostavljene izraze,

$$a_{L_x}(c, L_y) \approx \left[\frac{4c(1-c)L_y}{2\pi \ln L_x - \pi \ln 2\pi}\right]^{1/2}, \tag{5.18}$$

$$b_{L_x}(c, L_y) \approx cL_y + \left\{c(1-c)L_y\left[\ln\left(\frac{L_x^2}{2\pi}\right) - \ln\ln\left(\frac{L_x^2}{2\pi}\right)\right]\right\}^{1/2}. \tag{5.19}$$

$$\tag{5.20}$$

Iako usporedba $\omega^*(\alpha)$ i $\overline{\omega}^*$, prikazana u tablici 5.1 za $L_x = L_y = 200$, opravdava ocjenu $\omega^*(\alpha)$ njezinom srednjom vrijednošću, ni $\omega^*(\alpha)$ ni $\overline{\omega}^*$ ne daju puno bolju ocjenu maksimalne struje. Najbolja ocjena, prikazana u posljednjem stupcu tablice 5.1, dobiva se ako prepoznamo da najveći doprinos struji dolazi od onih čvorova koji imaju ulaznu i izlaznu kariku. Obzirom da je vjerojatnost da čvor ima obje karike jednaka $(1-c)^2$, tj. $1-(1-c)^2 = 2c - c^2$ da barem jednu nema, dolazimo do slijedeće ocjene maksimalne struje,

$$\begin{aligned} \max_{\rho}\{j_x(\rho, \alpha)\}/L_y &\approx \frac{1}{L_y}\min_i\left\{\sum_{j=1}^{L_y}\omega_{i-1,j}(\alpha)\omega_{ij}(\alpha)\right\} \cdot \frac{p_x}{4} \approx \\ &\approx [L_y - a_{L_x}(2c-c^2, L_y)\gamma - b_{L_x}(2c-c^2, L_y)] \cdot p_x/(4L_y). \end{aligned} \tag{5.21}$$

Pritom treba naglasiti da točnost ove ocjene ovisi o p_x: što je p_x manji (tj. p_y veći), to je veća vjerojatnost da će čestica ući i izaći iz stupca na različitim čvorovima. U to se možemo uvjeriti slijedećim računom. Izaberimo jedan stupac i, te zapišimo jednadžbu za stacionarnu gustoću $\rho_j^{(i)}$ u aproksimaciji srednjeg polja,

$$\frac{d\rho_j^{(i)}}{dt} = 0 = p_y(\rho_i^{(j+1)} + \rho_i^{(j-1)} - 2\rho_i^{(j)}) + \tag{5.22}$$

$$+ p_x\omega_j^{(i-1)}(\alpha)\rho_{i-1}^{(j)}(1-\rho_i^{(j)}) - p_x\omega_j^{(i)}(\alpha)\rho_i^{(j)}(1-\rho_{i+1}^{(j)}). \tag{5.23}$$

gdje smo umjesto $\omega_{ij}(\alpha)$ uveli notaciju $\omega_j^{(i)}$. Primijetimo da ovako zapisana jednadžba odgovara jednadžbi srednjeg polja u jednodimenzionalnom jednostavnom *simetričnom* procesu isključenja u kojem sustav izmjenjuje čestice s vanjskim spremnikom na nasumično odabranim čvorovima s vjerojatnostima apsorpcije i desorpcije $p_x\omega_j^{(i-1)}\rho_j^{(i-1)})$ i $p_x\omega_j^{(i)}(1-\rho_j^{(i+1)})$. Obzirom da je proces simetričan, jednadžba je linearna u gustoći pa se može zapisati u matričnom obliku,

$$T^{(i)}\rho^{(i)} = -p_x b^{(i-1)}, \tag{5.24}$$

gdje je $b_j^{(i-1)} = -p_x\omega_j^{(i-1)}\rho_j^{(i-1)}$, a $T^{(i)}$ matrica oblika

$$T_{kl}^{(i)} = \begin{cases} d_k^{(i)} & k = l, \\ & k = l \pm 1, \\ p_y & k = 1, l = L, \\ & k = L, l = 1, \\ 0 & \text{ostalo} \end{cases} \tag{5.25}$$

uz

$$d_k^{(i)} = -[2p_y + p_x\omega_k^{(i-1)}\rho_k^{(i-1)} + p_x\omega_k^{(i)}(1-\rho_k^{(i+1)})]. \tag{5.26}$$

Formalnim zapisom rješenja gornjeg sustava $\rho^{(j)} = -p_x[T^{(i)}]^{-1}b^{(i-1)}$ za struju j se dobiva

$$\begin{aligned} j &= \frac{1}{L_y}\sum_{j=1}^{L_y} p_x\omega_j^{(i)}\rho_j^{(i)}(1-\rho_j^{(i+1)}) = \\ &= -\frac{p_x}{L_y}\sum_{k=1}^{L_y}\rho_k^{(i-1)}[T_{kl}^{(i)}]^{-1}[1-\rho_l^{(i+1)}]\omega_k^{(i-1)}\omega_l^{(i)}, \end{aligned} \tag{5.27}$$

u kojem prepoznajemo bilinearnu formu u varijablama nereda $\omega_k^{(i-1)}\omega_l^{(i)}$. Kako bi ocijenili težinski faktor uz $\omega_k^{(i-1)}\omega_l^{(i)}$, trebali bi odrediti inverz $[T^{(i)}]^{-1}$. To što nažalost nije moguće u zatvorenom obliku, osim ako ne pretpostavimo reflektirajuće rubne uvjete u $\hat{y}$ smjeru za koje vrijedi $T_{1L}^{(i)} = T_{L1}^{(i)} = 0$. U tom slučaju se može pokazati da nedijagonalni elementi u $[T_{kl}^{(i)}]^{-1}$ opadaju eksponencijalno u $|k-l|$ [158],

$$[T_{kl}^{(i)}]^{-1} \propto p_y^{|k-l|} = e^{-|k-l|/(-1/\ln p_y)} \tag{5.28}$$

što nam za dani p_y daje ocjenu relevantne udaljenosti između čvorova ulaska i izlaska čestica iz stupca. Na primjer, za $p_y = 0.25$, $-1/\ln p_y \approx 0.72$, što znači da čestice uglavnom izlaze na istom ili susjednom čvoru, kao što smo i pretpostavili u 5.21.

5.3.1.2 Profili gustoće

U prethodnom poglavlju smo opisali utjecaj nereda na struju. U ovom poglavlju opisujemo utjecaj nereda na stacionarne profile gustoće. Slika 5.12 prikazuje prostornu raspodjelu lokalne gustoće dobivenu Monte Carlo simulacijama za različite gustoće ρ, označenu nijansama plave ($\langle\tau_{ij}\rangle = 0$) i crvene ($\langle\tau_{ij}\rangle = 1$), pri čemu bijela označava srednju gustoću ρ. Sa slike je jasno vidljivo kako se povećanjem gustoće ρ u početku stvaraju lokalne nehomogenosti, koje oko $\rho = 0.4$ poprimaju dimenzije sustava. To je još očitije ukoliko nacrtamo histogram lokalne gustoće, koji pri niskim/visokim gustoćama ima tek jedan maksimum (slika 5.13a), dok za gustoće oko 1/2 ima dva istaknuta maksimuma (slika 5.13b). Da li je prijelaz iz jednog režima u drugi posljedica konačnosti sustava ili postoji i u termodinamičkoj granici nije jednostavno za utvrditi numeričkim simulacijama, jer smo ograničeni na male sustave. U nastavku zato promatramo anizotropnu granicu $p_x \to 0$, koju je moguće analizirati analitički i u kojoj ćemo pokazati da ovakvog prijelaza uopće nema, bez obzira na vrijednost koncentracije nereda.

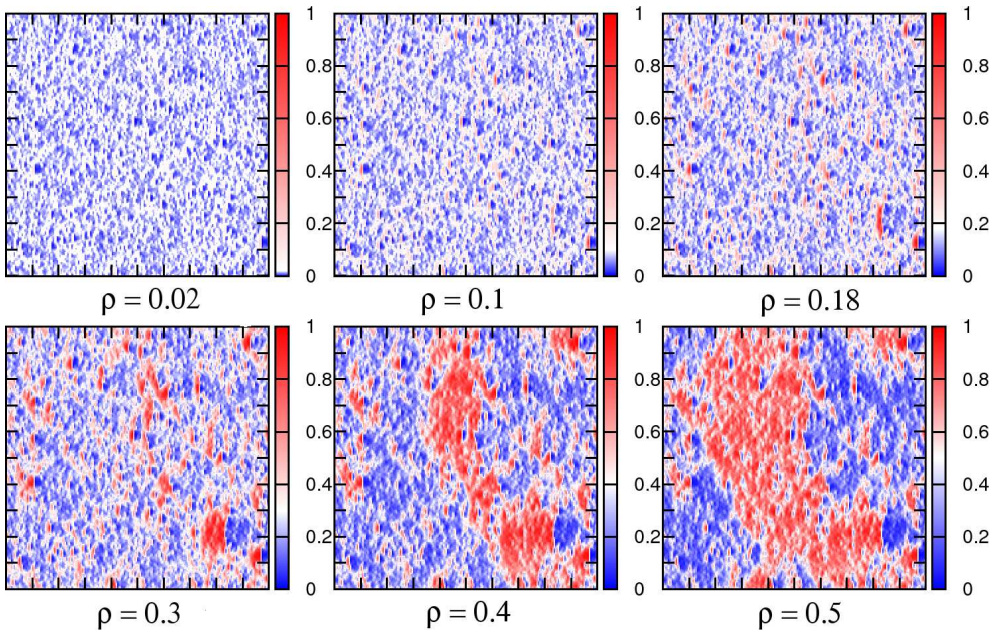

Slika 5.12: Raspodjela gustoće za različite ρ i koncentraciju nereda $c = 0.4$, dobivena Monte Carlo simulacijama ($L_x = L_y = 200$, $p_x = 2p_x = 1/2$, $t = 10^6$ MC koraka/čvoru) za jednu konfiguraciju nereda. Plava boja označava $\langle\tau_{ij}\rangle = 0$, bijela $\langle\tau_{ij}\rangle = \rho$, a crvena $\langle\tau_{ij}\rangle = 1$.

5.3.2 Aproksimacija srednjeg polja u granici $p_x \to 0$

U granici $p_x \to 0$, preskoci između stupaca su toliko rijetki u odnosu na preskoke unutar stupca da $n_i = \sum_{j=1}^{L_y}$ možemo uzeti kao sporu varijablu. Konfigura-

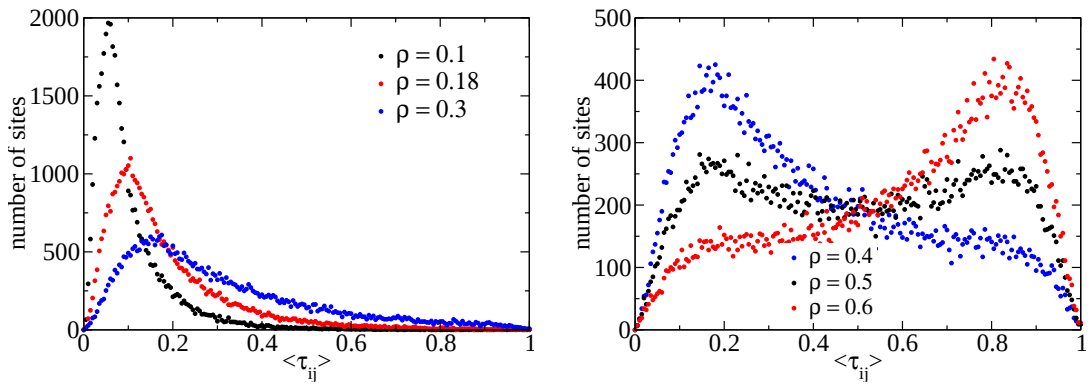

Slika 5.13: Histogram lokalne gustoće $\langle \tau_{ij} \rangle$ dobivene Monte Carlo simulacijama za jednu realizaciju nereda pri koncentraciji nereda $c = 0.4$ ($L_x = L_y = 200$, $p_x = 2p_x = 1/2$, $t = 10^6$ MC koraka/čvoru) koji prikazuje (a) jedan maksimum pri niskim/visokim gustoćama ρ i (b) dva maksimuma pri gustoćama oko $\rho = 1/2$.

ciju sustava tada možemo zapisati kao $C = \{n_i | i = 1, \ldots, L_x\}$, a evoluciju sustava opisati master jednadžbom

$$\frac{d}{dt}P(C,t) = \sum_i \left[W(C_+^{i,i+1} \to C) P(C_+^{i,i+1}, t) - W(C \to C_-^{i,i+1}) P(C,t) \right], \quad (5.29)$$

gdje je $C_\pm^{i,i+1} = \{n_1, \ldots, n_i \pm 1, n_{i+1} \mp 1, \ldots, n_{L_x}\}$. Obzirom da su preskoci između stupaca rijetki, možemo pretpostaviti da su čestice unutar stupca uvijek homogeno raspoređene, pa je vjerojatnost da se na nekom čvoru nalazi čestica jednaka n_i/L_y. Uz tu pretpostavku, brzine prijelaza W su oblika

$$W(C \to C_-^{i,i+1}) = p_x \cdot \left(\sum_{j=1}^{L_y} \omega_{ij} \right) \cdot \frac{n_i}{L_y} \cdot \left(1 - \frac{n_{i+1}}{L_y} \right), \quad (5.30)$$

$$W(C_+^{i,i+1} \to C) = p_x \cdot \left(\sum_{j=1}^{L_y} \omega_{ij} \right) \cdot \frac{n_i + 1}{L_y} \cdot \left(1 - \frac{n_{i+1} - 1}{L_y} \right), \quad (5.31)$$

gdje je $\omega_i \equiv \sum_{j=1}^{L_y} \omega_{ij}$. Na ovaj smo način reducirali početni dvodimenzionalni problem na jednodimenzionalni u kojem se nered javlja samo kroz ω_i. Jednodimenzionalni proces u kojem može biti više čestica na jednom čvoru, a vjerojatnosti preskoka ovise o broju čestica na čvorovima s kojeg i na koji se čestica pomiče zove se *mizantropski proces* [159].

Iz (5.29) i (5.31) se lako dobije jednadžba za srednji broj čestica n_i u stupcu i,

$$\frac{d}{dt}\langle n_i(t) \rangle = p_x \cdot \omega_{i-1} \cdot \left\langle \frac{n_{i-1}}{L_y} \cdot \left(1 - \frac{n_i}{L_y} \right) \right\rangle - p_x \cdot \omega_i \cdot \left\langle \frac{n_i}{L_y} \cdot \left(1 - \frac{n_{i+1}}{L_y} \right) \right\rangle. \quad (5.32)$$

Gornja se jednadžba pretvara u jednadžbu srednjeg polja u 1D dTASEP-u ukoliko zanemarimo korelacije, $\langle n_i n_{i+1}\rangle \approx \langle n_i\rangle\langle n_{i+1}\rangle$, te redefiniramo $\langle n_i\rangle \to \langle n_i\rangle/L_y \equiv \rho_i$ i $\omega_i \to \omega_i/L_y \equiv r_i$, što daje

$$\frac{d\rho_i}{dt} = p_x \cdot r_{i-1}\rho_{i-1}(1-\rho_i) - p_x \cdot r_i\rho_i(1-\rho_{i+1}), \tag{5.33}$$

gdje se r_i biraju prema binomnoj raspodjeli

$$P(n = r_i \cdot L_y) = \binom{L_y}{n}(1-c)^n c^{L_y-n}, \tag{5.34}$$

$$\{r_i\} = 1-c, \qquad \{r_i^2\} - \{r_i\}^2 = c(1-c)/L_y. \tag{5.35}$$

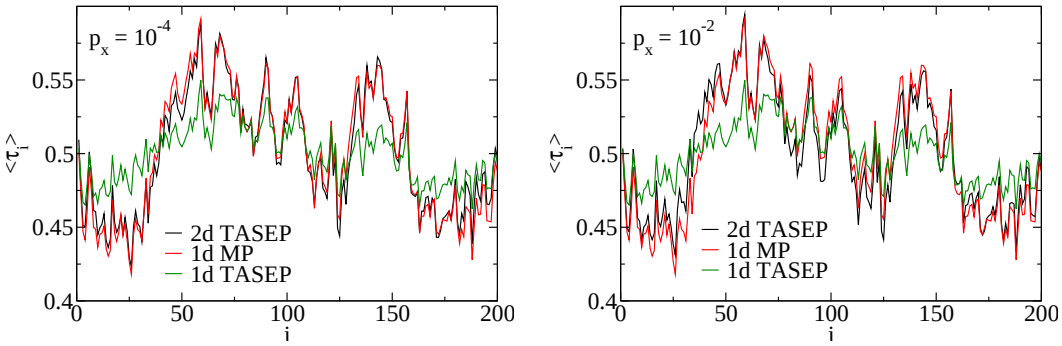

Slika 5.14: Usporedba stacionarnog profila gustoće $\langle\tau_i\rangle \equiv \sum_{j=1}^{L_y}\langle\tau_{ij}\rangle/L_y$ dobivenog iz Monte Carlo simulacija 2D TASEP-a za (a) $p_x = 10^{-4}$ i (b) $p_x = 10^{-2}$ ($L_x = L_y = 200$, $c = 0.2$, $\rho = 1/2$, $t = 10^6$ MC koraka/čvoru) i profila gustoće u ekvivalentnom 1D mizantropskom procesu (MP) i 1D dTASEP-u.

Slaganje mizantropskog procesa (5.29)-(5.31) s 2D TASEP-om provjerili smo tako što smo za zadanu konfiguraciju nereda konstruirali r_i, te u Monte Carlo simulacijama izabrali $p_x \ll 1$. Rezultati simulacija su prikazani na slikama 5.14a i 5.14b za $p_x = 10^{-4}$ i $p_x = 10^{-2}$, kojima smo pridodali rezultate 1D dTASEP-a s istim r_i. Sa slika uočavamo da mizantropski proces jako dobro opisuje 2D TASEP u granici malog p_x, dok 1D dTASEP pokazuje znatno manje varijacije. Povećamo li p_x, jasno je da će slika homogene raspodjele čestica unutar stupaca prestati vrijediti, pa se možemo pitati kako ocijeniti granični p_x. Gruba ocjena bi bila da usporedimo vrijeme relaksacije simetričnog 1D TASEP-a $\sim L_y^z$ s srednjim vremenom koji čestica provede u stupcu $\sim 1/p_x$. Kako je $z = 2$, to daje ocjenu $p_x \sim L_y^{-2}$, što bi za $L_y = 200$ dalo $p_x \sim 10^{-5}$, znatno manje nego što opažamo u simulacijama. Točna vrijednost graničnog p_x za koji još vrijede zaključci anizotropne granice ostavljamo kao otvoren problem i motivaciju za daljnja istraživanja.

Jednom kada smo reducirali originalni 2D problem s neredom na 1D problem u kojem nered reducira vjerojatnosti preskoka, možemo se pozvati na teoriju ekstremnih vrijednosti koja kaže da ćemo u tom slučaju u granici beskonačnog sustava uvijek moći naći beskonačni niz čvorova na kojima su r_i manji od neke ispodprosječne (ili iznadprosječne) vrijednosti $r_0 < 1-c$ (ili $r_0 > 1-c$). Drugim riječima, sve što trebamo napraviti je u izrazu (5.3) uvrstiti $p = P(r_i < r_0)$,

$$p = P(x < r_0) = \frac{1}{2}\left[1 + \mathrm{erf}\left(\frac{r_0 - \mu}{\sqrt{2\sigma^2}}\right)\right], \tag{5.36}$$

gdje smo binomnu raspodjelu aproksimirali Gaussovom (po Berry-Essenovom teoremu greška je reda $1/\sqrt{L_y}$) uz $\mu = 1-c$ i $\sigma^2 = c(1-c)/L_y$. Odavde slijedi da veličina "spore" domene u mizantropskom procesu divergira kao $\{l_{\max}\} \propto \ln L_x$, a samim time i da se u 2D TASEP-u neizbježno javlja separacija faza za *sve* p_x, obzirom da je zaobilaženje defekata najlakše upravo u granici $p_x \to 0$. Ovakav zaključak doista je ispravan ukoliko u granici $L_x \to \infty$ zadržimo *konačni* L_y (npr. TASEP s nekoliko paralelnih traka). No, ukoliko nas zanima pravi dvodimenzionalni problem, tj. granica $L_x \sim L_y \to \infty$, onda moramo biti oprezni jer tada $\sigma \to 0$. Izaberemo li $r_0 < \mu = 1-c$, tada Gaussovu funkciju greške možemo razvijati oko $-\infty$, pri čemu koristimo razvoj oko ∞,

$$\mathrm{erf}(x) = 1 - \frac{e^{-x^2}}{\sqrt{\pi}x}\left[1 - \frac{1}{2x^2} + \ldots\right], \quad x \to \infty. \tag{5.37}$$

i činjenicu da je $\mathrm{erf}(x)$ neparna funkcija, $\mathrm{erf}(x) = -\mathrm{erf}(-x)$. Konačni rezultat za nazivnik u (5.3) glasi

$$\ln(1/p) = \ln\left[\frac{2\sqrt{\pi}|r_0 - 1 + c|}{\sqrt{c(1-c)}}\right] + \frac{1}{2}\ln L_y + 2\frac{(r_0 - 1 + c)^2}{c(1-c)}L_y, \tag{5.38}$$

dok se za brojnik dobiva

$$\gamma + \ln[L_x(1-p)] \approx \gamma + \ln L_x + \sqrt{\frac{2}{\pi}}\frac{c(1-c)}{|r_0 - 1 + c|}\frac{1}{L_y}e^{-\frac{|r_0-1+c|^2}{2c(1-c)}L_y}. \tag{5.39}$$

Odavde vidimo da u granici $L_y \to \infty$ nazivnik raste brže od brojnika, pa $\{l_{\max}\}$ iščezava. Drugim riječima, u granici $p_x \to 0$ nered "uprosječuje sam sebe", pa argument u korist separacije faza zbog beskonačno velike domene "sporih" čvorova više ne vrijedi. U to se možemo uvjeriti ako za mali p_x pogledamo ovisnost struje o gustoći (slika 5.15a), te histogram profila gustoće za $\rho = 1/2$ (slika 5.15b). Na slici 5.15a ne uočavamo zaravan uobičajenu za separaciju faza, a sama struja slijedi

parabolički oblik $j(\rho) \propto \rho(1-\rho)$ s konstantom proporcionalnosti koja je blizu $1-c$. Također, histogram profila gustoće za $\rho = 1/2$, prikazan na slici 5.15b, pokazuje samo jedan maksimum.

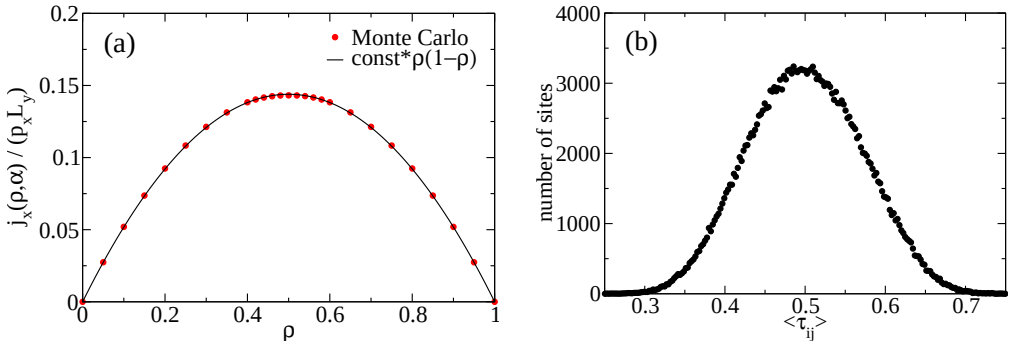

Slika 5.15: (a) Ovisnost struje o gustoći dobivena Monte Carlo simulacijama 2D TASEP-a za jednu konfiguraciju nereda pri koncentraciji $c = 0.4$ ($p_{\mathrm{x}} = 10^{-2}$, $L_{\mathrm{x}} = L_{\mathrm{y}} = 1000$ i $t = 10^5$ MC koraka/čvoru). Puna linija je prilagodba na izraz $j(\rho) = const. \times \rho(1-\rho)$ uz konstantnu $const. \approx 0.5756$, koja je blizu $1 - c = 0.6$. (b) Odgovarajući histogram profila gustoće za $\rho = 1/2$.

* * *

Prisutnost nereda u jednodimenzionalnom ASEP-u ima univerzalnu posljedicu: za dovoljno veliku struju, nered će uvijek inducirati separaciju faza, bez obzira na mikroskopske detalje nereda (oblik raspodjele vjerojatnosti preskoka, koncentraciju, itd.). U osnovi, razlog tome leži u činjenici da će nered uvijek proizvesti dugačku domenu s *jednakim*, ali reduciranim vjerojatnostima preskoka, koja će ograničiti struju na vrijednost manju od one koja bi se uspostavila da nereda nema. Jednom kad se ta vrijednost dostigne, daljnim porastom gustoće struja mora ostati nepromijenjena, što rezultira stvaranjem makroskopskog domenskog zida.

Univerzalnost ovog rezultata, koji vrijedi bez obzira na detalje nereda, u osnovi je geometrijske prirode: nered u jednoj dimenziji uvijek stvara dugačke domene sporo propusnih čvorova. To nas je motiviralo da istražimo mogućnost izbjegavanja separacije faza povećanjem povezanosti među čvorovima tako da čestice mogu zaobilaziti defektne čvorove [150]. Zaobilaženje defektnih čvorova izveli smo na dva načina: povećanjem dosega i dimenzionalnosti. U jednodimenzionalnom slučaju, pokazali smo da dugodosežni preskoci nisu dovoljni da se izbjegne separacija faza, pri čemu se separacija opaža tek u vrlo velikim sustavima, $\ln L \approx 50$. S druge strane, u dvodimenzionalnom slučaju smo jednostavnim argumentom pokazali upravo suprotno - izostanak separacije faza bez obzira na detalje nereda,

ali samo u anizotropnoj granici u kojoj je brzina kretanja čestica u smjeru polja puno manja od one u smjeru okomitom na polje. Naime, u toj granici se originalni 2d ASEP reducira na 1d proces sličan ASEP-u, s vjerojatnostima preskoka koje ovise o ukupnom broju defektnih čvorova u svakom stupcu, ali ne i njihovom rasporedu unutar stupca. Po središnjem graničnom teoremu, fluktuacije u broju defektnih mjesta po stupcu duljine L_y imaju standardnu devijaciju $\sim L_y^{-1/2}$, pa će za $L_y \to \infty$ biti nemoguće opaziti dugačku domenu "sporih" stupaca.

Kao potvrdu gornjih razmatranja, bilo bi zanimljivo pogledati utjecaj nereda na generalizaciju ASEP-a koja uključuje nekoliko lanaca koji međusobno izmjenjuju čestice. U tom slučaju gornji rezultat tvrdi da će za dovoljno jaku struju do separacije faza uvijek doći. Također, gornji rezultat koji isključuje mogućnost separacije faza u dvije dimenzije u anizotropnoj granici, može se u načelu primjeniti i u tri dimenzije, pretpostavimo li da nered ometa transport čestica samo u smjeru vanjskog polja. Otvorenim pitanjem pritom ostaje utvrditi režim parametara u kojem pretpostavka brze relaksacije fluktuacija gustoće u smjerovima okomitim na smjer polja više ne vrijedi.

6 Zaključak

Ogromni broj stupnjeva slobode, prisutan u svemu što nas okružuje, postavlja pred nas veliki izazov: kako razmatranjem mikroskopskih stupnjeva slobode objasniti makroskopska opažanja. Taj je program, barem u načelu, moguće provesti za sustave u termodinamičkoj ravnoteži, dok za sustave izvan ravnoteže ekvivalentne teorije, u toj općenitosti, još nema.

Jedno od najjednostavnijih neravnotežnih stanja su stacionarna stanja, koja se održavaju daleko od ravnoteže vanjskom silom i/ili neravnotežnim rubnim uvjetima. Nedostatak zaokružene teorije, čak i za stacionarna stanja, vraća nas proučavanju mikroskopskih modela, koji mogu imati dvije uloge: s jedne strane, to mogu biti vrlo složeni modeli s velikim brojem parametara, a s ciljem da se što vjernije objasni neka fizikalna pojava; nasuprot tome postavljaju se tzv. minimalni modeli, s malo parametara, za koje se vjeruje da sadrže tek nužne elemente, dostatne za kvalitativno razumijevanje općenitih principa.

U ovom radu proučavali smo jednostavni asimetrični proces isključenja (ASEP), minimalni model za transport (klasičnih) čestica koje se nalaze u vanjskom polju i međusobno osjećaju međudjelovanje "nultog" dosega, koje brani česticama da se približe jedna drugoj. Iako pojednostavljeno, ovakvo međudjelovanje opisuje niz realnih situacija, od zasjenjenih iona u superionskim vodičima do samovođenih čestica u mezoskopskim (ribosomi) i makroskopskim (pješaci, automobili) sustavima. S teorijske strane, ASEP je postao paradigma faznih prijelaza induciranih rubnim uvjetima i vođenih daleko od ravnoteže, koji se opažaju čak i u jednoj dimenziji.

U poglavlju 2 dali smo pregled najvažnijih dosadašnjih rezultata koji se tiču faznih prijelaza u jednodimenzionalnom potpuno asimetričnom modelu s otvorenim rubnim uvjetima. Lokalni, difuzijski karakter transporta u ASEP-u zamijenili smo u poglavlju 3 s dugodosežnim preskocima, čija vjerojatnost preskoka duljine l opada potencijski kao $p_l \sim l^{-(1+\sigma)}$, gdje je σ parametar dosega [107]. Promjenom difuzijskog karaktera transporta željeli smo istražiti univerzalnost faznih prijelaza u ASEP-u, koji su se pokazali robustnima na brojna poopćenja [78–82]. U slučaju jedne čestice, ovakvo kretanje odgovara Levyjevom nasumičnom gibanju i vodi na tzv. anomalnu difuziju [117].

Kratkodosežnim model naučio nas je koliko se toga može zaključiti samo iz hidrodinamičke jednadžbe, koja se kasnije može nadograđivati, npr. dinamikom domenskih zidova. To nas je motiviralo da potražimo hidrodinamičku jednadžbu i u dugodosežnom slučaju, koju smo izveli nerigorozno iz diskretnih jednadžbi u aproksimaciji srednjeg polja na beskonačnoj rešetci [108]. Pomalo iznenađujuće, konačni rezultat dao je istu hidrodinamičku (Burgersovu) jednadžbu, ali s nelokalnim (frakcionalnim) difuzijskim članom za $1 < \sigma < 2$ i lokalnim difuzijskim članom za $\sigma > 2$.

Dobivena hidrodinamička jednadžba dala nam je uvid u nekoliko stvari. Prvo, promjena režima na $\sigma = 2$ sugerira da kratkodosežna granica modela nastupa za $\sigma > 2$, što se potvrdilo kroz sve kasnije račune. Drugo, očekujemo da diskretni model naslijedi otprije poznata dinamička svojstva frakcionalno-viskozne jednadžbe, poput dinamičkog eksponenta koji opisuje relaksaciju k stacionarnom stanju. Doista, dinamički eksponent $z = \min\{\sigma, 3/2\}$, koji smo dobili Monte Carlo simulacijama iz vremenske korelacijske funkcije odstupanja gustoće od srednje vrijednosti za male pomake izvan stacionarnog stanja, $C(0,t) = \langle \delta\rho(0,0)\delta\rho(0,t)\rangle \sim t^{-1/z}$, jednak je otprije poznatoj vrijednosti dobivenoj iz teorijskih razmatranja metodama renormalizacijske grupe [126].

Uvođenje dugodosežnih preskoka u konačni sustav zahtjevalo je redefiniranje rubnih uvjeta, kako bi kretanje čestica u unutrašnjosti bilo kvalitativno isto onome blizu rubova. Novi rubni uvjeti, konzistentni s dugodosežnom prirodom preskoka, prirodno slijede ako zamislimo produžene spremnike, iste duljine kao i sustav. Sličan problem prirodno se javlja u definiciji rubnih uvjeta pri rješavanju diferencijalnih jednadžbi s frakcionalnim derivacijama na konačnim intervalima. Glavna novost ovakvih rubnih uvjeta je što se izmjena čestica sa spremnicima odvija na svim mjestima u sustavu, slično kao i u još jednom poopćenju, ASEP-u s Langmuirovom kinetikom [96].

Što se faznih prijelaza tiče, Monte Carlo simulacije na konačnom sustavu s otvorenim rubnim uvjetima pokazale su isti fazni dijagram kao i u kratkodosežnom slučaju, kao što bismo i naslutili iz sličnosti hidrodinamičkih jednadžbi, uz razlike na prijelazu prvog reda i u fazi maksimalne struje. Novost na prijelazu prvog reda je separacija faza za $1 < \sigma < 2$, koja se javlja zbog lokalizacije domenskog zida. U slici domenskog zida kao nasumičnog šetača, pokazuje se da nelokalni rubni uvjeti vode na problem nasumičnog šetača u vanjskom *potencijalu*, čiji globalni minimum, koji za $1 < \sigma < 2$ raste s veličinom sustava, naposljetku zarobljava domenski zid. Sličan mehanizam separacije faza opažen je i u ASEP-u s Langmuirovom kinetikom [96]. U fazi maksimalne struje i dalje se opaža potencijsko odstupanje gustoće od rubova, ali s eksponentom $(\sigma-1)/2$ za $1 < \sigma < 2$ i $1/2$ za $\sigma > 2$. σ-ovisni eksponent dobiven Monte Carlo simulacijama slijedi već iz hidrodinamičke jednadžbe, što sugerira da je aproksimacija srednjeg polja, za razliku od kratkodosežnog slučaja, u dugodosežnom slučaju dovoljna ne samo za opis faznog dijagrama, nego i za opis

faznih prijelaza.

Netrivijalno stacionarno stanje ne javlja se samo u kontaktu sa spremnicima. ASEP s periodičkim rubnim uvjetima, ali jednim defektnim čvorom, s kojeg se čestice pomiču s vjerojatnošću reduciranom za faktor r, poznati je i stari problem, koji još uvijek nije egzaktno riješen [59,132]. Poznato je da takav defekt u ASEP-u inducira globalnu, makroskopsku separaciju faza, ali je neriješenim ostalo pitanje dogodi li se globalna promjena uvijek, za sve "jakosti" defekta [143]. Naš doprinos tom problemu je eksplicitni, analitički dokaz promjene režima iz separirane u homogenu fazu u modificiranom, dugodosežnom modelu u kojem se defekt uvodi kao čvor na rešetci koji ne sudjeluje u dinamici, ali usporava čestice time što ga moraju preskočiti [131]. Iako smo rezultat dobili u modelu koji je u mnogome sličan kratkodosežnom, ali ipak esencijalno dugodosežan, ovim primjerom smo pokazali da je takav prijelaz ipak u načelu moguć. Vrijedi spomenuti da je postojanje netrivijalnog prijelaza nedavno demonstrirano i u modelu rasta površine u prisustvu linijskog defekta [134].

Za razliku od *jednog* defekta, Tripathy i Barma [102] su pokazali da će, za dovoljno veliku struju, prisutnost *punog* nereda u kratkodosežnom ASEP-u u jednoj dimenziji uvijek inducirati separaciju faza, bez obzira na mikroskopske detalje nereda (oblik raspodjele vjerojatnosti preskoka, koncentraciju, itd.). U osnovi, razlog tome leži u činjenici da će nered uvijek proizvesti dugačku domenu *jednakih*, ali reduciranih vjerojatnosti preskoka, koje će ograničiti struju na maksimalnu struju koja se može uspostaviti u toj domeni. Jednom kad se ta maksimalna vrijednost dostigne, daljnim porastom gustoće struja mora ostati nepromijenjena, što rezultira stvaranjem makroskopskog domenskog zida. Univerzalnost ovog rezultata, koji vrijedi bez obzira na detalje nereda, u osnovi je geometrijske prirode: nered u jednoj dimenziji uvijek stvara dugačke domene sporo propusnih čvorova. U poglavlju 5 istražili smo robustnost ovog rezultata u slučaju da povećamo povezanost među čvorovima, kako bi čestice lakše zaobilazile defektne čvorove [150]. Konkretno, promatrali smo dvije takve geometrije: jednodimenzionalnu rešetku s dugodosežnim preskocima i dvodimenzionalnu rešetku s kratkodosežnim preskocima. U dvodimenzionalnom slučaju nered je postavljen samo u smjeru polja, tako da čestice mogu zaobići defektna mjesta kretanjem u smjeru okomitom na smjer polja. Zaključak je slijedeći: bez obzira na dugodosežnost preskoka, geometrijski razlog uvijek će pobijediti u jednoj dimenziji, ali ne nužno i u dvije dimenzije. Naime, transport čestica u 2d neuređenoj matrici postaje efektivno 1d u anizotropnoj granici u kojoj je brzina kretanja čestica u smjeru polja puno manja od one u smjeru okomitom na polje. Razlog tome je što se u toj granici čestice puno brže raspoređuju unutar stupca (okomitog na smjer polja), nego što se kreću od stupca do stupca. Konfiguraciju 2d sustava moguće je stoga opisati ukupnim brojem čestica u svakom stupcu, kao da se radi o kutijama. Vjerojatnosti preskoka čestica iz jedne kutije u drugu ovisiti će pritom samo o ukupnom broju defektnih čvorova

u svakom stupcu, ali ne i njihovom rasporedu unutar stupca. To, međutim, ne znači da je će, jednom kad smo problem sveli na 1d, separacije faza uvijek biti. Naime, po središnjem graničnom teoremu, fluktuacije u broju defektnih mjesta po stupcu duljine L_y imaju standardnu devijaciju $\sim L_y^{-1/2}$, pa će za $L_y \to \infty$ biti nemoguće opaziti dugačku domenu "sporih" stupaca. U toj granici smo, dakle, dobili upravo suprotan rezultat: separacija faza nije moguća, bez obzira na detalje nereda! Otvorenim pitanjem pritom ostaje pronaći vjerojatnosti preskoka za koje anizotropna granica prestaje vrijedi, te mehanizam separacije u tom slučaju. Također, zanimljivom se čini mogućnost eksperimentalne provjere ovih rezultata u nedavno proučavanim mikrofluidicima na dvodimenzionalnim geometrijama [154].

A

Statistika ekstremnih vrijednosti

Označimo s X_i ukupan broj prekinutih karika u i-tom stupcu, $X_i = \sum_{j=1}^{L_y}(1 - \omega_{ij})$. Ako karike uklanjamo nasumično s vjerojatnošću c, tada je raspodjela od X_i binomna

$$P(X_i = n) = \binom{L_y}{n} c^n (1-c)^{L_y - n}. \tag{A.1}$$

Neka je $F(x) = P(x < X)$ odgovarajuća kumulativna raspodjela, a $x^* = sup\{x : F(x) < 1\}$. Zanima nas maksimalna vrijednost od $\{X_1, \ldots, X_{L_x}\}$ kada $L_x \to \infty$,

$$max\{X_1, \ldots, X_{L_x}\} \xrightarrow{P} x^*, \tag{A.2}$$

gdje $\to^P$ označava konvergenciju u vjerojatnosti u slijedećem smislu. Naime, kako su X_i nezavisne, vjerojatnost da u svih m pokušaja dobijemo X_i manje od nekog x jednaka je $P(max\{X_1, \ldots, X_m\} \leq x) = F^m(x)$. U granici $m \to \infty$, ta je raspodjela degenerirana, jer konvergira ili u 0 za $x < x^*$ ili u 1 za $x \geq x^*$. Zbog toga tražimo niz realnih brojeva $a_n > 0$ i b_m takvih da $lim_{m\to\infty} F^m(a_m x + b_m) = G(x)$ postoji, gdje se $G(x)$ zove raspodjela ekstremnih vrijednosti. Dovoljan uvjet da $G(x)$ postoji sadržan je u von Misesovom uvjetu [148], koji kaže da ako $F''(x)$ postoji i $F'(x) > 0$ za $x < x^*$, tada

$$\lim_{m\to\infty} F^m(a_m x + b_m) = \exp\left[-(1+\gamma' x)^{-1/\gamma'}\right], \quad 1 + \gamma' x > 0, \tag{A.3}$$

gdje je γ' dan s

$$\lim_{t\to x^{*+}} \left(\frac{[1-F(t)]F''(t)}{[F'(t)]^2} \right) = -\gamma' - 1. \tag{A.4}$$

Brojevi a_m i b_m pritom poprimaju vrijednosti $a_m = mU'(m)$ i $b_m = U(m)$, gdje je $U(m)$ inverzna funkcija od $1/(1 - F(x))$. Za $\gamma' = 0$, desna strana od (A.3) se tumači kao $\exp(-e^{-x})$.

Da bismo primijenili gornji kriterij, aproksimirati ćemo binomnu raspodjelu Gaussovom raspodjelom, $N(\mu, \sigma^2)$, gdje je $\mu = cL_y$ i $\sigma^2 = L_y c(1-c)$. To nije

velika greška, jer je prema Barry-Essenovom teoremu razlika u kumulativnim raspodjelama reda $1/\sqrt{L_y}$, a $L_y \gg 1$. Kumulativna raspodjela Gaussove raspodjele je dana s

$$F(x) = \frac{1}{2}\left[1 + \mathrm{erf}\left(\frac{x-\mu}{\sqrt{2\sigma^2}}\right)\right], \tag{A.5}$$

gdje je $\mathrm{erf}(x)$ Gaussova funkcija greške,

$$\mathrm{erf}(x) = \frac{2}{\sqrt{\pi}}\int_0^x e^{-t^2}dt. \tag{A.6}$$

Iz definicije funkcije $U(x)$

$$\frac{1}{1-F(U(x))} = x \tag{A.7}$$

slijedi da je

$$U(x) = F^{-1}(1-1/x) \tag{A.8}$$

pri čemu je domena od $U(x)$ $x \geq 1$. Inverz kumulativne raspodjele $F(y)$ može se dalje izraziti preko tzv. kvantilne funkcije $\Phi(y)$

$$F^{-1}(y) = \mu + \sigma \cdot \Phi(y), \quad \Phi(y) = \sqrt{2}erf^{-1}(2y-1) \tag{A.9}$$

odakle naposljetku slijedi izraz za $U(x)$

$$U(x) = \mu + \sqrt{2\sigma^2}\cdot \mathrm{erf}^{-1}\left(1-\frac{2}{x}\right), \quad x \geq 1. \tag{A.10}$$

Prva i druga derivacija kumulativne raspodjele dane su izrazima

$$F'(x) = P(x) = \frac{1}{\sqrt{2\pi\sigma^2}}e^{-\frac{(x-\mu)^2}{2\sigma^2}} \tag{A.11}$$

$$F''(x) = -\frac{x-\mu}{\sigma^2}P(x), \tag{A.12}$$

odakle se uvrštavanjem u (A.4) nakon sređivanja dobiva $\gamma' = 0$, što odgovara Gumbelovoj raspodjeli $G(x) = \exp(-e^{-x})$. Srednja vrijednost i varijanca Gumbelove raspodjele jednake su redom $\gamma = 0.5772\ldots$ i $\pi^2/6$, što daje srednju vrijednost i varijancu početne varijable x^*,

$$\langle x^* \rangle = a_{L_x}\gamma + b_{L_x}, \tag{A.13}$$

$$\langle x^{*2} \rangle - \langle x^* \rangle^2 = \frac{a_{L_x}^2\pi^2}{6}, \tag{A.14}$$

gdje su a_{L_x} i b_{L_x} dani s

$$a_{L_x}(c, L_y) = \frac{2\sqrt{2c(1-c)L_y}}{L_x}\cdot \exp\left\{\left[\mathrm{erf}^{-1}\left(1-\frac{2}{L_x}\right)\right]^2\right\}, \tag{A.15}$$

$$b_{L_x}(c, L_y) = cL_y + \sqrt{2c(1-c)L_y} \cdot \mathrm{erf}^{-1}\left(1 - \frac{2}{L_x}\right). \tag{A.16}$$

Za $L_x \gg 1$, $\mathrm{erf}^{-1}(1 - 2/L_x)$ se može razvijati oko $L_x \to \infty$, čime se gornji izrazi dodatno pojednostavljuju,

$$a_{L_x}(c, L_y) \approx \left[\frac{4c(1-c)L_y}{2\pi \ln L_x - \pi \ln 2\pi}\right]^{1/2}, \tag{A.17}$$

$$b_{L_x}(c, L_y) \approx cL_y + \left\{c(1-c)L_y\left[\ln\left(\frac{L_x^2}{2\pi}\right) - \ln\ln\left(\frac{L_x^2}{2\pi}\right)\right]\right\}^{1/2}. \tag{A.18}$$

Popis literature

[1] B. Schmittmann i R.K.P. Zia, *Statistical mechanics of driven diffusive systems* in *Phase Transtions i Critical Phenomena*, Ed. C. Domb i J.L. Lebowitz (Academic Press, San Diego, 1995)

[2] G.M. Schütz, *Exactly Solvable Models for Many-Body Systems Far From Equilibrium* in *Phase Transtions i Critical Phenomena*, Ed. C. Domb i J.L. Lebowitz (Academic Press, San Diego, 2001)

[3] B. Derrida, E. Domany i D. Mukamel, *J. Stat. Phys.* **69**, 667 (1992)

[4] G.M. Schütz i E. Domany, *J. Stat. Phys.* **72**, 109 (1993)

[5] B. Derrida, M.R. Evans, V. Hakim i V. Pasquier, *J. Phys. A* **26**, 1493 (1993)

[6] L.E. Reichl, *A Modern Course in Statistical Physics* (Wiley, New York, 1998)

[7] S.R. de Groot i P. Mazur, *Non-Equilibrium Thermodynamics* (Dover, New York, 1984)

[8] G. Gallavotti, *Statistical Mechanics: A Short Treatise* (Springer-Verlag, Berlin, 1999)

[9] G. Ódor, *Rev. Mod. Phys.* **76**, 663 (2004)

[10] H. E. Stanley, *Introduction to Phase Transitions i Critical Phenomena* (Oxford University Press, New York, 1987)

[11] K.G. Wilson, *Phys. Rev. B* **4**, 3174-3183 (1971)

[12] L. Onsager, *Phys. Rev.* **65**, 117-149 (1944)

[13] J. Krug, *Phys. Rev. Lett.* **67**, 1882 (1991)

[14] R. Peierls, *Proc. Cambridge Phil. Soc.* **32**, 477 (1936)

[15] S. Katz, J.L. Lebowitz i H. Spohn, *J. Stat. Phys.* **34**, 497-537 (1984)

[16] W. Dietrich, P. Fulde, i I. Peschel, *Adv. Phys.* **29**, 527 (1980)

[17] D.P. Landau i K. Binder, *Monte Carlo Simulations in Statistical Physics* (Cambridge University press, New York, 2000)

[18] A. Schadschneider, D. Chowdhury i K. Nishinari, *Stochastic Transport in Complex Systems: From Molecules to Vehicles* (Elsevier, Amsterdam, 2010)

[19] I. Prigogine, *The arrow of Time* u *The Chaotic Universe: Proceedings of the Second ICRA Network Workshop*, Advanced Series in Astrophysics i Cosmology, vol.10, ur. V. G. Gurzadyan i R. Ruffini (World Scientific, Singapur, 2000)

[20] J.L. Lebowitz, *Rev. Mod. Phys.* **71**, S346-S357 (1999)

[21] D.J. Evans, E.G.D. Cohen i G.P. Morriss, *Phys. Rev. Lett.* **71**, 2401 (1993)

[22] D. Evans i D. Searles, *Phys. Rev. E* **50**, 1645 (1994)

[23] G. Gallavotti i E.G.D. Cohen, *Phys. Rev. Lett.* **74**, 2694 (1995);
G. Gallavotti i E.G.D. Cohen, *J. Stat. Phys.* **80**, 931 (1995)

[24] J. Kurchan, *J. Phys. A* **31**, 3719 (1998)

[25] J.L. Lebowitz i H. Spohn, *J. Stat. Phys.* **95**, 333 (1999)

[26] E.D.G Cohen i G. Gallavotti, *J. Stat. Phys.* **96**, 1343-1349 (1999)

[27] O.G. Jepps i L. Rondoni, *J. Phys. A: Math. Theor.* **43** 133001 (2010)

[28] O. Penrose, *The Direction of Time* u *Chance in Physics: Foundations i Perspectives*, ur. J. Bricmont, D. Dürr, M.C. Galavotti, G. Ghirardi, F. Petruccione i N. Zanghi (Springer-Verlag, Berlin, 2002)

[29] C. Jarzynski, *Phys. Rev. Lett.* **78**, 2690-2693 (1997)

[30] R.J. Harris i G.M. Schütz, *J. Stat. Mech.* P07020 (2007)

[31] L.D. Landau i E.M. Lifshitz, *Statistical Physics* (Pergamon Press, Oxford, 1990)

[32] C. Bustamante, J. Liphardt i F. Ritort, *Physics Today* **58**, 43-48 (2005)

[33] D. Ruelle, *Physics Today* **57**, 48-53 (2004)

[34] A. Einstein, *Ann. d. Phys.* **17**, 549 (1905)

[35] P. Langevin, *C. R. Acad. Sci. Paris* **146**, 530 (1908)

[36] L. Onsager, *Phys. Rev.* **37**, 405-426 (1931)

[37] L. Onsager i S. Machlup, *Phys. Rev.* **91**, 1505-1512 (1953)

[38] H.B. Callen i T.A. Welton, *Phys. Rev.* **83**, 34 (1951)

[39] H.B. Callen i R.F. Greene, *Phys. Rev.* **86**, 702 (1952)

[40] R. Kubo, *Rep. Prog. Phys.* **29**, 255 (1966)

[41] M. Baiesi, C. Maes i B. Wynants, *Phys. Rev. Lett.* **103**, 010602 (2009)

[42] B. Schmittmann i R.K.P Zia, *Phys. Rep.* **301**, 45-64 (1998)

[43] J. Marro, *Nonequilibrium Phase Transitions in Lattice Models* (Cambridge University Press, Cambridge, 1999)

[44] G. Grinstein, *J. App. Phys.* **69**, 5441 (1991)

[45] C.T. MacDonald, J.H. Gibbs i Pipkin, *Biopolymers* **6**, 1 (1968)

[46] C.T. MacDonald i J.H. Gibbs, *Biopolymers* **7**, 707 (1969)

[47] F. Spitzer, *Adv. Math* **5**, 246 (1970)

[48] L. Bertini, A. De Sole, D. Gabrielli, G. Jona-Lasinio i C. Landim, *J. Stat. Phys.* **135** 857-72 (2009)

[49] V.B. Priezzhev, *Phys. Rev. Lett.* **91**, 050601 (2003)

[50] L-H. Gwa i H. Spohn, *Phys. Rev. A* **46**, 844 (1992)

[51] J. de Gier i F.H.L. Essler, *Phys. Rev. Lett.* **95**, 240601 (2005)

[52] J. de Gier i F.H.L. Essler, *J. Stat. Mech.* P12011 (2006)

[53] M.R. Evans i T. Hanney, *J. Phys. A: Math. Gen.* 38, R195 (2005)

[54] D. van der Meer, K. van der Weele i D. Lohse, *Phys. Rev. Lett.* **88**, 174302 (2002)

[55] K. Nagel i M. Schreckenberg, *J. Phys. I* **2**, 2221 (1992)

[56] D. Chowdhury, L. Santen i A. Schadschneider, *Phys. Rep.* **329**, 199-329 (2000)

[57] V. Popkov, L. Santen, A. Schadschneider i G.M. Schütz, *J. Phys. A:Math. Gen.* **34**, L45 (2001)

[58] N. H. Barton *et al.*, *Evolution* (Cold Spring Harbor Laboratory Press, 2007)

[59] S.A. Janowsky i J.L. Lebowitz, *Phys. Rev. A* **45**, 618 (1992)

[60] T. Chou i G. Lakatos, *Phys. Rev. Lett.* **93**, 198101 (2004)

[61] J.J. Dong, B. Schmittmann i R.K.P. Zia, *Phys. Rev. E* **76**, 051113 (2007)

[62] J.J. Dong, B. Schmittmann i R.K.P. Zia, *J. Stat. Phys.* **128**, 21 (2007)

[63] J.J. Dong, R.K.P. Zia i B. Schmittmann, *J. Phys. A: Math. Gen.* **42**, 015002 (2009)

[64] M. Ebrahim Foulaadvand, A.B. Kolomeisky i H. Teymouri, *Phys. Rev. E 78*, 061116 (2008)

[65] R.K.P. Zia, J.J. Dong i B. Schmittmann, *J. Stat. Phys.* **128**, 21 (2007)

[66] P. Meakin, P. Ramanlal, L.M. Sander i R.C. Ball, *Phys. Rev. A* **34**, 5091 (1986)

[67] S.-C. Park, D. Kim i J.-M. Park, *Phys. Rev. E* **65**, 015102 (2002)

[68] M. Kardar, G. Parisi Y.-C. Zhang, *Phys. Rev. Lett* **56**, 889 (1986)

[69] M.J. Lighthill i G.B. Whitham, *Proc. R. Soc. London* Ser. A **229**, 281 (1955)

[70] P. D. Lax, *Hyperbolic Systems of Conservation Laws i the Mathematical Theory of Shock Waves* (SIAM, New York, 1973)

[71] P.G. Drazin i R.S. Johnson, *Solitons: An Introduction* (Cambridge University Press, New York, 1989)

[72] A.B. Kolomeisky, G.M. Schütz, E.B. Kolomeisky i J.P. Straley, *J. Phys. A: Math. Gen.* **31**, 6911 (1998)

[73] L. Santen i C. Appert, *J. Stat. Phys.* **106**, 187 (2002)

[74] B. Derrida, S. A. Janowsky, J. L. Lebowitz i E. R. Speer, *J. Stat. Phys.* **73**, 813-842 (1993)

[75] J.S. Hager, J. Krug, V. Popkov i G.M. Schütz, *Phys. Rev. E* **63**, 056110 (2001)

[76] J. Krug *Advances in Physics* **46**, 139 (1997)

[77] H.K. Janssen i K. Oerding, *Phys. Rev. E* **53**, 4544 (1996)

[78] T. Sasamoto, *J. Phys. Soc. Jpn.*, **69**, 1055 (2000)

[79] M.R. Evans, N. Rajewski i E.R. Speer, *J. Stat. Phys.* **95**, 45 (1999)

[80] J. de Gier i B. Nienhuis, *Phys. Rev. E* **59**, 4899 (1999)

[81] R. Juhász i L. Santen, *J. Phys. A: Math. Gen.* **37**, 3933 (2004)

[82] M. Bengrine et al., *J. Phys. A: Math. Gen.* **32**, 2527 (1999)

[83] V. Popkov i G.M. Schütz, *J. Stat. Phys.* **112**, 523-540 (2003)

[84] V. Popkov, *J. Phys. A: Math. Gen.* **37**, 1545 (2004)

[85] E. Pronina i A.B. Kolomeisky, *J. Phys. A: Math. Gen.* **37**, 9907 (2004)

[86] J. Brankov, N. Pesheva i N. Bunzarova, *Phys. Rev. E* **69**, 066128 (2004)

[87] E. Pronina i A.B. Kolomeisky, *J. Stat. Mech.* P07010 (2005)

[88] K. Mallick, *J. Phys. A: Math. Gen.* **29**, 5375 (1996)

[89] H.-W. Lee, V. Popkov i D. Kim, *J. Phys. A: Math. Gen.* **30** 8497 (1997)

[90] M.R. Evans, *Europhys. Lett.* **36**, 13 (1996)

[91] J. Krug i P.A. Ferrari, *J. Phys. A: Math. Gen.* **29**, L465-71 (1996)

[92] V. Karimipour, *Europhys. Lett.* **47**, 304 (1999)

[93] T. Antal i G.M. Schütz, *Phys. Rev. E* **62**, 83-93 (2000)

[94] G. Lakatos i T. Chou, *J. Phys. A: Math. Gen.* **36**, 2027 (2003)

[95] L.B. Shaw, R.K.P. Zia i K.H. Lee, *Phys. Rev. E* **68**, 021910 (2003)

[96] A. Parmeggiani, T. Franosch i E. Frey, *Phys. Rev. Lett.* **90**, 086601 (2003)

[97] T. Reichenbach, T. Franosch i E. Frey, *Phys. Rev. Lett.* **97**, 050603 (2006)

[98] A. Alberts et al. *The Molecular Biology of the Cell* (Garland, New York, 1994)

[99] M.R. Evans, R. Juhász i L. Santen, *Phys. Rev. E* **68**, 026117 (2003)

[100] A. Rakoś, M. Paessens i G.M. Schütz, *Phys. Rev. Lett.* **91**, 238302 (2003)

[101] D.E. Wolf i L.-H. Tang, *Phys. Rev. Lett.* **65**, 1591-1594 (1990)

[102] G. Tripathy M. Barma, *Phys. Rev. Lett.* **78**, 3039-42 (1997)

[103] G. Tripathy i M. Barma, *Phys. Rev. E.* **58**, 1911–26 (1998)

[104] R. J. Harris i R.B. Stinchcombe, *Phys. Rev. E.* **70**, 016108 (2004)

[105] P. Pfeuty i G. Toulouse, *Introduction to the Renormalization Group i to Critical Phenomena* (John Wiley & Sons, Inc., New York, 1977)

[106] F. J. Dyson, *Commun. Math. Phys.* **12**, 91 (1969)

[107] J. Szavits-Nossan i K. Uzelac, *Phys. Rev. E* **74**, 051104 (2006)

[108] J. Szavits-Nossan i K. Uzelac, *Phys. Rev. E* **77**, 051116 (2008)

[109] B. Derrida, *J. Stat. Mech.* P07023 (2007)

[110] G.M. Schütz, R. Ramaswamy i M. Barma, *J. Phys. A: Math. Gen.* **29** 837 (1996)

[111] A. Benassi i J.-P. Fouque, *Ann. Prob.*, **15** 546 (1987)

[112] F. Rezakhanlou, *Comm. Math. Phys.* **140**, 417 (1991)

[113] M. D. Jara, *Comm. Pure Appl. Math.* **62**, 198-214 (2009)

[114] S.G. Samko, A.A. Kilbas i O.I. Marichev, *Fractional Integrals i Derivatives* (Yverdon, Switzerland, Gordon i Breach, 1993)

[115] P.L. Butzer i U. Westphal, *An Introduction to Fractional Calculus* u *Applications of fractional calculus*, Ed. R. Hilfer (World Scientific, Singapore, 2000)

[116] K. Miller i B. Ross, *An Introduction to the Fractional Calculus i Fractional Differential Equations* (John Wiley & Sons, Inc., New York, 1993)

[117] R. Metzler i J. Klafter, *J. Phys. A* **37**, R161-R208 (2004)

[118] R. Hilfer (Ed.), *Applications of fractional calculus*, (World Scientific, Singapore, 2000)

[119] L. Debnath, *Int. J. Math. Math. Sci.* **2003**(54), 3413-3442 (2003)

[120] V.E. Tarasov, *J. Phys. A: Math. Gen.* **39**, 14895 (2006)

[121] J.E. Robinson, *Phys. Rev.* **83**, 678 (1951)

[122] J. Droniou, *Electronic Journal of Differential Equations* **117**, 1 (2003)

[123] D. Kim, *Phys. Rev. E* **52**, 3512 (1995)

[124] M. Henkel i G. Schütz, *Physica A* **206**, 187-195 (1994)

[125] J.A. Mann i W.A. Woyczynski, *Physica A* **291**, 159 (2001)

[126] E. Katzav, *Phys. Rev. E* **68**, 031607 (2003)

[127] A.D. Riggs, S. Bourgeois i M. Cohn, *J. Mol. Biol.* **53** 401-17 (1970)

[128] L. Mirny et al., *J. Phys. A: Math. Gen.* **42** 434013 (2009)

[129] M.A. Lomholt, T. Ambjörnsson i R. Metzler, *Phys. Rev. Lett.* **95**, 260603 (2005)

[130] B. Duplantier, *J. Stat. Phys.* **54**, 581 (1989)

[131] J. Szavits-Nossan i K. Uzelac, *J. Stat. Mech.* P12019 (2009)

[132] S.A. Janowsky i J.L. Lebowitz, *J. Stat. Phys.* **77**, 35 (1994)

[133] D. Kandel i D. Mukamel *Europhys. Lett.* **20**, 325 (1992)

[134] V. Beffara, V. Sidoravicius i M. Eulalia Vares, *Probab. Th. Rel. Fields* **147**, 565-581 (2009)

[135] D.A. Huse, C. Henley i D.S. Fisher, *Phys. Rev. Lett.* **55**, 2924-2924 (1985)

[136] L.H. Tang i I.F. Lyuksyutov, *Phys. Rev. Lett.* **71**, 2745 (1993)

[137] L. Balents i M. Kardar, *Europhys. Lett.* **23**, 503 (1993)

[138] L. Balents i M. Kardar, *Phys. Rev. B* **49**, 13030 (1994)

[139] T. Hwa i T. Nattermann, *Phys. Rev. B* **51**, 455 (1994)

[140] H. Kinzelbach i M. Lassig, *J. Phys. A: Math. Gen.* **28**, 6535 (1995)

[141] J.H. Lee i J.M. Kim, *Phys. Rev. E* **79**, 051127 (2009)

[142] G.M. Schütz, *J. Stat. Phys.* **71**, 471-505 (1993)

[143] M. Ha, J. Timonen i M. den Nijs, *Phys. Rev. E* **68**, 056122 (2003)

[144] C. N. Yang i T. D. Lee, *Phys. Rev.* **87**, 404 (1952)

[145] T. D. Lee i C. N. Yang, *Phys. Rev.* **87**, 410 (1952)

[146] R. A. Blythe i M. R. Evans, *Phys. Rev. Lett.* **89**, 080601 (2002)

[147] J. Krug J, *Braz. J. Phys.* **30**, 97-104 (2000)

[148] L. de Haan i A. Ferreira, *Extreme Value Theory: An Introduction* (Springer, New York, 2006)

[149] L. Gordon, M.F. Schilling i M.S. Waterman, *Probab. Th. Rel. Fields* **72**, 279-87 (1986)

[150] J. Szavits-Nossan i K. Uzelac, *J. Stat. Mech.* P05030 (2011)

[151] R. Ramaswamy i M. Barma, *J. Phys. A: Math. Gen.* **20**, 2973-87 (1987)

[152] M. Barma i R. Ramaswamy, *Field-induced transport in random media* u *Non-linearity i Breakdown of Soft Condensed Matter*, ur. K. K. Bardhan *et al.* (Springer, Berlin, 1993) str. 309

[153] T. Saegusa, T. Mashiko i T. Nagatani, *Physica A* **387**, 4119-32 (2008)

[154] N. Champagne, R. Vasseur, A. Montourcy i D. Bartolo, *Phys. Rev. Lett.* **105**, 044502 (2010)

[155] Y. Kafri, E. Levine, D. Mukamel, G.M. Schütz i J. Török, *Phys. Rev. Lett.* **89**, 035702 (2002)

[156] F.J. Alexander i J.L. Lebowitz, *J. Phys. A: Math. Gen.* **27**, 683-96 (1994)

[157] B. Schmittmann B, K. Hwang i R.K.P. Zia, *Europhys. Lett.* **19**, (1) 19-25 (1992)

[158] R. Usmani, *Linear Algebra Appl.* **212-213**, 413 (1994)

[159] C. Cocozza-Thivent,*Z. Wahrsch. Verw. Gebiete* **70** 509-523 (1985)